

การปรับปรุงประสิทธิภาพในการเร่งปฏิกิริยาของตัวเร่งปฏิกิริยาแพลเลเดียมบนตัวรองรับอัลฟาอะลูมินา
ในปฏิกิริยาไฮโดรจิเนชันแบบเลือกเกิดของอะเซทิลีน
โดยการใช้อัลฟาอะลูมินาเฟสผสมและผลึกขนาดนาโน



นายสถาพร คำหอม

วิทยานิพนธ์นี้เป็นส่วนหนึ่งของการศึกษาตามหลักสูตรปริญญาวิศวกรรมศาสตรดุษฎีบัณฑิต

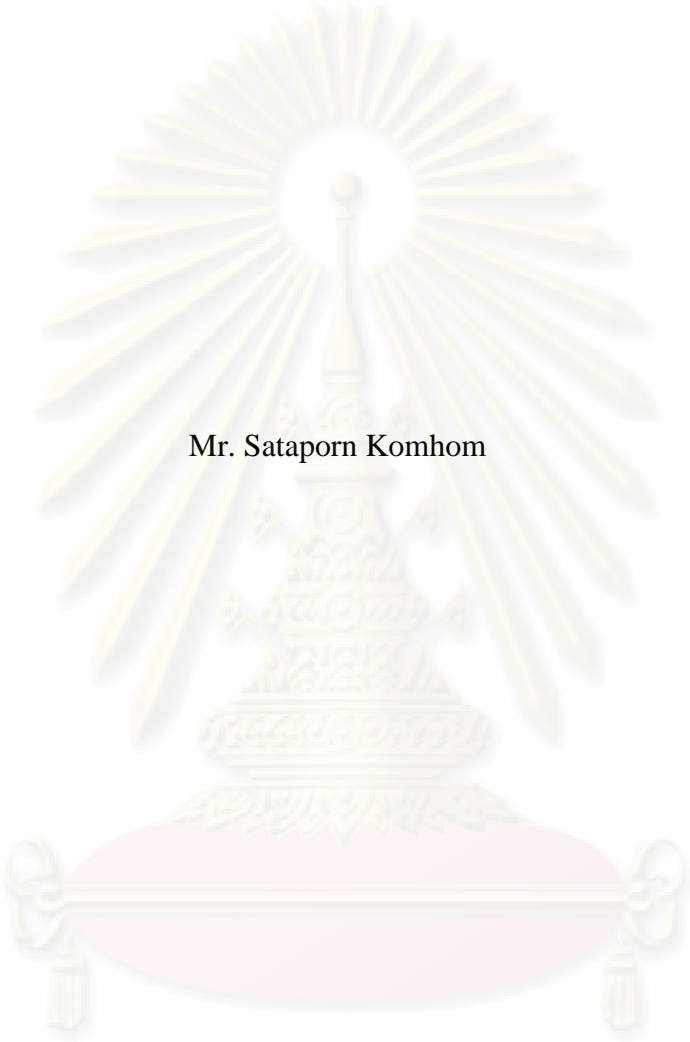
สาขาวิชาวิศวกรรมเคมี ภาควิชาวิศวกรรมเคมี

คณะวิศวกรรมศาสตร์ จุฬาลงกรณ์มหาวิทยาลัย

ปีการศึกษา 2551

ลิขสิทธิ์ของจุฬาลงกรณ์มหาวิทยาลัย

IMPROVEMENT OF CATALYTIC PERFORMANCE OF Pd/ α -Al₂O₃
IN SELECTIVE ACETYLENE HYDROGENATION
USING MIXED PHASES AND NANOCRYSTALLINE α -Al₂O₃



Mr. Sataporn Komhom

A Dissertation Submitted in Partial Fulfillment of the Requirements
for the Degree of Doctor of Engineering Program in Chemical Engineering
Department of Chemical Engineering

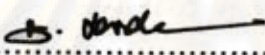
Faculty of Engineering
Chulalongkorn University

Academic year 2008

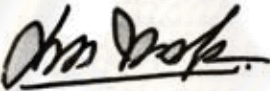
Copyright of Chulalongkorn University

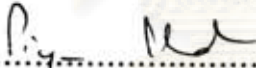
Thesis Title **IMPROVEMENT OF CATALYTIC PERFORMANCE
 OF Pd/ α -Al₂O₃ IN SELECTIVE ACETYLENE
 HYDROGENATION USING MIXED PHASES
 AND NANOCRYSTALLINE α -Al₂O₃**
 By **Mr. Sataporn Komhom**
 Field of Study **Chemical Engineering**
 Advisor **Professor Piyasan Prasertdam, Dr.Ing.**
 Co-Advisor **Assistant Professor Joongjai Panpranot, Ph.D.**


Accepted by the Faculty of Engineering, Chulalongkorn University in Partial Fulfillment of the Requirements for the Doctoral Degree

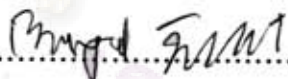

Dean of the Faculty of Engineering
 (Associate Professor Boonsom Lerdkhirunwong, Dr.Ing.)

THESIS COMMITTEE



Chairman
 (Associate Professor Supakanok Thongyai, Ph.D.)


Advisor
 (Professor Piyasan Prasertdam, Dr.Ing.)


Co-Advisor
 (Assistant Professor Joongjai Panpranot, Ph.D.)


Examiner
 (Assistant Professor Bunjerd Jongsomjit, Ph.D.)


Examiner
 (Assistant Professor Okorn Mekasuwandumrong, D.Eng.)


External Examiner
 (Assistant Professor Panida Sampranpiboon, D.Eng.)

สถาพร คำหอม : การปรับปรุงประสิทธิภาพในการเร่งปฏิกิริยาของตัวเร่งปฏิกิริยา
แพลเลเดียมบนตัวรองรับอัลฟาอะลูมินา ในปฏิกิริยาไฮโดรจิเนชันแบบเลือกเกิดของ
อะเซทิลีน โดยการใช้อัลฟาอะลูมินาเฟสผสมและผลึกขนาดนาโน (IMPROVEMENT OF
CATALYTIC PERFORMANCE OF Pd/ α -Al₂O₃ IN SELECTIVE
ACETYLENE HYDROGENATION USING MIXED PHASES AND
NANOCRYSTALLINE α -Al₂O₃) อ. ที่ปรึกษาวิทยานิพนธ์หลัก: ศ.ดร.ปิยะสาร
ประเสริฐธรรม, อ. ที่ปรึกษาวิทยานิพนธ์ร่วม: ผศ.ดร.จุงใจ ปั้นประณต, 156 หน้า.

ประสิทธิภาพในปฏิกิริยาไฮโดรจิเนชันแบบเลือกเกิดของอะเซทิลีน บนตัวเร่งปฏิกิริยา
แพลเลเดียมบนอัลฟาอะลูมินาปรับปรุงได้โดยการใช้อะลูมินาเฟสผสม และผลึกขนาดนาโนเมตร
การใช้เฟสผสมที่มีปริมาณของเฟสอัลฟา 64% ส่งผลต่อการปรับปรุงค่าการแปลงของอะเซทิลีน
และการเลือกเกิดเป็นเอทิลีน การมีอยู่ของทรานซิชันเฟสช่วยเพิ่มพื้นที่ผิวและการกระจายตัวของ
แพลเลเดียม นอกจากนี้ยังปรับปรุงความสามารถในการรีดักชันของตัวเร่งปฏิกิริยา และส่งเสริมให้
มีการดูดซับเอทิลีนในปริมาณต่ำลงด้วย การปรับปรุงการเลือกเกิดของอะเซทิลีน ไปเป็นเอทิลีน
สามารถกระทำได้โดยใช้การรีดักชันที่อุณหภูมิ 500 องศาเซลเซียส บนตัวเร่งปฏิกิริยาแพลเลเดียม
บนอัลฟาอะลูมินาที่มีผลึกขนาดนาโนเมตร พบว่าผลึกขนาดนาโนเมตรของอัลฟาอะลูมินาที่
สังเคราะห์โดยวิธีโซลโวลเทอรัมอล เมื่อใช้เป็นตัวรองรับแล้วให้ประสิทธิภาพที่ดีกว่าเมื่อ
เปรียบเทียบกับตัวรองรับที่มีขนาดไมโครเมตรทางการค้า ตัวรองรับอัลฟาอะลูมินาที่สังเคราะห์
จากวิธีโซลโวลเทอรัมอล โซล-เจล และการตกตะกอน ให้ขนาดผลึกอยู่ในช่วง 34 - 68 นาโนเมตร
โดยมีลักษณะความพรุนของผลึกที่ต่างกัน แม้ว่าขนาดผลึกของอัลฟาอะลูมินาจากวิธีโซล-เจล จะ
เล็กสุดแต่ความพรุนน้อยจึงทำให้พื้นที่ผิวและปริมาตรของรูพรุนน้อยลงไปด้วย อัลฟาอะลูมินาจาก
วิธีโซลโวลเทอรัมอลให้การกระจายตัวของขนาดรูพรุนที่แคบที่สุด (15 นาโนเมตร) เมื่อเปรียบเทียบกับ
วิธีโซล-เจลและวิธีการตกตะกอน เมื่อใช้ทำงานเป็นตัวรองรับโลหะแพลเลเดียมจึงให้การ
กระจายตัวที่สูง และมีประสิทธิภาพในปฏิกิริยาการเลือกเกิดของอะเซทิลีน ไปเป็นเอทิลีนได้ดีกว่า
จากการศึกษาด้วยวิธีการเปลี่ยนแปลงของอุณหภูมิพบว่าเมื่อใช้อัลฟาอะลูมินาที่เตรียมโดยวิธีโซล
โวลเทอรัมอลเป็นตัวรองรับ ทำให้ตัวเร่งปฏิกิริยามีการรีดักชันด้วยไฮโดรเจน และการคายซับของ
เอทิลีนและการบอมนอนออกไซด์ที่อุณหภูมิต่ำลง

ภาควิชา.....วิศวกรรมเคมี.....

สาขาวิชา.....วิศวกรรมเคมี.....

ปีการศึกษา.....2551.....

ลายมือชื่อนิติศ.....*ณัฐพร คำหอม*.....

ลายมือชื่อ. ที่ปรึกษาวิทยานิพนธ์หลัก.....*ปิยะสาร*.....

ลายมือชื่อ. ที่ปรึกษาวิทยานิพนธ์ร่วม.....*จุงใจ ปั้นประณต*.....

##4771829421: MAJOR CHEMICAL ENGINEERING

KEYWORDS: SELECTIVE ACETYLENE HYDROGENATION / MIXED PHASES / CRYSTALLITE SIZES EFFECT / NANOCRYSTALLINE POROSITY / SOLVOTHERMAL / Pd/Al₂O₃

SATAPORN KOMHOM: IMPROVEMENT OF CATALYTIC PERFORMANCE OF Pd/ α -Al₂O₃ IN SELECTIVE ACETYLENE HYDROGENATION USING MIXED PHASES AND NANOCRYSTALLINE α -Al₂O₃. ADVISOR: PROF. PIYASAN PRASERTHDAM, Dr.Ing., CO-ADVISOR: ASST. PROF. JOONGJAI PANPRANOT, Ph.D., 156 pp.

The performance in selective acetylene hydrogenation over Pd/ α -Al₂O₃ catalysts has been improved using mixed phases and nanocrystalline α -Al₂O₃. The use of mixed phases Al₂O₃ with approximately 64% of α -phase resulted in significant improvement for both acetylene conversion and ethylene selectivity. The presence of small amount of transition-phase in the alumina supports brought about higher BET surface area and Pd dispersion as well as improvement of reduction ability of the Pd/Al₂O₃ catalysts. On the other hand, significant amount of α -Al₂O₃ is necessary for high ethylene selectivity due to the lower amount of ethylene adsorbed. The improvement of ethylene selectivity can also obtained after reduction at 500°C on the solvothermal-derived nanocrystalline α -Al₂O₃ supported Pd. Moreover, the nanocrystalline α -Al₂O₃ powder with average crystallite size 34-68 nm have been synthesized by three different methods, namely, solvothermal, sol-gel, and precipitation. Nanocrystalline porosity of α -Al₂O₃ powder was varied by changing the preparation methods. Although smallest crystallite size of α -Al₂O₃ was obtained via the sol-gel synthesis, the α -Al₂O₃ sol-gel possessed the least amount of specific surface area and pore volume. A narrow pore size distribution with average pore diameter 15 nm can be obtained via solvothermal method while precipitation method yielded α -Al₂O₃ with larger pore size and wider pore size distribution. When employed as a support for Pd catalysts, the α -Al₂O₃ solvothermal provided the highest Pd dispersion and the best catalyst performance for selective hydrogenation of acetylene. The catalytic properties of Pd/ α -Al₂O₃ solvothermal were improved in terms of both acetylene conversion and ethylene selectivity. As shown by temperature program studies, the use of solvothermal-derived α -Al₂O₃ facilitated H₂ reduction at low temperature and desorption of ethylene and CO.

Department..... Chemical Engineering

Field of Study..... Chemical Engineering

Academic Year..... 2008

Student's Signature..... Sataporn

Advisor's Signature..... Piyasan Praserttham

Co-Advisor's Signature..... Joongjai Panpranot

ACKNOWLEDGEMENTS

First of all, I would like to express my sincere and deepest appreciation to my advisor, Professor Piyasan Prasertdam for his guidance, support, encouragement, kindness and help during the course of my graduate study. His in-depth knowledge, expertise and vision have guided me through the past five years of study and research. I am lucky enough to have him as my advisor. The research experience and knowledge gained here will benefit greatly my professional career. I would like to thank my thesis committee members, Associate Professor ML. Supakanok Tongyai, Assistant Professor Joongjai Panpranot, Assistant Professor Bunjerd Jongsomjit, Assistant Professor Okorn Mekasuwandumrong and Assistant Professor Panida Sampranpiboon for their valuable advice, help and support. I have learned a lot from all of the committee members in many different aspects. Without their help, I would not achieve what I have achieved today. Many thanks also go to many of my lab mates and friends. We have shared many happiness and some times, sadness during the past four years of study. At difficult times, they offered great help and encouragement. At good times, they shared the happiness with me.

The financial support from the Thailand Research Fund (TRF), Ministry of Education, Thailand and Commission on Higher Education is gratefully acknowledged.

Lastly, and also most importantly, I would like to thank my family for their love, support, encouragement, and understanding. I know I can always count on them for whatever I need. I would like to dedicate this thesis to them.

ศูนย์วิทยบริการ
จุฬาลงกรณ์มหาวิทยาลัย

CONTENTS

	Page
ABSTRACT (THAI).....	iv
ABSTRACT (ENGLISH).....	v
ACKNOWLEDGEMENTS.....	vi
CONTENTS.....	vii
LIST OF TABLES.....	x
LIST OF FIGURES.....	xi
CHAPTER	
I BACKGROUND.....	1
1.1 Overview.....	1
1.2 Acetylene hydrogenation.....	2
1.3 Palladium metal.....	3
1.4 Alumina (Al ₂ O ₃).....	4
1.5 Motivation.....	5
II RESEARCH OBJECTIVES AND SCOPE.....	7
2.1 Objectives.....	7
2.2 Research scope.....	7
2.3 Thesis outline.....	8
III LITERATURE REVIEW.....	9
3.1 The mechanism of acetylene hydrogenation.....	9
3.2 The α -PdH to β -PdH transformation.....	12
3.3 Formation of a PdC _x	15
3.4 Deposition of carbonaceous species on the palladium surface.....	17
3.5 Deposition of carbonaceous and “coke” on the support.....	19
3.6 Pd in selective hydrogenation.....	22
3.7 Catalyst.....	23
3.8 Catalyst deactivation.....	30
3.9 Industrial acetylene hydrogenation.....	32
3.10 Regeneration techniques.....	36

CHAPTER	Page
3.11 Current and future developments.....	37
IV EXPERIMENTAL.....	40
4.1 Catalyst preparation.....	40
4.2 Catalyst evaluation.....	44
4.3 Catalyst characterization.....	47
V RESULTS AND DISCUSSION.....	51
5.1 Mixed-phases Al ₂ O ₃ support.....	51
5.2 Micron-sized and nanocrystalline α -Al ₂ O ₃	66
5.3 Influence of preparation method on the nanocrystalline porosity.....	74
5.4 Influence of coke formation on Pd/ α -Al ₂ O ₃	87
5.5 Zinc modified α -Al ₂ O ₃ for supported Pd catalyst.....	92
VI CONCLUSIONS AND RECOMMENDATIONS.....	98
6.1 Conclusion.....	98
6.2 Recommendations.....	99
REFERENCES.....	100
APPENDICES.....	115
APPENDIX A CALCULATION FOR CATALYST PREPARATION.....	116
APPENDIX B CALCULATION CURVES.....	118
APPENDIX C CALCULATION OF THE CRYSTALLITE SIZE.....	121
APPENDIX D CALCULATION OF C ₂ H ₂ CONVERSION AND C ₂ H ₄ GAIN.....	124
APPENDIX E CALCULATION FOR CO-CHEMISORPTION.....	125
APPENDIX F PHYSISORPTION THEORY.....	128
APPENDIX G CALCULATION OF CONCENTRATION OF BOTH REACTANTS IN PRECIPITATION METHOD.....	133
APPENDIX H CALCULATION OF Zn MODIFIED ON Al ₂ O ₃ SUPPORT.....	135
APPENDIX I TABLE OF MESH SIZE.....	137
APPENDIX J CALCULATION OF GAS HOURLY SPACE VELOCITY (GHSV).....	138

LIST OF PUBLICATIONS.....	140
VITA.....	156



ศูนย์วิทยทรัพยากร
จุฬาลงกรณ์มหาวิทยาลัย

LIST OF TABLES

TABLE	Page
1.1 Some physical properties of palladium.....	4
3.1 General mechanism of catalytic acetylene hydrogenation.....	12
3.2 Contains a list and classification of poisons that are commonly present in feeds to acetylene converters.....	32
3.3 Typical acetylene concentration in the feed gas and conversion rate.....	34
3.4 Typical feed composition to ethyne hydrogenation reactors and the operating conditions for front-end and tail-end processes.....	36
4.1 Details of chemical reagents used for the catalyst preparation.....	41
4.2 Operating conditions of gas chromatographs.....	45
5.1 The physical properties of alumina with various phase compositions.....	53
5.2 Physicochemical properties of Pd supported on alumina with various phase compositions.....	57
5.3 The amount of H ₂ consumption and C ₂ H ₄ desorption.....	63
5.4 The physicochemical properties of Pd catalysts supported on micron-sized and nanocrystalline α -Al ₂ O ₃	69
5.5 Physicochemical properties of α -Al ₂ O ₃ various preparation methods and 0.3%Pd/Al ₂ O ₃ catalysts.....	77
5.6 Consumption of hydrogen in TPR, amount of ethylene and CO desorption.....	83

ศูนย์วิทยทรัพยากร
 จุฬาลงกรณ์มหาวิทยาลัย

LIST OF FIGURES

FIGURE	page
1.1 Thermal transformation sequence of the aluminum hydroxides.....	5
3.1 The network of the main reactions proceeding during acetylene hydrogenation in ethylene-rich streams.....	10
3.2 Changes to the catalyst during reaction.....	13
3.3 The phase diagram for PdH solutions.....	14
3.4 The scheme of the proposed changes of carbon concentration.....	17
3.5 Schematic diagram of carbonaceous species identified on palladium surface in acetylene and ethylene chemisorptions, decomposition, and hydrogenation.....	18
3.6 The diagram of plane view of adsorbed molecules of acetylene and ethylene including van der Waals radii and plane view of palladium atom for comparison.....	19
3.7 Ethane selectivity obtained during aging of 0.05% Pd/ α -Al ₂ O ₃ . Triangles show the performance of the deactivated 3.0 mm pellets after crushing to less than 0.5 mm.....	22
3.8 Location of front-end ethyne hydrogenation reactors in a simplified scheme of downstream treatment of steam cracker effluents.....	35
3.9 Location of tail- and ethyne-hydrogenation reactors in a simplified scheme of downstream treatment of steam cracker effluents.....	35
3.10 Computer designed shape (CDS).....	38
4.1 Flow diagram of the selective hydrogenation of acetylene.....	46
5.1 The XRD patterns of the Al ₂ O ₃ supports containing various % of α - phase.....	52
5.2 The BJH pore size distribution curves of the Al ₂ O ₃ supports.....	54
5.3 ESR spectra of the Al ₂ O ₃ supports.....	55
5.4 A plot between relative amplitudes of resonance at $g'=13$ and α -phase concentration.....	55
5.5 TG/DTA curve for the γ -Al ₂ O ₃	56
5.6 Transmission electron micrographs of the Pd/Al ₂ O ₃ catalyst.....	58

FIGURE	page
5.7 The XPS patterns of the Pd/Al ₂ O ₃ catalyst.....	59
5.8 Pd/Al ratios per BET surface area of the various Pd/Al ₂ O ₃ catalysts from XPS results.....	60
5.9 TPR profiles of the Pd/Al ₂ O ₃ catalysts.....	61
5.10 Ethylene TPD results of the Pd/Al ₂ O ₃ catalysts.....	62
5.11 Catalyst performances in selective hydrogenation of acetylene in terms of GHSV values and acetylene conversion (%).....	64
5.12 Catalyst performances in selective hydrogenation of acetylene in terms of GHSV values and ethylene gain (%).....	64
5.13 Catalyst performances in selective hydrogenation of acetylene in terms of acetylene conversion (%) and ethylene gain (%).....	66
5.14 The catalytic performances of Pd catalysts supported on micron-sized and nanocrystalline α -Al ₂ O ₃ reduced at 150°C and 500°C in selective acetylene hydrogenation under various feed flow rates.....	67
5.15 XRD patterns of the micron-sized and nanocrystalline α -Al ₂ O ₃	68
5.16 H ₂ temperature program reduction results.....	70
5.17 Ethylene temperature program desorption results.....	71
5.18 Ratios of Pd/Al/BET.....	72
5.19 Pd active sites results on different reduction temperature.....	73
5.20 The catalytic performances of Pd catalysts supported on micron-sized and nanocrystalline α -Al ₂ O ₃ reduced at 150°C, N ₂ O pretreatment and reaction temperature at 90°C in selective acetylene hydrogenation under various feed flow rates.....	74
5.21 XRD patterns of the α -Al ₂ O ₃ supports: solvothermal, sol-gel, and Precipitation method.....	75
5.22 IR spectra of α -Al ₂ O ₃ from solvothermal (a), sol-gel (b), and precipitation (c) method.....	76
5.23 Pore size distribution results of the α -Al ₂ O ₃ supports from solvothermal (a), sol-gel (b), and precipitation (c) method.....	78
5.24 N ₂ adsorption isotherms.....	79

FIGURE	page
5.25 TEM image of the Pd supported by α -Al ₂ O ₃ from solvothermal (a), sol-gel (b), and precipitation (c) method, showed Pd characteristics within the circles.....	81
5.26 H ₂ -TPR profiles for the various Pd/ α -Al ₂ O ₃ catalysts.....	82
5.27 C ₂ H ₄ -TPD profiles for the various Pd/ α -Al ₂ O ₃ catalysts.....	84
5.28 CO-TPD profiles for the various Pd/ α -Al ₂ O ₃ catalysts.....	85
5.29 Performance of Pd/ α -Al ₂ O ₃ catalysts in the selective acetylene hydrogenation.....	86
5.30 TPO profiles for the various Pd/ α -Al ₂ O ₃ catalysts.....	87
5.31 NH ₃ -TPD profiles for the various α -Al ₂ O ₃ supports.....	88
5.32 Performance of Pd/ α -Al ₂ O ₃ catalysts in the selective acetylene hydrogenation with GHSV = 9800 h ⁻¹ and various temperatures.....	89
5.33 Performance of Pd/ α -Al ₂ O ₃ catalysts in the selective acetylene hydrogenation with GHSV = 18800 h ⁻¹ and various temperatures.....	90
5.34 Performance of Pd/ α -Al ₂ O ₃ catalysts in the selective acetylene hydrogenation with GHSV = 25700 h ⁻¹ and various temperatures.....	91
5.35 Performance of Pd/ α -Al ₂ O ₃ catalysts in the selective acetylene hydrogenation with various GHSV at 40°C.....	92
5.36 XRD patterns of the α -Al ₂ O ₃ supports (Zn-modified and non-modified): solvothermal, sol-gel, and precipitation method.....	93
5.37 Performance of Pd/ α -Al ₂ O ₃ catalysts supported on α -Al ₂ O ₃ from solvothermal method in the selective acetylene hydrogenation with various temperature in the four GHSV values	95
5.38 Performance of Pd/ α -Al ₂ O ₃ catalysts supported on α -Al ₂ O ₃ from sol-gel method in the selective acetylene hydrogenation with various temperature in the four GHSV values.....	96
5.39 Performance of Pd/ α -Al ₂ O ₃ catalysts supported on α -Al ₂ O ₃ from precipitation method in the selective acetylene hydrogenation with various temperatures in the four GHSV values.....	97

CHAPTER I

BACKGROUND

1.1 Overview

Ethylene is one of the most widely produced petrochemicals in the world, with a production history reaching back to the early 20th century. It has been recovered since 1930 as a product of coke-oven gas and in the 1940's became an important industrial intermediate when American companies began producing it by separation from waste gas. This era also saw deliberate ethylene production from ethane and natural gas.

The chemical properties of ethylene result from the carbon-carbon double bond, with a bond length of 0.134 nm and a planar structure. Ethylene is a very reactive intermediate, which can undergo all typical reactions of a short-chain olefin. Due to its reactivity ethylene gained importance as a chemical building block. The complex product mixtures that have to be separated during the production of ethylene are also due to the reactivity of ethylene. Ethylene can be converted to saturated hydrocarbons, oligomers, polymers, and derivatives thereof. Chemical reactions of ethylene with commercial importance are: addition, alkylation, halogenation, hydroformylation, hydration, oligomerization, oxidation, and polymerization. More recently, ethylene has taken the place of acetylene in virtually all large-scale chemical syntheses. However, acetylene itself is a byproduct of modern ethylene production processes, and the removal of this contaminant is necessary.

More than 97% of ethylene around the world is produced by thermal cracking of hydrocarbons in the presence of steam, and by recovery from refinery cracked gas. This process can be described as the heating of a mixture of steam and hydrocarbon to the necessary cracking temperature, which can range from 260°C to 340°C depending on the hydrocarbon used. This mixture is then fed to a fired reactor or furnace and heated to between 400°C and 470°C. As a result, the original saturated hydrocarbon "cracks" into smaller unsaturated molecules. This process is extremely endothermic, and the product must be cooled back to the original feed temperature upon leaving the reactor in order to minimize secondary reactions. Possible alkane feedstocks for

pyrolysis include ethane, propane, n-butane, isobutane, naphthas, kerosene, and various gas oils. In the U.S., ethane and natural gas liquids (often a mixture of ethane and propane) are most commonly used in ethylene production. Incidentally, using an ethane feedstock produces the smallest amount of acetylene byproduct, which averages about 0.26% by weight of the product stream. For other feeds, this quantity can become as large as 0.95% by weight. Ethylene to be used for polymerization processes has to be 99.90% pure. This is known as polymer-grade ethylene and the maximum allowable limit of acetylene should not be higher than 5 ppm [1].

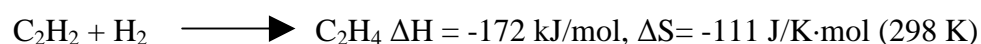
1.2 Acetylene hydrogenation

1.2.1 Polyethylene

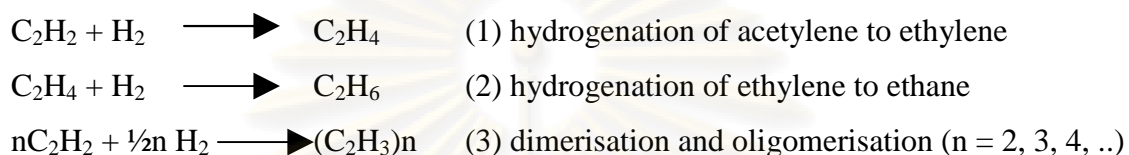
Polyethylene (PE) is a polymer consisting of a long backbone of covalently linked carbon atoms connected to two hydrogen atoms. Polyethylene is formed by polymerization of n molecules of the monomer ethylene. The chemical formula of polyethylene in its simplest form is $C_{2n}H_{4n+2}$, where n is the degree of polymerization. Different kinds of polyethylene exist depending on the concentration of side chains and of the presence of linked or functional groups like acids or esters. The total production of polyethylene exceeds 40 million tons per year [2]. PE is used in large quantities of non-expensive synthetic material with modest physical properties like stiffness and excellent chemical resistance for nondurable applications which do not require properties like hardness or thermal resistance. Industrial production of polyethylene is performed by two different processes. The Ziegler-Natta process consists of ethylene polymerization using transition metal organic complexes and transition metal chlorides [3]. Other processes are based on supported transition metal oxides like chromium oxide in the so-called Phillips process and metallocene catalysts [4].

1.2.2 Acetylene hydrogenation

Ethylene for the polymerization to polyethylene is produced by cracking of light alkanes in a steam cracker. The ethylene stream has to be purified and one step in the purification process is the selective hydrogenation of acetylene to ethylene [5].



Presence of acetylene in ethylene stream leads to poisoning of the polymerization catalyst because acetylene adsorbs at the active sites for ethylene and blocks the polymerization process. Therefore, the acetylene content in the ethylene feed has to be reduced to the low ppm-range. Hydrogenation of acetylene in the presence of ethylene requires high selectivity to ethylene to prevent hydrogenation of ethylene to ethane [5,6]. Following reactions occur in an acetylene hydrogenation reactor:



Main product of reaction (3) is 1,3-butadiene which can be further hydrogenated to so-called C₄ hydrocarbons 1-butene, n-butane, cis- and trans-butene. C₆-hydrocarbons and the so called green oil of higher hydrocarbons are formed in small quantities. Hydrocarbon deposits and hydrocarbon decomposition with subsequent formation of carbonaceous deposits on the catalyst surface lead to deactivation [6-8].

1.3 Palladium metal

1.3.1 Elemental palladium

Palladium as a group VIII noble metal has unique catalytic properties in homogeneous and in heterogeneous reactions. In heterogeneous catalysis palladium is used for oxidation and hydrogenation reactions. One of the most remarkable properties of palladium is the ability to dissociate and dissolve hydrogen. Atomic hydrogen occupies the octahedral interstices between the Pd atoms of the cubic-closed packed metal. Palladium can absorb up to 935 times of its own volume of hydrogen. Depending on hydrogen partial pressure and temperature a so-called α - and β -hydride is formed [9].

Table 1.1 Some physical properties of palladium [10].

Atomic number	46
Atomic weight	106.42
Atomic diameter	275.2 pm
Melting point	1827 K
Crystal structure	cubic closed packed
Electron configuration	[Kr] 4d ¹⁰
Electron negativity (Allred & Rochow)	1.4

1.3.2 Palladium in heterogeneous hydrogenation reactions

Like other group VIII metals, palladium can be used for hydrogenation of unsaturated hydrocarbons. Palladium shows the highest selectivity of these metals in heterogeneously catalyzed semi-hydrogenation of alkynes and dienes to the corresponding alkenes [6]. Activity of palladium for hydrocarbon hydrogenation is based on the ability for the dissociative adsorption of hydrogen and chemisorption of unsaturated hydrocarbons. The chemisorption of alkenes and alkynes is based on the interaction of the d-band of the Pd metal with the π -bonding system of the unsaturated hydrocarbons [11,12]. Industrially used catalysts for acetylene hydrogenation contain relatively low Pd content (< 0.1 wt%) and are supported on metal oxides like alumina. Palladium shows high activity but only limited selectivity and long-term stability for hydrogenation of acetylene. The limited selectivity is mainly due to enhanced ethane formation and the formation of by-products like C₄ and higher hydrocarbons. Palladium shows a strong deactivation behavior because of hydrocarbon and carbon deposits. Catalyst deactivation by hydrocarbon and carbon deposits requires a frequent exchange or regeneration of the catalyst in the hydrogenation reactor. Moreover, fresh or regenerated catalysts show high activity and consequently lead to increased ethylene consumption and reduced selectivity. Furthermore, high activity of fresh or regenerated catalysts can lead to overheating (“thermal run away”) of the reactor because of the exothermic hydrogenation reaction [7,8].

1.4 Alumina (Al₂O₃)

Alumina (Al₂O₃) is a white powder normally produced from bauxite ores. It is one of the most widely used advanced ceramic materials with applications ranges

from spark plugs to catalyst materials. In processing of alumina, the reactions can be divided into 3 different stages. The first is the formation of aluminium hydroxide. Aluminium hydroxides are either in well-characterised crystalline or amorphous forms. The most common trihydroxides are gibbsite, bayerite and nordstrandite, while boehmite and diaspore are in the hydroxide forms.

Alumina exists both in the transition or metastable and stable forms. Of the different forms of aluminas (α , χ , η , δ , κ , θ , γ , ρ), all are in the transition forms except for α -alumina. γ -alumina and α -alumina are the only two types of commercial alumina that are produced. The crystal structure of γ -alumina is that of hexagonal plate with large surface area. This made the alumina used being mainly in catalysis and in absorbent applications. There are different crystal structures of α -alumina most of which are rounded shape and hexagonal. The crystals also have small surface area. The usual way to synthesize the α -phase is the heat treatment of the transition alumina powders at relatively high temperatures, e.g., 1000-1200°C. The transition sequence is illustrated as follows [13,14]:

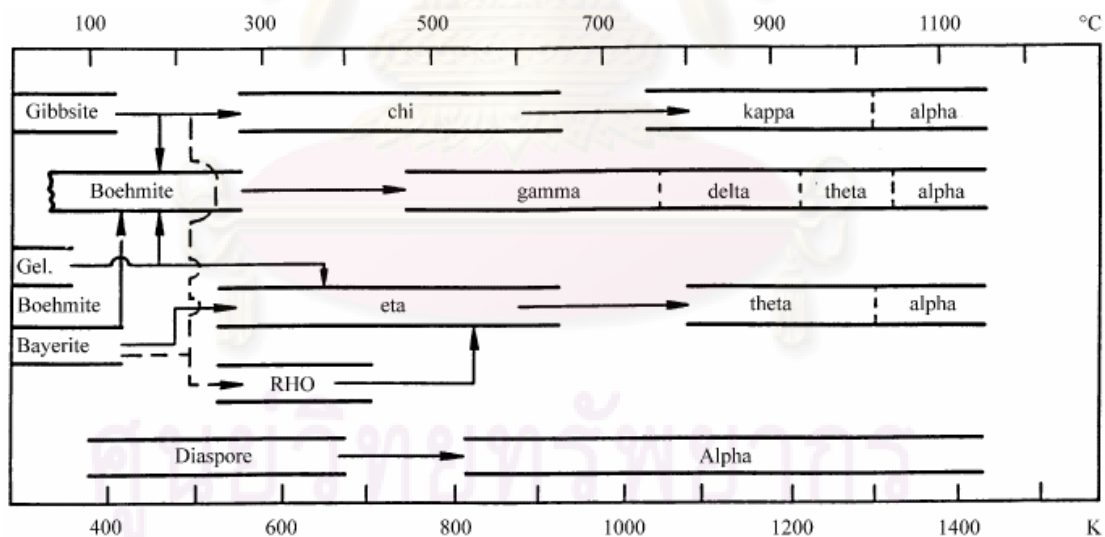


Figure 1.1 Thermal transformation sequence of the aluminum hydroxides.

1.5 Motivation

The reason that acetylene removal from the ethylene stream is so vital is that acetylene acts as a poison to the catalysts used for making polyethylene out of the ethylene product. In addition, acetylene can form metal acetylides, which are

explosive contaminants [15]. Therefore, acetylene in the ethylene stream must be hydrogenated aiming at reducing its concentration with a minimum loss of ethylene to ethane [16-17]. The selective hydrogenation of acetylene to ethylene is an important process used to purify ethylene streams containing trace amount of acetylene, for the production of polyethylene. It is desirable that the abundant ethylene component remains intact during the acetylene hydrogenation. Typically, Pd-based catalysts are efficient and widely utilized for this process due to its good activity and selectivity. During long-time investigations, the researchers have found the sequence of catalytic activity is Pd > Pt > Ni; Rh > Co > Fe > Cu/Au in the reaction of selective hydrogenation of acetylene and alumina supported low Pd content catalyst is widely used [18-25]. However, the catalyst performances could be improved by using novel supports or promoters and preparation advance of catalyst in order to obtain a high acetylene activity and high ethylene selectivity, as well as a long lifetime.

Recently, high ethylene selectivity for Pd/TiO₂-Anatase compared to Pd/TiO₂-Rutile has been suggested to be due to the promotional effect of the Ti³⁺ present on the TiO₂ surface [26]. The presence of Ti³⁺ in contact with Pd can probably lower adsorption strength of ethylene resulting in an ethylene gain. A recent study by Li et al. [27] reveals that the SMSI of Pd/TiO₂ catalyst was influenced by the titania polymorph. Diffusion of Ti³⁺ from the lattice of anatase TiO₂ to surface Pd particle can lower the temperature to induce SMSI. Therefore, Ti³⁺ species that were in contact with palladium surface can simultaneously promoted SMSI effect and ethylene desorption. Ag addition shows a negative effect for Pd/TiO₂-Anatase because suppression of the beneficial effect of the Ti³⁺ on anatase TiO₂ by Ag addition hence lower ethylene selectivity was obtained. Although it was found that the TiO₂ phases had been reported, the mixed-phases of alumina have not studied. In addition, the parameters via crystallite size and porosity of nanocrystalline on the selective acetylene hydrogenation have not been reported yet.

CHAPTER II

RESEARCH OBJECTIVES AND SCOPE

2.1 Objectives

The objectives of the study are to investigate the influence of mixed phases of alumina on the performance of Pd catalysts and to comparatively study of micron-sized and nanocrystalline of α -Al₂O₃ supported catalysts. Besides, the properties of α -Al₂O₃ by different preparations are to analyze for Pd catalysts in selective hydrogenation of acetylene to ethylene. Specifically, this study is aimed to fulfill the following three objectives:

1. To study the effect of mixed transition- and alpha-phase alumina on the performance of Pd/Al₂O₃ catalysts.
2. To comparatively study the effect of micron-sized and nanocrystalline of α -Al₂O₃ supported catalysts on the performance of Pd catalysts.
3. To determine the properties of α -Al₂O₃ prepared by different manners for application Pd catalyst support.

2.2 Research scope

The experiments carried out in this research are divided into three categories: catalyst preparation, characterization, and reaction study. The research scope for each part is shown below:

Part I

1. Preparation of α -Al₂O₃ supports which consisted of various transition- and alpha-phase alumina.
2. Preparation of micron-sized and nanocrystalline α -Al₂O₃. The micron-sized α -Al₂O₃ was the commercially available α -Al₂O₃ from Aldich. The nanocrystalline α -Al₂O₃ was prepared by the solvothermal method.
3. Preparation of α -Al₂O₃ supports by solvothermal, sol-gel, and precipitation method.
4. Preparation of Pd/Al₂O₃ catalysts by the incipient wetness impregnation technique.

Part II

1. The Al₂O₃ supports were characterized XRD, ESR, and BET.
2. The Pd/Al₂O₃ catalysts were characterized using TEM, XPS, TPR, TPD, TPO, TGA-DTA, and CO-chemisorption techniques.

Part III

1. The catalytic performance of Pd/Al₂O₃ catalysts was studied in the selective hydrogenation of acetylene to ethylene. The catalyst was reduced in situ with hydrogen by heating from room temperature to 150°C at a heating rate of 10°C/min. Then the reactor was purged with argon and cooled down to the reaction temperature. The reaction was carried out using a feed composition of 1.5% C₂H₂, 1.7% H₂, and balanced C₂H₄ with a vary GHSV.

2.3 Thesis outline

This thesis is arranged into five chapters. The background chapter is presented in **Chapter I**, and following a research objectives and scope is obtained in **Chapter II**. **Chapter III** describes the literature review and the industrial acetylene hydrogenation. The experimental works are covered in **Chapter IV**. Finally, **Chapter V** contains the results and discussion as well as the conclusions from this research and some recommendations for conundrum studies in this area are shown in **Chapter VI**.

ศูนย์วิทยทรัพยากร
จุฬาลงกรณ์มหาวิทยาลัย

CHAPTER III

LITERATURE REVIEW

Selective acetylene hydrogenation has been known about for many years, although the information in the literature is somewhat sparse. There are few references on experimental studies of various factors influencing the Pd catalysts performance. In light of this, the literature review presented here covers a large number of topics that are concerned with the various factors influence to the Pd catalyst. In addition, some fundamental reaction concepts are briefly introduced because they are the basis understanding of the Pd catalyst performance.

3.1 The mechanism of acetylene hydrogenation

In a constant volume system, high selectivity of ethylene could be maintained as long as any acetylene remained, even in the presence of excess hydrogen but, while it was possible in the region of room temperature, the use of higher temperatures encouraged the simultaneous formation of ethane. When this occurred, however, the two processes occurred in parallel; but the selectivity remained constant while any acetylene was left. When all of the acetylene had reacted, the ethylene was then hydrogenated more quickly, so that the rate of pressure fall increased [28-30]. This proved very clearly that under these conditions there were no sites available for ethylene hydrogenation that were not occupied by acetylene, that is, re-adsorption of gaseous ethylene was forbidden. The simultaneous formation of ethane must, therefore, have arisen by reaction of ethylene before it had desorbed. This led to the recognition of two factors in high selectivity shown by palladium: (i) a thermodynamic factor, which secures the preferential coverage of the surface by acetylene through its greater heat of adsorption; and (ii) a mechanistic factor, by which ethylene desorbs and is replaced by acetylene before it has a chance to react [31-34].

The network of the main reactions proceeding during acetylene hydrogenation in ethylene-rich streams is shown in **Figure 3.1**.

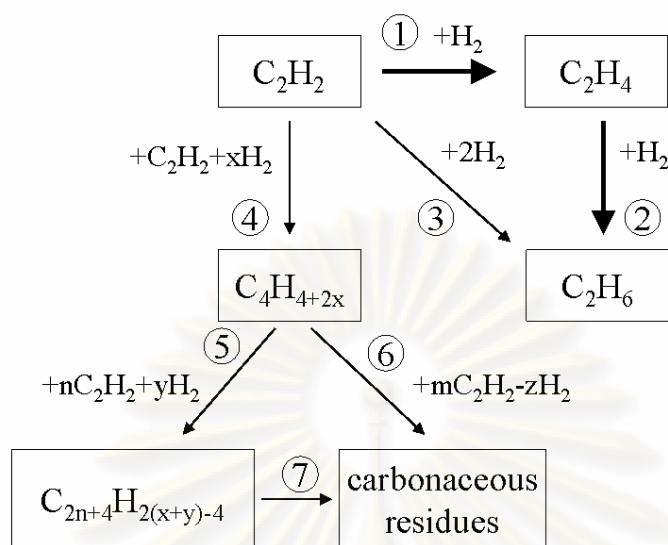


Figure 3.1 The network of the main reactions proceeding during acetylene hydrogenation in ethylene-rich streams. The reactions are denoted by numbers in the circles: 1) acetylene half-hydrogenation to ethylene, 2) ethylene hydrogenation to ethane, 3) acetylene hydrogenation to ethane, 4) hydro-oligomerization of acetylene to C_4 hydrocarbons (value x may be equal to: 0, 1, 2), 5) formation of C_{6+} hydro-oligomers of acetylene (value y may be equal to: 0, 1, 2, 3, . . . n), 6), and 7) formation of carbonaceous residues (value z may be equal to: 0, 1, 2, 3, . . . z).

This scheme does not show the mechanism of the reactions but rather the reactions having a main influence on the mass balance of the process and on the process operation. The only desired reaction is acetylene half-hydrogenation to ethylene. During acetylene hydrogenation in ethylene-rich streams, at steady state conditions, the rates of reactions (3-6) are small as compared to the rates of reactions (1) and (2). However, reactions (4-6) play an important role in the process. Reaction (4) produces C_4 hydrocarbons, which were suggested to be the precursors of heavier C_{6+} hydro-oligomers containing even numbers of carbon atoms (5) and of carbonaceous residues (6). The liquid part of the hydrocarbons accumulates in the catalyst's pores and also appears downstream, where it can cause plugging of pipes. When carbon monoxide is co-fed the liquid hydrocarbons have a green color and are called "green oil". The irreversibly adsorbed heavy hydrocarbons on the catalyst

surface (6,7) modify the catalyst properties [increase or decrease of the catalyst's activity and selectivity to ethylene] [35-38].

In the partial catalytic hydrogenation of acetylenic compounds, the triple bond has to be converted into a double bond. In doing so, there arise the following problems of selectivity [39]:

- (a) The double bond which is formed can be further hydrogenated.
- (b) The double bond which is formed can be displaced (position isomerism).
- (c) The double bond which is formed can have cis or trans configuration (geometric isomerism).

Since acetylene only have two carbon atoms, the problems stated in (c) is not applicable. To achieve high selectivity, the catalyst must not further hydrogenate the partially hydrogenated product. This can be affected by two factors, the kinetics and the thermodynamic factors. Kinetic and thermodynamic effects are frequently combined, and they cannot readily be distinguished. Further, not only the catalyst but also the chemical structure can have an influence on the selectivity.

In case of the subsequent reactions (undesired reaction) proceeding much more slowly than the partial hydrogenation (desired reaction); the selectivity is then based on a mechanistic (kinetic) factor. Besides, the partially hydrogenated product can also be protected from subsequent reactions by being rapidly desorbed from the catalyst surface and then not being re-adsorbed again. This thermodynamically dependent selectivity is based on the triple bond being more strongly adsorbed than the corresponding double bond, because it is more electrophilic character. Even relatively small differences in the adsorption energy are sufficient for the acetylenic compound to immediately displace the primary resulting hydrogenation product from the catalyst surface and accordingly act as a "poison" for the subsequent reactions. The poisoning action is naturally only effective as long as the acetylenic compound is still present.

Acetylene itself is a good example of thermodynamically controlled selectivity. This can be proven from the effluence of a fixed bed palladium catalyst reactor, where the resulting ethylene only contains 1-5 % ethane although this catalyst have 10 to

100 times greater activity for the hydrogenation of ethylene than for the hydrogenation of acetylene [39].

A general mechanism shown in **Table 3.1** suggested that selectivity is controlled by the equilibrium between the two forms of adsorbed C_2H_3 (step 3 and step 4). The hydropolymerisation (formation of oligomer or “green oil”) is considered to be a polymerisation of adsorbed acetylene, $H\overset{\cdot}{C}=\overset{\cdot}{C}H$, in which the free radical $-H\overset{\cdot}{C}-\overset{\cdot}{C}H_2$ is the initiator [40].

Table 3.1 General mechanism of catalytic acetylene hydrogenation.

Step 1 : Adsorption	Acetylene is associatively adsorbed on the longer lattice spacing of the transition group metal, and that it reacts with a H_2 molecule (there being no independently adsorbed hydrogen on Ni) or	$H\overset{\cdot}{C}=\overset{\cdot}{C}H + H_2 \rightarrow H\overset{\cdot}{C}=\overset{\cdot}{C}H_2 + H^{\cdot}$
	with an adsorbed H atom (on Pd or Pt)	$H\overset{\cdot}{C}=\overset{\cdot}{C}H + H^{\cdot} \rightarrow H\overset{\cdot}{C}=\overset{\cdot}{C}H_2$
Step 2: Isomerisation	The adsorbed vinyl radical is thought to isomerise in part into a free radical form	$-H\overset{\cdot}{C}-\overset{\cdot}{C}H_2$
Step 3: Hydrogenation to ethylene	The vinyl form hydrogenates to give ethylene which leaves the surface	$H\overset{\cdot}{C}=\overset{\cdot}{C}H_2 + H^{\cdot} \rightarrow CH_2=CH_2$
Step 4: Hydrogenation to ethane	The free radical form gives an adsorbed ethylene which can react with more hydrogen	$-H\overset{\cdot}{C}-\overset{\cdot}{C}H_2 + H^{\cdot} \rightarrow \overset{\cdot}{C}H_2-\overset{\cdot}{C}H_2$ $\overset{\cdot}{C}H_2-\overset{\cdot}{C}H_2 + H^{\cdot} \rightarrow \overset{\cdot}{C}H_2-CH_3 \rightarrow CH_3-CH_3$

The asterisks indicate adsorption links.

3.2 The α -PdH to β -PdH transformation

Ethylene adsorption and the detailed mechanism of its hydrogenation on metal surfaces is still one of the most widely studied and debated problems in catalysis. The great complexities of hydrogenation of acetylene/ethylene mixtures over palladium catalysts is the reason for slow progress in establishing a molecular mechanism for the process, and the nature and the types of active site. The role of carbonaceous species adsorbed on metal surfaces has been studied using various techniques. There are two main difficulties in these studies: (i) the existence of the pressure gap between studies on model catalysts and kinetic measurements on supported catalysts, (ii) the species active in hydrogenation reactions may be moderately adsorbed, so their surface coverage may be very low, whereas strongly adsorbed species, which are much easier

to determine, may only play the role of spectator [41-43]. The catalytic process may proceed via several parallel and sequential steps on various specific types of active sites both on metal and support surfaces. An additional difficulty is connected with the various types of change that may occur in parallel to catalysts during use, such as phase transformations ($\text{Pd} \rightarrow \beta\text{-PdH}_x$ and $\text{Pd} \rightarrow \text{PdC}_x$) and deposition of unreactive hydrogen-deficient polymeric species on the metal surface and in the catalyst's pores, which may affect the catalyst's properties [44]. Explanation of unusually high selectivity of palladium in hydrogenation of acetylene to ethylene is one of the most interesting questions addressed by this process.

When a palladium catalyst is stabilized during hydrogenation of acetylene or acetylene-ethylene mixtures, it undergoes fast and slow changes that modify its properties, as schematically shown in **Figure 3.2**.

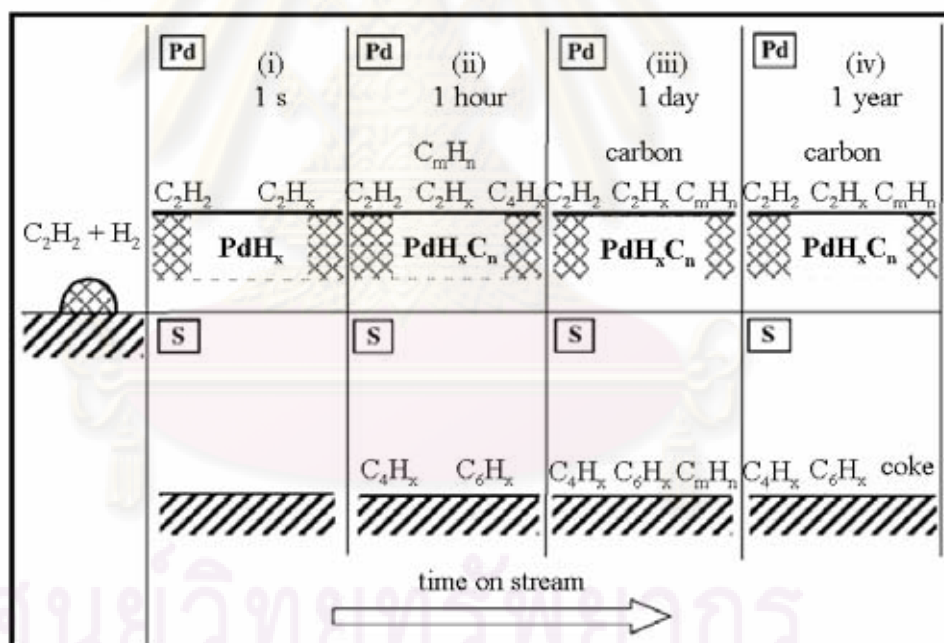


Figure 3.2 Changes to the catalyst during reaction.

First, the palladium surface is immediately covered by associatively $[(\text{C}_2\text{H}_2)_{\text{ad}}]$ and dissociatively $[(\text{C}_2\text{H})_{\text{ad}}]$ chemisorbed acetylene, and the half-hydrogenated state $(\text{C}_2\text{H}_3)_{\text{ad}}$ (ethynylidyne, as is shown in **Figure 3.2**) [45]. Secondly, the $\alpha\text{-PdH} \rightarrow \beta\text{-PdH}$ phase transition may rapidly occur at room or higher temperatures and high hydrogen

pressure [46,47]; and, thirdly, carbon is gradually incorporated into palladium lattice [48,49] and acetylene-derived oligomers and polymers are covering the palladium [50,51] as well as support surfaces [52,53]. After about 4-24 hours a pseudo-steady state is achieved, but very slow deactivation of the catalyst proceeds as a result of deposition of coke (high polymer, perhaps graphitic, certainly with a low H/C ratio) in the catalyst pores [54,55]. At the pseudo-steady state of the reaction carbonaceous deposits are present in the catalyst pores and the palladium surface is covered by a carbonaceous overlayer, which consists of various species, such as: C_2H_x ($x = 1, 2,$ and 3), and surface oligomers/polymers ($C_{2n}H_m$) [56].

Palladium has the specific ability to form a β -PdH phase at relatively low hydrogen pressures. The properties of palladium hydrides were widely investigated and described in several monographs and reviews [57]; the phase diagram of PdH system is shown in **Figure 3.3**. It represents the experimental relations between hydrogen pressure and concentration of hydrogen in PdH solution (H/M atomic ratio) derived from solid/gas equilibration studies at various temperatures.

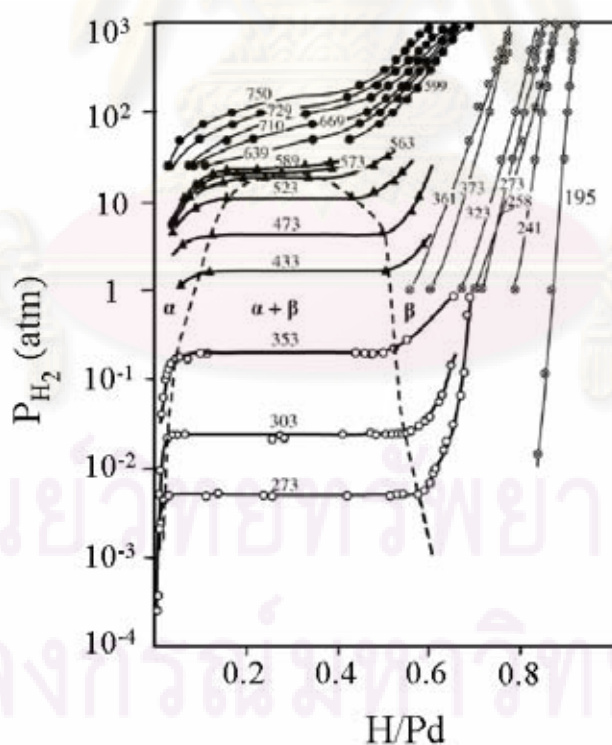


Figure 3.3 The phase diagram for PdH solutions. The numbers indicate the temperature in K for given hydrogen sorption isotherms. The broken line enclosed the area of coexistence of α -PdH and β -PdH phases.

The presence of the β -PdH phase during the hydrogenation of alkynes or alkenes cannot be proved simply on the basis of thermodynamics of the palladium-hydrogen system. The reason is that the hydrogenations may consume hydrogen from the hydride, so the partial pressure of hydrogen must be increased to allow formation of the β -PdH phase. This decomposes (or forms) very fast, so it has to be detected in situ, during the reaction. The amount of β -PdH phase present was assessed only by TPR measurements starting at room temperature after helium flushing, but of course the phase transformation may have occurred during the cooling and flushing. Interpretation of results obtained using catalysts having different palladium particle sizes is fraught with difficulty, as the pressure needed for hydride formation increases with decreasing size [58] and also the rate of decomposition of β -PdH phase for highly dispersed catalysts can be higher. Thus the β -PdH phase is more likely to have decomposed in the case of the more highly dispersed catalyst.

In summary, the studies of acetylene hydrogenation performed with in situ measurements of the extent of β -PdH phase formation are self-consistent and show that this phase is more active and less selective to ethylene than is the α -PdH phase.

3.3 Formation of a PdC_x phase

It was discovered that during acetylene hydrogenation at moderate temperature (373 K) carbon atoms, being the product of acetylene decomposition on the palladium surface, penetrate into the lattice, and a solid solution of carbon in palladium (PdC_x where $0 < x \leq 0.13$) is formed, whereas in contact with graphite much lower amounts of carbon are dissolved.

Further in situ studies of the state of palladium during the reaction showed that a supersaturated solid solution PdC_{0.13} can be obtained upon heating catalysts during acetylene hydrogenation at temperatures from 470 K to 510 K, depending on the average metal crystallite size (8-50 nm) and gas composition [59], and at 413 K with acetylene/ethylene mixtures. PdC_{0.15} solid solution is also formed when metallic palladium is heated above 523 K in the atmosphere of 1% C₂H₂/He, in ethylene above 403 K, or in carbon monoxide above 773 K (114, 115). The PdC_x phase decomposes above ca. 403 K in hydrogen or oxygen and at 873 K in an inert atmosphere.

The carbon atoms in the interstitial solid solution PdC_x occupy octahedral holes in the palladium lattice, which is similar to hydrogen atoms in the β -PdH phase, and competition between hydrogen and carbon atoms in the Pd-C-H ternary system is observed [60]. Increase of carbon concentration in palladium (C/Pd) caused a decreasing tendency to form the β -PdH phase and ultimately $\text{PdC}_{0.13}$ did not form this hydride phase at all. A similar effect of alloying on the decrease of hydrogen absorption ability was observed earlier for a PdB_x interstitial solution [61] and for substitutional solid palladium solutions [62]. An analogous relation between the carbon solubility and the amount of aluminum in Pd-Al alloys has been found, alloying thus hindering the penetration of carbon into palladium lattice.

Carburization of palladium during hydrogenation of acetylene-ethylene mixtures is responsible for the increase of the rate of acetylene disappearance in the course of aging the catalyst. Thus, the effect of carbon penetration to the palladium lattice on the activity of the catalyst is analogous to the effect of hydrogen. The rate of acetylene disappearance and the concentration of carbon dissolved in the bulk palladium increased similarly for samples with metal crystallite sizes of 12 nm. Similar effects of carburization have been suggested for hydrogenation of acetylene but the suggestion was not supported by in situ measurements of carbon concentration during the reaction. The maximum concentration of carbon in palladium at the steady state of the reaction also increased with carburization temperature and decreased with increase of crystallite size. During carburization the rate of the process was limited by the formation rate of the carbon atoms on the palladium surface, so diffusion of carbon into the bulk was fast and there was no concentration gradient in the palladium crystallites.

However, during carburization of larger palladium crystallites (20 nm) at the same temperature, the rate of the process was limited by hydrogen diffusion from the surface to bulk and the parallelism between the rate of acetylene hydrogenation and carbon concentration in the bulk no longer existed. It was also found that two catalysts having different initial phase compositions ($\text{PdC}_{0.13}$ and Pd) had the same activities at steady state conditions at 323 K. The proposed changes of carbon concentration in the surface layer and in the bulk of crystallites are shown in **Figure 3.4**. In the $\text{PdC}_{0.13}$ sample, the carbon concentration in the bulk did not change,

whereas in the other sample the value of x increased to 0.016. This result indicates that $\text{PdC}_{0.13}$ at 323 K is in the diffusion-hindered frozen state in the bulk, but the concentrations of carbon on the surfaces of $\text{PdC}_{0.13}$ and $\text{PdC}_{0.016}$ are very similar at steady-state conditions [48].

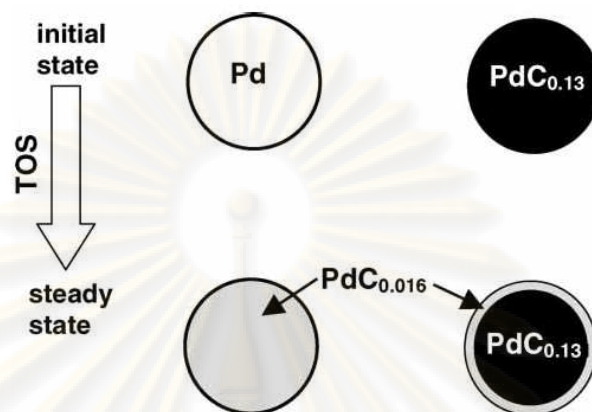


Figure 3.4 The scheme of the proposed changes of carbon concentration in the surface layer and in the bulk of palladium crystallites during acetylene hydrogenation at 323 K; average crystallite size of palladium black was 12.2 nm; $P_{\text{C}_2\text{H}_2} = 0.0215$ kPa; $P_{\text{H}_2} = 0.57$ kPa.

3.4 Deposition of carbonaceous species on the palladium surface

3.4.1 Interaction of acetylene and ethylene with the palladium surface

During adsorption or hydrogenation of acetylene/ethylene mixtures over palladium catalysts, various forms of adsorbed C_2 species and carbonaceous deposits may be present on the palladium surface depending on temperature, hydrogen surface coverage, and type of crystallographic surface plane. Extensive studies have been carried out to establish the structure and mode of decomposition of adsorbed acetylene and ethylene molecules.

Some of the identified adsorbed states of acetylene and ethylene [63,64] on the palladium surface are shown in **Figure 3.5**. Increase of the adsorption temperature generally causes progressive loss of hydrogen atoms from adsorbed carbonaceous species, and these unsaturated molecules become multiply bonded to the metal surface and, therefore, more strongly held. Further increase of temperature causes C-C bond breaking, with ultimate formation of amorphous carbon or a graphitic layer, and also oligomers C_nH_m strongly bonded to the palladium surface. When hydrogen is co-

adsorbed with acetylene or ethylene, then carbonaceous species are partly hydrogenated and become less hydrogen-deficient with increasing surface coverage by hydrogen.

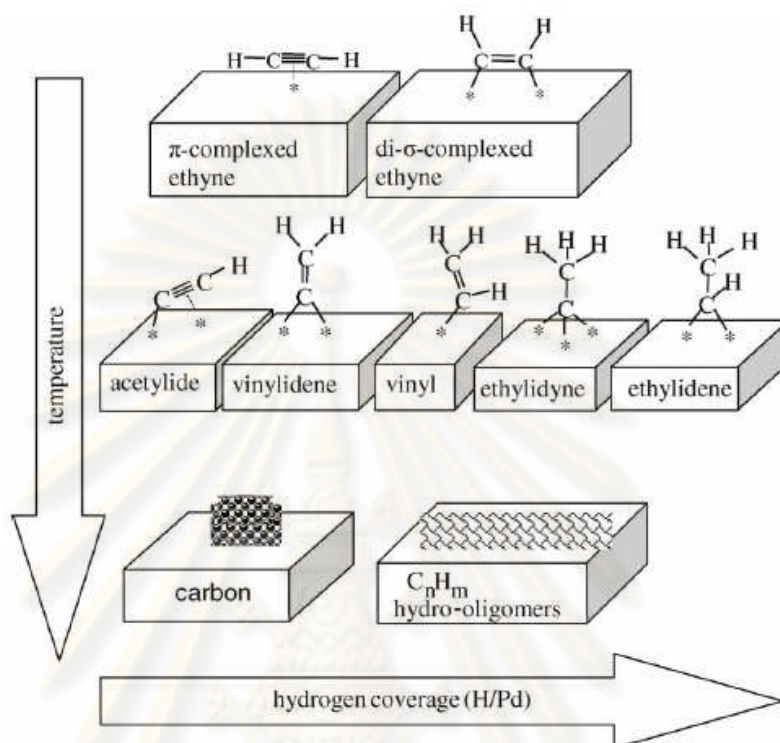


Figure 3.5 Schematic diagram of carbonaceous species identified on palladium surface in acetylene and ethylene chemisorptions, decomposition, and hydrogenation.

3.4.2 Deposits on the palladium surface during hydrogenation of acetylene, ethylene, and their mixtures

The carbonaceous overlayer is immediately formed on the palladium surface during hydrogenation of acetylene at atmospheric pressure and temperatures above 273 K, and the reaction then occurs in the presence of these carbonaceous deposits. It was proposed that two types of catalytic site are created on the palladium surface by the hydrocarbonaceous overlayer deposited during the reaction: A and E sites responsible respectively for acetylene and ethylene conversion. These deposits are composed of dissociatively adsorbed acetylene (CCH , CCH_2 , CCH_3), surface polymeric species, C_nH_m , and carbon [65,66]. The active sites represent small (A site) and large (E site) spaces on the palladium surface between the carbonaceous species. The A sites are composed of a series of narrow adsorption sites able to adsorb acetylene and hydrogen but too narrow to adsorb ethylene and are therefore inactive for ethylene hydrogenation [67]. E sites adsorb all reactants including ethylene, which

are hydrogenated on them. The rate of acetylene conversion on E sites was found negligible, hence it was assumed that the concentration of the large E sites is much lower than that of small A sites, for the catalyst working at the steady state. To explain the larger steric hindrance of adsorbed ethylene compared to that of adsorbed acetylene, it was suggested that the key intermediate of acetylene hydrogenation is π -bonded acetylene [68] is adsorbed parallel to the palladium surface and is hydrogenated by sequential addition of single hydrogen atoms to the adsorbed C_2H_x ($x = 2-3$) species, the vinyl group existing in normal and free radical state in equilibrium [69,70]. The lack of ethylene adsorption on A sites may be explained by the difference in width of the molecules in the directions perpendicular to C-C axis, 0.43 nm and 0.34 nm, respectively, as is illustrated in diagrams of plane view of adsorbed molecules including van der Waals radii (Figure 3.6).

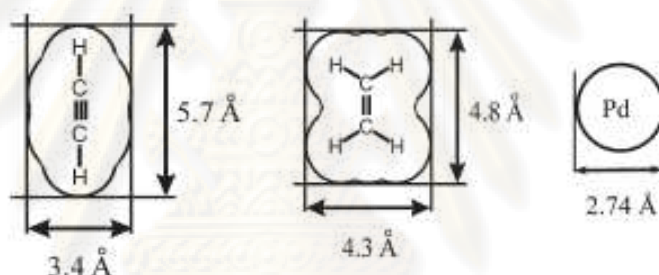


Figure 3.6 The diagram of plane view of adsorbed molecules of acetylene and ethylene including van der Waals radii and plane view of palladium atom for comparison.

3.5 Deposition of hydrocarbons and “coke” on the support

3.5.1 Oligomerization

Adsorbed acetylene species undergo slow hydro-oligomerization, which leads to the formation of heavy oligomers containing an even number of carbon atoms [71]. About 25%-30% of acetylene is converted to C_{4+} hydrocarbons and about 2% is deposited on the catalyst during tail-end hydrogenation at 1 atm under steady-state conditions. However, at the beginning of acetylene hydrogenation at 308 K the selectivity of coke deposition was very high (about 60%) and then at steady-state conditions, the decrease of the rate of coke deposition was found.

Acetylene oligomerization occurs on palladium and on the Al₂O₃ support surface [72]. It was suggested that butadiene and larger conjugated dienes, which are formed on the palladium surface, are precursors of the carbon deposits (coke) formed on the support [73]. Some of the oligomers desorb from the catalyst and form the liquid hydrocarbon products in the outlet mixture. The hydrocarbons may push palladium particles away from the alumina support and may be responsible for rapid metal sintering during the catalyst regeneration. The oligomers are produced in smaller amounts on palladium catalyst promoted by the addition of a second metal [74], a transition metal oxide [72], and silicon [75].

The amounts and types of the carbonaceous deposits depend on the type of the catalyst and on the reaction conditions [8]. It was postulated on the basis of kinetic measurements conducted after stabilization of the catalyst at various compositions of reaction mixture that two types of coke are deposited on the catalyst: “harmful coke” and “harmless coke” [76]. The first is formed at low hydrogen coverage of the palladium surface during the stabilization.

3.5.2 Influence of “coke” on intraparticle mass transport of hydrogen and acetylene

It was shown that coke deposition in the catalyst pores may decrease the effective diffusion coefficient of acetylene (D_{eA}) by nearly one order of magnitude [37]. This effect may increase its internal diffusion resistance during aging of the catalysts. The Weisz-Prater criterion [77] should be satisfied to assure the absence of internal diffusion limitation, which is necessary if the reaction kinetics are to be controlled by the surface chemistry, the inequality is

$$\frac{\rho \cdot r_w \cdot d_p^2}{36 \cdot D_{eA} \cdot C_{sA}} \cdot \left(\frac{n+1}{2} \right) < 0.15.$$

where ρ is the catalyst particle density; r_w the specific reaction rate, (mol/(kg_{cat}·s)); d_p is the catalyst particle diameter, (m); n is the order of reaction (for $n \geq -1$); D_{eA} is the effective diffusion coefficient of molecule A, (m²/s); and C_{sA} is the molar concentration of A at the exterior surface of a catalyst particle, (mol/m³).

In agreement with the earlier criterion it was found that the internal diffusion limitation of acetylene decreases with: (i) particle diameter, (ii) decreasing depth of palladium penetration for eggshell catalysts, (iii) increase of D_{eA} [by increase of pore size or decrease of coke formation], (iv) decrease of the specific reaction rate of acetylene [by decrease of palladium concentration, temperature, or hydrogen pressure, or by increase of carbon monoxide pressure or poisoning of the palladium surface] [78].

3.5.3 Ethylene hydrogenation on the support by spillover hydrogen catalyzed by carbonaceous species

It was found that in the case of Pd/ γ -Al₂O₃ catalysts hydrogen dissociated on the metal surface can spill over to the support and react with adsorbed ethylene to form ethane, whereas acetylene is only hydrogenated on palladium. The carbonaceous species accumulated on the support act as bridges that accelerate the process and consequently greatly increase the undesirable ethylene hydrogenation and ethane selectivity. It can also be said that the accumulations of oligomers on the support may influence both hydrogen spillover and internal diffusion limitations of the acetylene.

The hydrogenation of ethylene on α -Al₂O₃ and on SiO₂ supports is negligible, so that these are suitable supports for commercial catalysts [56,79]. A small increase of the rate of ethane formation was found during aging of Pd/ α -Al₂O₃ or Pd/SiO₂ in spite of elimination of internal diffusion limitation of acetylene by using very small catalyst particles, as shown in **Figure 3.7**. It was probably caused by an increase of the rate of hydrogenation of acetylene to ethane on the palladium surface, because a similar increase of ethane formation was observed on this catalyst during hydrogenation of acetylene alone [37]. Results shown in **Figure 3.7** suggest that $S_{C_2H_6}$ increases on palladium during about the first 20 h of aging of the catalyst in the form of 2.3mm spheres, but then the amount of oligomers accumulated in the support pores exceeds the critical value and additional ethylene is hydrogenated owing to the internal diffusion limitation of acetylene.

Therefore, the accumulations of oligomers on the support may influence both hydrogen spillover and internal diffusion limitations of the acetylene. These two phenomena are manifested by similar changes of ethane selectivity during aging of

the catalyst, so they are difficult to distinguish. Their relative importance depends on the catalyst support and reaction conditions.

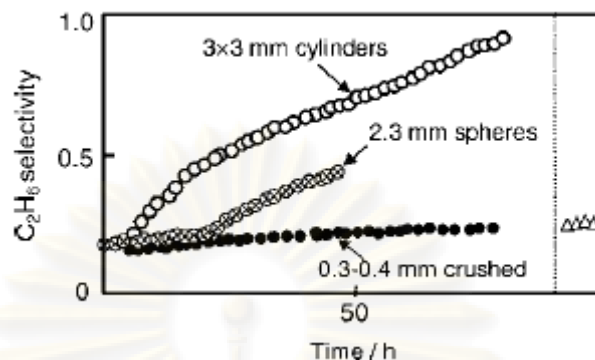


Figure 3.7 Ethane selectivity obtained during aging of 0.05% Pd/ α -Al₂O₃. Triangles show the performance of the deactivated 3.0mm pellets after crushing to less than 0.5 mm.

3.6 Pd in selective hydrogenation

High selectivity to ethylene is not a feature that is unique to palladium: other metals, especially nickel and copper [80], can also perform well; and it has recently been shown that gold also gives ethylene with total selectivity [81]. Other metals such as platinum and iridium show much lower mechanistic selectivities. Industrial usage employs only palladium, because its high selectivity is accompanied by very high activity, so that supported catalysts containing only very small amounts of palladium can be used. Palladium particles are able to add one hydrogen molecule to both alkenes and alkynes. To do so in the latter case, the surface-near region has to undergo strong modifications, in which a significant amount of carbon from hydrogenolysed feed molecules penetrates into the palladium surface, modifying its geometric as well as its electronic structure. In situ XPS experiments proved the presence of a surface Pd-C phase, as established previously [82]. Pd-C formation was found to be a general process in any selective alkyne hydrogenation reaction we studied, while it was always absent with alkene feed. Its role, in line with the hydrogenation model suggested by the Chemical Physics Department of FHI [83], is to inhibit the emergence of bulk-dissolved hydrogen to the surface, or even hinder its population. Bulk-dissolved/subsurface hydrogen was shown to be a very reactive but unselective species. To distinguish between the possible scenarios, an in situ cell for Prompt Gamma Activation Analysis was developed allowing the quantification of

dissolved hydrogen in situ. These experiments revealed that both scenarios were possible. The population of subsurface hydrogen is becoming probable above a certain H_2 /alkyne ratio, since the initial alkyne hydrogenolysis decreases, shifting the equilibrium of hydrogen vs. carbon penetration towards hydrogen diffusion. High-pressure XPS experiments have clearly shown the correlation between diminishing Pd-C and changing hydrogenation selectivity favoring alkane formation. As we have seen, by cutting down subsurface hydrogen population, total hydrogenation can be avoided. However, e.g. in the semi-hydrogenation of small amounts of acetylene in a large excess of ethylene, the reaction has to be prevented from running into the oligo- and polymerization path. Both requirements can be met by using different palladium intermetallic compounds, IMCs ($PdGa$, Pd_3Ga_7 , $Pd_{15}Cu_{85}$, $PdZn$), as suggested by the site isolation concept. Samples were prepared by melting the elements under argon atmosphere followed by further annealing in evacuated quartz glass ampoules. These compounds exhibit well-ordered crystal structures with Pd atoms solely coordinating to the second metal atoms in the first shell. Analysis of the chemical bonding by quantum chemical calculation of the electron localization function (ELF) reveals pronounced directed (covalent) bonding in $PdGa$ and Pd_3Ga_7 . The intermetallic compounds were characterized by FT-IR and in situ XPS, and the site isolation concept as well as the modified electronic state was validated by the experiments. (For further details, consult the corresponding poster abstract.) Catalytically the samples are active, despite the low specific surface area, long-term stable and possess superior selectivity, significantly higher than the industrially relevant alloy $Pd_{20}Ag_{80}$ or supported Pd catalysts. The site isolation on the surface of a hydrogenation catalyst results in three modifications of the active surface that account for the increased catalytic performance: (i) reduced number of different adsorption sites on structurally non-isolated active Pd atoms (“geometric effect”); (ii) reduced availability of hydrogen from the bulk (“kinetic effect”); and (iii) electronic modification of the active sites (“electronic effect”). By fine-tuning those properties, the rational synthesis of hydrogenation catalysts has now been made possible.

3.7 Catalysts

There is not just one universal catalyst suitable for the hydrogenation of acetylene. Different catalyst modifications are applied depending principally upon the

gas composition and operating conditions. For satisfactory performance, the catalyst should exhibit these characteristics [84]:

- 1) High activity sustained over long operating periods, high space velocity, and consequently a low-catalyst inventory.
- 2) High selectivity over a relatively wide temperature range to avoid losses of ethylene and to prevent polymer and carbon formation. These latter products result from temperature variations within the catalyst bed due to the exothermic nature of the reactions.

Many attempts have been made to develop catalysts of improved ethylene selectivity [85-88]. One approach is to prepare catalysts of high metal dispersions. Small Pd particles in highly dispersed catalysts allow few Pd planar sites, i.e. multiple adsorption sites, which results in suppression of the ethylidyne or ethylidene species. Small Pd particles also accommodate less amount of β -Pd hydride than large particles. Since, the β -Pd hydride is responsible for non-selective hydrogenation of acetylene, small Pd particles are beneficial to improved selectivity.

Another approach to improve the selectivity is to add a second metal to the catalyst, so that the added metal either forms an alloy with Pd or modify the Pd surface [89,90]. β -Pd hydride is suppressed on many Pd alloys. Additionally, proper dilution of the Pd surface with a second metal will inhibit formation of the multiple bound intermediates species, which is directly hydrogenated to ethane and C_2 polymerization. Polymerization to yield green oil will obviously be retarded when the Pd surface is geometrically blocked by promoter. A second metal sometimes modifies the Pd surface electronically, so that its adsorption strength for acetylene and ethylene is altered. Moreover, it was found that an increase in the Pd d-band electron density and reduction of absorption hydrogen spill over from the bulk of the metals to react with acetylene by the addition of promoters was responsible for the enhanced selectivity [91].

The role of the additives or selectivity promoters, improves the performance of the Pd catalysts, particularly in achieving a high selectivity for ethylene production. In the previous research, that has proposed the following geometric and electronic effect of promoters. Geometric modification is considered because the promoter atoms

located on the Pd surface decrease the amounts of the multiple Pd sites responsible for the selectivity deterioration. The promoter also modifies the Pd surface electronically to alter the adsorption strength between Pd and the adsorbates.

The analogy between the role of selectivity promoters of Pd catalysts in acetylene hydrogenation and the role of reducible oxide supports in the SMSI phenomenon, TiO_2 was selected as a candidate promoter because it has been observed the phenomenon of “the strong metal-support interaction” (SMSI). The performance of TiO_2 -modified Pd catalysts [92-94], in the selective hydrogenation of acetylene, showed a higher selectivity for ethylene production due to the following effect.

- The amounts of chemisorbed H_2 and CO were significantly reduced and, in particular, the adsorption of multiply coordinated CO species was suppressed because the Ti species added to the catalyst covers the Pd surface, thus blocking the multiply coordinated Pd sites, which characteristic of the well-known strong metal-support interaction (SMSI) phenomenon. To obtain additional evidence for the SMSI phenomenon on catalyst, the H/Pd ratio after oxidation, is nearly the same as the initial value prior to oxidation. The above reversible behavior of gas adsorption on catalyst after oxidation-reduction treatments is characteristic of the SMSI phenomenon [95-96]. The case in which the hydrogen coverage of the catalyst is low is similar to the case wherein a low H_2 /acetylene ratio is used in the reactant stream, which allows for the improved ethylene selectivity by reducing the rate of ethane formation. Lowering the hydrogen concentration on the catalyst usually increases the rate of green oil formation [97,98] because the hydrogen-deficient condition accelerates the C_2 polymerization step.
- A clear advantage of using TiO_2 as an additive instead of a support is that highly dispersed Pd catalysts can be obtained and is maintained even after reduction at high temperature.
- An electronic modification of Pd by TiO_2 has appeared the shift in metal binding energy, but this effect is influenced not only by the electronic interaction of the metal with other components but also by the size of metal crystallites.

- The TPD of ethylene from the catalyst showed the weakening in ethylene adsorption on the Pd surface and the decomposition of ethylene is suppressed because of the charge transfer from the Ti species to Pd.
- The polymerization of C₂ species leading to catalyst deactivation proceeds at slower rates because large ensembles of Pd are blocked by the Ti species, thus suppressing the formation of green oil. Moreover, small Pd crystallites are advantageous for the suppression of green oil because they have small fractions of the low index Pd surface, e.g., Pd(100), than on the high-index surface, e.g., Pd(111) [88].

The existence of well dispersed metallic phase in a matrix with a spinel-like structure can be crucial in the selective hydrogenation of acetylene. This is a non structure-sensitive reaction, but acetylene hydrogenolysis does, and takes place simultaneously to the hydrogenation reactions giving undesirable products, such as coke and methane. Thus, acetylene hydrogenation is in fact a reaction with an apparent structure sensitivity. Coke and methane are formed from ethylidene species and acetylene dissociatively adsorbed on three-atom arrangements at the catalyst surface [99-101]. Thus, coke and methane yields can be reduced by physical isolation of surface metallic nickel atoms, e.g., in a solid in which metallic nickel is finely dispersed in a stable ZnAl₂O₄ spinel-like phase [102]. These hydrogenation catalysts can be successfully modified by the addition of other components such as Co, to improve the ethylene selectivity [103], or Cr, lowering the coke formation.

Along this line, the role of added Zn on Ni-Al-Cr oxide catalysts with a spinel-like structure hinders coke formation. An increase of Ni leads to the decrease of activity to gaseous products (ethane, ethylene, methane). While the initial formation of coke increases along with the larger of initial catalyst deactivation, thus the initial conversion decreased as the Ni/Zn ratio increased. Because it can be seen the size of the Ni crystallites increases with increasing the Ni content. The large Ni particles are weakly interacted with the support and behave as 'strong' active sites where a higher rate of coke formation is related to a larger metal particle size, and that Zn plays a geometrical role, 'diluting' the Ni particles (i.e., leading to a larger dispersion) and thus decreasing coke formation, without decreasing the activity in the

main reaction. However, an increase in coke concentration increases activity and selectivity to ethylene, especially in those samples with not too high Ni contents. When, as the reaction proceeds, amorphous coke is formed as layers on the so-called 'weak' sites. These sites interact strongly with the support and the crystallite size is markedly smaller, ethylidene is formed as a monolayer on their surface, and acetylene is hydrogenated to ethylene [36]. Because of the presence of Zn as a spinel-like structure, the Ni crystallites are 'diluted' or digged in the support, thus increasing the Ni-support interaction and exposing a lower area to the gaseous phase. As mentioned above, methane is formed on the 'strong' metal sites. Ethane can be formed either by direct hydrogenation of acetylene, or by hydrogenation of ethylene [102], while hydrogenation of acetylene to ethylene takes place on the 'weak' sites, where a monolayer of ethylidene is formed. Direct hydrogenation of acetylene to ethane takes place on the 'strong' sites, where methane is also formed; as the strong sites become deactivated by spinel-like structure or coke deposition, the yield to methane decreases, and that to ethane increases. When the activity of the strong sites approximates to zero, ethane production reaches a maximum, then decreasing due to formation of ethylidene on the 'weak' sites (the only active sites under these conditions), thus favouring formation of ethene instead of ethane. As a result, the coke concentration increases, selectivity to ethylene increases, but as the Ni/Zn ratio (i.e., the strong/weak sites ratio) increases, the ethane/ethene ratio also does [22].

One can see an excellent agreement that acetylene over Ni-Si-Al mixed oxides has shown the existence of two different types of sites. Firstly, the hydrogenolytic (naked) metallic centers, corresponding to nickel without (or little) interaction with the support, are responsible for a large part of the coke and are active for side-reactions. Secondly, the hydrogenating sites correspond to nickel interacted with the support and are active for the main reaction. The formation of coke favors the ethylene selectivity for the small (<16 nm) particles because of the deactivation of hydrogenolytic sites which is mainly related to the metal in strong interaction with the support and the geometric effects of dilution due to the presence of unreduced surface-Ni species [104-107].

The Al_2O_3 used as Pd catalyst support in this reaction contains mostly the α -phase Al_2O_3 since it possesses relatively low specific surface area and low acidity compared to other 'transition' alumina (such as β -, γ -, η -, χ -, κ -, δ -, θ -phase Al_2O_3). With respect to selectivity changes, catalysts with low dispersion were suggested to give better selectivity toward ethylene [108-109]. Modification of nanocrystalline α - Al_2O_3 with zinc is studied because it can form ZnAl_2O_4 spinel which is an interesting material with low acidity that can exhibit the strong metal-support interaction (SMSI) with noble metal [110-112]. Pd catalysts on the nanocrystalline Zn-modified α - Al_2O_3 also showed less deactivation by coke formation. Based on the mechanisms in the literature [113], acetylene hydrogenation was suggested to take place on the active sites on Pd surface while most of the carbonaceous deposits were found to be accumulated on the support. The carbon deposits acted as a hydrogen bridge for the hydrogen spillover from Pd to the support facilitating ethylene hydrogenation to ethane. Modification of Pd/ α - Al_2O_3 catalysts with Zn considerably reduced coke deposition thus ethylene selectivity was improved. Moreover, the proper palladium particle size leads to the enhancement of catalytic activity because many researchers have shown that the specific activity of Pd decreased by an order of magnitude when the size of palladium particle were very small (1-5 nm) [114-116].

Formation of NiAl_2O_4 spinel during the preparation of Ni-modified Al_2O_3 resulted in a decreased acidity of α - Al_2O_3 . A decrease of alumina acidity, however, was less pronounced due probably to for the presence of NiO. As a consequence, the catalysts exhibited high ethylene selectivities at high acetylene conversions and lower amounts of coke deposited. Formation of NiAl_2O_4 in Ni-based hydrogenation catalysts has also shown high resistance to deactivation by coke formation [117-119].

The plasma technology provides several varieties for surface treatment. The surface of supported palladium catalyst was undertaken the actions of high-energy atoms, electrons and ions during the plasma treatment. It resulted in a decreasing of the decomposition temperature and also that of reduction, the oligomers (green oil) formation and coke-forming reactions were suppressed, and then the dispersion of active Pd component could be improved. The enhanced selectivity was related to that the chemisorption of ethylene was much weaker on plasma treated sample, and the

adsorbed ethylene could be replaced by acetylene molecule more easily. Thus, the treatment by the glow discharge plasma, as a new kind of surface modification technique, could change effectively the interaction between metal and support, obtaining new active materials with higher reaction performances [120-122].

The other techniques for surface modification is found that the pretreatment with oxygen and/or oxygencontaining compounds result in the formation of Ag_2O , which will expose the accessible Pd sites to react with C_2H_2 and H_2 in the feed stream, thereby enhancing the catalytic activity of Pd-Ag/ Al_2O_3 catalysts. In addition, the different behaviors of the pretreatment with O_2 , NO_x and CO_x are examined. NO_x -treated catalysts give higher ethylene gains because the numbers of sites for direct ethane formation is lessened, whereas the opposite behaviors are revealed for O_2 -treated or CO_x -treated catalysts [23].

Although most of the selective acetylene hydrogenation studies to date have involved Pd-based systems, other catalysts have also been considered. A well-dispersed Au catalysts show extremely high selectivity for ethylene formation, and also depends on the size of ultrafine gold particles [123]. For Au-Pd/ TiO_2 catalysts prepared by a redox method showed improvement of catalyst [124], there is interaction between Pd and Au, therefore the catalyst behaves essentially as a bimetallic Au-Pd catalyst. Presence of Au decreased the carbon coverage and improved the ethene selectivity. Decoration of Pd by Au and the morphology of particles explain the ethene selectivity improvement.

A novel composite material based on carbon nanofibers (CNF) grown on sintered metal fibers ($\text{SMF}_{\text{Inconel}}$) filter was investigated for its favorable properties as catalytic support. The TOF was one order of magnitude higher for $\text{Pd}^0/\text{CNF}/\text{SMF}_{\text{Inconel}}$ catalysts as compared with Pd supported on activated carbon fibers (Pd^0/ACF). This effect was attributed to a strong metal-support interaction of Pd^0 -nanoparticles with the graphitized CNF. Graphitic nature inherent to the CNF enhances the palladium activity for hydrogenation as compared to the amorphous form of activated carbon (ACF). Electron transfer between the conductive CNF support and the palladium particles, inducing electronic perturbations of the metal could explain this activity increase [125,126]. The reaction was found to be structure sensitive leading to a

decrease of TOF for the Pd⁰-particles <3 nm. As claimed by several works in the field [127], the relationship between the Pd particles size and their electronic properties affects the Pd catalytic behavior. Small particles, being electron deficient [128], adsorb more strongly electron-rich substrates, like alkynes, lowering the turnover frequency. For bigger particles, their electronic properties approach those of bulk metal, and therefore the metal–substrate interaction decreases, leading to a higher reactivity of adsorbed alkyne. Another explanation involves a change in the ratio between the different types of surface atoms [7]. As the Pd particle size decreases, the fraction of Pd surface atoms with a low coordination number (edge atoms) increase, and this modifies the catalytic properties of the metal. The catalysts based on CNF/SMF_{Inconel} support presented a much higher selectivity when the CNF surface was activated by H₂O₂. Since this treatment modifies the acidity of the support due to the formation of O-containing surface groups, the adsorption strength of acetylene as compared to ethylene may be enhanced favoring acetylene hydrogenation. This leads to higher selectivity to ethylene. This result is in line with the results for the ACF support. The ACF was shown to possess a high amount of acid surface groups. Therefore, Pd/ACF catalysts showed a rather high selectivity.

The removal of trace acetylene from ethylene is performed industrially by palladium hydrogenation catalysts (often modified with silver) that avoid the hydrogenation of ethylene to ethane [129]. In an effort to identify catalysts based on less expensive and more available metals, density functional calculations were performed that identified relations in heats of adsorption of hydrocarbon molecules and fragments on metal surfaces. This analysis not only verified the facility of known catalysts but identified nickel-zinc alloys as alternatives. Experimental studies demonstrated that these alloys dispersed on an oxide support were selective for acetylene hydrogenation at low pressures.

3.8 Catalyst deactivation

The causes of deactivation are basically of three kinds: chemical, mechanical, and thermal. The five intrinsic mechanisms of catalyst decay, (1) poisoning, (2) fouling, (3) thermal degradation, (4) chemical degradation, and (5) mechanical failure, vary in their reversibility and rates of occurrence (Bartholomew, 2003). Poisoning and thermal degradation are generally slow, irreversible processes while fouling with coke

and carbon is generally rapid and reversible by regeneration with O_2 or H_2 . Catalyst deactivation is more easily prevented than cured. Poisoning by impurities can be prevented through careful purification of reactants. Carbon deposition and coking can be prevented by minimizing the formation of carbon or coke precursors through gasification, by careful design of catalysts and process conditions and by controlling reaction conditions to minimize effects of carbon and coke formation on activity. Sintering is best avoided by minimizing and controlling the temperature of reaction.

Poisons reduce the activity of palladium catalysts in two major ways: first, by hindering or blocking the access of the reactants to palladium sites, and second, by changing the electronic properties of the palladium such that the adsorption strength of the reactant on the palladium is greatly reduced. Sulfur compounds represent the first class of poisons. Compounds like hydrogen sulfide (H_2S) or carbonyl sulfide (COS) adsorb strongly on the palladium. In this manner, these poisons block the acetylene from the reaction sites.

Poisons like the sp metals, such as arsenic and mercury, form “alloys” with the palladium. Electron transfer between the sp metals and the palladium drastically reduces the associated adsorption strength of acetylene. Since the reaction rate of acetylene is directly proportional to the rate of adsorption, which in turn depends exponentially on the heat of adsorption, a small reduction in the adsorption strength will translate to a significant drop in catalyst activity. Although to a limited extent, silver behaves like a sp metal, however, its impact on palladium is less drastic in comparison to arsenic or mercury. Palladium catalysts with a silver promoter are not as active as catalysts containing only palladium. The beneficial effect of the silver is its modification of the relative adsorption strength of acetylene and ethylene on the palladium. The result is a catalyst with a small reduction in activity but an improvement in selectivity.

The poisons can be categorized among three types as defined below:

- (a) Inhibitor – those poisons whose effects subside when the concentration of the species diminishes.
- (b) Temporary – those poisons whose effects subside only after the catalyst undergoes proper steam/air regeneration.

- (c) Permanent – those poisons whose effects cannot be alleviated, even after the catalyst undergoes proper steam/air regeneration.

Table 3.2 contains a list and classification of poisons that are commonly present in feeds to acetylene converters [130].

Classification	Type of poison	Examples
Inhibitor	oxides MA/PD amines/nitrogen sulfides	CO, O ₂ , H ₂ O $CH_3C \equiv CH$, $H_2C = C = CH_2$ NH ₃ , NH ₂ R COS, H ₂ S, MeSH
Temporary	phosphines carbon oligomers (green oil) chlorides	PH ₃ , PH ₂ R Precursors: BD, acetylene Cl ⁻
Permanent	mercury arsenic heavy metals main group metals	Hg AsH ₃ Fe, Mn, Pb, Ti Na, Ca, Mg

3.9 Industrial acetylene hydrogenation

3.9.1 Acetylene hydrogenation reaction

The basic requirements for acetylene hydrogenation units include the following:

- Safe operation; e.g., it shouldn't occur the exothermic runaway reactions or "hot spots" during operation.
- Maintain acetylene in ethylene product below specification. The typical maximum is 5 ppm; however, ethylene customers may expect the acetylene level to be maintained below 1 ppm; perhaps, below 0.5 ppm.
- Do not be the cause of interruptions to continuous operation of the ethylene plant; e.g., a target for continuous operation may be over 5 years.
- Operating with a net gain of ethylene; the higher, the better.
- "Low investment cost" within the context of the overall cost considerations for ethylene plant investment, project execution, feedstocks, energy, etc.
- Good catalyst life and reasonable catalyst cost.

3.9.2 Acetylene removal technology

Treatment of the C₂-stream can take various routes, depending on the acetylene content and whether or not high-purity acetylene is to be recovered. There are

basically two main paths, to extract the acetylene from the C₂-stream and recover it as a product, or to convert the acetylene into useful product which is ethylene. Each paths involved different unit operations and it affects the overall process sequences.

3.9.2.1 Acetylene recovery through solvent extraction

Acetylene recovery facilities can be located between the deethanizer and the ethylene-ethane fractionator or downstream of the latter. The typical acetylene recovery process makes use of three towers, the first to absorb acetylene in a suitable solvent, the second to reject and return co-absorbed ethylene and ethane from the solution, and the third to desorb acetylene [131]. Acetone, dimethylformamide (DMF), methanol and n-methyl pyrrolidone are the preferred solvents [132]. Certain C₃-hydrocarbons in the deethanizer overhead have solubilities in these solvents comparable to the solubility of acetylene and therefore have to be completely removed from the feed. Location of acetylene recovery facilities downstream of the main ethylene-ethane fractionators eliminates this problem but involves high concentrations of acetylene in this tower, resulting in partial pressure that, however, remain well below established safety limits. Acetylene recovery systems in both locations are presently in operation with a better overall safety record than acetylene hydrogenation systems have had.

3.9.2.2 Acetylene hydrogenation system

The acetylene hydrogenation reactor is typically a fixed bed catalytic reactor, normally operated adiabatically. There are also isothermal tubular reactors operated commercially. There are three major reactor configurations, i.e. the cracked gas train, the back-end and the front-end reactor. **Table 3.3** shows the typical feed compositions as the function of reactor location [92,130]. Basically, acetylenes (inclusive of acetylene and methyl acetylene) in a naphtha cracker is higher than an ethane cracker.

จุฬาลงกรณ์มหาวิทยาลัย

Table 3.3 Typical acetylene concentration in the feed gas and conversion rate [133].

	Feedstock	Concentration (vol %)			Conversion Rate (%)		
		C ₂ H ₂	C ₃ H ₄	C ₄ H ₆	C ₂ H ₂	C ₃ H ₄	C ₄ H ₆
Back-end Hydrogenation	Naphtha	1.3	-	-	100	-	-
Front-end Hydrogenation (deethanizer)	Naphtha	0.61	-	-	100	-	-
Front-end Hydrogenation (depropanizer)	Naphtha	0.53	0.067	-	100	> 60	-
Raw Gas Hydrogenation	Ethane/ propane	0.3	0.13	0.85	100	> 60	> 90

- *Raw gas catalytic hydrogenation reactors*

In raw gas catalytic hydrogenation, the effluent of the cracked gas compressor, after minimal treatment, enters the acetylene converters for catalytic hydrogenation of the acetylene contained in the feed. Although the use of nickel catalysts has endured in this type of application, a progression to the use of the higher selective palladium technologies is occurring. In raw gas applications where the reactors precede the caustic tower, effective utilization of palladium catalyst is not possible without process modification. The feed in this case contains copious amounts of sulfur, which necessitate the use of supported, nickel-based catalysts. It has been suggested cobalt molybdate and Ni-Co-Cr catalysts to be used and steam to be added to improve the selectivity and inhibit the fouling of the catalyst [40].

- *Commercial front-end and tail-end processes*

There are two basic methods of selective hydrogenation of acetylene in ethylene-rich streams, the so-called front-end (**Figure 3.8**) and tail-end (**Figure 3.9**) processes [134].

ศูนย์วิทยทรัพยากร
จุฬาลงกรณ์มหาวิทยาลัย

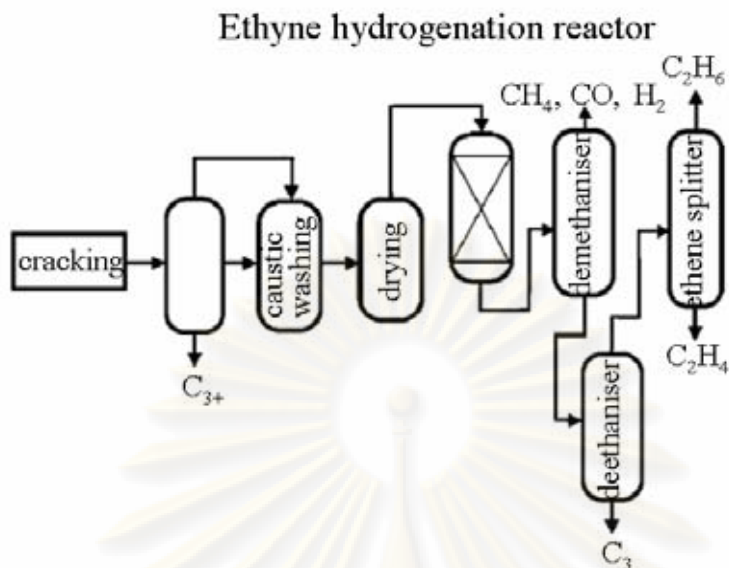


Figure 3.8 Location of front-end acetylene hydrogenation reactors in a simplified scheme of downstream treatment of steam cracker effluents.

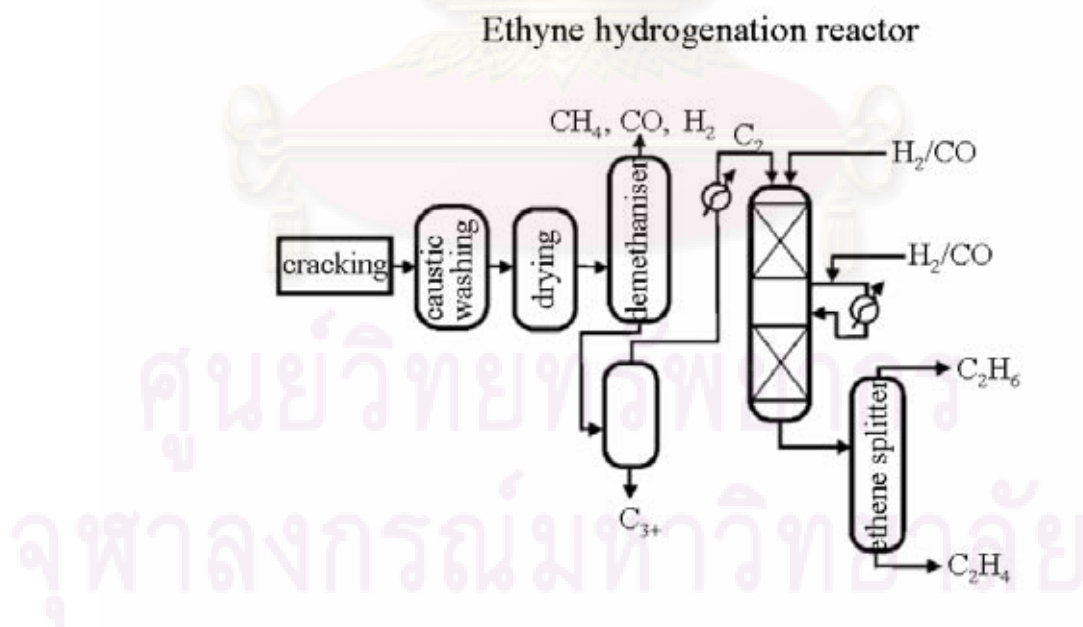


Figure 3.9 Location of tail- and acetylene-hydrogenation reactors in a simplified scheme of downstream treatment of steam cracker effluents.

The methods differ in the location of the acetylene hydrogenation reactors [97,98,135-138]. In the tail-end method the reactors for acetylene hydrogenation are located after the demethanizer units, so the inlet hydrogenation stream mainly consists of C₂ hydrocarbons. Stoichiometric amounts of hydrogen with respect to acetylene are added to this C₂-rich stream to ensure an optimal concentration of hydrogen in the reactor feed (1%-4% by volume). In some cases small amounts of carbon monoxide are also separately added to the inlet stream. In the front-end method the reactors for acetylene hydrogenation precede the demethanizer in the process. Consequently, the reactor feed contains typically 10-35 mol% of hydrogen, together with C₂ and lighter hydrocarbons. The comparison of the typical reactor feed compositions and the operating conditions for front-end and tail-end processes are shown in **Table 3.4**.

Table 3.4 Typical feed composition to acetylene hydrogenation reactors and the operating conditions for front-end and tail-end processes.

	Front-end mole %	Tail-end mole %
Hydrogen (mole %)	22	2.4
Ethyne (mole %)	0.2	2
Ethene (mole %)	37	71
Methane (mole %)	12	—
Ethane (mole %)	28.4	25
Propene (mole %)	0.12	—
Carbon monoxide (ppm by vol.)	2800	40
H ₂ /C ₂ H ₂ (inlet mol ratio)	110	1.5
Pressure (bar)	35	20
Temperature (K)	343	333
Space velocity (m ³ m _{cat} ⁻³ h ⁻¹)	2000	3000

3.10 Regeneration techniques

Regeneration of deactivated catalysts is possible for many catalytic processes and is widely practiced. The main purpose is to remove the temporary poisons on the catalyst surface and restore the free adsorption sites. Generally regeneration can be categorized into two, i.e. the off-site and the on-site regeneration. In the off-site (ex-situ) regeneration, the catalyst is to be unloaded from the reactor and regeneration is performed in moving-bed belt calciners or conical-shaped rotating drum calciners [139].

The on-site (in-situ) regeneration does not require removing the catalyst from reactor. The most common procedure is to burn off, or oxygenate, the temporary poisons, such as green oil, in order to resume the catalyst activity. Regeneration of the catalyst may be accomplished by heating the catalyst in air at a temperature lower than 500 °C, to burn off any organic material, polymers or char. Huang, et al. (1994) invented an improved method for regenerating acetylene hydrogenation catalysts which does not require an oxygenation step. The hydrogen stripping involves feeding a mixture of 5-10 % hydrogen and the balance nitrogen to the spent catalyst at 350°C and 50 psig. This is much less time consuming than oxygenation, since the whole procedure takes between 16-24 hours. The only disadvantage to hydrogen stripping is that the catalyst deactivates more quickly so that the procedure must be performed more often.

3.11 Current and future developments

Research and development in the partial catalytic acetylene hydrogenation are mainly to improve the acetylene removal efficiency and lower the ethylene losses. Past research is basically focused on optimizing the acetylene reactor operating temperature and pressure, changing reactor configuration and location, optimizing H₂ to acetylene ratio, changing catalyst formulation, etc. In this paper, we will discuss the revamp on the catalyst shape and the research in membrane catalytic reactor.

3.11.1 CDS (computer designed shape) catalyst

The catalyst manufacturers are competing in the catalyst design and manufacturing technologies. Besides changing the formulation and the palladium impregnating techniques, the catalyst manufacturer also look into possibilities of improving catalyst performance by varying the size and shape of the catalyst. The Süd-Chemie, Inc or known as Nissan Girdler Catalyst Co. Ltd. had came out a technology called CDS (computer designed shape). **Figure 3.10** shows some of these CDS catalyst.

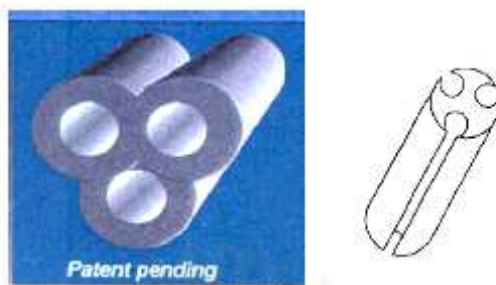


Figure 3.10 Computer designed shape (CDS).

Some features claims by inventor are listed below (Lai: 2000; Süd-Chemie product catalogue):

1. Shape avoids catalyst interlocking, thus maintaining the high geometric surface area and void volume.
2. High void volume results in low pressure drop, thus higher space velocity.
3. Pd is skin impregnated and since there is high geometric surface area, the Pd is better dispersed, resulting in high activity and excellent poison resistance.

Till dates, there isn't been much technical papers discussing the performance of the CDS catalyst. Further warranted from laboratory tests and exact operating precedent are needed to confirm the CDS catalyst performance.

3.11.2 Catalytic membrane reactor

A membrane reactor may be either a supported ceramic layer on a porous support or an ultra-thin solid noble metal. Some metal membrane studies include Pd, Pd/Ni, Pd/Ru and Pd/Ag (Vincent and Gonzalez, 2002). Studies found that the permeate hydrogen was very active and that ethylene was the main product. However, the membrane must be very thin in order to provide the appropriate selectivity. Porous ceramic membranes can support highly dispersed metals on an inorganic oxide to combine the properties of higher permeability with thermal stability, which are absent in the dense metal membranes. A novel approach to the selective hydrogenation of acetylene involves a short contact time reactor is suggested by Vincent and Gonzalez (2002). The experiment by forcing a dilute $C_2H_2/H_2/Ar$ mixture through a thin Pd/ γ -

Al_2O_3 catalytic membrane (about 5 mm thick) produced high conversions coupled with high selectivity at high temperatures. Membrane reactors achieve efficiencies by combining in one unit of reactor that generates a product with a semi-permeable membrane that extracts it. Studies have been done on methanol reforming [140], photocatalytic oxidation of volatile organic carbon [141], Direct synthesis of Hydrogen Peroxide [142] and others catalytic reactions. Membrane reactors fundamentally change the pressure dependence of conversion in gas phase decomposition reactions so that the reactions are preferentially performed at high pressures rather than low. Higher pressures allow much smaller reactors and more efficient purification. Membrane reactors can be advantageous also for sequential endothermic and exothermic reactions, by using the product extraction to promote heat transfer. The net result is smaller reactors, improved heat transfer, lower capital costs, and often fewer side-reactions.



ศูนย์วิทยทรัพยากร
จุฬาลงกรณ์มหาวิทยาลัย

CHAPTER IV

EXPERIMENTAL

This chapter discussed the preparation methodology of the mixed phases Al_2O_3 including an expanded discussion about the effect of $\alpha\text{-Al}_2\text{O}_3$ micron-sized and nanocrystalline $\alpha\text{-Al}_2\text{O}_3$. The properties of nanocrystalline $\alpha\text{-Al}_2\text{O}_3$ from the three different methods, namely, solvothermal, sol-gel, and precipitation are later discussed. The catalyst characterization and the catalytic reaction are also explained. The chemicals, apparatus and procedures for catalyst preparation are explained in **section 4.1**. Details of catalyst evaluation to study catalytic activity and selectivity are given in **section 4.2**. Finally, the composition, structure and surface properties of the synthesized catalysts characterized by various techniques are discussed in **section 4.3**.

4.1 Catalysts preparation

Since this research focuses on the mixed phases Al_2O_3 , the $\alpha\text{-Al}_2\text{O}_3$ micron-sized and nanocrystalline $\alpha\text{-Al}_2\text{O}_3$, and the nanocrystalline $\alpha\text{-Al}_2\text{O}_3$ from the three different methods for supported Pd; therefore, the details of preparation procedures are important to understand. The Pd catalyst is chosen as commercial alkynes hydrogenation because of minimize the formation of surface oligomers, resulting from the conjugation of adsorbed acetylene molecules, and to avoid the undesirable hydrogenation of alkenes.

4.1.1 Material

The support and metal precursors used for the catalyst preparation are listed in **Table 4.1**.

Table 4.1 Details of chemical reagents used for the catalyst preparation.

Chemical	Formula	Manufacturer
1. Gamma alumina	$\gamma\text{-Al}_2\text{O}_3$	JRC Co., Ltd., Japan
2. Alpha alumina	$\alpha\text{-Al}_2\text{O}_3$	Sigma-Aldrich Chemical Co., Ltd., U.S.A.
3. Aluminum isopropoxide (98%+)	$((\text{CH}_3)_2\text{CHO})_3\text{Al}$	Sigma-Aldrich Chemical Co., Ltd., U.S.A.
4. Aluminium nitrate (98%)	$\text{Al}(\text{NO}_3)_3 \cdot 9\text{H}_2\text{O}$	Sigma-Aldrich Chemical Co., Ltd., U.S.A.
5. Ammonium aluminum sulfate (99%+)	$\text{NH}_4\text{Al}(\text{SO}_4)_2 \cdot 12\text{H}_2\text{O}$	Merck Co., Ltd., Germany
6. Ammonium hydrogencarbonate (98%)	NH_4HCO_3	Unilab
7. Toluene (95.5%)	$\text{C}_6\text{H}_5\text{CH}_3$	Carlo Erba Reagenti, Italy
8. Acetone (99.5%)	$\text{C}_3\text{H}_6\text{O}$	Merck Co., Ltd., Germany
9. Methanol (99.9%)	CH_3OH	Merck Co., Ltd., Germany
10. Ethanol (99.9%)	$\text{CH}_3\text{CH}_2\text{OH}$	Mallinckrodt Baker Co., Ltd.,
11. Urea (99.5%)	$(\text{NH}_2)_2\text{CO}$	Univar, Australia
12. Palladium nitrate	$\text{Pd}(\text{NO}_3)_2$	Wako Pure Chemical Industries Co., Ltd., Japan

4.1.2 Preparation procedures

4.1.2.1 Mixed phases Al_2O_3 and $\alpha\text{-Al}_2\text{O}_3$

The mixed phases with various phase compositions were prepared by calcination of the $\gamma\text{-Al}_2\text{O}_3$ at 1100°C for 120, 200, or 240 min. The $\alpha\text{-Al}_2\text{O}_3$ was obtained by calcination of the $\gamma\text{-Al}_2\text{O}_3$ at 1175°C for 120 min. In this research, the alumina samples consisting of 0, 14, 47, 64, and 100% alpha phase are referred to as Al- α 0, Al- α 14, Al- α 47, Al- α 64, and Al- α 100, respectively. The percentage of alpha

phase was calculated using a calibration curve from XRD results of the physically mixed γ -, and α - Al_2O_3 (**APPENDIX B**).

4.1.2.2 Nanocrystalline α - Al_2O_3 via solvothermal method

An appropriate amount of aluminum isopropoxide (AIP, 25g) was suspended in 100 ml of toluene within a test tube, which was placed in an autoclave and then added with 30 ml of toluene in the gap between the test tube and the autoclave wall. The autoclave was completely purged by nitrogen before heating up to 300°C at a rate of 2.5°C/min, and kept at that temperature for 2 h. After cooling to room temperature, the resulting product was collected after repeated washing with methanol or acetone by centrifugation and air-dried overnight. The obtainable powder was put into a box furnace and heated to 1150°C with a rate of 10°C/min and kept at 1150°C for 1 h. Finally, white powder of α - Al_2O_3 was obtained. For Zn modified alumina, Zinc (II) acetylacetonate was added by suspending in test tube before the reaction tool place, for the calculation of Zn-modified according to a procedure in **APPENDIX H**.

For some experiments, a different drying was applied as follows. After the reaction, the valve of the autoclave was slightly opened to release the organic solvent from the autoclave by flash evaporation while keeping at the reaction temperature. The valve was opened until the pressure inside the autoclave was decreased to atmospheric level. Dry products were obtained directly after the process was cooled down without the step of washing by methanol and centrifugation. The obtained products were calcined in the box furnace in the same manner as described in upper.

4.1.2.3 Nanocrystalline α - Al_2O_3 via sol-gel method

A mixture of aluminium nitrate nonahydrate and ethanol used as starting solution was prepared by dissolving 24g of aluminium nitrate in 50 ml of ethanol at room temperature. The experiment was conducted in the reflux-condenser reactor at the temperature about 70-80°C for 18 h. Then urea solution which consists of urea (60g) and distilled water (50 ml) was added to adjust pH of solution. The mixture was rested at the same temperature for 24 h to be gelled at neutral condition. After that it was calcined with 2 steps of heating rate to avoid overflowing of gel during calcination, i.e. 3°C/min from room temperature to 500°C and continue heating at

5°C/min to 1150°C. Temperature was hold for 3 h. For Zn modified alumina, Zinc (II) nitrate hexahydrate was added to the starting solution of aluminium precursor, for the calculation of Zn-modified according to a procedure in **APPENDIX H**.

4.1.2.4 Nanocrystalline α -Al₂O₃ via precipitation method

Ammonium aluminium sulfate solution was gradually added to ammonium hydrogen carbonate aqueous solution with concentration ratio of 0.2:2.0 mol/l (**APPENDIX G**). The experiment was controlled at the temperature in range of 40-45°C, 450 rpm for mixing speed, 3 ml/min for addition rate, and constant pH value at 9. The mixture was aged for 15 minutes to permit growth of crystal. White precipitate formed was separated from the final solution by centrifugation, repeatedly washed with methanol and dry in the oven at 110°C overnight. The obtainable powder was calcined in depleted-oxygen atmosphere in a box furnace at 1175°C for 4 h with rate 10°C/min for the obtained α -Al₂O₃ [143]. For Zn modified alumina, Zinc (II) nitrate hexahydrate used as Zn source was added into AAS solution which before dropping into AHC solution, for the calculation of Zn-modified according to a procedure in **APPENDIX H**.

4.1.2.5 Pd/Al₂O₃ catalysts

The 0.3%Pd/ α -Al₂O₃, 0.5%Pd/ α -Al₂O₃, and 1%Pd/ α -Al₂O₃ catalysts were prepared by an incipient wetness impregnation using Pd(NO₃)₂·x(H₂O) as the Pd precursor and de-ionized water as a solvent (**APPENDIX A**). The alumina support (2 g) was placed in an Erlenmeyer flask then the impregnating solution from the palladium solution was gradually dripped into the support. Shaking the flask continuously during impregnation was required to ensure the homogeneous distribution of metal component on the support. After impregnation, the catalysts were stand at room temperature for 6 h, dried at 110°C in an oven overnight, the catalyst was further calcined in N₂ flow 60 cm³/min with a rate of 10°C/min until the temperature reached 500°C and then switched to air flow 100 cm³/min at 500°C for 2 h.

4.2 Catalyst evaluation

The catalytic performance for the selective hydrogenation of acetylene was measured at different GHSV and temperature in order to cover the industrial window operation [144,145]. Materials, apparatus and operating procedures are detailed as below:

4.2.1 Materials

The reaction was carried out using a feed composition of 1.5% C₂H₂, 1.7% H₂, and balanced C₂H₄. Ultra high purity hydrogen and high purity argon were used for reduction and cooling processes. All of the gases were supplied by Thai Industrial Gas Limited (TIG).

4.2.2 Apparatus

The catalytic test was performed in a flow system as shown diagrammatically in **Figure 4.1**. The apparatus consisted of a pyrex tubular reactor, an electrical furnace and an automation temperature controller. The instruments used in this system are listed and explained as follows:

4.2.2.1 Reactor

The reaction was performed in a conventional pyrex tubular reactor (inside diameter = 10.1 mm), at atmospheric pressure.

4.2.2.2 Automation temperature controller

This unit consisted of a magnetic switch connected to a variable transformer and a thermal overload relay (HITACHI, TR1 2B-1E, AC 600 V) linked to a temperature controller (Shinks, ECS, 220-R/E) in which connected to a thermocouple attached to the catalyst bed in a reactor. A dial setting established a set point at any temperature within the range between 0 and 999°C. The accuracy was of $\pm 2^\circ\text{C}$.

4.2.2.3 Electrical furnace

The furnace supplied the required temperature to the reactor which could be operated from room temperature up to 500°C at maximum voltage of 220 volts.

4.2.2.4 Gas controlling system

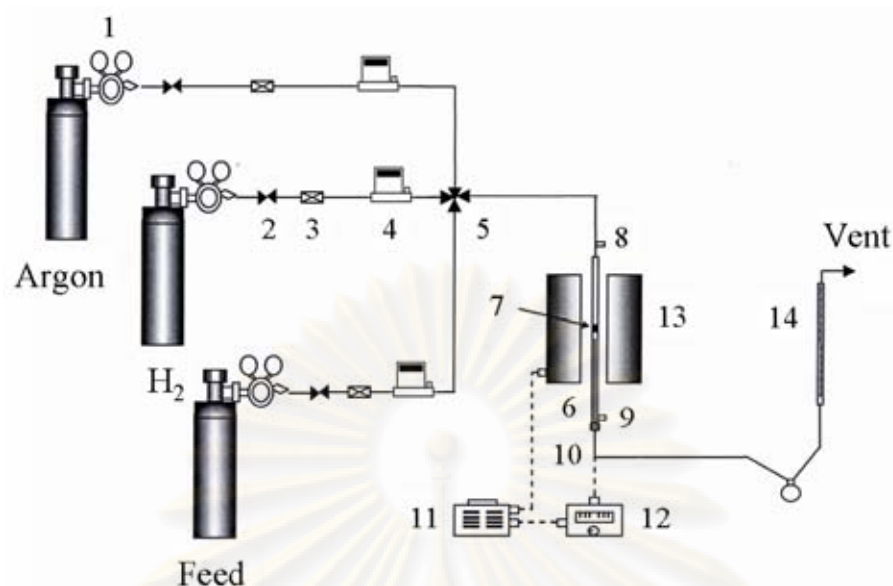
Reactant, hydrogen and carrier gas for the system was each equipped with a pressure regulator and on-off valve and the gas flow rates were adjusted by using mass flow controller (AALBORG, GFC).

4.2.2.5 Gas chromatograph

The products and feeds were analyzed by a gas chromatograph equipped with a FID detector (SHIMADZU FID GC 8APF, carbosieve column S-II) for separating CH₄, C₂H₂, C₂H₄ and C₂H₆. H₂ was analyzed by a gas chromatograph equipped with a TCD detector (SHIMADZU TCD GC 8APT, molecular sieve 5A). The operating conditions for each instrument are summarized in **Table 4.2**.

Table 4.2 Operating conditions of gas chromatographs.

Gas chromatograph	SHIMADZU GC-8APF	SHIMADZU GC-8APT
Carrier gas	Ultrahigh purity N ₂	Ultrahigh purity Ar
Carrier gas flow rate (ml/min)	40-60	40-60
Injector temperature (°C)	180	80
Initial column temperature (°C)	100	50
Programmed rate (°C/min)	10	-
Final column temperature (°C)	160	50
Current (mA)	-	70



- | | |
|-------------------------|----------------------------------|
| 1. Pressure regulator | 8. Sampling point (feed) |
| 2. On-off valve | 9. Sampling point (product) |
| 3. Filter | 10. Thermocouple |
| 4. Mass flow controller | 11. Variable voltage transformer |
| 5. 4-ways fitting | 12. Temperature controller |
| 6. Reactor | 13. Electric furnace |
| 7. Catalyst bed | 14. Bubble flow meter |

Figure 4.1 Flow diagram of the selective hydrogenation of acetylene.

4.2.3 Procedures

The catalyst was packed in a pyrex tubular downflow reactor by setting up catalyst bed length was about 1.5 mm. The reactor was placed into the furnace and argon was introduced into the reactor in order to remove remaining air. Prior to the start of each experimental run, the catalyst was reduced *in situ* with 100 ml/min hydrogen by heating from room temperature to 150°C at a heating rate of 10°C/min and held at that temperature for 2 h. Then the reactor was purged with argon and cooled down to the reaction temperature 40°C, sampling was taken every 1 h.

The reaction was carried out using a feed composition of 1.5% C₂H₂, 1.7% H₂, and balanced C₂H₄ with a vary GHSV of 52580, 32577, 22534, 12385, 9366, 6660, and 4282 h⁻¹ (for calculation according to **APPENDIX J**). In addition to various temperatures such as 40, 60, and 80°C were used to test the catalytic performance. At

each condition, sampling was undertaken when the steady state of the system was reached, which was approximately within 1 h. The products and feeds were analyzed by a two gas chromatographs equipped with a FID detector (SHIMADZU FID GC 9A, carbosieve column S-2) and TCD detector (SHIMADZU TCD GC 8A, molecular sieve-5A). Details of the calculation of the catalyst activity to convert acetylene and the selectivity towards ethylene in term of ethylene gain are given in **APPENDIX B and D**.

4.3 Catalyst characterization

Various characterization techniques were used in this study in order to clarify the catalyst structure, the morphology and the surface composition. The effect of mixed phases Al_2O_3 , the $\alpha\text{-Al}_2\text{O}_3$ micron-sized and nanocrystalline $\alpha\text{-Al}_2\text{O}_3$, and the nanocrystalline $\alpha\text{-Al}_2\text{O}_3$ from the three different methods, on the behavior of Pd catalysts was characterized by using the following techniques.

4.3.1 Bulk structure and morphology of the catalyst

4.3.1.1 Specific surface area measurement

The BET surface areas of the Al_2O_3 supports were measured by N_2 physisorption, with nitrogen as the adsorbate using a Micromeritics model ASAP 2000 automated system degassing at 200°C for 1 h prior to N_2 physisorption. Calculations were performed on the basis of the BET (Stephen Brunauer-Paul Hugh Emmett-Edward Teller) isotherm for specific surface area and pore size distribution was calculated by BJH (Barrett-Joyner-Halenda) desorption branch analysis. Specific pore volume was determined from the single point adsorption total pore volume of pores at relative pressure (P/P_0) ~ 0.99 and the average pore diameter was calculated from BJH desorption branch. It can see the physisorption theory in **APPENDIX F**

4.3.1.2 X-ray diffraction (XRD) analysis

The crystallinity, structure and composition of the Al_2O_3 supports and Pd/ Al_2O_3 catalysts showed by X-ray diffraction (XRD) pattern were carried out using *ex situ* employing an X-ray diffractometer, SIEMENS XRD D5000, with Cu K_α radiation with a Ni filter in the 2θ range of 20-80 degrees resolution 0.04° .

4.3.1.3 Particle size by TEM

The distribution of palladium on Al₂O₃ supports were observed using JEOL Model JEM-2010 transmission electron microscope operated at 200 keV at the National Metal and Materials Technology Center (MTEC). The sample powder was dispersed in absolute ethanol and sonicated for about 15 minutes before dropping on a copper grid (with Formvar film) or a carbon grid.

4.3.1.4 Electron spin resonance spectroscopy (ESR)

ESR will be performed to determine the defect of surface Al₂O₃ support by JEOL JAPAN. The ESR was carried out by using model JES-RE2X at the Scientific and Technological Research Equipment Center, Chulalongkorn University (STREC).

4.3.2 Surface analysis

4.3.2.1 Metal active site measurement

The amounts of CO chemisorbed on the Pd/Al₂O₃ catalysts were measured at room temperature by using a Micromeritic Chemisorb 2750 automated system attached with ChemiSoft TPx software. Approximately 0.1 g of catalyst was placed in a sample cell. Prior the measurement, 30 ml/min of He gas was introduced into the sample cell in order to remove the remaining air. The system was switched to 50 ml/min of hydrogen and heated to 150°C with a heating rate of 10°C/min. The temperature was kept constant for 2 h and then cooled down to the room temperature. Carbon monoxide was pulsed over the reduced catalyst until the TCD signal became constant. Palladium dispersion was estimated from the amount of CO chemisorbed assuming a stoichiometry of CO/Pd = 1 [146]. For the **Section 5.3**, the chemisorption mean stoichiometry of Pd metal to CO molecule ($X_{\text{Pd-CO}}$) was determined according to the iterative method [147]. In brief, the starting value of 0.5 was used for $X_{\text{Pd-CO}}$ and a first value of Pd dispersion was calculated from the CO monolayer uptake. Joyal and Butt [148] determined $X_{\text{Pd-CO}}$ as a function of dispersion in Pd/SiO₂ catalysts, which based on the obtained data, a polynomial function was fitted (**APPENDIX B**). Using this fitted function, a new value of $X_{\text{Pd-CO}}$ was determined corresponding to the precedent obtained dispersion value; this new value of $X_{\text{Pd-CO}}$ was used to calculate a new value of dispersion. The iterative cycle was repeated until convergence. Using

this iterative method, the values of $X_{\text{Pd-CO}}$ were determined to be 0.51, 0.34, and 0.29 for Pd supported on solvothermal-, sol-gel and precipitation-made $\alpha\text{-Al}_2\text{O}_3$ catalyst, respectively; these values were used to determine the Pd active sites and Pd dispersion of the three catalysts. Calculation details of Pd active sites and %Pd dispersion are given in **APPENDIX E**.

4.3.2.2 Surface analysis by X-ray photoelectron spectroscopy (XPS)

The XPS analysis was performed using an AMICUS photoelectron spectrometer equipped with an Mg K_α X-ray as primary excitation and KRATOS VISION2 software. XPS elemental spectra were acquired with 0.1 eV energy step at a pass energy of 75 kV. The C 1s line was taken as an internal standard at 285.0 eV.

4.3.2.3 Temperature programmed experiments

Temperature program experiments were carried out in a Micromeritic Chemisorb 2750 automated system. The temperature ramping was controlled by temperature controller, Furnace Power 48 VAC 8A MAX.

A mixture of 10% H_2 in Ar with a flow rate of 15 cm^3/min was used in TPR experiment. Prior the experiment, the sample was treated in N_2 flow at 200°C for 1 h in order to remove any adsorbed gas. The TPR was performed with a constant heating rate of 10°C/min from 35 to 200°C. For ethylene-TPD experiments, the samples were pre-reduced at 150°C in H_2 for 2 h (flow rate 50 cm^3/min) and cooled down to room temperature. Then adsorption of ethylene was performed at room temperature for 3 h. The temperature-programmed desorption was performed with a constant heating rate of 10°C/min from 35 to 800°C. The amount of desorbed ethylene was measured by analyzing the effluent gas with a thermal conductivity detector.

For CO-TPD experiment, the sample was pre-reduced at 150°C in H_2 for 2 h (flow rate 50 cm^3/min) and following cooled down to room temperature. Then CO adsorption was performed at room temperature by continuous injection until disappear of CO adsorption. The temperature-programmed desorption was applied with a constant rate of 10°C/min from 35 to 800°C. The amount of desorbed CO was measured by analyzing the effluent gas with a thermal conductivity detector.

Temperature programmed desorption of ammonia (NH₃-TPD) was performed with 0.1 g of supports which placed in a quartz tube. The sample was heated from room temperature to 200°C under helium flow rate at 15 ml/min with a heating rate of 10°C/min and hold for 1 hour. Then, the sample was cooled down to 40°C, 15 vol% ammonium in helium gas with flow rate at 15 ml/min flowed through sample and hold for 1 h. Consequently, helium gas at the same flow flowed through sample and also holds for 1 h. In the last step, sample was heated from 40°C to 780°C with a heating rate of 10°C/min.

For temperature program oxidation (TPO) experiments were carried out in the spent catalysts, sending a 1 vol% O₂ in helium flow (30 cm³/min) onto 0.05 g of sample, and heating up to 760°C (10°C/min). Prior experiment, the spent catalyst was pre-treated in He (30 cm³/min) at 200°C for 1 h.

The thermogravimetric analyzer-differential scanning calorimeter (TGA-DSC) analysis was performed with an SDT Q600 instrument from TA Instruments, USA. The sample powder of about 5-10 mg was put in a 90 µl Al₂O₃ cup and heated to 1300°C with a heating rate of 5°C/min, under oxygen flowing at 100 ml/min. The derivative thermogravimetric analysis (DTG) data was calculated using the % weight data, derivative to temperature (°C).

ศูนย์วิจัยทรัพยากร
จุฬาลงกรณ์มหาวิทยาลัย

CHAPTER V

RESULTS AND DISCUSSION

This chapter presents the results with a discussion to clarify effects of the mixed phases Al_2O_3 , the $\alpha\text{-Al}_2\text{O}_3$ micron-sized, and the nanocrystalline $\alpha\text{-Al}_2\text{O}_3$ on the reactivity behavior of $\text{Pd}/\text{Al}_2\text{O}_3$ catalysts for the selective hydrogenation of acetylene. In order to accommodate the detailed consideration, this is categorized into 3 sections as follow: **Section 5.1** describes mixed phases Al_2O_3 , **Section 5.2** describes micron-sized and nanocrystalline $\alpha\text{-Al}_2\text{O}_3$, **Section 5.3** describes nanocrystalline $\alpha\text{-Al}_2\text{O}_3$ via various preparations, **Section 5.4** describes effect of coke formation during reaction, and **Section 5.5** describes modification of Al_2O_3 support with Zn.

5.1 Mixed-phases Al_2O_3 support

The mixed phases Al_2O_3 supports used for preparation of the $\text{Pd}/\text{Al}_2\text{O}_3$ catalysts in this study were obtained by varying the calcination conditions of the $\gamma\text{-Al}_2\text{O}_3$ (calcination temperature 1100-1175°C and holding time 2-4 h). The XRD patterns of Al_2O_3 are shown in **Figure 5.1**. The weight (%) of α -phase in these samples were calculated to be 0, 14, 47, 64 and 100% using a calibration from XRD results of the physically mixed γ -, and $\alpha\text{-Al}_2\text{O}_3$ (**APPENDIX B**) and were designated herein as Al- α 0, Al- α 14, Al- α 47, Al- α 64, and Al- α 100, respectively.

ศูนย์วิทยทรัพยากร
จุฬาลงกรณ์มหาวิทยาลัย

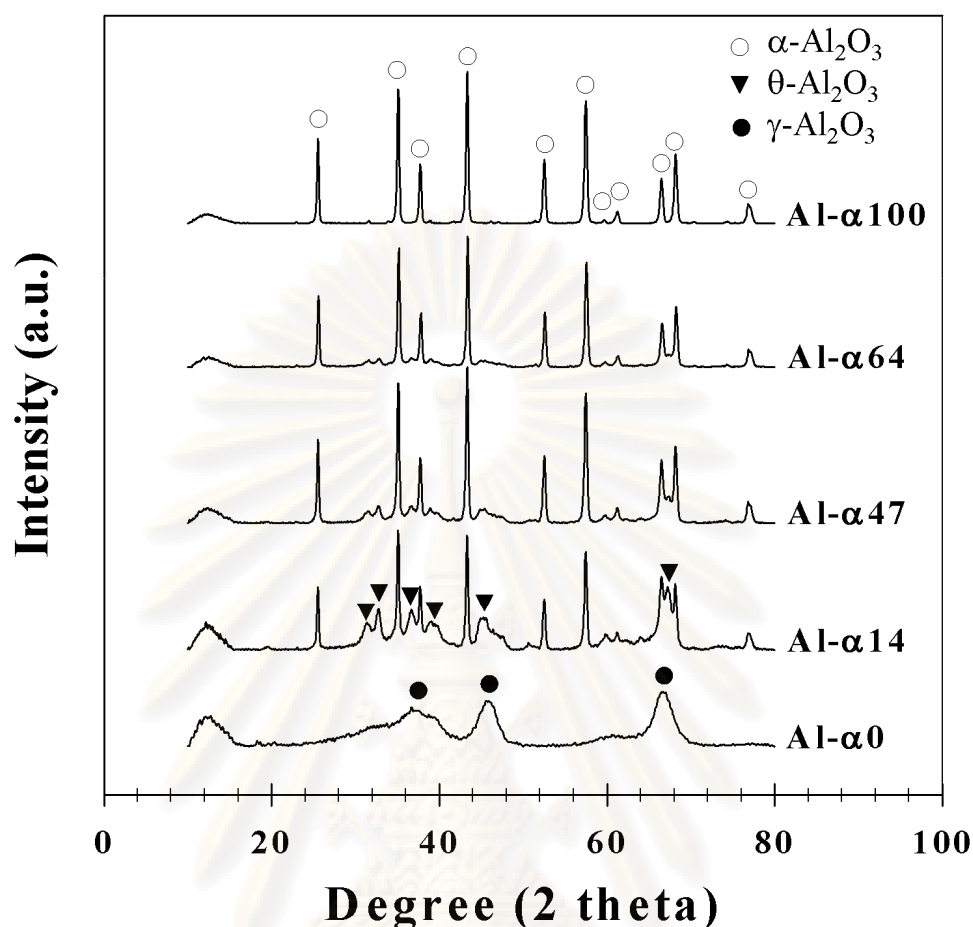


Figure 5.1 The XRD patterns of the Al₂O₃ supports containing various % of α-phase.

Table 5.1 summarized physical properties of the various Al₂O₃ supports. The crystallite size of transition-phase was increased from 3.7 nm to 28.3 nm (**APPENDIX C**) as the weight (%) of α-phase content increased from 0 to 64%, while the crystal size of α-phase remained constant at around 45 nm. The specific surface area and total pore volume calculated from BJH method decreased from 244 to 12 m²/g and 0.66 to 0.03 cm³/g with increasing amount of α-phase alumina. A drastically decrease in BET surface area and total pore volume of alumina during phase transformation can be explained by the rapidly increase of alumina crystal size. It is generally known that calcination of γ-Al₂O₃ at high temperature results in phase transformation from γ- to θ- and then α-Al₂O₃.

Table 5.1 The physical properties of alumina with various phase compositions.

Samples	α -Phase (%)	BET Surface Area (m ² /g)	Crystallite Size (nm) ^a		Pore Volume ^b (cm ³ /g)	Average Pore Diameter ^b (Å)
			γ -phase	α -phase		
Al- α 100	100	12.3	n.d.	44.5	0.03	90.1
Al- α 64	64	36.1	28.3	45.8	0.14	129.6
Al- α 47	47	45.4	17.8	48.9	0.20	151.9
Al- α 14	14	67.3	11.8	46.0	0.30	143.8
Al- α 0	0	244.1	3.7	n.d.	0.66	78.9

^a Calculated from XRD results

^b Based on BJH method

n.d. = not determined

The XRD characteristic peaks of all the Pd/Al₂O₃ catalysts were not different from the Al₂O₃ supports after Pd loading. No XRD peaks for PdO or Pd⁰ metal were observed due probably to the low loading of palladium (results not shown).

The BJH pore size distribution curves of the Al₂O₃ supports are also given in **Figure 5.2**. The commercial γ -Al₂O₃ (Al- α 0) gave two types of pore structures; (1) a narrow pore size distribution in the range of 2-10 nm and (2) a broad pore size distribution in the range of 10-100 nm. After calcination at high temperature, the first type of pore size distribution decreased and became distinct after complete transformation to α -Al₂O₃ (Al- α 100). The crystallite size of commercial γ -Al₂O₃ calculated from XRD was around 3.7 nm. This value was smaller than the average pore diameter (7 nm). It is indicated that the pore structure of γ -Al₂O₃ does not present in the crystal but it formed between the crystal of γ -Al₂O₃. By increasing the calcination temperature, the crystal of γ -Al₂O₃ was growth and some was transformed to α -phase which gave the larger particles. By increasing of crystal size, the pore between small particles was collapsed and shifted to the larger size.

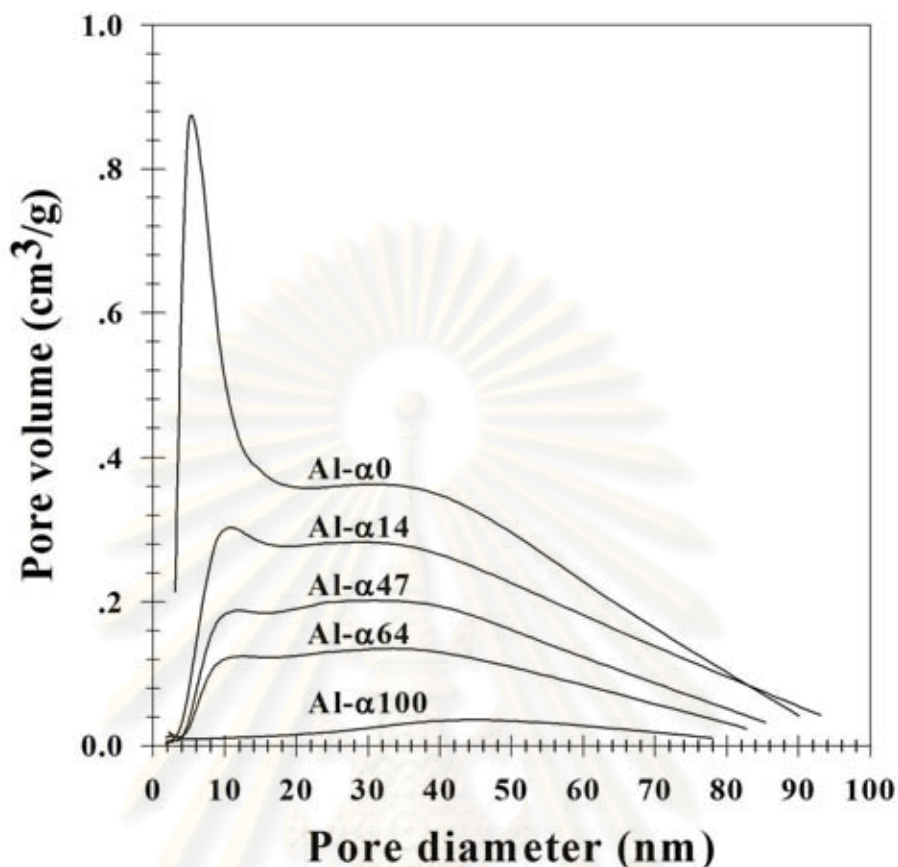


Figure 5.2 The BJH pore size distribution curves of the Al_2O_3 supports.

Figure 5.3 shows ESR spectra of the various Al_2O_3 supports. No spin resonance was observed for $\gamma\text{-Al}_2\text{O}_3$ sample suggesting that there was no other metal contamination in our supports [149]. After treated the Al_2O_3 supports at high temperature, the resonances assigned to α -phase was evidenced by signal at $g'=13$ and 5.2 [150]. The amplitudes of these resonances increased as the α -phase contents increased. Plot between relative amplitudes of resonance at $g'=13$ and α -phase concentration is presented in **Figure 5.4**. The experimental data are fitted well by the linear plot. This result was in good agreement with the weight (%) of α -phase calculated from the calibration of XRD pattern.

จุฬาลงกรณ์มหาวิทยาลัย

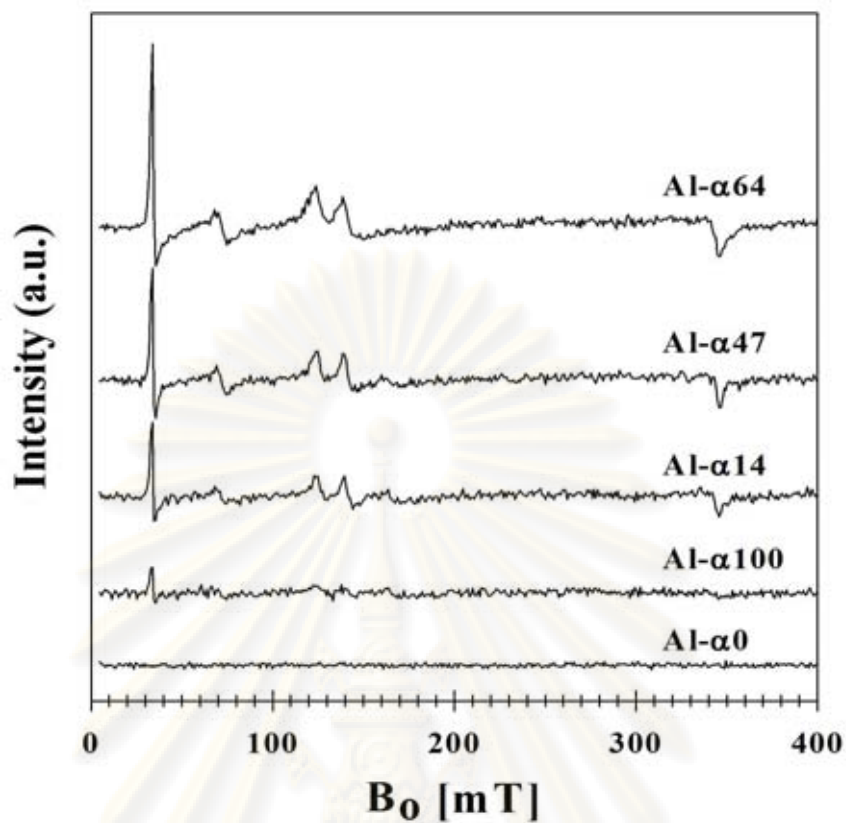


Figure 5.3 ESR spectra of the Al_2O_3 supports.

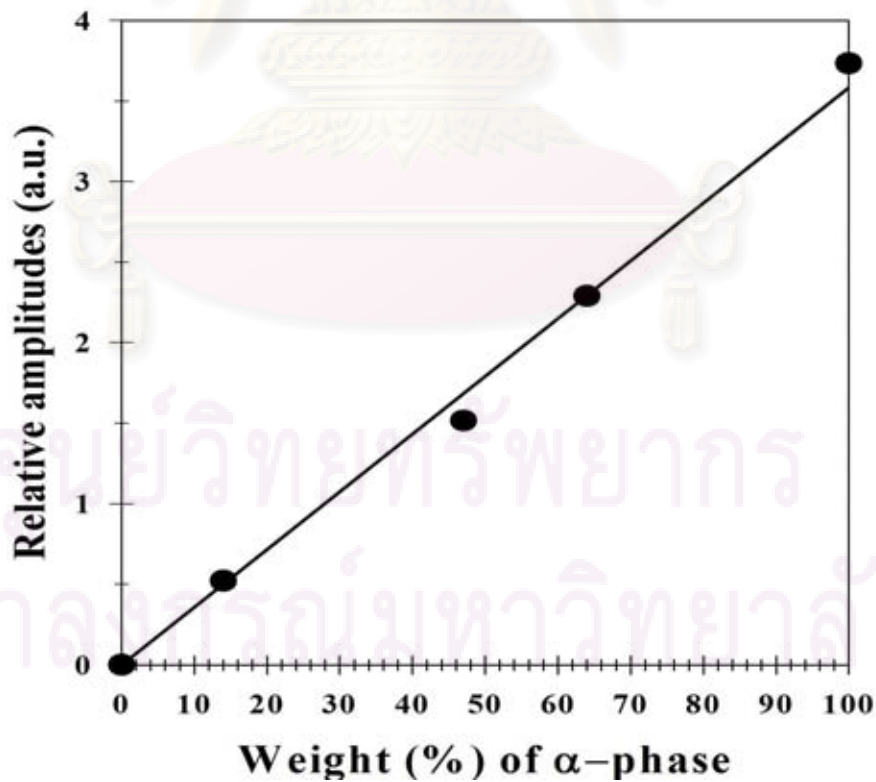


Figure 5.4 A plot between relative amplitudes of resonance at $g=13$ and α -phase concentration.

Figure 5.5 shows the TG/DTA curve for the γ - Al_2O_3 . Three stages of weight loss occurred at three temperature regions, namely, below 300°C , around 300 to 900°C , and from 900 to 1100°C . In the first and the second stage, a weight loss about 14% was observed corresponding with the presence of two endothermic peaks on DTA curve around 180 and around 400 to 800°C . This loss was probably due to the removal of physisorbed water and chemisorbed hydroxyl groups. In the third stage, a small weight loss of about 2% was due to phase transformation of alumina. The loss was probably related to transformation of the last phase and removal of water during formation of the α -phase. The smaller exothermic features observed at temperature above 800°C corresponds to the formation of better crystallized phases of alumina. This was attributed to the phase transformation from γ -, to θ - Al_2O_3 . While the last exothermic at around 1230°C would be attributed to the α -phase transformation. All phase transformation steps were confirmed by the XRD pattern of Al_2O_3 samples calcined at various temperatures.

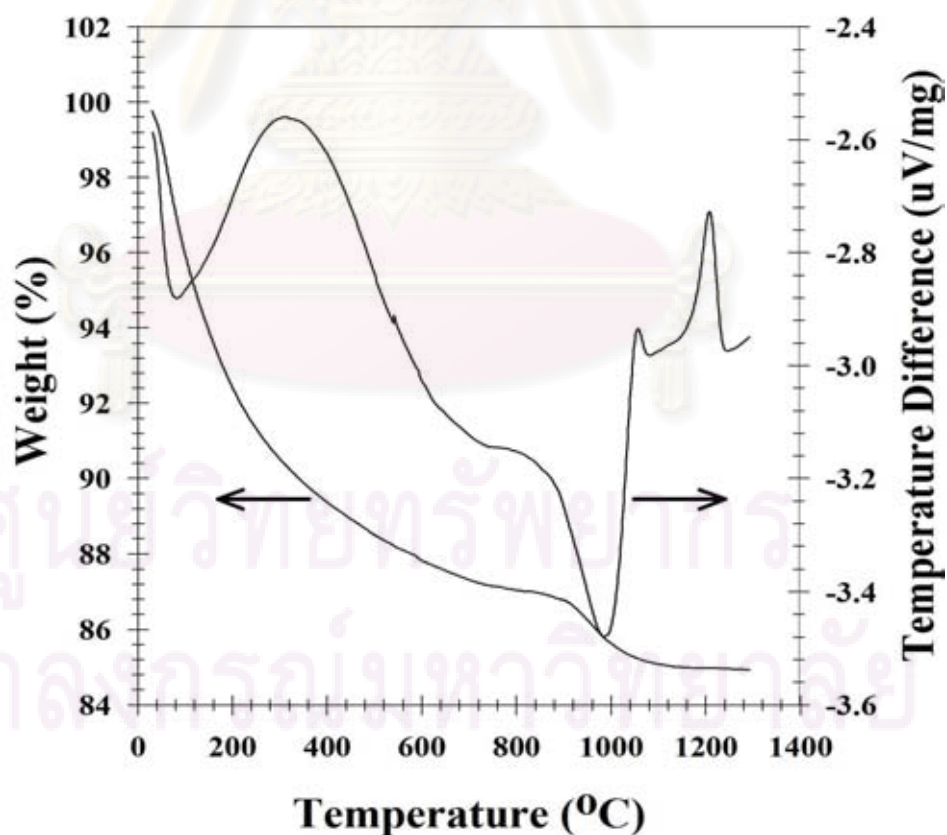


Figure 5.5 TG/DTA curve for the γ - Al_2O_3 .

The CO chemisorption results such as the number of active Pd atoms, Pd dispersion (%), and average Pd metal particle size are summarized in **Table 5.2 (APPENDIX E)**. Palladium dispersion was estimated from the amount of CO chemisorbed assuming a stoichiometry of CO/Pd = 1 [146]. The number of Pd active sites decreased from 35.1 to 7.4×10^{18} sites/g-catalyst corresponding to an decrease in Pd dispersion (%) from 59.5 to 12.5 and an increase in Pd metal particle size from 1.9 to 8.9 nm as the weight (%) of α -phase contents increased from 0 to 100%.

Table 5.2 Physiochemical properties of Pd supported on alumina with various phase compositions.

Samples	Pd Active Sites ^a ($\times 10^{18}$ CO molecule/g-cat)	%Pd Dispersion ^b	d_p^c (Pd ⁰) (nm)	Pd 3d _{5/2} ^d		Atomic Concentration ^d Pd/Al
				B.E. (eV)	FWHM	
Pd/Al- α 100	7.4	12.5	8.9	336.9	1.8	0.034
Pd/Al- α 64	11.0	18.5	6.1	336.9	2.0	0.027
Pd/Al- α 47	25.4	42.9	2.6	336.4	2.4	0.020
Pd/Al- α 14	31.7	53.5	2.1	336.4	2.3	0.011
Pd/Al- α 0	35.1	59.2	1.9	336.4	2.2	0.001

^a Pd active sites = $(V_{ads}/V_g) \times (6.02 \times 10^{23}) \times S_f$, error of measurement = $\pm 5\%$

^b %Pd dispersion = $[\text{Pd active sites} \times (\text{M.W.}/\%M) \times 100\% \times 100\%]/(6.02 \times 10^{23})$

^c Based on $d_p = 1.12/D$ (nm), where $D = \%Pd$ dispersion [151]

^d Based on XPS results

where V_{ads} = volume adsorbed
 V_g = molar volume of gas at STP
 S_f = stoichiometry factor, CO on Pd
M.W.= molecular weight of the metal
%M = %metal loading

In order to verify the Pd particle size, TEM micrographs have been acquired and are shown in **Figure 5.6**. The Pd supported on pure γ -Al₂O₃ consisted of particles with primarily spherical shape with some needlelike structure. The particle shape appeared more uniformly spheroidal for those supported on mixed phases Al₂O₃. Large fingerlike shape particles were observed for the catalysts containing 100% α -

phase Al_2O_3 . Increasing α -phase content of the alumina supports from 0 to 100% resulted in an increase of Pd cluster/particle size from about 2 to 10 nm.

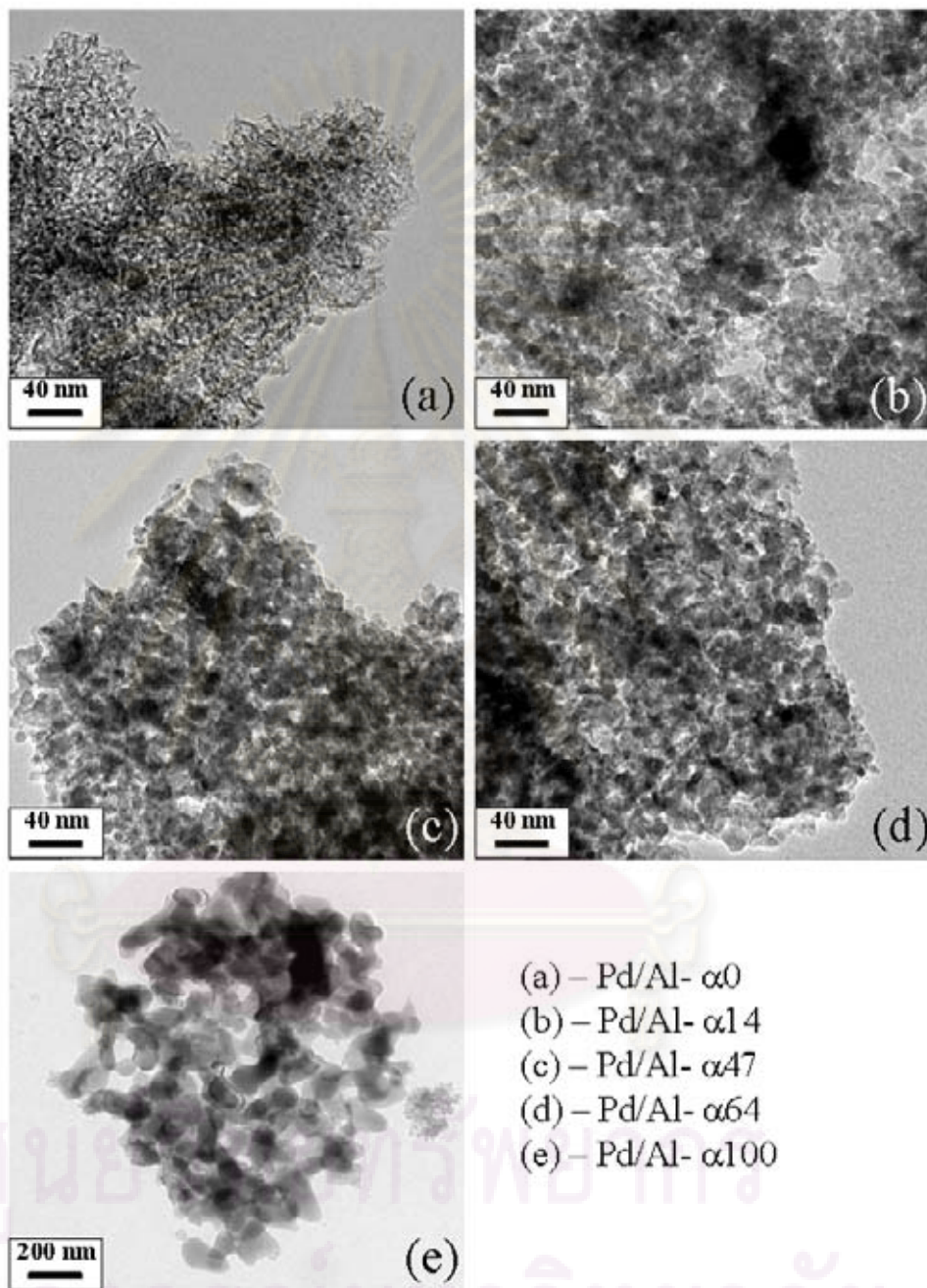


Figure 5.6 Transmission electron micrographs of the Pd/ Al_2O_3 catalyst.

XPS is used to determine the surface compositions of the catalysts and the interaction between Pd and the Al_2O_3 supports. The deconvoluted XPS photoelectron spectra for the Pd 3d core level region of all the catalysts are shown in **Figure 5.7**.

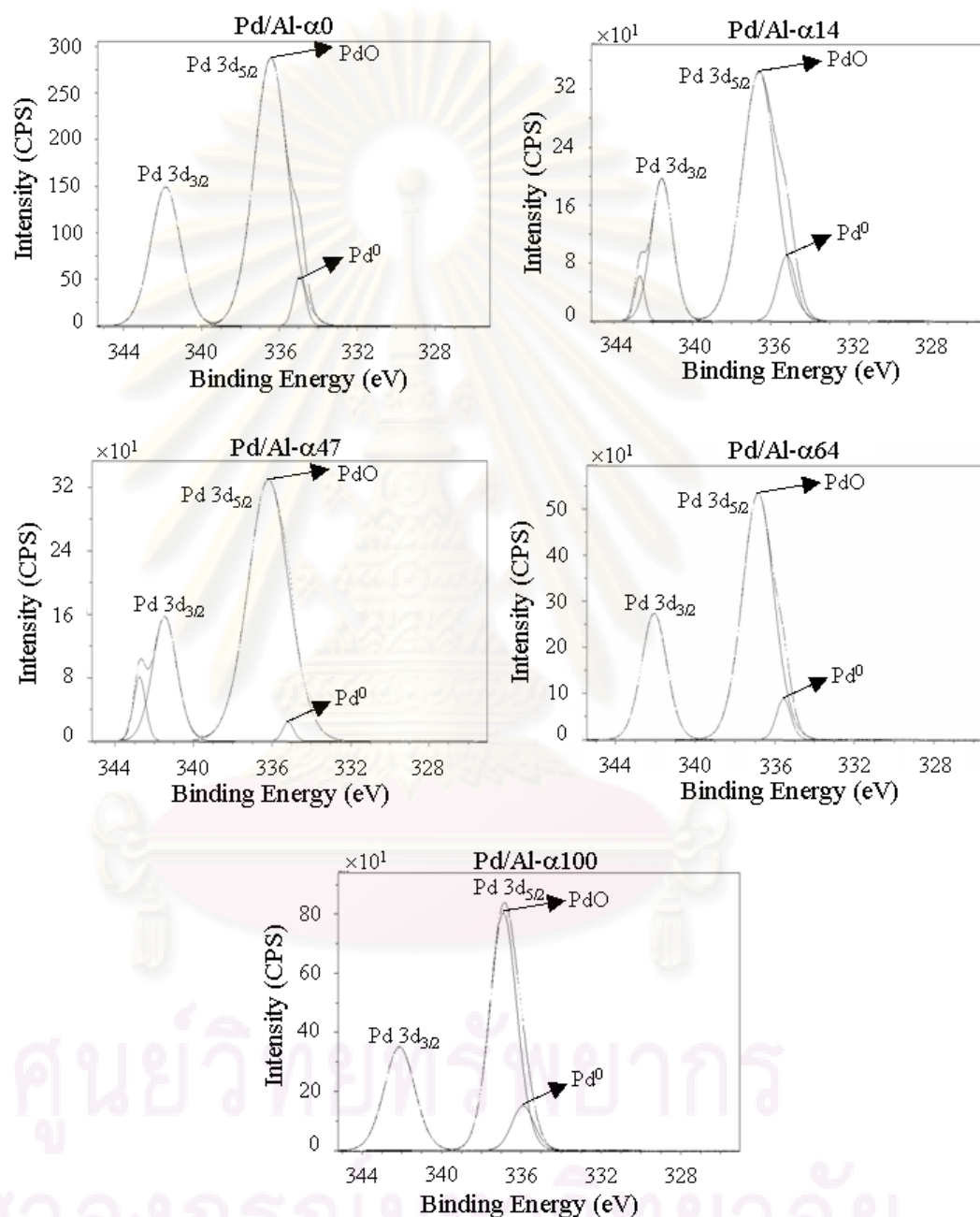


Figure 5.7 The XPS patterns of the Pd/Al₂O₃ catalyst.

From the figure, the Pd doublet was clearly evident. A small shoulder at the binding energy around 335.1-335.8 eV was present in every samples and was attributed to metallic Pd⁰ [152]. Such results indicated that partial reduction occurred during analysis. PdO species was observed at the binding energies in the range of 336.9-336.4 eV which was consistent to the values reported in the literature [153-154]. The percentages of atomic concentration, the binding energy, and FWHM of Pd 3d are also given in **Table 5.2**. The atomic concentration ratios for Pd/Al decreased with the decrease in α -phase Al₂O₃ contents. The results were consistent with the CO chemisorption results that larger Pd particle sizes were obtained on α -Al₂O₃. The FWHM values larger than 2 for Pd 3d_{5/2} may be due to some differential charging that contributed to the widening of the palladium peaks [155-156]. The Pd/Al ratio per BET surface area was calculated to equally compare the contents of Pd species on catalyst surface, the results are shown in **Figure 5.8**. These values decreased from 2.8×10^{-3} to 4.3×10^{-6} as the weight (%) of α -phase contents increased from 0 to 100%.

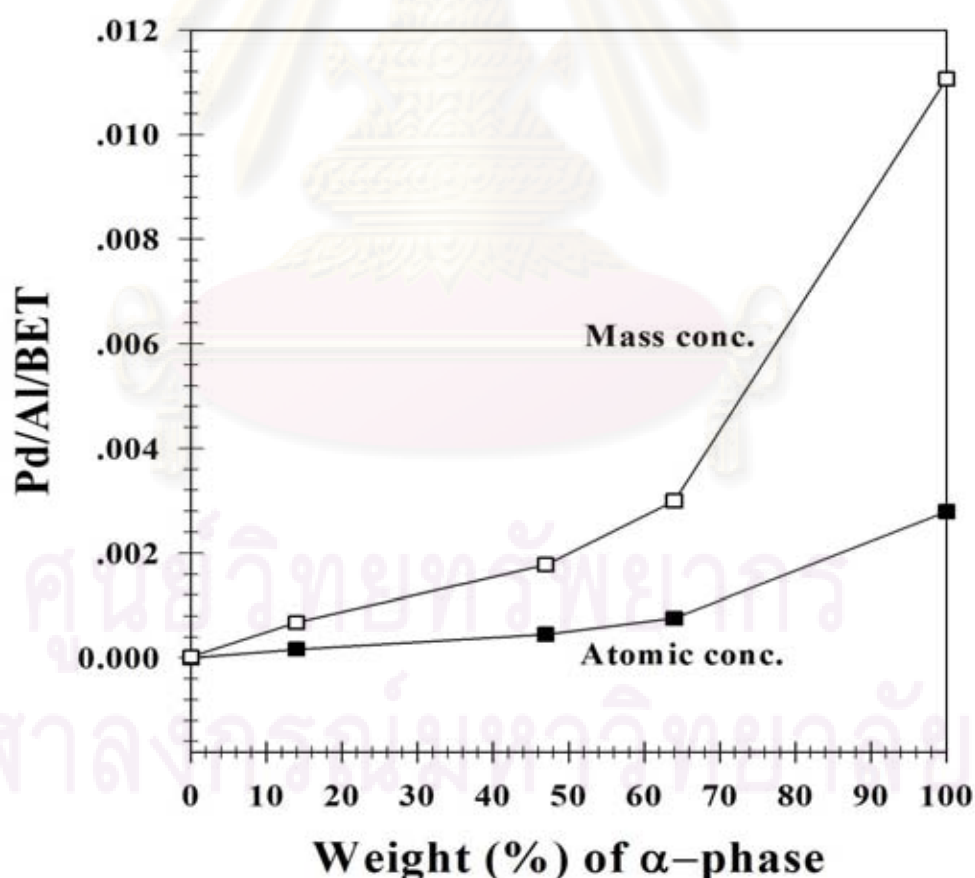


Figure 5.8 Pd/Al ratios per BET surface area of the various Pd/Al₂O₃ catalysts from XPS results.

Reduction behavior and reducibility of the catalysts were investigated by means of H₂-temperature programmed reduction and the results are shown in **Figure 5.9**.

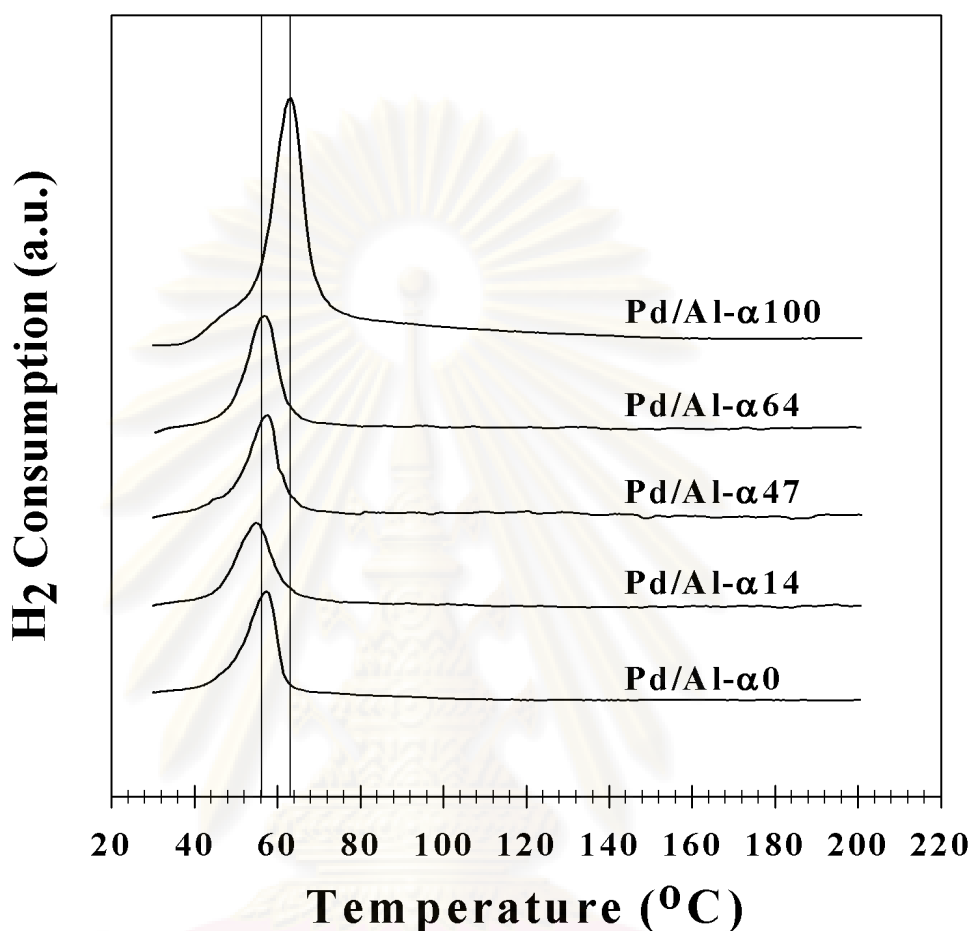


Figure 5.9 TPR profiles of the Pd/Al₂O₃ catalysts.

All the Pd/Al₂O₃ catalysts exhibited TPR profiles with one main reduction peak which can be assigned to the reduction of PdO to Pd⁰ metal. This peak remained constant at around 55°C for those with the weight (%) of α -phase contents between 0 and 64%. The reduction peak was slightly shifted to 65°C for the Pd/Al- α 100 catalyst (100% α -phase). It is suggested that the existence of transition phase Al₂O₃ (either γ - or θ -Al₂O₃) in the Al₂O₃ supports facilitated reduction at low temperature. However, the hydrogen consumptions during the transformation of PdO to metallic Pd as determined from the areas of the reduction peak for all the catalysts were essentially the same.

Ethylene-temperature programmed desorption (C_2H_4 -TPD) was performed in order to obtain an information about ethylene adsorption behavior on the catalyst surfaces. The C_2H_4 -TPD experiments were carried out at 35-800°C after the samples were reduced in H_2 at 150°C and purged with He at the same adsorption temperature. The temperature programmed study profiles of the catalysts are shown in **Figure 5.10**.

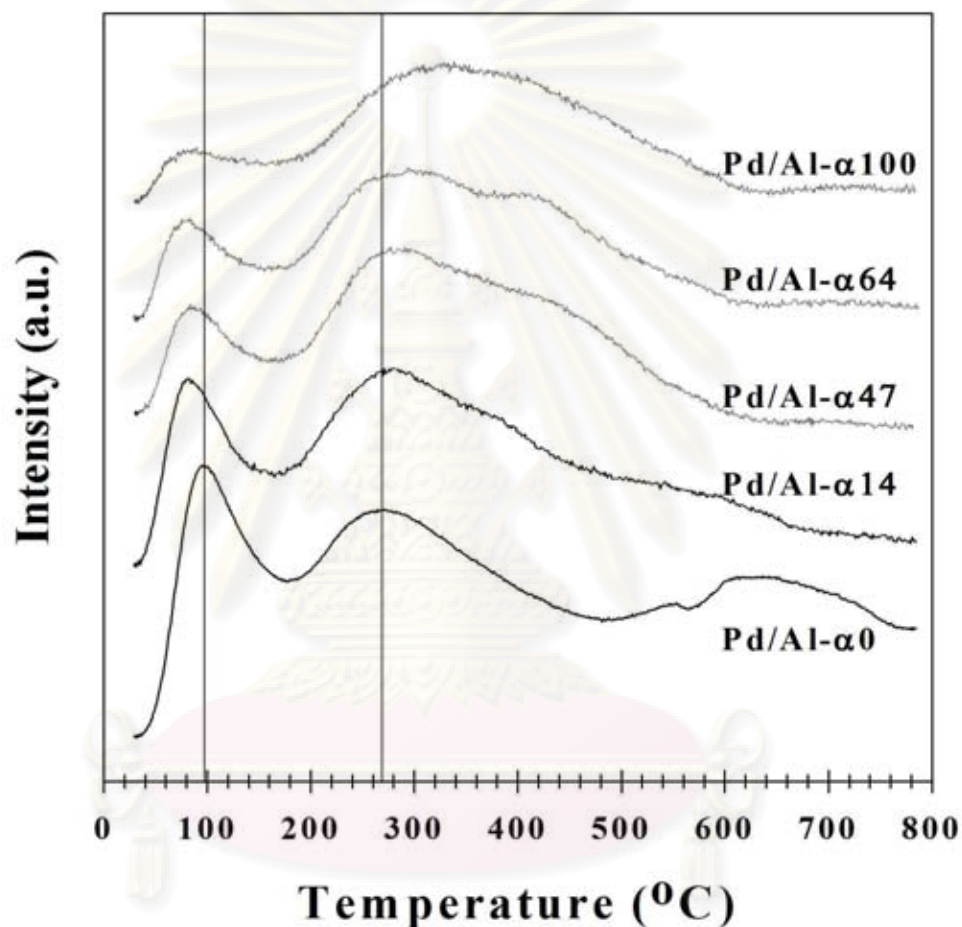


Figure 5.10 Ethylene TPD results of the Pd/Al₂O₃ catalysts.

Two main desorption peaks at ca. 80-105°C and 275-300°C were observed for all the catalyst samples. As suggested by Moon et al. [157], the lower temperature desorption peak was assigned to π -bonded ethylene species while the higher temperature was assigned to di- σ -bonded ethylene. The latter species were suggested to be the species that recombined with surface hydrocarbon and produced ethane. In some cases, the third peak at temperature range around 450-650°C was observed. It

was suggested to be due to decomposition of C₂ hydrocarbons adsorbed on Pd surface [18]. In the present study, the intensities of the TCD signals during ethylene temperature programmed desorption was significantly decreased when the content of α -phase in the Al₂O₃ supports increased from 0 to 100%. In other words, the amount of ethylene adsorbed was much lower when the Al₂O₃ supports contained significant amounts of α -Al₂O₃. The obtained results from TPR profiles and C₂H₄-TPD were translated to the quantity of hydrogen and ethylene as **Table 5.3** with calibration curve in **APPENDIX B**.

Table 5.3 The amount of H₂ consumption and C₂H₄ desorption (**APPENDIX B**).

Catalysts	H ₂ Consumption (μmol)	C ₂ H ₄ Desorption (μmol)
Pd/Al- α 100	2408	32
Pd/Al- α 64	982	42
Pd/Al- α 47	796	51
Pd/Al- α 14	699	68
Pd/Al- α 0	668	174

For the details of catalyst and reaction as giving information: 1%Pd/Al₂O₃, reaction temperature = 40°C, GHSV = 12385, 22534, 32577, and 52580 h⁻¹ (**APPENDIX J**). The catalytic performances of Pd/Al₂O₃ catalysts containing α -Al₂O₃, γ -Al₂O₃, or mixed phases alumina were evaluated in the selective hydrogenation of acetylene at 40°C under various feed flow rates (GHSV 52580, 32577, 22534, and 12385 h⁻¹). Acetylene conversion is defined as moles of acetylene converted with respect to acetylene in feed. Ethylene gain is defined as the percentage of acetylene hydrogenated to ethylene over totally hydrogenated acetylene. The ethylene being hydrogenated to ethane (ethylene loss) is the difference between all the hydrogen consumed and all the acetylene which has been totally hydrogenated (**APPENDIX D**). The plots of acetylene conversion and ethylene selectivity versus GHSV are shown in **Figure 5.11** and **5.12**, respectively.

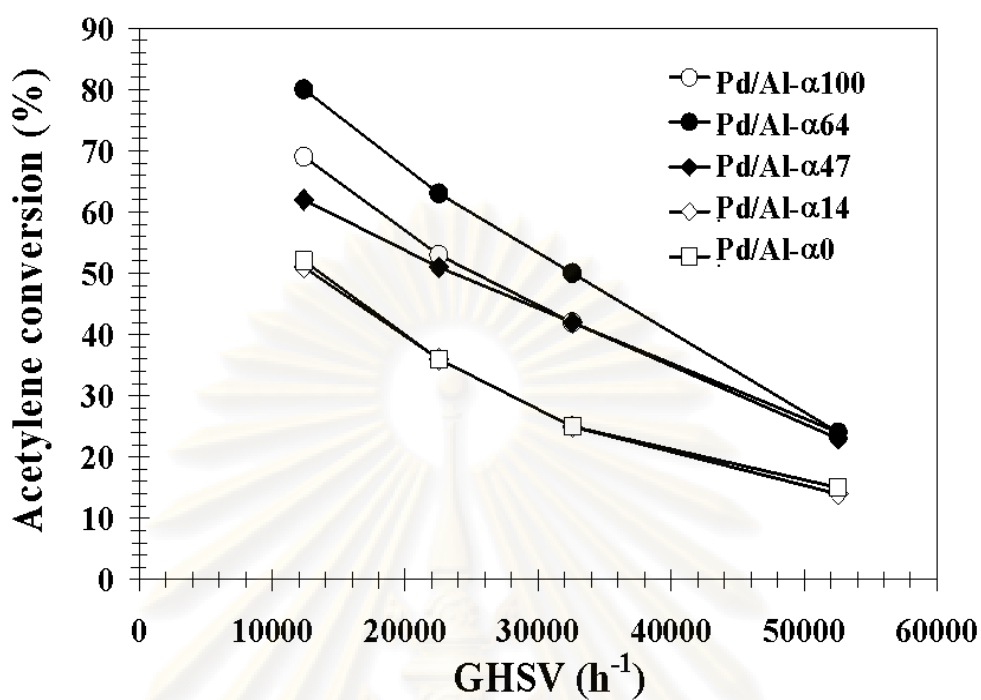


Figure 5.11 Catalyst performances in selective hydrogenation of acetylene in terms of GHSV values and acetylene conversion (%).

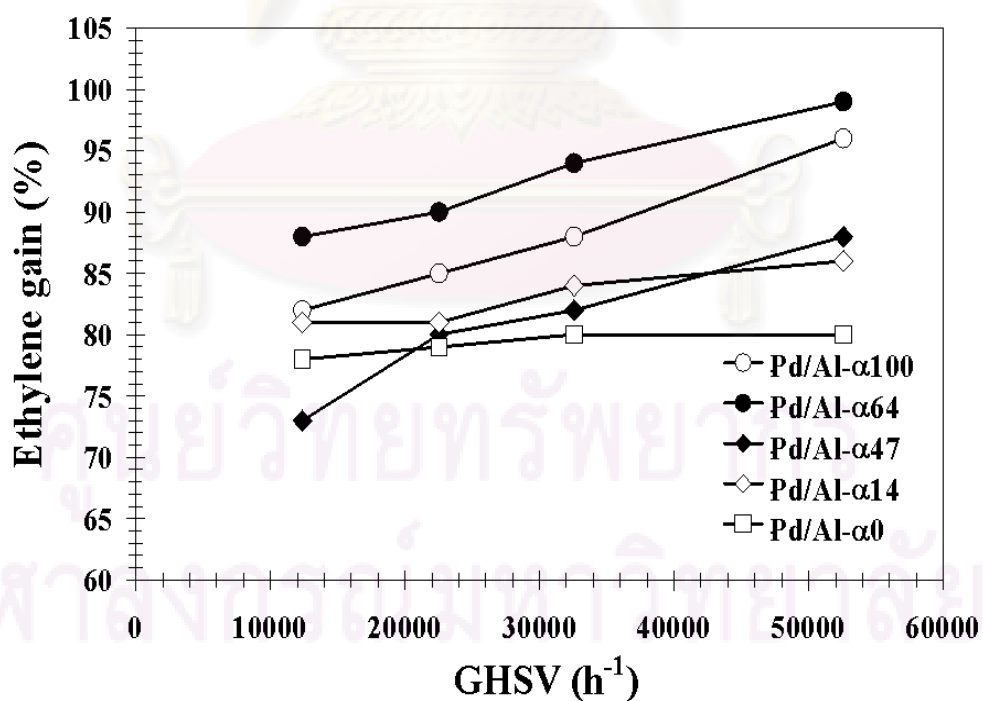


Figure 5.12 Catalyst performances in selective hydrogenation of acetylene in terms of GHSV values and ethylene gain (%).

In general, acetylene conversion decreased with increasing GHSV while ethylene gain increased. Since ethylene is produced as an intermediate in acetylene hydrogenation, which is a typical consecutive reaction, the ethylene selectivity decreases with acetylene conversion [92]. The performance of Pd/Al₂O₃ catalysts was improved in the order of Pd/Al- α 64 > Pd/Al- α 100 > Pd/Al- α 47 > Pd/Al- α 14 > Pd/Al- α 0. It is clearly shown that the Pd catalyst supported on mixed phase Al₂O₃ that contained 64% of α -phase (Pd/Al- α 64) exhibited the best catalytic performance among the five catalysts studied.

Based on the characterization results, the presence of the transition-phase in α -Al₂O₃ supports increased the specific surface area, total pore volume, Pd active sites and the dispersion of Pd on Al₂O₃ supports and facilitated the reduction of PdO at lower temperature, which promoted acetylene conversion. However, the TPD profiles suggest that the amount of ethylene adsorbed on the catalyst surface decreased with increasing α -phase content. The feature is important for the improvement of ethylene gain especially at high acetylene conversion. The results in this study revealed that the beneficial properties of both α -Al₂O₃ and transition alumina can be combined to give the best catalytic performance of Pd/Al₂O₃ catalyst in selective acetylene hydrogenation. Among the five catalysts studied, the optimum amount of α -phase content was found to be at 64 wt%. Moreover, the small shift in XPS pattern of 100 and 64 wt.% α -phase to higher binding energies (0.5 eV) was probably due to the stronger interaction between Pd and Al₂O₃ supports, which promotes ethylene gain and acetylene conversion. The best catalytic performance of Pd catalyst supported on mixed phase Al₂O₃ that contained 64% of α -phase (Pd/Al- α 64) can be confirmed by the plot between acetylene conversion (%) and ethylene gain (%) which is shown in **Figure 5.13**.

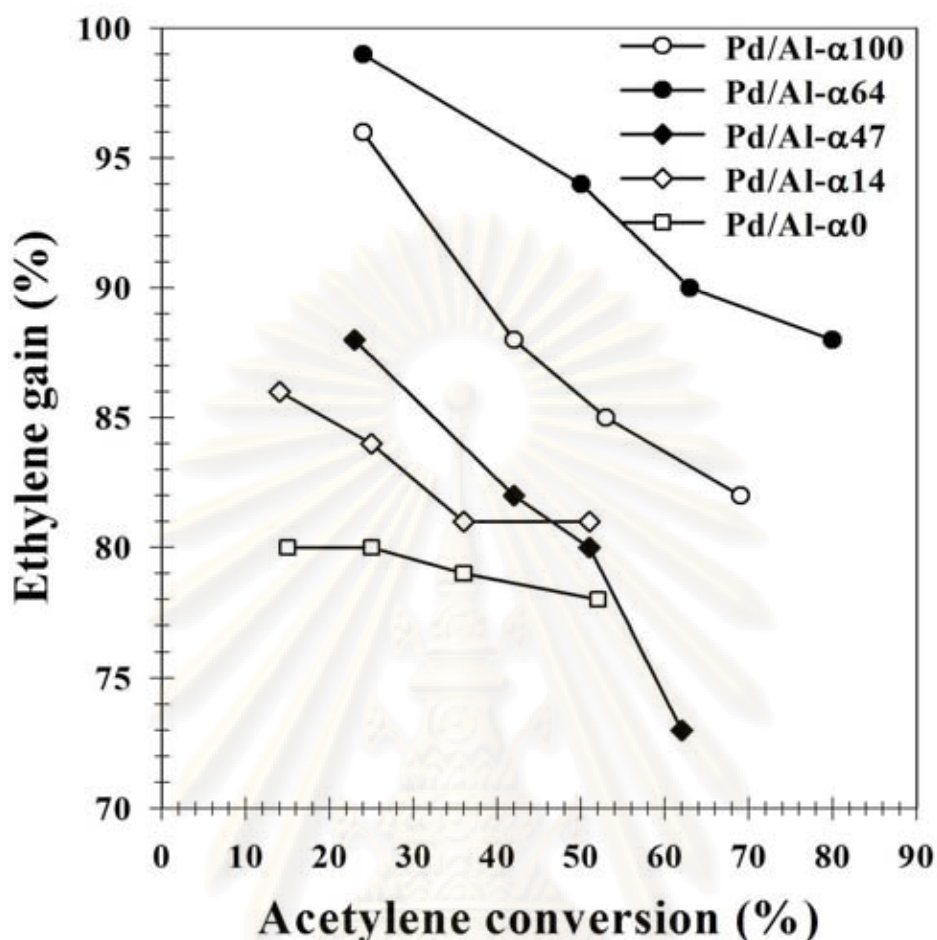


Figure 5.13 Catalyst performances in selective hydrogenation of acetylene in terms of acetylene conversion (%) and ethylene gain (%).

5.2 Micron-sized and nanocrystalline α - Al_2O_3

For the details of catalyst and reaction as giving information: 1%Pd/ Al_2O_3 , reaction temperature = 60°C, GHSV = 52580, 32577, 22534, 12385, 9366, 6660 and 4282 h^{-1} (**APPENDIX J**). The plots between acetylene conversion \times ethylene selectivity versus GHSV are shown in **Figure 5.14**. Acetylene conversion is defined as moles of acetylene converted with respect to acetylene in feed and ethylene selectivity is defined as the percentage of acetylene hydrogenated to ethylene over totally hydrogenated acetylene. However, due to the difficulty in precise measurement of the ethylene change in the feed and product, the indirect calculation using the difference in the hydrogen amount (hydrogen consumed) was used. The ethylene

being hydrogenated to ethane is the difference between all the hydrogen consumed and all the acetylene totally hydrogenated.

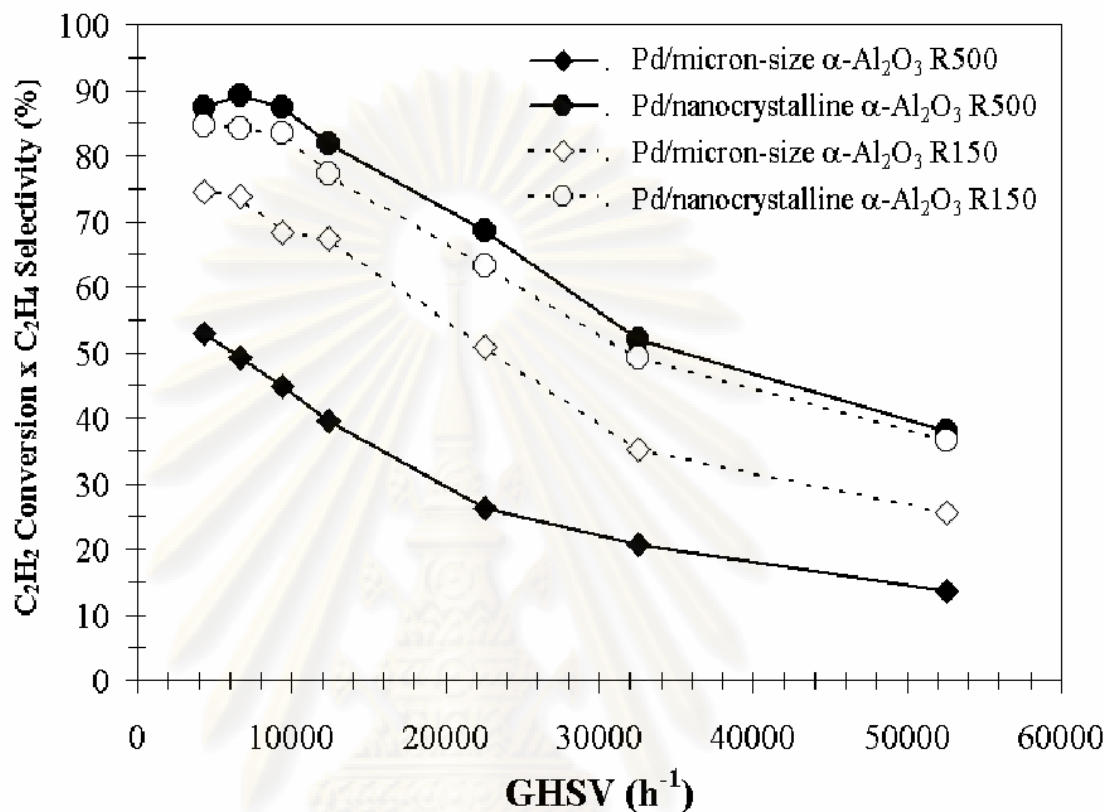


Figure 5.14 The catalytic performances of Pd catalysts supported on micron-sized and nanocrystalline α -Al₂O₃ reduced at 150°C and 500°C in selective acetylene hydrogenation under various feed flow rates.

It is clearly seen that ethylene yield (%) was improved in order of Pd/nanocrystalline Al₂O₃-R500°C > Pd/nanocrystalline Al₂O₃-R150°C > Pd/micron-sized Al₂O₃-R150°C > Pd/micron-sized Al₂O₃-R500°C. The Pd catalysts supported on nanocrystalline α -Al₂O₃ exhibited superior performance than the micron-sized supported ones. It should be noticed that the catalytic performance of Pd/nanocrystalline α -Al₂O₃ was improved by reduction at 500°C while the Pd/micron-sized α -Al₂O₃ showed the opposite trend. The results suggest that the interaction between Pd metal and α -Al₂O₃ support was affected by the crystallite size of α -Al₂O₃. Reduction at 500°C could result in stronger metal-support interaction between Pd metal and α -Al₂O₃ for the nanocrystalline α -Al₂O₃ supported catalysts and as a

consequence, ethylene selectivity was enhanced due to the lower adsorption strength of ethylene as can be found in other catalyst systems such as Pd/TiO₂ [92]. The absence of strong metal-support interaction in the case of Pd/micron-sized α -Al₂O₃ was probably due to sintering of Pd⁰ metal during high temperature reduction.

Based on XRD results (Figure 5.15), both supports showed only the crystal structure for α -phase Al₂O₃. The average crystallite size of nanocrystalline α -Al₂O₃ calculated from the XRD peak at $2\theta = 43.32^\circ$ using Scherrer's equation was 45 nm while those of the commercial one could not be determined by this method due to the calculation limit of the Scherrer equation (the crystallite size may be too large).

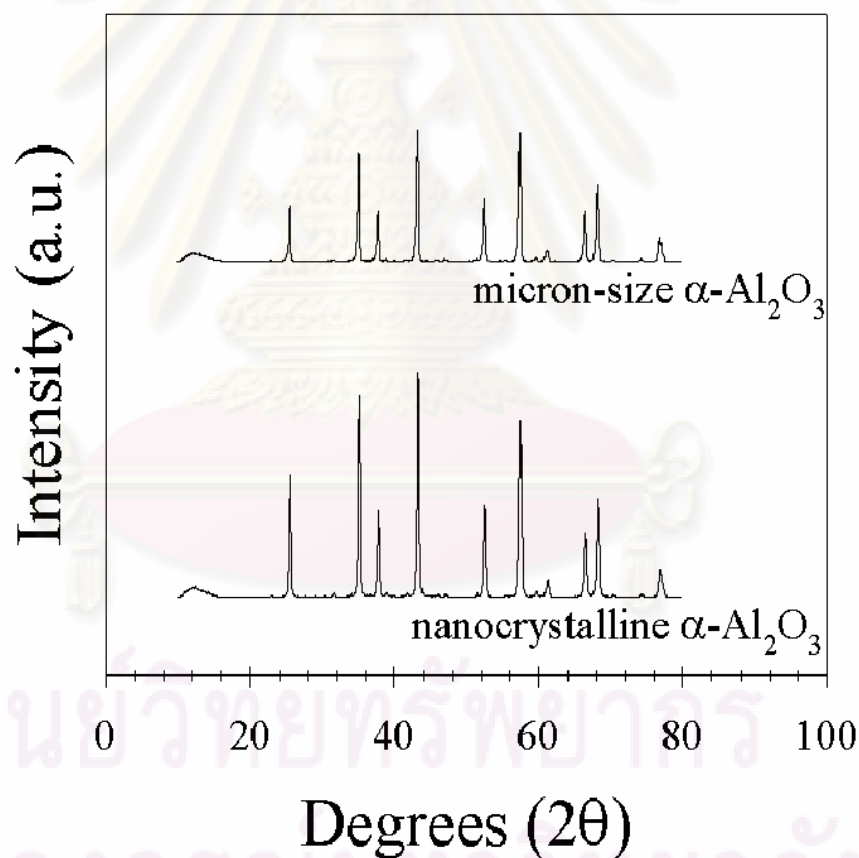


Figure 5.15 XRD patterns of the micron-sized and nanocrystalline α -Al₂O₃.

The physicochemical properties of α -Al₂O₃ supports are summarized in Table 5.4. The specific surface area of nanocrystalline α -Al₂O₃ was about 6 times higher than micron-sized one. The total pore volume and average pore diameter of the

micron-sized sample can not be determined, while nanocrystalline sample could find the total pore volume and average pore diameter. The physical properties of nanocrystalline α -Al₂O₃ promoted the CO chemisorption results such as the number of active Pd atoms, Pd dispersion (%), and average Pd metal particle size for the Pd/ α -Al₂O₃ catalysts, it was also shown in **Table 5.4**. The active sites of Pd supported on nanocrystalline α -Al₂O₃ catalyst are higher than micron-sized α -Al₂O₃. The lower Pd dispersion obtained for the Pd/micron-sized α -Al₂O₃ would be due to the lower specific surface area and large size of α -Al₂O₃ support. The higher acetylene hydrogenation activity obtained over Pd/nanocrystalline α -Al₂O₃ was probably due to the increase of Pd active sites [158].

Table 5.4 The physicochemical properties of Pd catalysts supported on micron-sized and nanocrystalline α -Al₂O₃.

Catalyst	BET surface area (m ² /g)	Pore volume (cm ³ /g)	Average pore diameter (nm)	Pd active sites ($\times 10^{-17}$ sites/g-catalyst)	%Pd dispersion	Average Pd ^o particle size (nm)	XPS binding energy of Pd 3d _{5/2}
Pd/micron-sized α -Al ₂ O ₃	1.9	n.d.	n.d.	11.6	2.3	48.6	336.0
Pd/nanocrystalline α -Al ₂ O ₃	12.3	0.0259	9.0	41.1	8.2	13.7	337.0

n.d. = not determined

Temperature program reduction (TPR) was performed in order to identify the reduction behaviors and reducibility of catalysts. The TPR profiles for Pd/nanocrystalline and Pd/micron-sized α -Al₂O₃ catalysts are shown in **Figure 5.16**. Only one main reduction peak was observed which could be assigned to the reduction of PdO to Pd⁰ metal. The reduction peaks were at 65 and 55°C for the catalysts

supported on micron-sized and nanocrystalline α -Al₂O₃, respectively. The 10°C shift of TPR profile suggests that PdO/Pd supported on the nanocrystalline α -Al₂O₃ facilitated reduction at lower temperature.

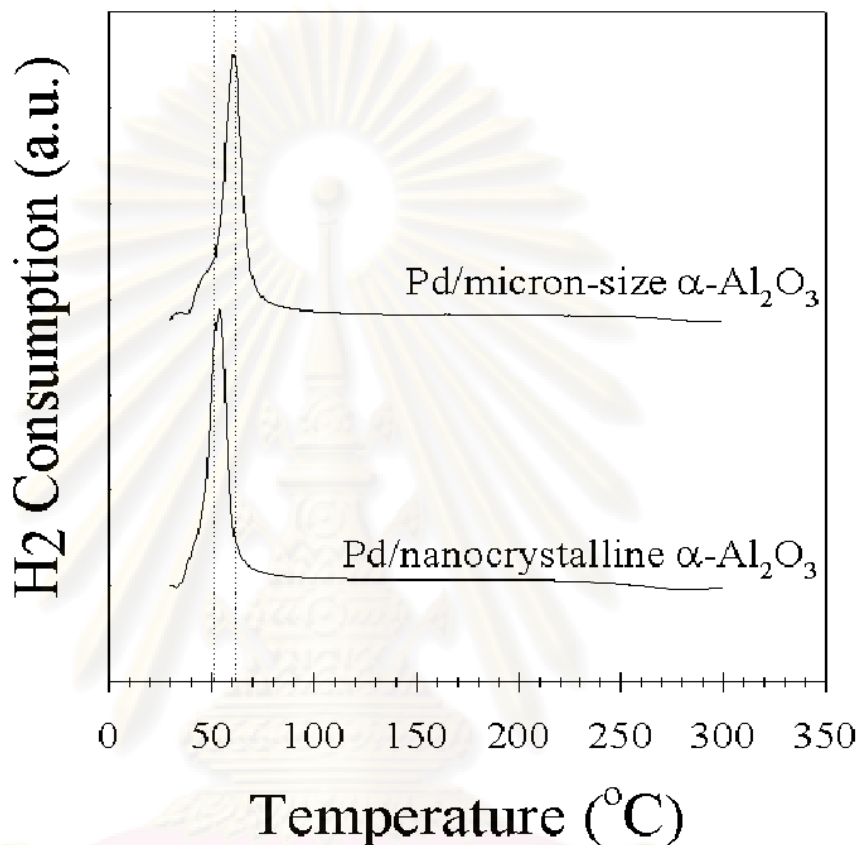


Figure 5.16 H₂ temperature program reduction results.

The behaviors for adsorption and desorption of ethylene on the catalyst surface were investigated by ethylene temperature program desorption (ethylene-TPD) and the results are shown in **Figure 5.17**. The amounts of desorbed ethylene increased as the α -Al₂O₃ support changed from micron-sized to nanocrystalline α -Al₂O₃. This was probably due to the increasing of BET surface area and Pd dispersion of the catalyst. However, TPD profile of the Pd/nanocrystalline α -Al₂O₃ catalyst exhibited two main peaks ranged around 80°C and 300°C, while the Pd/micron-sized α -Al₂O₃ catalyst exhibited only one broad peak at around 340°C. According to Moon et al. [157], the first peak at low temperature was assigned to π -bonded ethylene species, which were weakly adsorbed to catalyst surface and desorbed from Pd without decomposition. The second one was assigned to di- σ -bonded ethylene species, which were desorbed

dissociatively followed by the recombination of the surface hydrocarbon species to produce either ethylene or ethane. Disappearance of the first TPD peak and a shift of the second desorption peak to higher temperature for the Pd/micron-sized α -Al₂O₃ indicate that chemisorption of ethylene on the Pd/micron-sized α -Al₂O₃ was stronger than on the Pd/nanocrystalline α -Al₂O₃. In other words, weaker ethylene chemisorption strength on the Pd/nanocrystalline α -Al₂O₃ promoted ethylene selectivity [92,159].

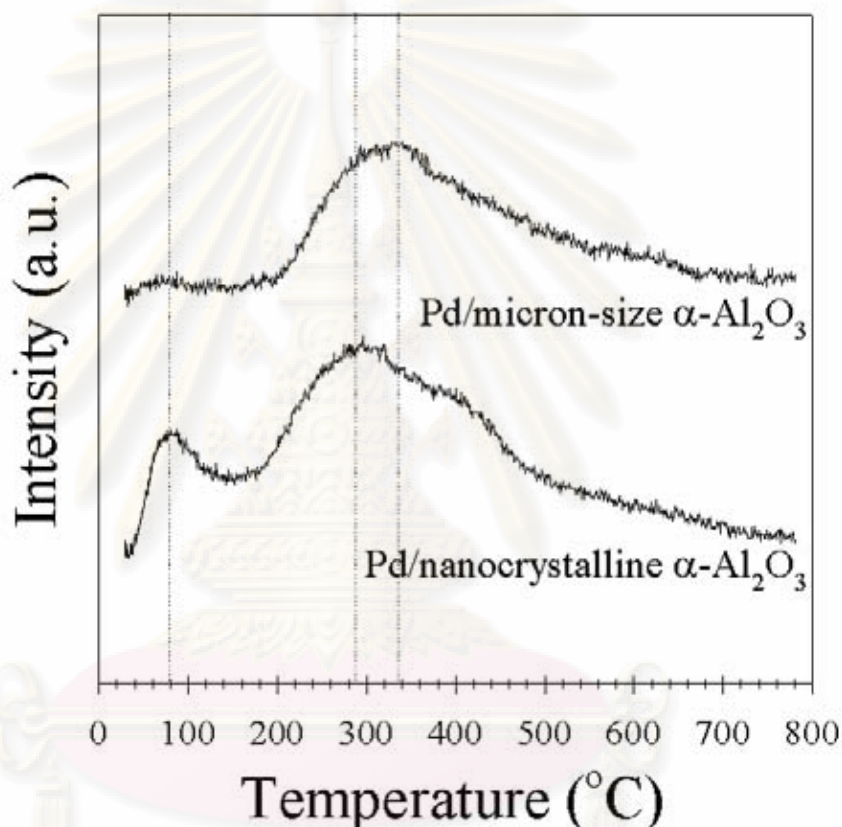


Figure 5.17 Ethylene temperature program desorption results.

The comparison of the Pd metal on surface among the Pd supported with nanocrystalline and micron-sized α -Al₂O₃ are presented in **Figure 5.18**. X-ray photoelectron spectroscopy (XPS) studies indicated that the atomic and mass concentration of Pd metal on support surface for Pd/nanocrystalline α -Al₂O₃ is higher than Pd/micron-sized α -Al₂O₃, which is due to specific surface area, pore volume and average pore diameter. The higher Pd metal on surface is responsible for the higher acetylene hydrogenation activity due to the increase of Pd active sites.

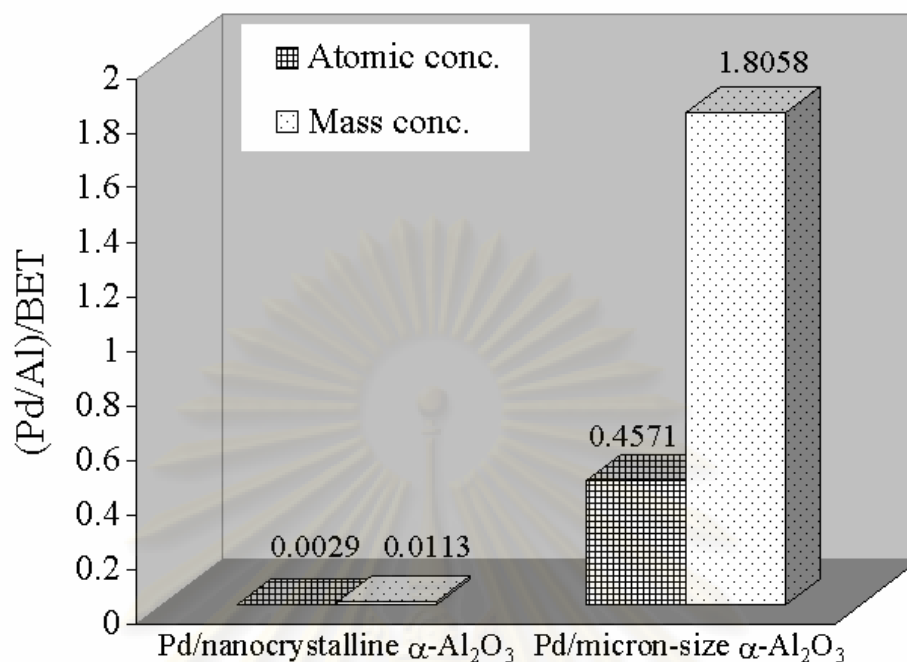


Figure 5.18 Ratios of Pd/Al/BET.

The characteristic of Pd metal on nanocrystalline and micron-sized α -Al₂O₃ are shown in **Figure 5.19**. As already found for the Pd/nanocrystalline α -Al₂O₃ catalysts has more the strong interaction between Pd metal and support than Pd/micron-sized α -Al₂O₃ when it is reduced at high temperature (500°C) because of a little decrease of Pd active sites. After that, the catalysts are recalcined by air and then it is again measured the Pd active sites at normal temperature reduction (150°C), it seems that the high temperature reduction lead to restructure of Pd/nanocrystalline α -Al₂O₃ which promote the Pd dispersion of catalyst. So, it was found that the Pd active sites of Pd/nanocrystalline α -Al₂O₃ show higher than Pd/micron-sized α -Al₂O₃ when recalcined after high reduction temperature. This suggests that, the nanocrystalline α -Al₂O₃ is strongly affected to Pd metal under extreme conditions in the reduction temperature of 500°C the changes on the catalyst structure was occurred. This restructuring of the catalyst, which is connected with a change in the oxidation properties, causes surface decorations and induces different metal-support interactions [160].

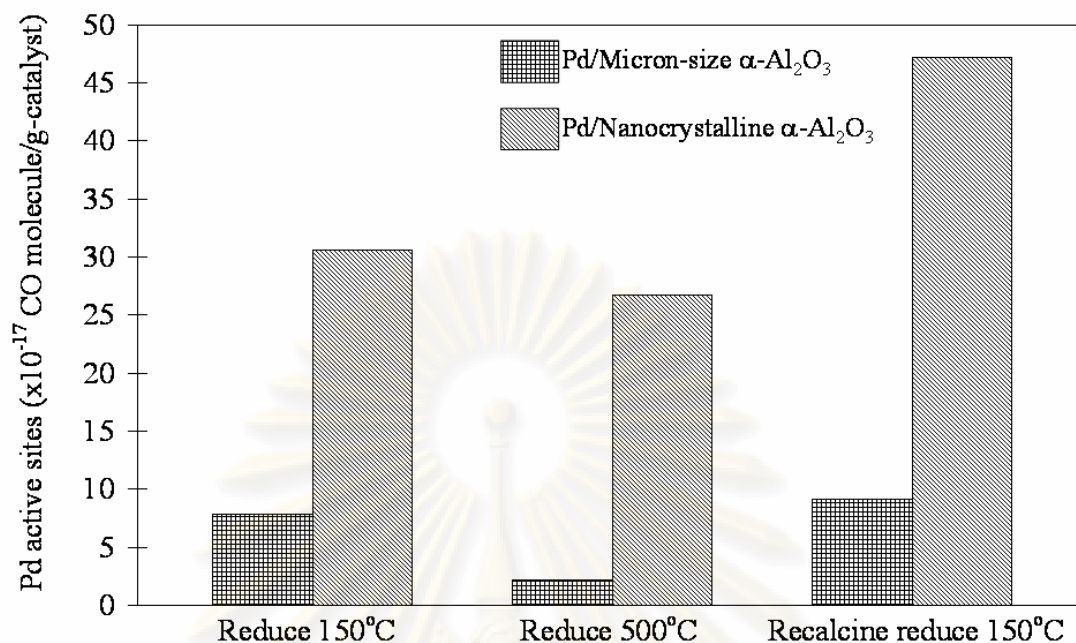


Figure 5.19 Pd active sites results on different reduction temperature.

Figure 5.20 shows that the pretreatment with N₂O on the Pd-Ag/nanocrystalline α -Al₂O₃ and Pd-Ag/micron-sized α -Al₂O₃. The performance of the Pd-Ag/nanocrystalline α -Al₂O₃ catalyst in the acetylene hydrogenation was higher than that of the Pd-Ag/micron-sized α -Al₂O₃. So, these results appear to be in agreement with the Pd catalyst does not modify by Ag metal. The Pd-Ag/micron-sized α -Al₂O₃ show less improvement with N₂O-treat for acetylene hydrogenation while of more improvement effect for Pd-Ag/nanocrystalline α -Al₂O₃.

ศูนย์วิทยทรัพยากร
จุฬาลงกรณ์มหาวิทยาลัย

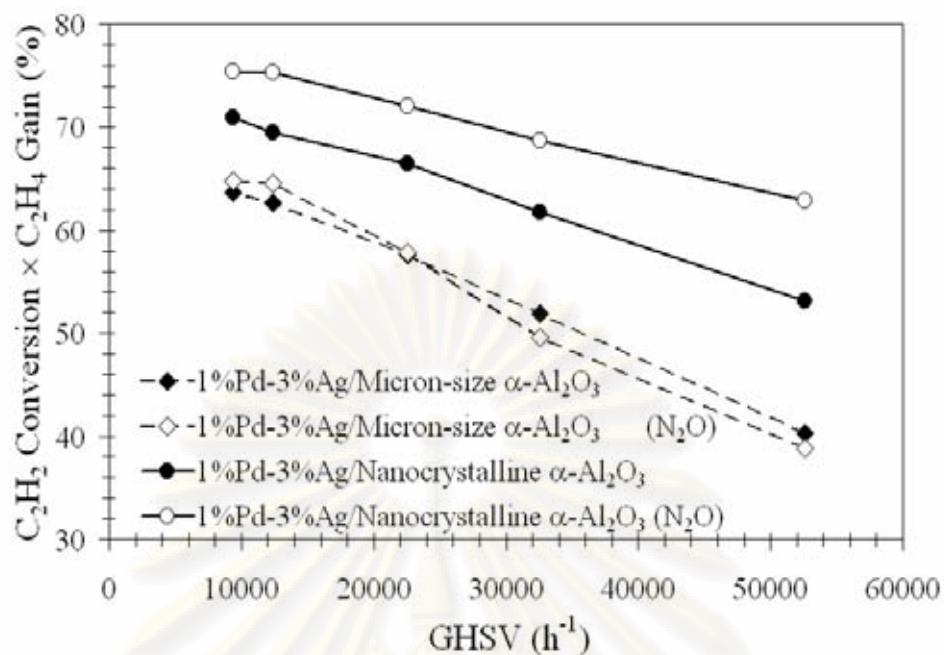


Figure 5.20 The catalytic performances of Pd catalysts supported on micron-sized and nanocrystalline α -Al₂O₃ reduced at 150°C, N₂O pretreatment and reaction temperature at 90°C in selective acetylene hydrogenation under various feed flow rates.

5.3 Influence of preparation method on the nanocrystalline porosity

5.3.1. Characteristics of α -Al₂O₃

Figure 5.21 shows the XRD patterns of Al₂O₃ supports prepared by different preparation methods. The typical characteristic peaks for α -phase alumina were detected for all the samples without any contamination of other transition alumina phases.

ศูนย์วิทยทรัพยากร
จุฬาลงกรณ์มหาวิทยาลัย

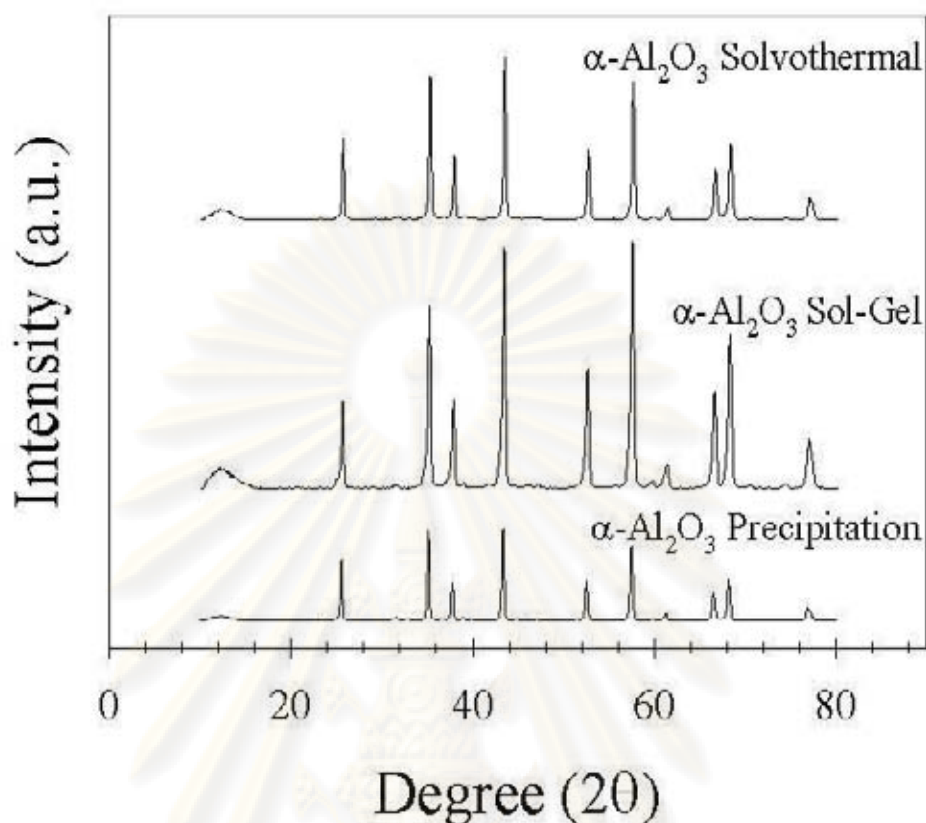


Figure 5.21 XRD patterns of the α - Al_2O_3 supports: solvothermal, sol-gel, and precipitation method.

The IR spectra of as-synthesized and calcined products are shown in **Figure 5.22**. In all cases, the strong H_2O peak at wave number around 3450 cm^{-1} disappeared after calcination suggesting that moisture trapped between crystals were removed by heat treatment. For the α - Al_2O_3 prepared by precipitation method, absorption bands at 860 and 1425 cm^{-1} corresponding to organic groups (CO_3^{2-} and NH_4^+) were eliminated during calcination. For the α - Al_2O_3 sol-gel, disappearance of the absorption peaks at 1400 , 1700 , and 3500 cm^{-1} after calcination indicated that organic groups and NO_3^- ion have been removed. The characteristic absorption bands of boehmite observed at 773 and 615 cm^{-1} from the as-synthesized solvothermal powder also disappeared after calcination. Boehmite was resulted from the presence of small amount of water which was by-product from AIP decomposition [161]. From IR analyses, it is confirmed that the α - Al_2O_3 powders obtained after calcination in all cases were pure Al_2O_3 without residual organic moiety. The calcination conditions

were also satisfactory for complete phase transformation or decomposition to α - Al_2O_3 .

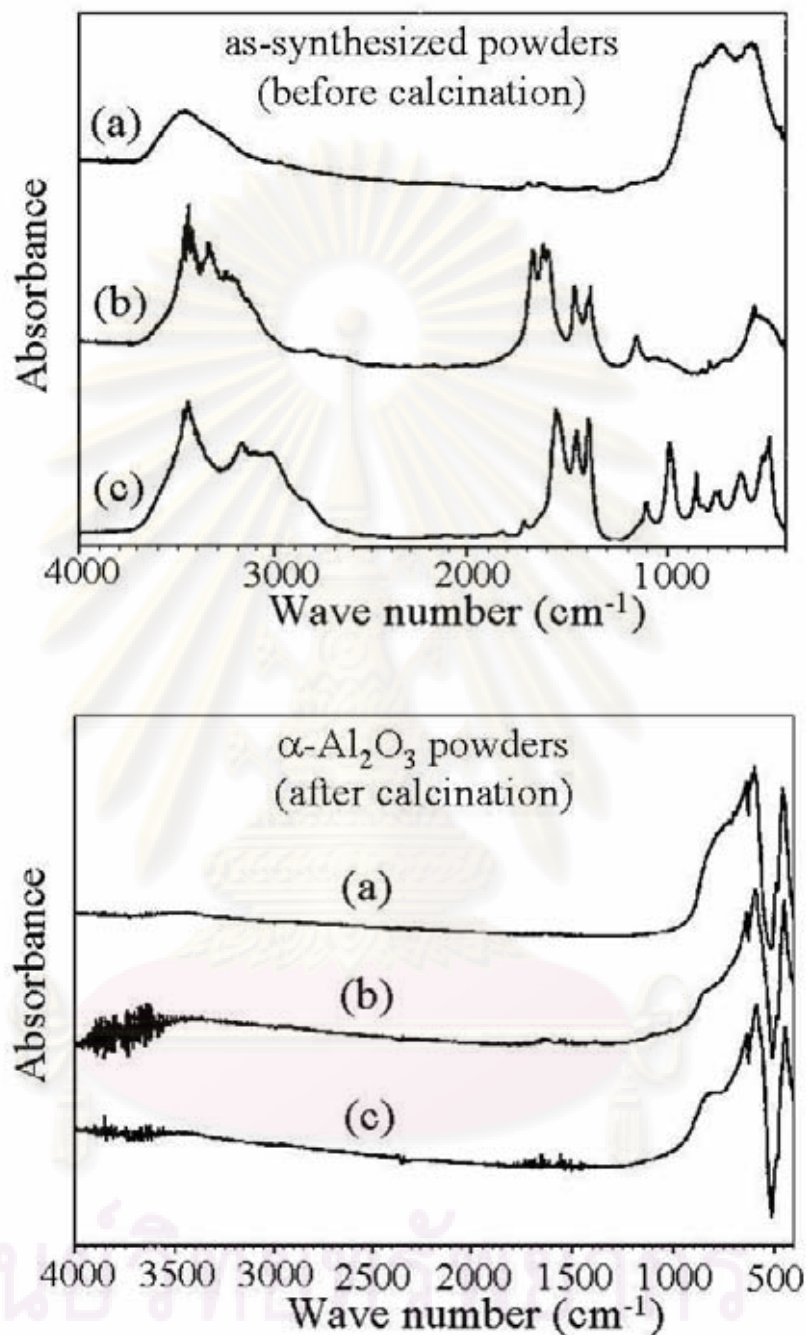


Figure 5.22 IR spectra of α - Al_2O_3 from solvothermal (a), sol-gel (b), and precipitation (c) method.

The BET surface area, pore volume, average pore diameter, and the average crystallite size of Al_2O_3 supports are given **Table 5.5**. The average crystallite sizes of α - Al_2O_3 were calculated from XRD results using Scherrer equation and the

characteristic peak of α -Al₂O₃ at $2\theta = 43^\circ$. The crystallite size of sol-gel made α -Al₂O₃ support was smallest at 33.8 nm, while the solvothermal- and precipitation-made α -Al₂O₃ support gave larger crystallite size at 53 and 67.6 nm, respectively. The specific surface area usually shows a reversed tendency with crystallite size. However, in this study, the α -Al₂O₃ obtained from sol-gel method not only possessed the smallest crystallite size but also had the minimum value of specific surface area (1.7 m²/g) as compared to those obtained by the solvothermal (19.8 m²/g) and precipitation (41.2 m²/g) method. This could possibly be due to the difference on degree of agglomeration. From **Table 5.5**, total pore volume of sol-gel made α -Al₂O₃ (0.0065 cm³/g) was much lower than those obtained from other preparation methods (0.2020 cm³/g for precipitation and 0.0739 cm³/g for solvothermal). These results indicated that the sol-gel made support had lowest space between particles comparing to the other supports, which prohibited the adsorption of N₂ molecules on catalyst surface and led to the lowest surface area.

Table 5.5 Physicochemical properties of α -Al₂O₃ various preparation methods and 0.3%Pd/Al₂O₃catalysts.

Catalysts	BET surface area (m ² /g) ^{a,*}	Pore volume (cm ³ /g) ^{b,*}	Average pore diameter (nm) ^{b,*}	Crystallite size (nm) ^{c,*}	Pd active sites ($\times 10^{-17}$ sites/g-catalyst) ^d	%Pd dispersion ^e	Average Pd ⁰ particle size (nm) ^f
Pd/Al ₂ O ₃ Solvothermal	19.8	0.0739	14.9	53	11.5	7.6	14.7
Pd/Al ₂ O ₃ Sol-Gel	1.7	0.0065	46	33.8	3.9	2.6	43.2
Pd/Al ₂ O ₃ Precipitation	41.2	0.2020	26.9	67.6	2.1	1.4	80.2

* Measured only catalyst supports.

^a Error of measurement = 10%.

^b Calculated from BJH method.

^c Determined from XRD line broadening.

^d Determined from CO chemisorption.

$$\text{Pd active sites} = (V_{\text{ads}}/V_{\text{g}}) \times (6.02 \times 10^{23}) \times S_{\text{f}}$$

Error of measurement = $\pm 5\%$.

^e Based on $D = [\text{Pd active sites} \times (\text{M.W}/\%M) \times 100\% \times 100\%]/(6.02 \times 10^{23})$.

^f Based on $d \text{ (nm)} = (1.12/D)$. [151]

Where	D	=	fractional metal dispersion
	V_{ads}	=	volume adsorbed
	V_{g}	=	molar volume of gas at STP
	S_{f}	=	stoichiometry factor, CO on Pd
	M.W	=	molecular weight of the metal
	%M	=	%metal

The pore size distribution curves of $\alpha\text{-Al}_2\text{O}_3$ supports are shown in **Figure 5.23**. While the solvothermal- and precipitation-made $\alpha\text{-Al}_2\text{O}_3$ exhibited the typical characteristic of mesopore system with average pore size 16-32 nm, the sol-gel made did not show any distinguish curve. Peak areas under the pore size distribution curves which were directly correlated with the pore volume increased in the order of precipitation > solvothermal >> sol-gel.

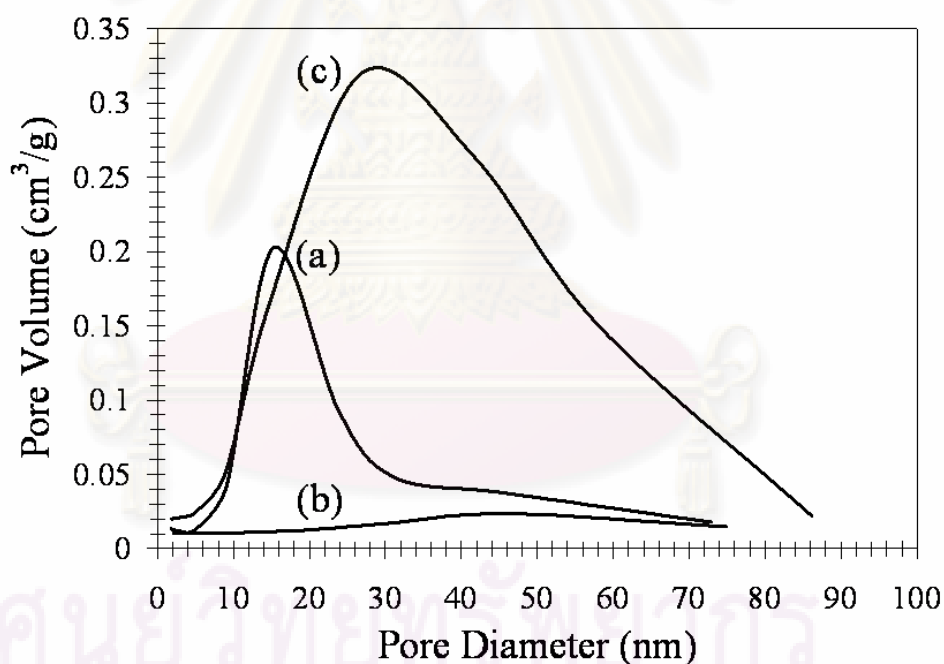


Figure 5.23 Pore size distribution results of the $\alpha\text{-Al}_2\text{O}_3$ supports from solvothermal (a), sol-gel (b), and precipitation (c) method.

The nitrogen adsorption isotherms for the $\alpha\text{-Al}_2\text{O}_3$ prepared by different methods are shown in **Figure 5.24**. It can be seen that the precipitation-made support represented adsorption isotherms with hysteresis loops with type-A adsorption

characteristic, which is corresponding to the presence of two-ended tabular pore structure. Whilst, the solvothermal- and sol-gel made alumina exhibited type-E hysteresis loop, which is an indication for the presence of tabular, through short pores with winded parts of various widths [162,163]. These pores were formed among the primary particles of alumina.

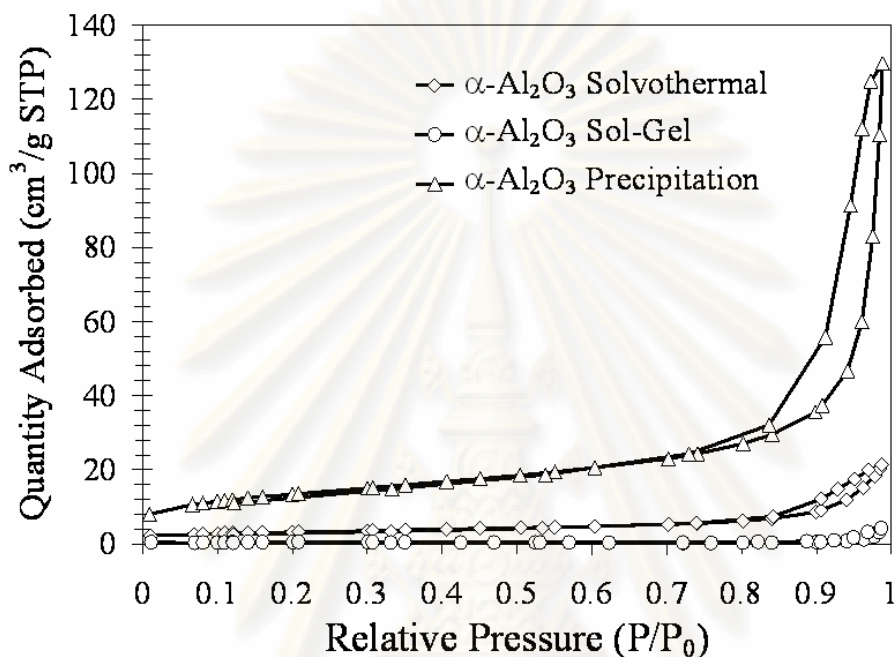


Figure 5.24 N₂ adsorption isotherms.

5.3.2 Physicochemical Properties of Pd/ α -Al₂O₃

The CO chemisorption results such as the number of active Pd atom, Pd dispersion (%), and average Pd metal particle size for the Pd/ α -Al₂O₃ catalysts are given in **Table 5.5**. The mean stoichiometry of Pd metal to CO molecule ($X_{\text{Pd-CO}}$) was determined by the iterative method according to those of Lambert et al. [147]. A polynomial function was fitted based on the table established by Joyal and Butt [148], who determined $X_{\text{Pd-CO}}$ as a function of Pd dispersion. The values of $X_{\text{Pd-CO}}$ were found to be 0.51, 0.34, and 0.29 for Pd catalysts supported on solvothermal-, sol-gel-, and precipitation-made α -Al₂O₃, respectively. The active site of Pd supported on solvothermal-, sol-gel and precipitation-made α -Al₂O₃ catalyst was 11.5, 3.9 and 2.1 $\times 10^{17}$ sites/g-catalyst corresponding to the %Pd dispersion of 7.6, 2.6 and 1.4, respectively. The lower Pd dispersion obtained for the Pd/sol-gel made α -Al₂O₃ would be due to the lower specific surface area and pore volume. On the other hand, the larger pore size of precipitation-made α -Al₂O₃ could also result in low Pd

dispersion due to agglomeration of Pd particles within the pores. Among the various Pd/ α -Al₂O₃, the maximum CO chemisorption was obtained on the solvothermal-made α -Al₂O₃ with medium pore size. In a previous study from our group about Pd dispersed on silica and MCM-41 with various pore sizes, lower Pd dispersion was found on the small pore SiO₂ owing to the significant amount of Pd being located out of the pores of the supports [164]. Similar result was obtained when Pd was supported on the sol-gel α -Al₂O₃ with very low amount of porosity.

The TEM micrographs of Pd/ α -Al₂O₃ catalysts were also taken in order to physically measure the size of the palladium oxide particles and/or palladium clusters on the various α -Al₂O₃ and are shown in **Figure 5.25**. The Pd catalyst supported on sol-gel made support consisted of agglomerated particles with primarily irregular shape structure whereas for those prepared by solvothermal and precipitation method, agglomeration of finger-like and rod-like particles were observed. The Pd metal cluster size on the various alumina supports increased in the order of α -Al₂O₃ precipitation \approx α -Al₂O₃ sol-gel > α -Al₂O₃ solvothermal.

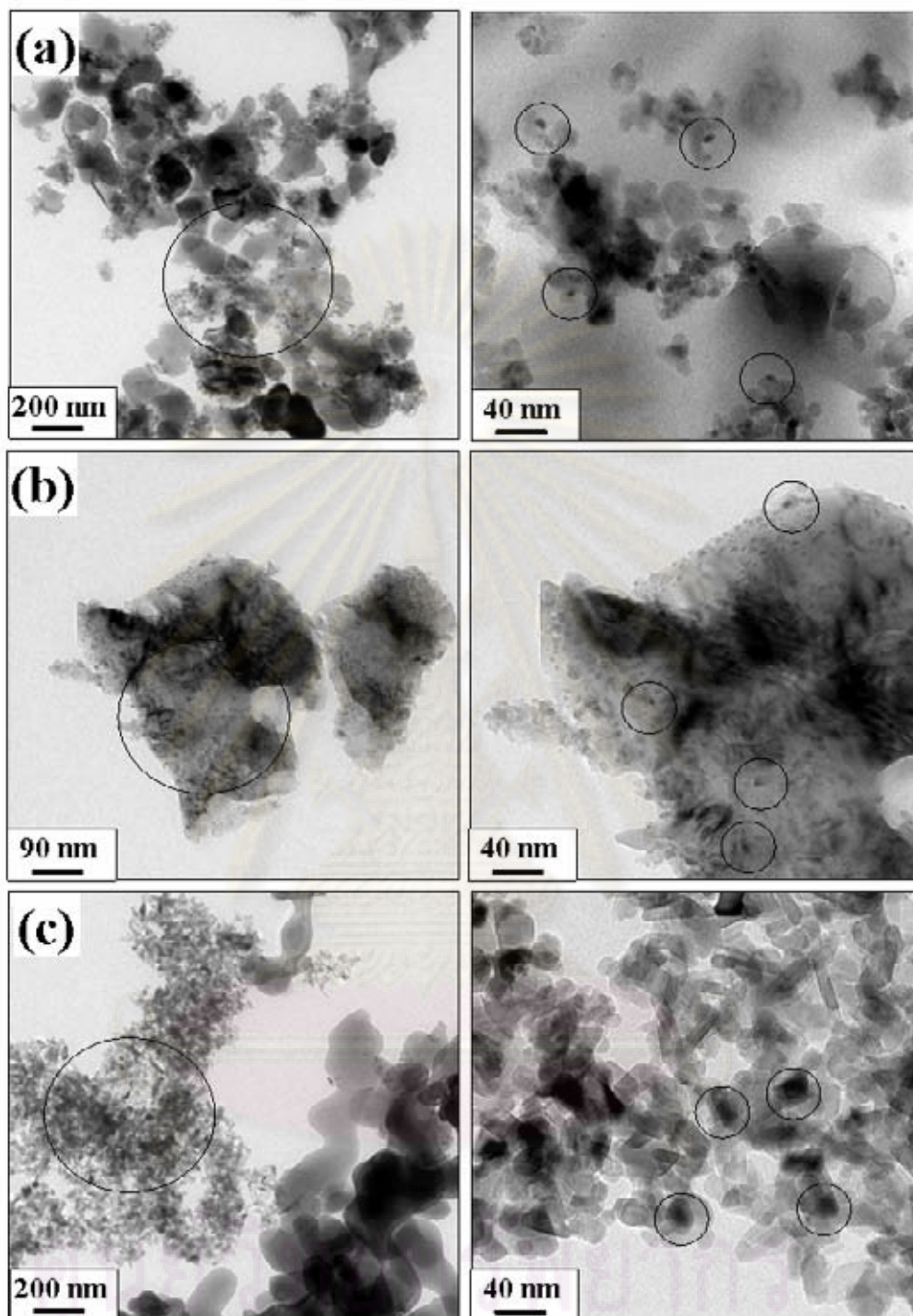


Figure 5.25 TEM images of the Pd supported by α -Al₂O₃ from solvothermal (a), sol-gel (b), and precipitation (c) method, showed Pd characteristics within the circles.

The reduction behaviors and reducibility of catalysts were studied by temperature program reduction technique (TPR). The TPR profiles of Pd/ α -Al₂O₃

catalysts are shown in **Figure 5.26**. All the TPR profiles showed single reduction peak in the range of 60-70°C corresponding to the reduction of PdO to Pd metal [165-167]. This peak was shifted to higher temperature for the catalysts that were supported on sol-gel and precipitation-made α -Al₂O₃ by approximately 10°C. The lower reduction temperature of TPR profile suggested that PdO/Pd supported on the solvothermal-made α -Al₂O₃ facilitated reduction at lower temperature.

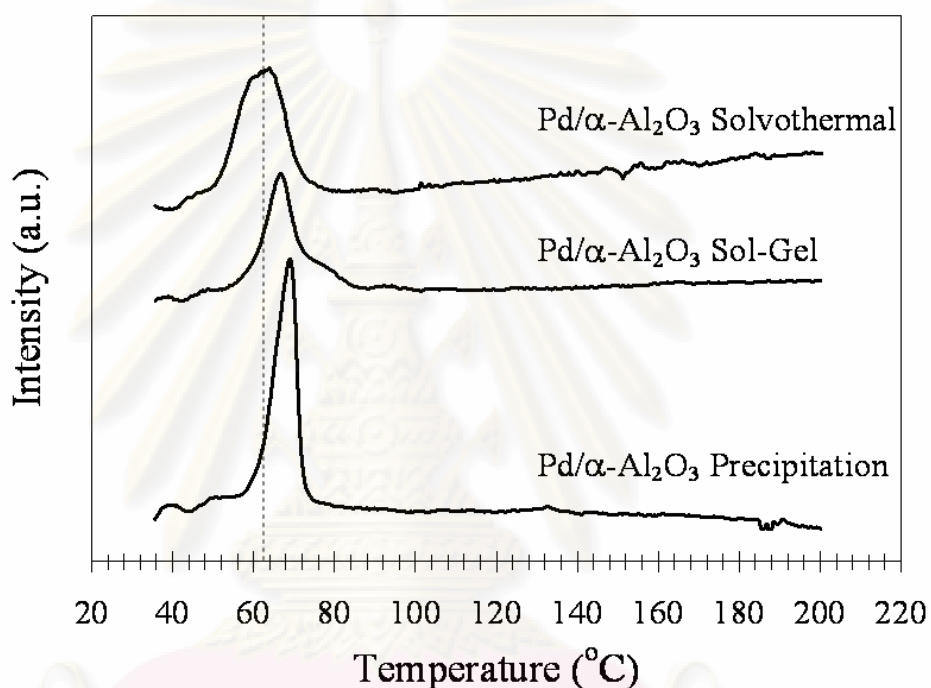


Figure 5.26 H₂-TPR profiles for the various Pd/ α -Al₂O₃ catalysts.

The average oxidation states of palladium were calculated according to the amount of H₂ consumption and the results are given in **Table 5.6**. The Pd/Al₂O₃ solvothermal possessed the highest Pd active sites due probably to the smallest PdO/Pd sizes produced as determined by TEM measurement.

จุฬาลงกรณ์มหาวิทยาลัย

Table 5.6 Consumption of hydrogen in TPR, amount of ethylene and CO desorption.

Catalysts	Temperature at maximum (°C)			H ₂ consumption (μmol)*	Amount of ethylene desorption (μmol)*	Amount of CO desorption (μmol)*
	Peak 1	Peak 2	Peak 3			
Pd/Al ₂ O ₃ Solvothermal	60 ^a ,90 ^b ,90 ^c	240 ^b ,230 ^c	420 ^b	658	131	76
Pd/Al ₂ O ₃ Sol-Gel	65 ^a ,100 ^b ,90 ^c	280 ^b ,230 ^c	500 ^b	488	75	10
Pd/Al ₂ O ₃ Precipitation	70 ^a ,100 ^b ,90 ^c	260 ^b ,250 ^c	440 ^b	610	122	33

* Measured using the same weight of catalysts. (Transformation of area to mol see in **APPENDIX B**)

^a Based on H₂-TPR results.

^b Based on C₂H₄-TPD results.

^c Based on CO-TPD results.

Ethylene-temperature programmed desorption (C₂H₄-TPD) was performed in order to obtain an information about ethylene adsorption behavior on the catalyst surface and the results are shown in **Figure 5.27**. We observed the peak locations and found that it appeared at different temperature ranges depending on the characteristic modes of the ethylene adsorbed on the surface. All of the catalysts showed that the three major peaks had difference of temperature positions and peak intensity. According to Shin et al. [18,93], the first peak at around 95°C was assigned to π -bonded ethylene which was weakly adsorbed and consequently desorbed without decomposition. The peak at around 240°C was due to di- σ -bonded ethylene which undergoes decomposition followed by the recombination of the surface hydrocarbon species with hydrogen to produced ethylene as well as ethane. The last peak at around 420°C was CH₃ group, for the CH₃ signal was due to the decomposition of C₂ hydrocarbons adsorbed on catalyst tentatively ethane or ethylene [168,169]. In the present study, the low temperature ethylene desorption peak decreased and slightly shifted to higher temperature as the preparation methods changed from solvothermal to sol-gel and to precipitation method. In other words, the adsorption strength of

ethylene on Pd/ α -Al₂O₃ catalysts was influenced by the nature of Al₂O₃ support obtained from different preparation methods.

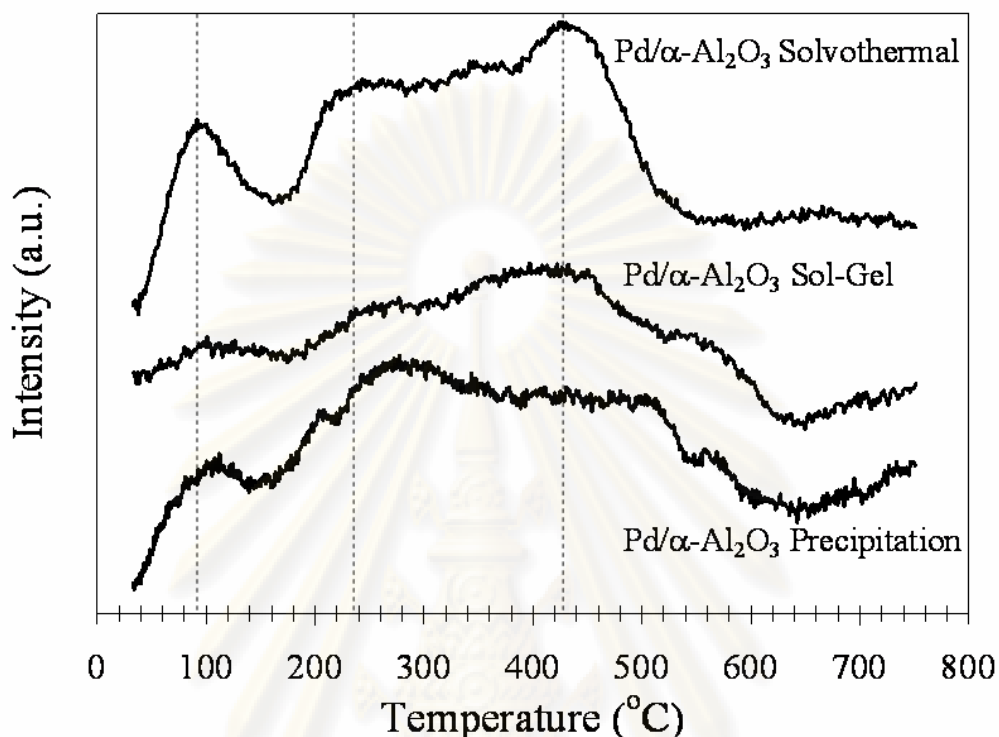


Figure 5.27 C₂H₄-TPD profiles for the various Pd/ α -Al₂O₃ catalysts.

CO temperature program desorption behavior for the Pd catalysts supported on Al₂O₃ from different preparation methods are shown in **Figure 5.28**. Two desorption peaks, one with strong intensity at ca. 95°C and another small peak located at ca. 220°C were observed for all the catalysts which could be attributed to CO adsorption on two adsorptive site groups. The first group gave the strong peak ranging from 95 to 180°C, which was weak CO species over the catalyst. The second one was characteristic of the strong chemically adsorbed CO molecules. The amount of chemisorbed CO (**Table 5.6**) on Pd/ α -Al₂O₃ (solvothermal-made support) was 7 and 2 times more than those on Pd/ α -Al₂O₃ (sol-gel made support) and Pd/ α -Al₂O₃ (precipitation-made support), respectively. The difference may be related to different geometry states of the adsorptive sites on catalysts occurred from the different support configurations of the Pd/ α -Al₂O₃ catalysts. Moreover, it has been reported that the activation energy of CO desorption decreased with decreasing size of Pd particles [170]. The results from this study also show that the Pd/Al₂O₃ (solvothermal-made

support) with the smallest Pd particle size facilitated CO desorption. The atomic structure of CO and ethylene was similar in term of double bond that consisted of π and σ bond thus both of ethylene and CO TPD results show the same trend.

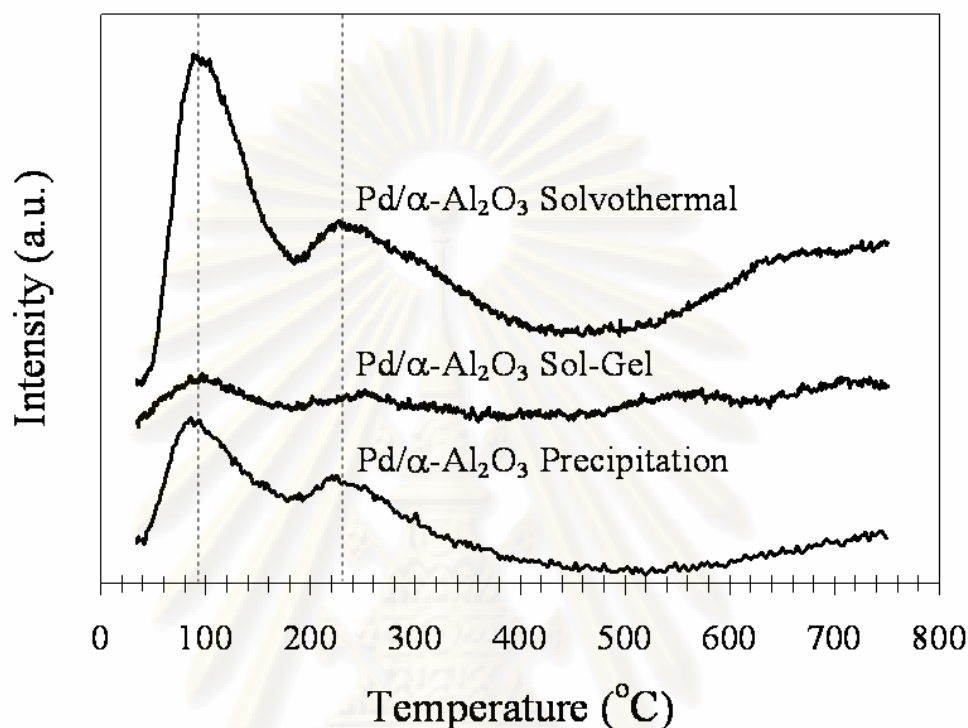


Figure 5.28 CO-TPD profiles for the various Pd/ α -Al₂O₃ catalysts.

5.3.3 Catalytic performance in selective acetylene hydrogenation

For the details of catalyst and reaction as giving information: 0.3%Pd/Al₂O₃, reaction temperature = 80°C, GHSV = 52580, 32577, 22534, 12385, 9366, 6660 and 4282 h⁻¹ (**APPENDIX J**). The effect of nanocrystalline porosity of α -Al₂O₃ obtained from various preparation methods on the catalytic properties of Pd/ α -Al₂O₃ was investigated in selective acetylene hydrogenation. The catalyst performances are shown by the plots of acetylene conversion \times ethylene selectivity versus the gas hourly space velocity (GHSV) in **Figure 5.29**. It was clearly seen that ethylene yield (%) was improved in the order of Pd/solvothermal-made α -Al₂O₃ > Pd/sol-gel made α -Al₂O₃ > Pd/precipitation-made α -Al₂O₃ catalysts. Among the three catalyst systems, the Pd/solvothermal-made α -Al₂O₃ showed better performance than catalysts supported on the other α -Al₂O₃ supports. Based on our characterization results, Pd/solvothermal-made α -Al₂O₃ had the appropriate total pore volume, highest Pd

active sites and metal dispersion of Pd on Al_2O_3 support and facilitated the reduction of PdO at lower temperature, which promoted acetylene conversion. Moreover, the TPD profiles of Pd/solvothermal-made $\alpha\text{-Al}_2\text{O}_3$ suggested that the amount of ethylene adsorbed at low temperature on the catalyst surface was highest which was important for the improvement of ethylene gain especially at high acetylene conversion.

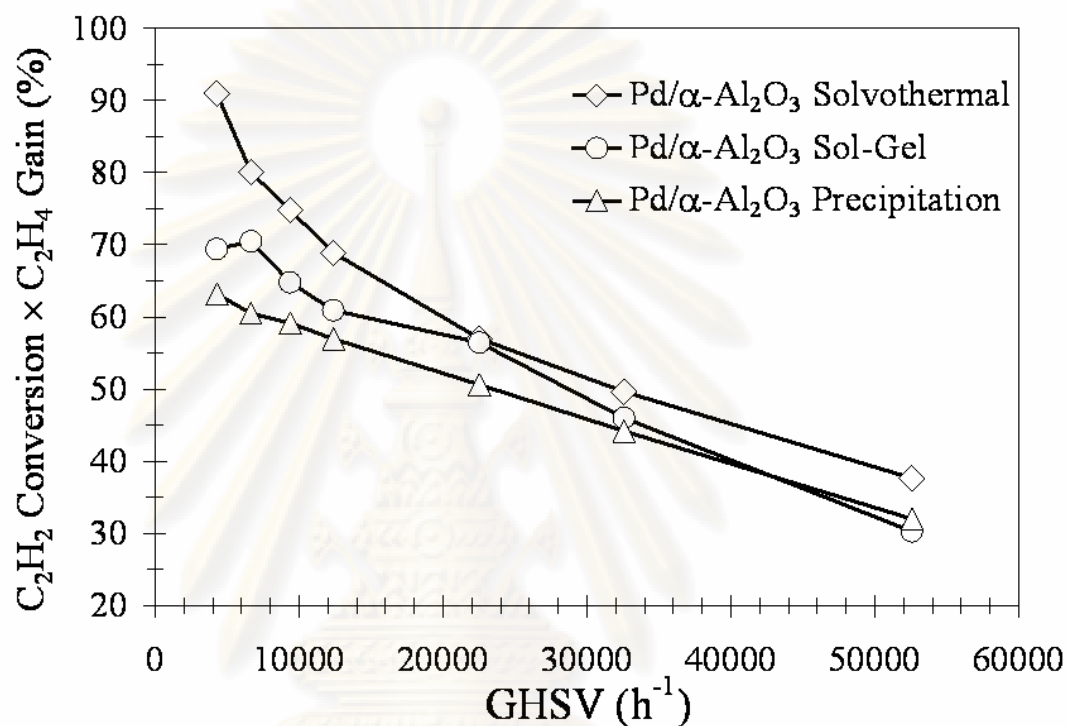


Figure 5.29 Performance of Pd/ $\alpha\text{-Al}_2\text{O}_3$ catalysts in the selective acetylene hydrogenation.

ศูนย์วิทยทรัพยากร
จุฬาลงกรณ์มหาวิทยาลัย

5.4 Influence of coke formation on Pd/ α -Al₂O₃

As it is known that Pd/ α -Al₂O₃ does a good job in the conversion of acetylene into ethylene, but its performance unavoidably slows down following the reaction process as the most acidic catalysts do. The main reason for this is due to the coke deposits on the surface of the catalysts. Therefore, one may say that a study of acidity and coke deposits on the surface could help in solving the problem of reducing the coke deposits and as a result, prolonging the catalyst life. Comparing the Pd catalyst supported on α -Al₂O₃ which received from different preparation methods, we found that coke deposit on Pd/ α -Al₂O₃ sol-gel was relatively less than the other ones, as shown in **Figure 5.30**. The acidity changes of the catalysts with temperature were shown in **Figure 5.31**. It can be seen that both the strong and weak acid sites decreased for the Pd/ α -Al₂O₃ sol-gel catalysts. These phenomena suggest that both the strong and weak acid sites could be coke deposit centers.

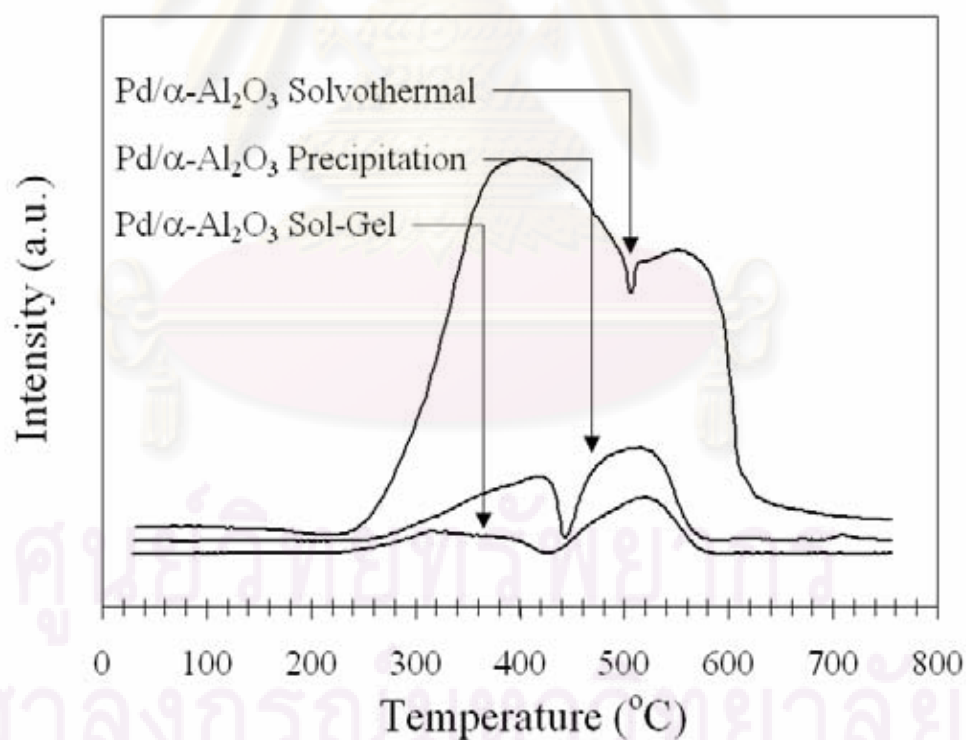


Figure 5.30 TPO profiles for the various Pd/ α -Al₂O₃ catalysts.

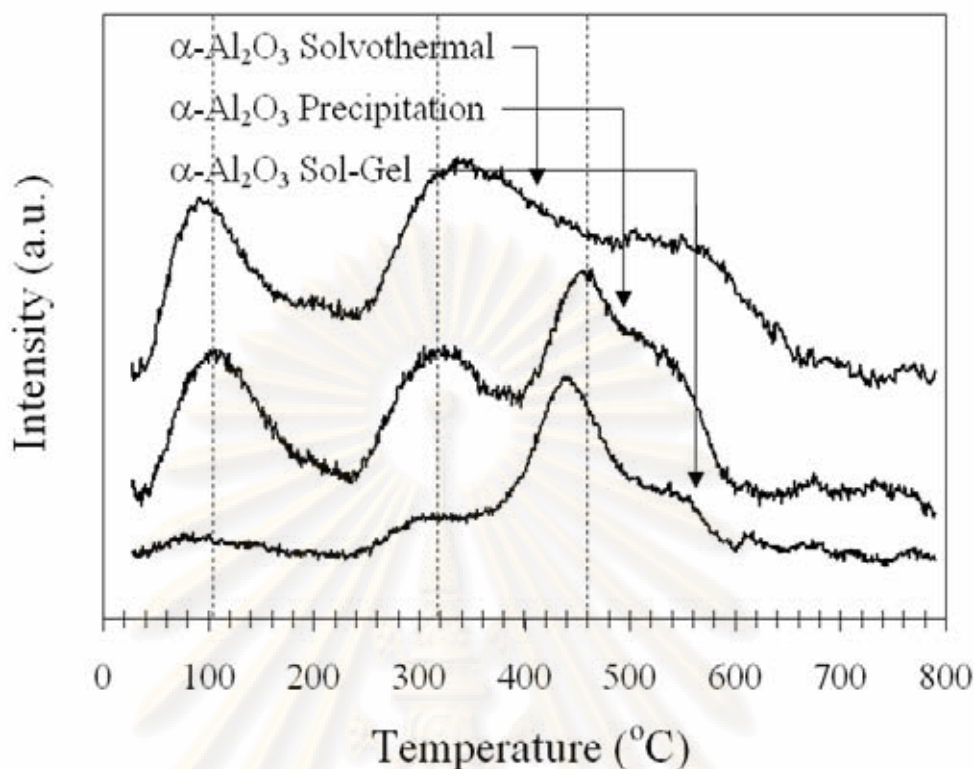


Figure 5.31 NH_3 -TPD profiles for the various $\alpha\text{-Al}_2\text{O}_3$ supports.

The selective hydrogenation of acetylene to form ethylene was carried out over Pd supported on solvothermal-, sol-gel and precipitation-made $\alpha\text{-Al}_2\text{O}_3$ catalyst at GHSV 9800 h^{-1} , 18800 h^{-1} , and 25700 h^{-1} with various temperatures as shown in **Figure 5.32**, **5.33**, and **5.34**, respectively. The activity of hydrogenation over Pd/ $\alpha\text{-Al}_2\text{O}_3$ sol-gel is higher than other ones at 40°C but activity of this catalyst is relatively lower at 60°C and 80°C which may possible be covered by coke deposition on the partial Pd particles during the reaction. It seems that the coke deposition is retarded on Pd/ $\alpha\text{-Al}_2\text{O}_3$ sol-gel due to the characteristic structure of sol-gel made $\alpha\text{-Al}_2\text{O}_3$. However, the ethylene selectivity was found to be little dropped when the Pd/ $\alpha\text{-Al}_2\text{O}_3$ sol-gel are performed at 80°C while the other catalysts was found to be apparently lower. It was demonstrated that the coke deposition on catalyst is much more that induced to hydrogen spillover which lead to ethane production. On the other hand, a little of coke deposition can create irreversibly on the palladium surface small A types of active site (responsible for selective to ethylene) [67].

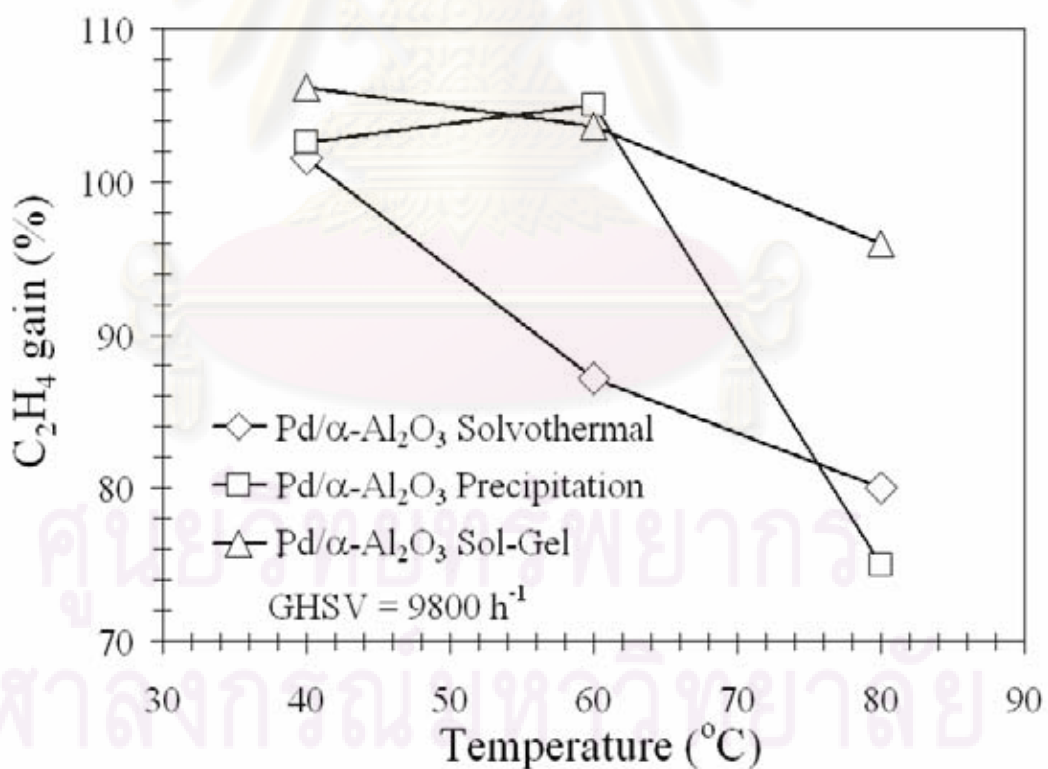
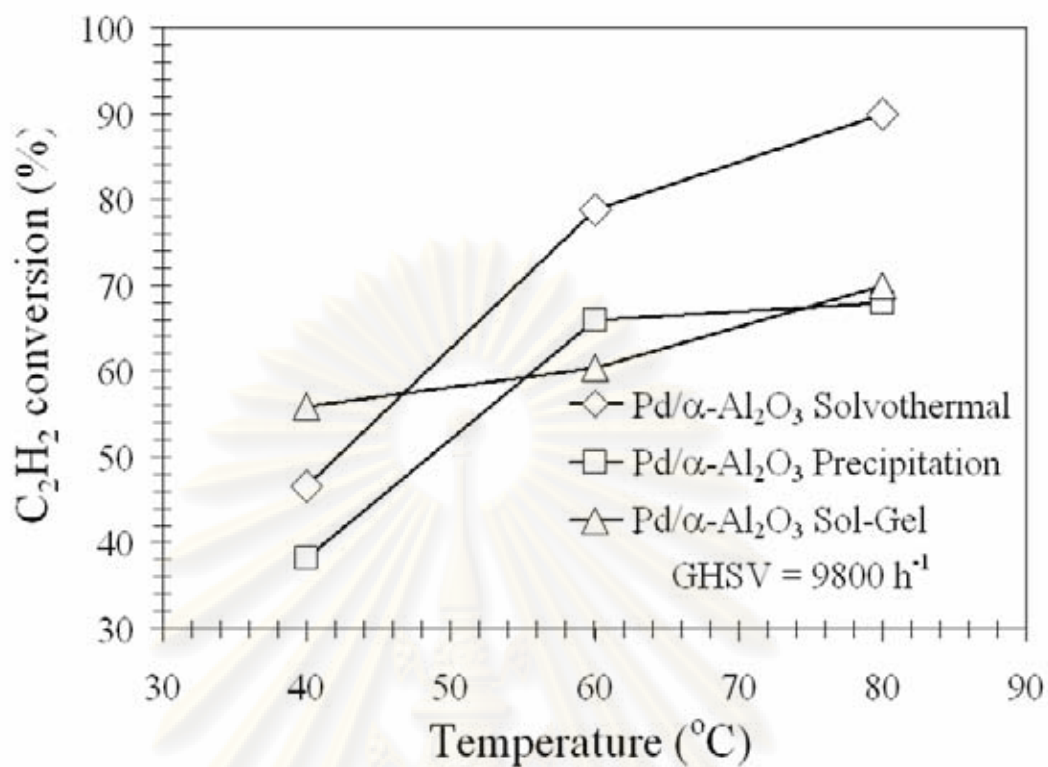


Figure 5.32 Performance of $Pd/\alpha-Al_2O_3$ catalysts in the selective acetylene hydrogenation with $GHSV = 9800\ h^{-1}$ and various temperatures.

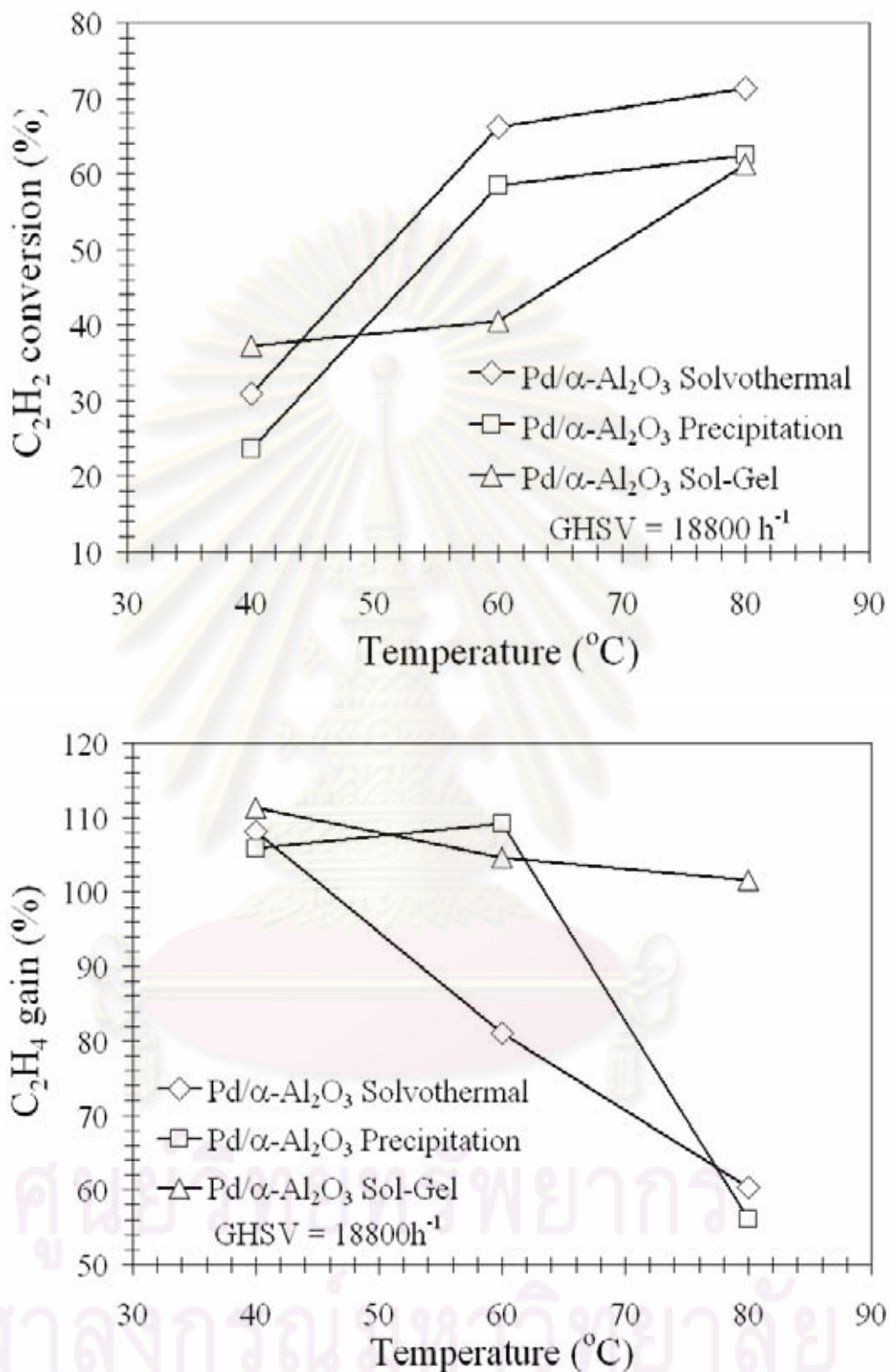


Figure 5.33 Performance of Pd/ α - Al_2O_3 catalysts in the selective acetylene hydrogenation with GHSV = 18800 h^{-1} and various temperatures.

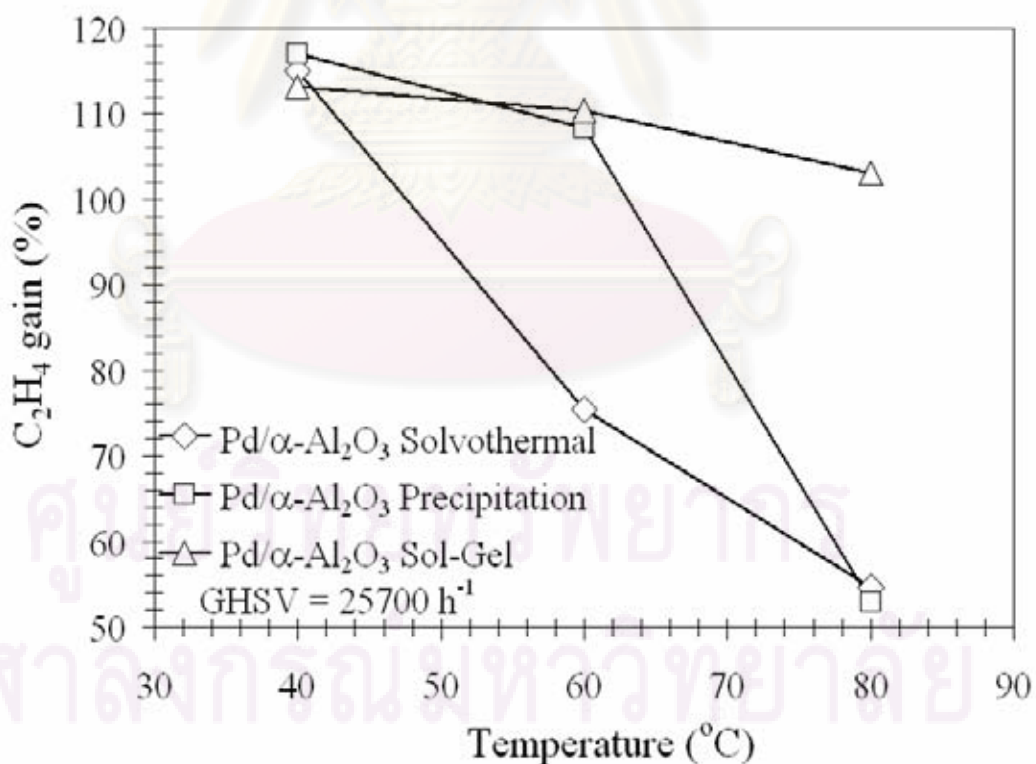
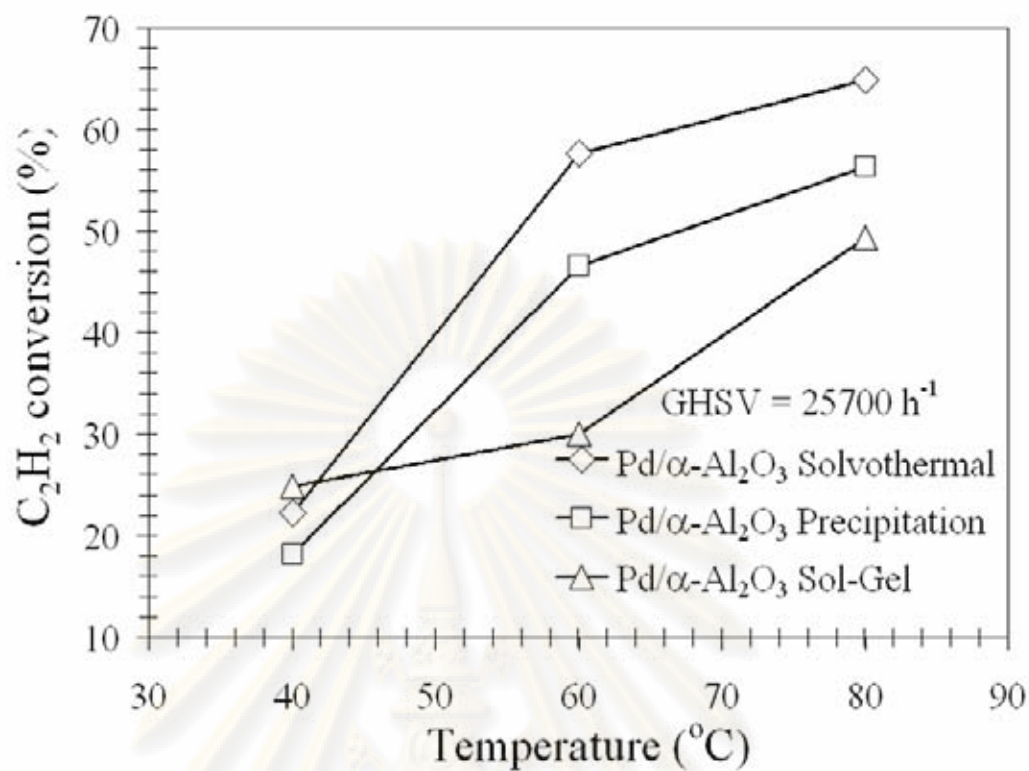


Figure 5.34 Performance of $Pd/\alpha-Al_2O_3$ catalysts in the selective acetylene hydrogenation with $GHSV = 25700\ h^{-1}$ and various temperatures.

5.5 Zinc modified α -Al₂O₃ for supported Pd catalyst

Performance of the Zn-modified α -Al₂O₃ for supported Pd catalyst in acetylene hydrogenation with various GHSV (52580, 32577, 22534, 12385 h⁻¹) has been compared with one of the Zn-modified α -Al₂O₃ from sol-gel and precipitation method as shown in **Figure 5.35**. Obviously, the ethylene selectivity is improved when the 0.5%Pd/(Zn/Al=0.3)Precipitation catalyst are used which compared to 0.5%Pd/(Zn/Al=0.3)Sol-Gel catalyst. These may possible be attribution of complete structure of ZnAl₂O₄ because the Zn-modified α -Al₂O₃ from precipitation method had disclosed this structure, as indicated in the **Figure 5.36**. Modification of α -Al₂O₃ with zinc can lead to form ZnAl₂O₄ spinel which is an interesting material with low acidity that can exhibit the strong metal-support interaction (SMSI) with noble metal [100]. Thus, the presence of ZnAl₂O₄ alone in the Zn-modified α -Al₂O₃ may improve the catalytic performance in the selective acetylene hydrogenation as well.

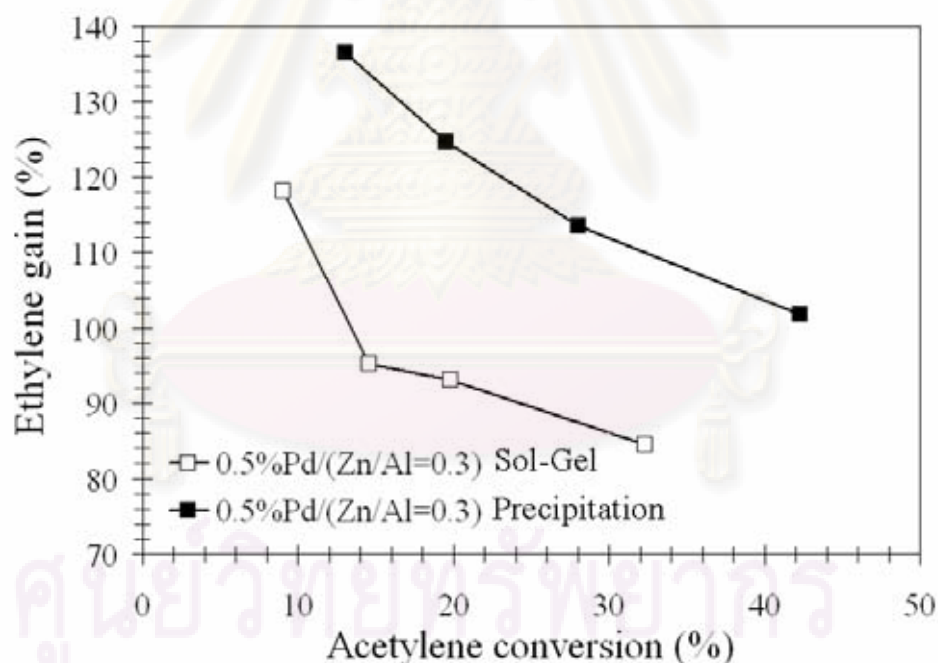


Figure 5.35 Performance of Pd/ α -Al₂O₃ catalysts in the selective acetylene hydrogenation with various GHSV at 40°C.

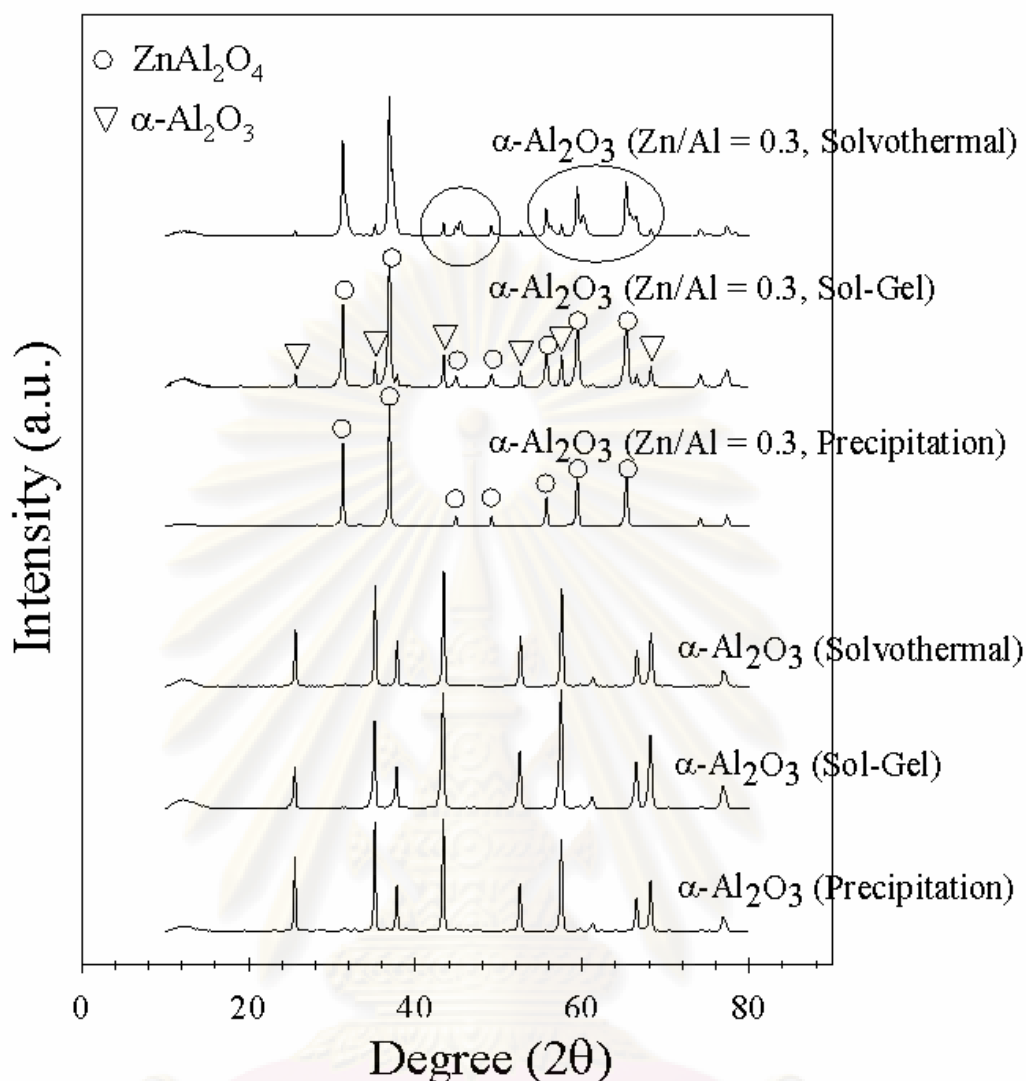


Figure 5.36 XRD patterns of the α - Al_2O_3 supports (Zn-modified and non-modified): solvothermal, sol-gel, and precipitation method.

It can be noticed from **Figure 5.36** that Zn-modified α - Al_2O_3 shows a complete structure of ZnAl_2O_4 in the order: Zn-modified α - Al_2O_3 -precipitation > Zn-modified α - Al_2O_3 -solvothermal > Zn-modified α - Al_2O_3 -sol-gel. The surface areas of the supports (non-modified) were similar to Zn-modified support for three preparation methods as shown in **Table 5.7**. The Zn-modified and non-modified α - Al_2O_3 by sol-gel possessed the surface area 1.1 and 1.8 m^2/g , respectively, while those prepared by precipitation and solvothermal was found to be apparently higher. The surface areas were quite low probably due to high agglomeration of these nanocrystalline particles during calcination at high temperature.

Table 5.7 Specific surface area of catalyst supports (Zn-modified and non-modified) from various preparation methods.

Catalyst supports	BET surface area (m ² /g)
α -Al ₂ O ₃ (Precipitation)	5.1
α -Al ₂ O ₃ (Sol-Gel)	1.8
α -Al ₂ O ₃ (Solvothermal)	8.3
α -Al ₂ O ₃ Zn/Al = 0.3 (Precipitation)	6.2
α -Al ₂ O ₃ Zn/Al = 0.3 (Sol-Gel)	1.1
α -Al ₂ O ₃ Zn/Al = 0.3 (Solvothermal)	10.7

The catalytic properties of Pd/ α -Al₂O₃ and Pd/Zn-modified α -Al₂O₃ catalysts which α -Al₂O₃ obtained via solvothermal method were evaluated in the selective hydrogenation of acetylene with a various temperature (40, 60, and 80°C) by SV-4 or SV-Zn-4, SV-3 or SV-Zn-3, SV-2 or SV-Zn-2, SV-1 or SV-Zn-1 represent as GHSV at 52580, 32577, 22534, 12385 h⁻¹, respectively. For performance comparison of catalysts based on α -Al₂O₃ support via solvothermal method are shown in **Figure 5.37**. In all cases, acetylene conversion increased with increasing temperature while ethylene selectivity decreases due to the fact that the ethylene is produced as an intermediate in acetylene hydrogenation reaction. These results are in good agreement of any GHSV which with a decrease in GHSV, the catalytic performance of catalysts was enhanced to attain a better value for acetylene conversion and ethylene gain. It was clearly seen that the use of Zn-modified α -Al₂O₃ prepared by solvothermal method resulted in much better acetylene conversion but to lower ethylene gain when compared to the non-modified α -Al₂O₃. Modification of Pd/ α -Al₂O₃ catalysts with Zn, however, resulted in significantly improvement of both acetylene conversion and ethylene selectivity at high temperature (80°C).

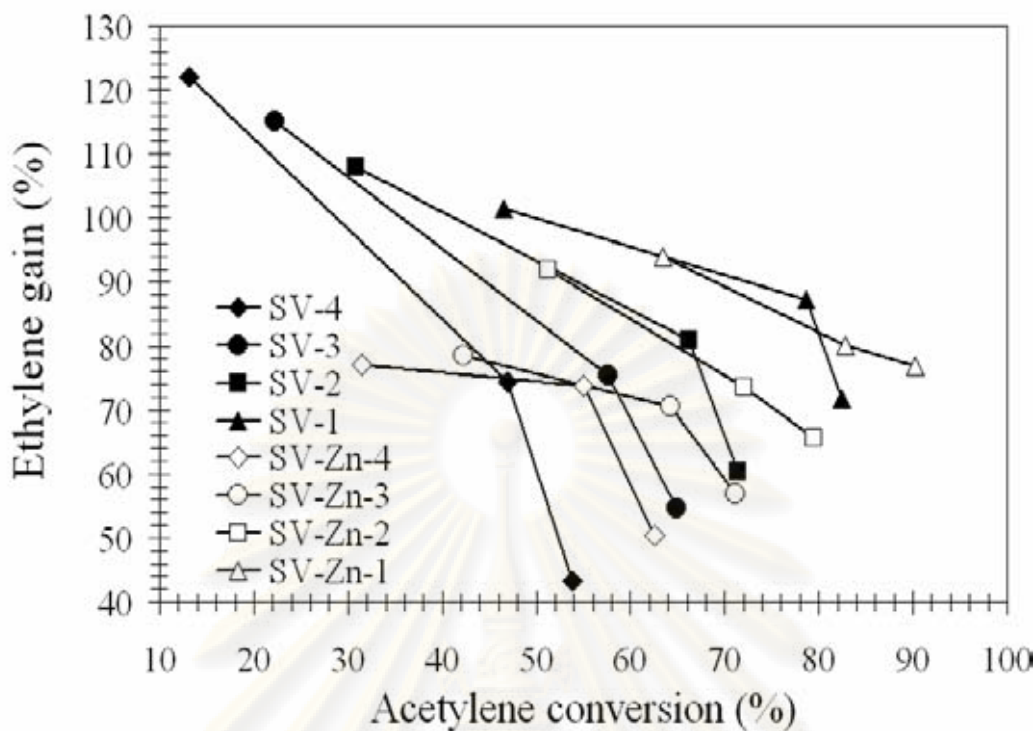


Figure 5.37 Performance of Pd/ α -Al₂O₃ catalysts supported on α -Al₂O₃ from solvothermal method in the selective acetylene hydrogenation with various temperatures in the four GHSV values.

As shown in **Figure 5.38**, the modification of Zn to α -Al₂O₃ support via sol-gel method had no effect on improvement of acetylene conversion and ethylene gain for Pd/Zn-modified α -Al₂O₃ catalysts. However, the decreasing of acetylene conversion and ethylene gain for Pd/Zn-modified α -Al₂O₃, suggesting that the incomplete of Zn penetrate to α -Al₂O₃ structure lead to poor dispersion of Pd particles on support, which may be occurs because the Pd metal is covered by Zn. It has been reported that ethylene selectivity is lower on the low-index Pd surface, e.g., Pd(100), than on the high-index surface, e.g., Pd(111) [88].

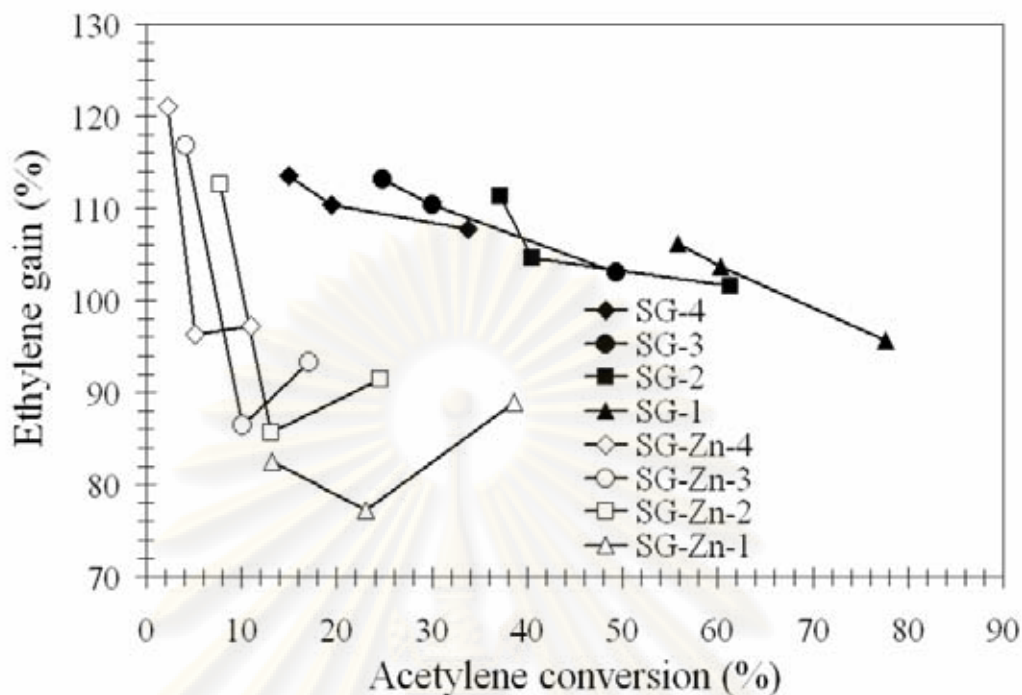


Figure 5.38 Performance of Pd/ α -Al₂O₃ catalysts supported on α -Al₂O₃ from sol-gel method in the selective acetylene hydrogenation with various temperatures in the four GHSV values.

The zinc-modified α -Al₂O₃ catalysts had a complete structure of ZnAl₂O₄ by using precipitation method. The physicochemical properties of Pd/zinc-modified α -Al₂O₃ used in selective hydrogenation of acetylene were investigated, as shown in **Figure 5.39**. It was found that the activity and selectivity to ethylene of the Pd/zinc-modified α -Al₂O₃ with complete structure of ZnAl₂O₄ of support were negatively modified by incorporation of zinc into Al₂O₃ structure. However, this influence of complete structure of ZnAl₂O₄ was much more significant for high temperature, which means that ethylene gain of Pd/zinc-modified α -Al₂O₃ is higher than Pd/ α -Al₂O₃ at temperature about 80°C.

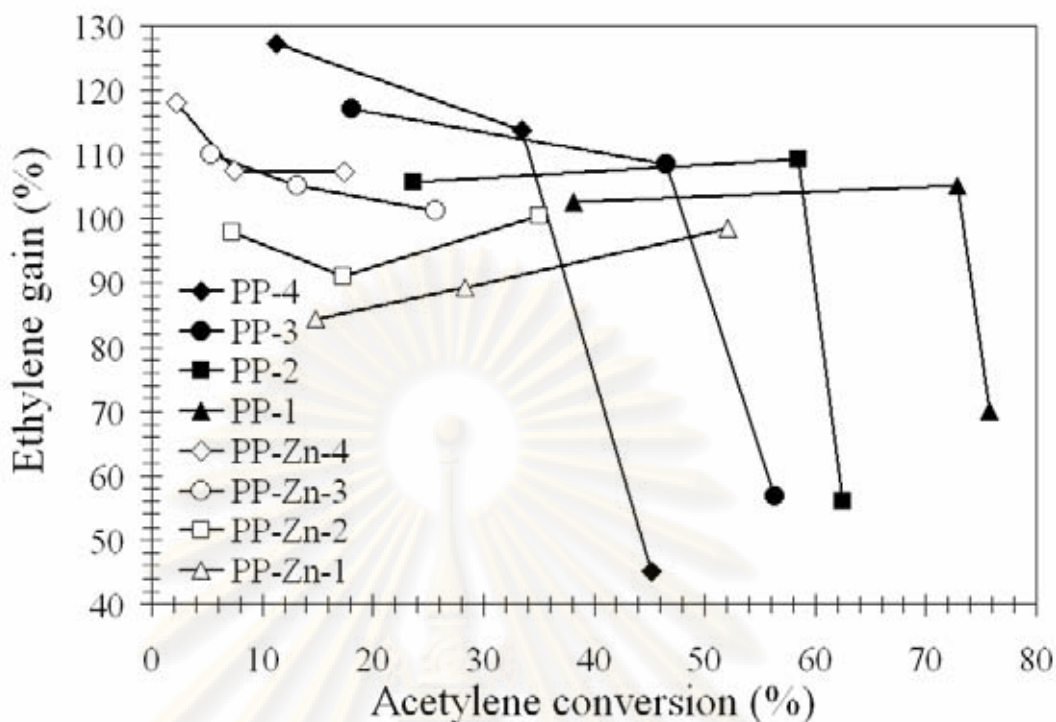


Figure 5.39 Performance of Pd/ α -Al₂O₃ catalysts supported on α -Al₂O₃ from precipitation method in the selective acetylene hydrogenation with various temperatures in the four GHSV values.

The activity and selectivity to ethylene of Pd/ α -Al₂O₃ catalysts depends on the degree of depletion in the Zn-modified α -Al₂O₃. As above results indicate that it is possible to obtain perfection of ZnAl₂O₄ via precipitation method when all of zinc is part of the solid structure. This occurrence of Zn-modified α -Al₂O₃ when used as catalyst support for Pd metal led to enhance the ethylene gain whereas the deterioration of acetylene conversion at high temperature reaction. Moreover, Zn-modified α -Al₂O₃ prepared by solvothermal method was not complete to ZnAl₂O₄ but it had remain together of α -Al₂O₃ and ZnAl₂O₄ resulted in the enhancement of acetylene conversion ranging from 40 to 60°C and the both of acetylene conversion and ethylene gain in the vicinity of 80°C. However, the Zn-modified α -Al₂O₃ prepared by sol-gel method had not improvement the catalyst because of overabundant incomplete of support structure. One of the probable interpretations of it was that ZnAl₂O₄ structure within α -Al₂O₃ support from sol-gel method less than the solvothermal method.

CHAPTER VI

CONCLUSIONS AND RECOMMENDATIONS

6.1 Conclusions

- In the mixed-phases Al_2O_3 support for supported Pd catalyst in selective acetylene hydrogenation, the conclusion could be drawn as follows:

Among the five crystalline phase compositions of alumina used in this study, the one containing 64% $\alpha\text{-Al}_2\text{O}_3$ was found to be the best (optimum) composition to prepare Pd/ Al_2O_3 catalysts with high acetylene conversion and high ethylene selectivity. The presence of transition-phase Al_2O_3 in $\alpha\text{-Al}_2\text{O}_3$ resulted in combined properties of the transition Al_2O_3 .

- In the effects of support crystallite size and reduction temperature on the properties of Pd/ $\alpha\text{-Al}_2\text{O}_3$ catalysts in selective acetylene hydrogenation, the following conclusions were drawn:

The improvement of activity would be due to the increasing of Pd active sites while the reduction on lower temperature and lower ethylene chemisorption would promote the ethylene selectivity. The catalytic performance of Pd/nanocrystalline $\alpha\text{-Al}_2\text{O}_3$ catalyst increased after reduction at higher temperature due to the formation of SMSI, which promoted the ethylene selectivity. While the Pd/micron-sized $\alpha\text{-Al}_2\text{O}_3$ catalyst exhibited lower catalytic activity, which due to the sintering of Pd metal. The different between Pd behaviors on those two supports after reduction at high temperature would be explained by the different of interaction between Pd and $\alpha\text{-Al}_2\text{O}_3$ support, which confirmed by the XPS results.

- In influence of preparation method on the nanocrystalline porosity of $\alpha\text{-Al}_2\text{O}_3$ and the catalytic properties of Pd/ $\alpha\text{-Al}_2\text{O}_3$ in selective acetylene hydrogenation, the conclusion could be drawn as follows:

Suitable properties of the solvothermal-derived α -Al₂O₃ such as high surface area and narrow pore size distribution were found to result in the best catalyst performance of Pd/ α -Al₂O₃ catalysts in the selective hydrogenation of acetylene. The α -Al₂O₃ solvothermal not only provided the highest Pd dispersion and smallest Pd particle size but it also facilitated H₂ reduction at low temperature and desorption of ethylene and CO.

- The coke deposition on catalyst during reaction increases in the following order: Pd/ α -Al₂O₃ sol-gel < Pd/ α -Al₂O₃ precipitation < Pd/ α -Al₂O₃ solvothermal.
- Modification of Pd/ α -Al₂O₃ catalysts with Zn which prepared from solvothermal method resulted in significantly improvement of both acetylene conversion and ethylene selectivity at temperature 80°C.

6.2 Recommendations

The studies in effect of Al₂O₃ support for supported Pd catalyst via selective acetylene hydrogenation are still some unclear explanation needed to be further studied in the aspect of:

1. The alumina support as various phases are different crystal structures which maybe to characteristic properties in each phases of alumina. There are several problems connected with the explanation of the role the mixed phases which require further investigation such as the restructuring of various phase within mixed phases and the adsorption ability of π - and σ -bond of reactant on mixed phases.
2. The results from temperature programmed desorption are still open for discussion to complete understanding of the characteristic of peak.

จุฬาลงกรณ์มหาวิทยาลัย

REFERENCES

-
- [1] A.J. Peacock. Handbook Polyethylene: Structures, properties, and applications. New York: Marcel Decker, Basel (2000).
- [2] P.M. Morse. Ethylene market stretched thin. *Chemical & Engineering News* 77 (1999): 20-22.
- [3] L.L. Bohm. The ethylene polymerization with Ziegler catalysts: Fifty years after the discovery. *Angewandte Chemie-International Edition* 42 (2003): 5010-5030.
- [4] E. Groppo, C. Lamberti, S. Bordiga, G. Spoto, A. Zecchina. The structure of active centers and the ethylene polymerization mechanism on the Cr/SiO₂ catalyst: A frontier for the characterization methods. *Chemical Reviews* 105 (2005): 115-183.
- [5] A.N.R. Bos, K.R. Westerterp. Mechanism and kinetics of the selective hydrogenation of ethyne and ethene. *Chemical Engineering and Processing* 32 (1993): 1-7.
- [6] H. Arnold, F. Dobert, J. Gaube. Hydrogenation reaction, in: G. Ertl, H. Knozinger, J. Weitkamp (Eds.): Handbook of Heterogeneous Catalysis, Wiley, New York, 5 (1997): 2165-2186.
- [7] A. Molnar, A. Sarkany, M. Varga. Hydrogenation of carbon-carbon multiple bonds: chemo-, regio- and stereo-selectivity. *Journal of Molecular Catalysis A-Chemical* 173 (2001): 185-221.
- [8] P. Albers, J. Pietsch, S.F. Parker. Poisoning and deactivation of palladium catalysts. *Journal of Molecular Catalysis A-Chemical* 173 (2001): 275-286.
- [9] F.A. Lewis. The Palladium Hydrogen System, Academic Press, London (1967).
- [10] Periodic table of elements. 3. Edt., Weinheim, Wilye-VCH (2002).
- [11] V. Pallassana, M. Neurock. Electronic factors governing ethylene hydrogenation and dehydrogenation activity of pseudomorphic Pd-ML/Re(0001), Pd-ML/Ru(0001), Pd(111), and Pd-ML/Au(111) surfaces. *Journal of Catalysis* 191 (2000): 301-317.
- [12] F. Mittendorfer, C. Thomazeau, P. Raybaud, H. Toulhoat. Adsorption of unsaturated hydrocarbons on Pd(111) and Pt(111): A DFT study. *Journal*

-
- of Physical Chemistry B* 107 (2003): 12287-12295.
- [13] R.S. Zhou, R.L. Snyder. Structure and transformation mechanisms of the eta, gamma and theta transition aluminas. *Acta Crystallograp B* 47 (1991): 617-630.
- [14] H.P. Santos, P.S. Santos. Pseudomorphic formation of aluminas from febrile pseudoboehmite. *Material Letters* 13 (1992): 175-179.
- [15] N.S. Schbib, M.A. García, C.E. Gigola, A.F. Errazu. Kinetics of front-end acetylene hydrogenation in ethylene production. *Industrial & Engineering Chemistry Research* 35 (1996): 1496-1505.
- [16] W. Huang. Optimize Acetylene Removal. *Hydrocarbon Processing* 59 (1979): 131.
- [17] M.W. Brown, A. Penlidis, G. Sullivan. Control policies for an industrial acetylene hydrogenation reactor. *The Canadian Journal of Chemical Engineering* 69 (1991): 152-164.
- [18] E.W. Shin, J.H. Kang, W.K. Kim, J.D. Park, S.H. Moon. Performance of Si-modified Pd catalyst in acetylene hydrogenation: the origin of the ethylene selectivity improvement. *Applied Catalysis A: General* 223 (2002): 161-172.
- [19] K.R. Westerterp, A.N.R. Bos. *Inzynieria Chemiczna I Procesowa* 21 (2000): 7.
- [20] J. Gislason, W.S. Xia, H. Sellers. Selective hydrogenation of acetylene in an ethylene rich flow: Results of kinetic simulations. *Journal of Physical Chemistry A* 106 (2002): 767-774.
- [21] M.M. Johnson. *US Patent* 4 404 124 (1983).
- [22] V. Rives, F.M. Labajos, R. Trujillano, E. Romeo, C. Royo, A. Monzón. Acetylene hydrogenation on Ni-Al-Cr oxide catalysts: the role of added Zn. *Applied Clay Science* 13 (1998): 363-379.
- [23] P. Prasertdam, B. Ngamsom, N. Bogdanchikova, S. Phatanasri, M. Pramotthana. Effect of the pretreatment with oxygen and/or oxygen-containing compounds on the catalytic performance of Pd-Ag/Al₂O₃ for acetylene hydrogenation. *Applied Catalysis A: General* 230 (2002): 41-51.
- [24] G. Deganello, D. Duca, F. Frusteri, A. Parmaliana. Selective hydrogenation of acetylene in ethylene feedstocks on Pd catalysts. *Applied Catalysis A:*

General 146 (1996): 269-284.

- [25] C.L. Gordon, R.G. Mallinson, L.L. Lobban. *Abstracts of Papers of the American Chemical Society* 220 (2000): 9-CATL Part 2.
- [26] J. Panpranot, K. Kontapakdee, P. Prasertthdam. Effect of TiO₂ crystalline phase composition on the physicochemical and catalytic properties of Pd/TiO₂ in selective acetylene hydrogenation. *Journal of Physical Chemistry B* 110 (2006): 8019-8024.
- [27] Y. Li, B. Xu, Y. Fan, N. Feng, A. Qiu, J. Miao, J. He, H. Yang, Y. Chen. The effect of titania polymorph on the strong metal-support interaction of Pd/TiO₂ catalysts and their application in the liquid phase selective hydrogenation of long chain alkadienes. *Journal of Molecular Catalysis A* 216 (2004): 107-114.
- [28] J. Sheridan. The metal-catalysed reaction between acetylene and hydrogen. Part V. Reaction over palladium, iron, and some other catalysts. *Journal of Chemical Society* (1945): 470-476.
- [29] K. Tamaru. On retardation of catalysis. The catalytic reaction between acetylene and hydrogen. *Bulletin of the Chemical Society of Japan* 23 (1950): 64-66.
- [30] G.C. Bond, P.B. Wells. The hydrogenation of acetylene. II. The reaction of acetylene with hydrogen catalyzed by alumina-supported palladium. *Journal of Catalysis* 5 (1965): 65-73.
- [31] G.C. Bond, G. Webb, P.B. Wells, J.M. Winterbottom. Patterns of behavior in catalysis by metals. *Journal of Catalysis* 1 (1962): 74-84.
- [32] G.C. Bond, D.A. Dowden, N. Mackenzie. The selective hydrogenation of acetylene. *Transaction of the Faraday Society* 54 (1958): 1537-1546.
- [33] G.C. Bond, J. Newham, P.B. Wells. The selective hydrogenation of unsaturated hydrocarbons, In Proceedings of 2nd International Congress on Catalysis, Technip, Paris, (1960): 1177-1180.
- [34] A. Borodziński, A. Cybulski. The kinetic model of hydrogenation of acetylene-ethylene mixtures over palladium surface covered by carbonaceous deposits. *Applied Catalysis A: General* 198 (2000): 51-66.
- [35] W.T. McGown, C. Kemball, D.A. Whan. Hydrogenation of acetylene in excess ethylene on an alumina-supported palladium catalyst at atmospheric pressure in a spinning reactor. *Journal of Catalysis* 51 (1978): 173-184.

-
- [36] J. Margitfalvi, L. Guzzi, A.H. Weiss. Reaction of acetylene during hydrogenation on Pd black catalyst. *Journal of Catalysis* 72 (1981): 185-198.
- [37] S. Asplund. Coke formation and its effect on internal mass transfer and selectivity in Pd-catalysed acetylene hydrogenation. *Journal of Catalysis* 158 (1996): 267-278.
- [38] G.C. Battiston, L. Dalloro, G.R. Tauszik. Performance and aging of catalysts for the selective hydrogenation of acetylene: a micropilot-plant study. *Applied Catalysis A: General* 2 (1982): 1-17.
- [39] H. Cutmann, H. Lindlar. Partial Catalytic Hydrogenation of Acetylenes. In: Viehe, H.G. ed., *Chemistry of Acetylenes*. New York: Marcel Dekker (1969): 355-362.
- [40] S.A. Miller. *Acetylene: Its Properties, Manufacture and Uses, vol. 2*. London: Ernest Benn Ltd. (1966).
- [41] S.M. Davis, F. Zaera, G.A. Somorjai. The reactivity and composition of strongly adsorbed carbonaceous deposits on platinum. Model of working hydrocarbon conversion catalyst. *Journal of Catalysis* 77 (1982): 439-459.
- [42] F. Zaera. On the mechanism for the hydrogenation of olefins on transition-metal surfaces: The chemistry of ethylene on Pt(111). *Langmuir* 12 (1996): 88-94.
- [43] P. Cremer, X. Su, Y.R. Shen, G.A. Somorjai. Ethylene hydrogenation on Pt(111) monitored in situ at high pressures using sum frequency generation. *Journal of the American Chemical Society* 118 (1996): 2942-2949.
- [44] W.J. Kim, J.H. Kang, I.Y. Ahn, S.H. Moon. Deactivation behavior of a TiO₂-added Pd catalyst in acetylene hydrogenation. *Journal of Catalysis* 226 (2004): 226-229.
- [45] A. Sandell, A. Beutler, A. Jaworski, M. Wiklund, K. Heister, R. Nyholm, J.N. Andersen. Adsorption of acetylene and hydrogen on Pd(111): formation of well-ordered ethylidyne overlayer. *Surface Science* 415 (1998): 411-422.
- [46] W. Palczewska. Catalytic reactivity of hydrogen on palladium and nickel

-
- hydride phases. *Advance Catalysis* 24 (1975): 235-291.
- [47] W. Palczewska. Catalytic properties of metal hydrides. In *Hydrogen Effects in Catalysis*; Z. Paál and P.G. Menon (eds); Marcel Dekker: New York, (1988): 373-395.
- [48] A. Borodziński. The effect of carburization of palladium catalysts on the hydrogenation of acetylene-ethylene mixtures. *Polish Journal of Chemistry* 72 (1998): 2455-2462.
- [49] R.H. Siller, W.A. Oates, R.B. McLellan. Solubility of carbon in palladium and platinum. *Journal of the Less-Common Metals* 16 (1968): 71-73.
- [50] R.-J. Liu, P.A. Crozier, C.M. Smith, D.A. Hucul, J. Blackson, G. Salaita. Metal sintering mechanisms and regeneration of palladium/alumina hydrogenation catalysts. *Applied Catalysis A: General* 282 (2005): 111-121.
- [51] S. LeViness, V. Nair, A.H. Weiss, Z. Schay, L. Gucci. Acetylene hydrogenation selectivity control on PdCu/Al₂O₃ catalysts. *Journal of Molecular Catalysis* 25 (1984): 131-140.
- [52] A.H. Weiss, S. LeViness, V. Nair, L. Gucci, A. Sárkány, Z. Schay. The effect of Pd dispersion in acetylene selective hydrogenation. In *Proceedings of the 8th International Congress on Catalysis*; Verlag: Weinheim; 5 (1984): 591.
- [53] A. Borodziński. The effect of carbonaceous deposits of alumina on hydrogenation of acetylene-ethylene mixture on Pd/Al₂O₃ catalyst. *Polish Journal of Chemistry* 69 (1995): 111-117.
- [54] G.C. Bond. The role of carbon deposits in metal-catalysed reaction of hydrocarbons. *Applied Catalysis A: General* 149 (1997): 3-25.
- [55] G.C. Bond, J. Sheridan. The hydrogenation of methylacetylene. *Transactions of the Faraday Society* 48 (1952): 651-658.
- [56] A. Borodziński, A. Golebiowski. Surface heterogeneity of supported palladium catalyst for the hydrogenation of acetylene-ethylene mixtures. *Langmuir* 13 (1997): 883-887.
- [57] E. Wicke, H. Brodowsky, H. Zuechner. Hydrogen in palladium and palladium alloys. In *Hydrogen in Metals*. G. Alefeld and J. Völkl (eds.); Springer Verlag: Berlin, 2 (1978): 73-155.
- [58] M. Boudart, H.S. Hwang. Solubility of hydrogen in small particles of

-
- palladium. *Journal of Catalysis* 39 (1975): 44-52.
- [59] A. Frackiewicz, A. Janko, J. Stachurski. Carburization of palladium catalysts during hydrogenation of acetylene. *Geterog. Katal.* (1979): 135-138.
- [60] L. Kepiński, M. Wołczyr, J.M. Jabłoński. Effect of high-temperature reduction on carburization of alumina-supported palladium: evidence for palladium-aluminium alloys formation. *Applied Catalysis* 54 (1989): 267-276.
- [61] R. Burch, F.A. Lewis. Absorption of hydrogen by palladium + boron and palladium + silver + boron alloys. *Transactions of the Faraday Society* 66 (1970): 727-735.
- [62] T.-C. Chang, J.-J. Chen, C.-T. Yeh. Temperature-programmed reduction and temperature-resolved sorption of strong-support interaction in supported palladium catalysts. *Journal of Catalysis* 96 (1985): 51-57.
- [63] H. Hoffmann, F. Zaera, R.M. Ormerod, R.M. Lambert, J.M. Yao, D.K. Saldin, L.P. Wang, D.W. Bennett, W.T. Tysoe. A near edge X-ray absorption fine structure and photoelectron spectroscopic study of the structure of acetylene on Pd(111) at low temperature. *Surface Science* 268 (1992): 1-10.
- [64] M. Kaltchev, A.W. Thompson, W.T. Tysoe. Reflection-absorption infrared spectroscopy of ethylene on palladium(111) at high pressure. *Surface Science* 391 (1997): 45-149.
- [65] L.L. Kesmodel, J.A. Gates. Ethylene adsorption and reaction on Pd(111): an angle-dependent EELS analysis. *Surface Science* 111 (1981): L747-L754.
- [66] W.T. Tysoe, G.L. Nyberg, R.M. Lambert. Selective hydrogenation of acetylene over palladium in ultra high vacuum. *Journal of Physical Chemistry* 90 (1986): 3188-3192.
- [67] A. Borodziński. Hydrogenation of acetylene-ethylene mixtures on commercial palladium catalyst. *Catalysis Letters* 63 (1999): 35-42.
- [68] J.J. Rooney, G. Webb. The importance of π bonded intermediates in hydrocarbon reactions on transition metal catalysts. *Journal of Catalysis* 3 (1964): 488-501.
- [69] G.C. Bond, P.B. Wells. The hydrogenation of acetylene. IV. The reaction of acetylene with deuterium catalyzed by alumina-supported rhodium, palladium, iridium, and platinum. *Journal of Catalysis* 6 (1966): 397-410.

-
- [70] G. Webb. Catalytic Hydrogenation. In *Comprehensive Chemical Kinetics*; C.H. Bamford, C.F.H. Tipper, Eds.; Elsevier: Amsterdam, 20 (1978): 1-121.
- [71] V. Ponec, G.C Bond. Catalysis by metals and alloys. *Studies in Surface Science and Catalysis* 95 (1995): 477-539.
- [72] J. Heaviside, P. Hendra, P. Tsai, R. Cooney. Adsorption and polymerization of acetylene on oxide surfaces. *Faraday Transactions I* 74 (1978): 2542-2549.
- [73] M. Larsson, J. Jansson, S. Asplund. Incorporation of deuterium in coke formed on an acetylene hydrogenation catalyst. *Journal of Catalysis* 162 (1996): 365-367.
- [74] A. Sárkány, Zs. Révay. Some features of acetylene and 1,3-butadiene hydrogenation on Ag/SiO₂ and Ag/TiO₂ catalysts. *Applied Catalysis A: General* 243 (2003): 347-355.
- [75] W.J. Kim, E.W. Shin, J.H. Kang, S.H. Moon. Performance of Si-modified Pd catalyst in acetylene hydrogenation: the origin of the ethylene selectivity improvement. *Applied Catalysis A: General* 223 (2002): 161-172.
- [76] M. Larsson, J. Jansson, S. Asplund. The role of coke in acetylene hydrogenation on Pd/ α -Al₂O₃. *Journal of Catalysis* 178 (1998): 49-57.
- [77] F. Kapteijn, G.B Marin, J.A. Moulijn. Catalytic reaction engineering. *Studies in Surface Science and Catalysis* 123 (1999): 375-431.
- [78] H.H. Lee. Local effective diffusivity in a pellet deactivated by multilayer coking. *AIChE Journal* 40 (1994): 2022-2027.
- [79] A. Borodziński. The effect of palladium particle size on the kinetics of hydrogenation of acetylene-ethylene mixtures over Pd/SiO₂ catalysts. *Catalysis Letters* 71 (2001): 169-175.
- [80] G.C. Bond. The addition of hydrogen to carbon-carbon triple bonds. In *Catalysis*; P.H. Emmett (ed); Reinhold: New York, (1955): 109-148.
- [81] J. Tai, K. Haraki, J.H. Kondo, K. Domen, K. Tamaru. Selective hydrogenation of acetylene over Au/Al₂O₃. *Journal of Physical Chemistry B* 104 (2000): 11153-11156.
- [82] Fachbeirat Report 2005; Teschner et al. Alkyne hydrogenation over Pd catalysts: A new paradigm. *Journal of Catalysis* 242 (2006): 26-37.

-
- [83] A.M. Doyle, Sh. Shaikhutdinov, S.D. Jackson, H.-J. Freund. *Angewandte Chemie* 42 (2003): 5240.
- [84] S.B. Zdonik, L.P. Hallee, E.J. Green. *Manufacturing Ethylene*. Tulsa, Oklahoma: Petroleum Publishing Co. (1970).
- [85] A. Borgna, B. Moraweck, J. Massardier, A. Renouperz. New supported palladium-chromium catalysts: characterization and catalytic properties. *Journal of Catalysis* 128 (1991): 99-112.
- [86] A. Sarkany, Z. Zsoldos, G. Stefler, J.W. Hightower, L. Gucci. Promoter effect of Pd in hydrogenation of 1,3-butadiene over Co-Pd catalysts. *Journal of Catalysis* 157 (1995): 179-189.
- [87] Y.H. Park, G.L. Price. Promotional effects of potassium on palladium/alumina selective hydrogenation catalysts. *Industrial & Engineering Chemistry Research* 31 (1992): 469-474.
- [88] A. Sárkány, A.H. Weiss, L. Gucci. Structure sensitivity of acetylene-ethylene hydrogenation over Pd catalysts. *Journal of Catalysis* 98 (1986): 550-553.
- [89] J. Phillips, A. Auroux, G. Bergeret, J. Massardier, A. Renoupez. Phase behavior of palladium-silver particles supported on silica. *Journal of Physical Chemistry* 97 (1993): 3565-3570.
- [90] H. Aduriz, D. Bodnariuk, B. Coq, F. Figueras. Alumina-supported bimetallics of palladium alloyed with germanium, tin, lead, or antimony from organometallic precursors II. gas-phase hydrogenation of 2-methyl-1-buten-3-yne (valylene) and 2-methyl-1,3-butadiene (isoprene) *Journal of Catalysis* 129 (1991): 47-57.
- [91] D.C. Huang, K.H. Chang, W.F. Pong, P.K. Tseng, K.J. Hung, W.F. Hung. Effect of Ag-promotion on Pd catalysts by XANES. *Catalysis Letters* 53 (1998): 155-159.
- [92] J.H. Kang, E.W. Shin, W.J. Kim, J.D. Park, S.H. Moon. Selective Hydrogenation of Acetylene on TiO₂-Added Pd Catalysts. *Journal of Catalysis* 208 (2002): 310-320.
- [93] J.H. Kang, E.W. Shin, W.J. Kim, J.D. Park, S.H. Moon. Selective hydrogenation of acetylene on Pd/SiO₂ catalysts promoted with Ti, Nb and Ce oxides. *Catalysis Today* 63 (2000): 183-188.
- [94] W.J. Kim, J.H. Kang, I.Y. Aha, S.H. Moon. Deactivation behavior of a

-
- TiO₂-added Pd catalyst in acetylene hydrogenation. *Journal of Catalysis* 226 (2004): 226-229.
- [95] S.J. Tauster, S.C. Fung. Strong metal-support interactions: Occurrence among the binary oxides of groups IIA–VB. *Journal of Catalysis* 55 (1978): 29-35.
- [96] S.J. Tauster, S.C. Fung, R.L. Garten. Strong metal-support interactions. Group 8 noble metals supported on titanium dioxide. *Journal of the American Chemical Society* 100 (1978): 170-175.
- [97] S.H. Chien, B.N. Shelimov, D.E. Resasco, E.H. Lee, G.L. Haller. Characterization of the interaction between rhodium and titanium oxide by XPS. *Journal of Catalysis* 77 (1982): 301-303.
- [98] E.M. Stuve, R.J. Madix. Use of the π - σ parameter for characterization of rehybridization upon adsorption on metal surfaces. *Journal of Physical Chemistry* 89 (1985): 3183-3185.
- [99] L.S. Lobo, D.L. Trimm. Carbon formation from light hydrocarbons on nickel. *Journal of Catalysis* 29 (1973): 15-19.
- [100] G.A. Somorjai, L.L. Kesmodel, L.H. Dubois. LEED analysis of acetylene and ethylene chemisorption on the platinum (111) surface: evidence for ethylidene formation. *Journal of Chemical Physics* 20 (1979): 2180-2188.
- [101] J.H. Moses, A.H. Weiss, K. Matusek, L. Guzzi. The effect of catalyst treatment on the selective hydrogenation of acetylene over palladium/alumina. *Journal of Catalysis* 86 (1984): 417-426.
- [102] J.C. Rodríguez, A.J. Marchi, A. Borgna, A. Monzón. Effect of Zn content on catalytic activity and physicochemical properties of Ni-based catalysts for selective hydrogenation of acetylene. *Journal of Catalysis* 171 (1997): 268-278.
- [103] J.C. Rodríguez, C. Guimon, A. Marchi, A. Borgna, A. Monzón. Activity, selectivity and coking of bimetallic Ni-Co-spinel catalysts in selective hydrogenation reactions. *Studies in Surface Science and Catalysis* 111 (1997): 183-190.
- [104] P. Turlier, H. Praliaud, P. Moral, G.A. Martin, J.A. Dalmon. Influence of the nature of the support on the reducibility and catalytic properties of nickel: evidence for a new type of metal support interaction. *Applied Catalysis* 19

-
- (1985): 287-300.
- [105] G.A. Martin, C.F. Ng. Poisoning of small metal particles by poison islands: A statistical approach based on the ensemble model. *Applied Catalysis* 31 (1987): 235-241.
- [106] L. Bonneviot, G.L. Haller. Morphology and site blocking effects on chemisorption properties and reactivity of Pt/TiO₂ and sulfided Pt/Al₂O₃ catalysts. *Journal of Catalysis* 130 (1991): 359-373.
- [107] L. Bonneviot, G.L. Haller. EPR characterization of Ti³⁺ ions at the metal-support interface in Pt/TiO₂ catalysts. *Journal of Catalysis* 113 (1988): 96-105.
- [108] S. Hub, L. Hilaire, R. Touroude. Hydrogenation of But-1-yne and But-1-ene on palladium catalysts : Particle size effect. *Applied Catalysis* 36 (1988) : 307-322.
- [109] J.P. Boitiaux, J. Cosyns, S. Vasudevan. Hydrogenation of highly unsaturated hydrocarbons over highly dispersed palladium catalyst: Part I: behaviour of small metal particles. *Applied Catalysis* 6 (1983): 41-51.
- [110] M.A. Valenzuela, J.P. Jacobs, P. Bosch. The influence of the preparation method on the surface structure of ZnAl₂O₄. *Applied Catalysis A: General* 148 (1997): 315-324.
- [111] M. Zawadzki, J. Wrzyszc. Hydrothermal synthesis of nanoporous zinc aluminate with high surface area. *Materials Research Bulletin* 35 (2000): 109-114.
- [112] M. Zawadzki, W. Miśta, L. Kepński. *Journal of Vacuum* 63 (2001): 291.
- [113] A. Sarkarny, L. Gucci, A.H. Weiss. On the aging phenomenon in palladium catalysed acetylene hydrogenation. *Applied Catalysis* 10 (1984): 369-388.
- [114] C.E. Gigola, H.R. Aduriz, P. Bodnariuk. Particle size effect in the hydrogenation of acetylene under industrial conditions. *Applied Catalysis* 27 (1986): 133-144.
- [115] Y.A. Ryndin, M.V. Stenin, A.I. Boronin, V.I. Bukhtiyarov, V.I. Zaikovskii. Effect of Pd/C dispersion on its catalytic properties in acetylene and vinylacetylene hydrogenation. *Applied Catalysis* 54 (1989): 277-288.
- [116] J. Panpranot, K. Phandinthong, T. Sirikajorn, M. Arai, P. Prasertthdam. Impact of palladium silicide formation on the catalytic properties of Pd/SiO₂

-
- catalysts in liquid-phase semihydrogenation of phenylacetylene *Journal of Molecular Catalysis* 261 (2007): 29-35.
- [117] A. Al-Ubaid, E.E. Wolf. Steam reforming of methane on reduced non-stoichiometric nickel aluminate catalysts. *Applied Catalysis* 40 (1988): 73-85.
- [118] A. Bhattacharyya, V.W. Chang. CO₂ reforming of methane to syngas: Deactivation behavior of nickel aluminate spinel catalysts *Studies in Surface Science and Catalysis* 88 (1994): 207-213.
- [119] J.A. Peña, J. Herguido, C. Guimon, A. Monzón, J. Santamaría. Hydrogenation of acetylene over Ni/NiAl₂O₄ catalyst: characterization, coking, and reaction studies. *Journal of Catalysis* 159 (1996): 313-322.
- [120] C.J. Liu, G.P. Vissokov, B.W.L. Jang. Catalyst preparation using plasma technologies. *Catalysis Today* 72 (2002): 173-184.
- [121] J.G. Wang, C.J. Liu, Y.P. Zhang, X.L. Zhu, J.J. Zou, K.L. Yu, B. Eliasson. Partial oxidation of methane to syngas over plasma treated Ni-Fe/La₂O₃ catalyst. *Chemistry Letters* 10 (2002): 1068.
- [122] Y. Zhang, W. Chu, W.M. Cao, C.R. Luo, X.G. Wen, K.L. Zhou. A plasma-activated Ni/ α -Al₂O₃ catalyst for the conversion of CH₄ to syngas. *Plasma Chemistry and Plasma Processing* 20 (2000): 137-144.
- [123] J. Jia, K. Haraki, J.N. Kondo, K. Domen, K. Tamaru. Selective hydrogenation of acetylene over Au/Al₂O₃ catalyst. *Journal of Physical Chemistry B* 104 (2000): 11153-11156.
- [124] T.V. Choudhary, C. Sivadinarayana, A.K. Datye, D. Kumar, D.W. Goodman. Acetylene hydrogenation on Au-based catalysts. *Catalysis Letters* 86 (2003): 1-8.
- [125] N.M. Rodriguez, M.S. Kim, R.T.K. Baker. Carbon nanofibers-A unique catalyst support medium. *Journal of Physical Chemistry* 98 (1994): 13108-13111.
- [126] C. Park, M.A. Keane. Catalyst support effects: gas-phase hydrogenation of phenol over palladium. *Journal of Colloid and Interface Science* 266 (2003): 183-194.
- [127] Y.A. Ryndin, L.V. Nosova, A.I. Boronin, A.L. Chuvilin. Effect of dispersion of supported palladium on its electronic and catalytic properties in the hydrogenation of vinylacetylene. *Applied Catalysis* 42 (1988): 131-141.

-
- [128] M.G. Mason. Electronic structure of supported small metal clusters. *Physical Review B* 27 (1983): 748.
- [129] C.N. Thanh, B. Didillon, P. Sarrazin, C. Cameron, U.S. Patent 6 054 409 (2000).
- [130] D.B. Tiedtke, et al. Chemical Influencing the Activity of Palladium-Based Catalysts for the Selective Hydrogenation of Acetylene to Ethylene in Acetylene Converters [online]. Texas: Chevron Phillips Chemical Company LP. Available from: <http://www.cpchem.com/specialtychem/library/CatalystPoisons.pdf> [Accessed 3 February 04]
- [131] L. Kniel, O. Winter, K. Stork. Ethylene: Keystone to the Petrochemical Industry. New York: Marcel Dekker (1980).
- [132] S.A. Miller. Acetylene: Its Properties, Manufacture and Uses, vol. 1. London: Ernest Benn Ltd. (1965).
- [133] R. Walzl. Acetylene removal in ethylene plants. In: The 3rd Asian Ethylene Symposium on Catalyst and Processes, 4-6 October 2000. Yokohama, Japan.
- [134] W.K. Lam, L. Lloyd. Catalyst aids selective hydrogenation. *Oil Gas Journal* (1972): 66-70.
- [135] M.L. Derrien. Selective hydrogenation applied to the refining of petrochemical raw materials produced by steam cracking. *Studies in Surface Science and Catalysis* 27 (1986): 613-666.
- [136] S.A. Blankenship, R.W. Voight, J.A. Perkins, J.E. Fried Jr. U.S. Patent: 6 509 292 (2001).
- [137] R.E. Reitmeier, H.W. Fleming. Acetylene removal from polyethylene grade ethylene. *Chemical Engineering Progress* 54 (1958): 48-51.
- [138] J.Y. Livingston. Performance of selective hydrogenation catalysts. *Chemical Engineering Progress* May (1973): 65-68.
- [139] D.W. Robinson. Catalyst regeneration, metal catalysts. Kirk-Othmer Encyclopedia of Chemical Technology [online], 4 December 2000. Available from: <http://www.mrw.interscience.wiley.com/kirk/articles/rel0001/noblrobi.a01/frame.html> [Accessed 1 March 2004]

-
- [140] R. Buxbaum. 1997. Membrane reactors, fundamental and commercial advantages, e.g. for methanol reforming [online]. Available from: <http://www.rebresearch.com/MRessay.html> [Accessed 9 March 2004].
- [141] K.L. Yeung, et al. Performance of a membrane-catalyst for photocatalytic oxidation of volatile organic compounds [online] Available from: <http://ihome.ust.hk/~kyeung/pdf/CES5803959.pdf> [Accessed 9 March 2004].
- [142] K. Svajda, et al., 2002. Development of catalytic membranes for direct synthesis of hydrogen peroxide [online]. Available from: http://kwi.dechema.de/tc/images/Svajda_hydrogenperoxide.pdf [Accessed 9 March 2004].
- [143] K. Shuzo, I. Takeo, H. Shogo, I. Yuichi. *U.S. Patent: 45 053 579* (1975).
- [144] J. Cosyns, J.-P. Boitiaux: Process for selectively hydrogenating acetylene in a mixture of acetylene and ethylene. *U.S. Patent: 4 571 442* (Institut Français du Pétrole) (1984).
- [145] J.-P. Boitiaux, J. Cosyns, M. Derrien, G. Leger. Newest hydrogenation catalyst. *Hydrocarbon Processing* March (1985): 51-59.
- [146] V.H. Sandoval, C.E Gigola. Characterization of Pd and Pd---Pb/ α -Al₂O₃ catalysts. A TPR-TPD study. *Applied Catalysis A: General* 148 (1996): 81-96.
- [147] S. Lambert, C. Cellier, P. Grange, J.P. Pirard, B. Heinrichs. Synthesis of Pd/SiO₂, Ag/SiO₂, and Cu/SiO₂ cogelled xerogel catalysts: study of metal dispersion and catalytic activity. *Journal of Catalysis* 221 (2004): 335-346.
- [148] C.L.M. Joyal, J.B. Butt. Chemisorption and disproportionation of carbon monoxide on palladium/silica catalysts of differing percentage metal exposed. *Journal of the Chemical Society, Faraday Transactions I* 83 (1987): 2757-2764.
- [149] V.B. Kazanskii, in: Proceedings of the 6th International Congress on Catalysis, London, (1976): 50.
- [150] R. Stößer, M. Nofz, M. Feist and G. Scholz. Fe³⁺-assisted formation of α -Al₂O₃, starting from sol-gel precursors. *Journal of Solid State Chemistry* 179 (2006): 652-664.

-
- [151] N. Mahata, V. Vishwanathan. Influence of palladium precursors on structural properties and phenol hydrogenation characteristics of supported palladium catalysts. *Journal of Catalysis* 196 (2000): 262-270.
- [152] J.F. Moulder, W.W. Stickle, P.E. Sobol, K.D. Bombier, in: J. Chastain (Ed.), Handbook of X-ray photoelectron spectroscopy, Perkin Elmer, Eden Prairie, USA (1992).
- [153] P. Legare, F. Finck, R. Roche, G. Maire. XPS investigation of the oxidation of the Al/Pd interface: The Al₂O₃/Pd interface. *Journal of Surface Science* 217 (1989): 167-178.
- [154] M. Brun, A. Berthet, J.C. Bertolini. XPS, AES and Auger parameter of Pd and PdO. *Journal of Electron Spectroscopy and Related Phenomena* 104 (1999): 55-60.
- [155] A.M. Venezia, A. Rossi, L.F. Liotta, A. Martorana, G. Deganello. Effect of sodium on the electronic properties of Pd/silica-alumina catalysts. *Applied Catalysis A: General* 147 (1996): 81-94.
- [156] A.B. Gaspar, L.C. Dieguez. Dispersion stability and methylcyclopentane hydrogenolysis in Pd/Al₂O₃ catalysts. *Applied Catalysis A: General* 201 (2000): 241-251.
- [157] I.Y. Ahn, W.J. Kim, S.H. Moon. Performance of La₂O₃- or Nb₂O₅-added Pd/SiO₂ catalysts in acetylene hydrogenation. *Applied Catalysis A: General* 308 (2006): 75-81.
- [158] J. Panpranot, K. Kontapakdee, P. Praserttham. Selective hydrogenation of acetylene in excess ethylene on micron-sized and nanocrystalline TiO₂ supported Pd catalysts. *Applied Catalysis A: General* 314 (2006): 128-133.
- [159] G.C. Bond. Catalysis by metals, Academic Press, London (1962).
- [160] A.M. Venezia, R. Bertoncello, G. Deganello. X-ray photoelectron spectroscopy investigation of pumice-supported nickel catalysts. *Surface and Interface Analysis* 23 (1995): 239-247.
- [161] O. Mekasuwandumrong, P.L. Silveston, P. Praserttham, M. Inoue, V. Pavarajarn, W. Tanakulrungsank. Synthesis of thermally stable micro spherical γ -alumina by thermal decomposition of aluminum isopropoxide in mineral oil. *Inorganic Chemistry Communications* 6

-
- (2003): 930-934.
- [162] B.C. Lippens, J.H. de Boer. Studies on pore systems in catalysts I. The adsorption of nitrogen; apparatus and calculation. *Journal of Catalysis* 3 (1964): 32-37.
- [163] B.C. Lippens, J.H. de Boer. Studies on pore systems in catalysts: V. The *t*-Method. *Journal of Catalysis* 4 (1965): 319-323.
- [164] J. Panpranot, K. Pattamakomsan, J.G. Goodwin Jr., P.A. Praserthdam. Comparative study of Pd/SiO₂ and Pd/MCM-41 catalysts in liquid-phase hydrogenation. *Catalysis Communications* 5 (2004): 583-590.
- [165] N.S. Figoli, P.C. Largentiere, A. Arcoya, X.L. Seoane. Modification of the properties and sulfur resistance of a Pd/SiO₂ catalyst by La addition. *Journal of Catalysis* 155 (1995): 95-105.
- [166] X.L. Seoane, N.S. Figoli, P.C. L'Argentiere, J.A. González, A. Arcoya. Palladium-Lanthanum interaction phenomena in Pd-LaCl₃/SiO₂ and Pd-La₂O₃/SiO₂ Catalysts. *Catalysis Letters* 47 (1997): 213-220.
- [167] C. Yang, J. Ren, Y. Sun. Role of La₂O₃ in Pd-supported catalysts for methanol decomposition. *Catalysis Letters* 84 (2002): 123-129.
- [168] S. Tsuchiya, M. Nakamura. Study of chemisorption and hydrogenation of ethylene on platinum by temperature-programmed desorption. *Journal of Catalysis* 50 (1977): 1-7.
- [169] Y.H. Park, G.L. Price. Temperature-Programmed-Reaction study on the effect of carbon monoxide on the acetylene reaction over palladium/alumina. *Industrial & Engineering Chemistry Research* 30 (1991): 1700-1707.
- [170] V. Matolin. Rheed and TPD studies of the effect of particle size on CO desorption from Al₂O₃ supported Pd and Rh model catalysts. *FIZIKA A*. 4 (1995): 181-189.



APPENDICES

ศูนย์วิทยทรัพยากร
จุฬาลงกรณ์มหาวิทยาลัย

APPENDIX A

CALCULATION FOR CATALYST PREPARATION

The calculation shown below is for 0.1%Pd/Al₂O₃. The alumina support weight used for all preparation is 4 g.

Based on 100 g of catalyst used, the composition of the catalyst will be as follows:

$$\begin{aligned} \text{Palladium} &= 0.1 \text{ g} \\ \text{Alumina} &= 100-0.1 = 99.9 \text{ g} \end{aligned}$$

For 4 g of alumina

$$\text{Palladium required} = (4 \times 0.1) / 99.9 = 0.004004 \text{ g}$$

Palladium nitrate 0.2 g dissolved in de-ionised water.

$$\begin{aligned} \text{Then Pd content in stock solution} &= \frac{\text{Weight of Pd(NO}_3)_2 \times \text{M.W. of Pd}}{\text{M.W. of Pd(NO}_3)_2} \\ &= (0.2 \times 106.4) / 230.4 \\ &= 0.0924 \text{ g} \end{aligned}$$

Pd(NO₃)₂ taken from stock solution (10 g including solvent and solute)

$$\begin{aligned} &= (0.004004 \times 10) / 0.0924 \\ &= 0.4333 \text{ g} \end{aligned}$$

The calculation shown below is for 0.1%Pd-0.3%Ag/Al₂O₃. The alumina support weight used for all preparation is 4 g.

Based on 100 g of catalyst used, the composition of the catalyst will be as follows:

$$\begin{aligned} \text{Palladium} &= 0.1 \text{ g} \\ \text{Silver} &= 0.3 \text{ g} \\ \text{Alumina} &= 100-0.4 = 99.6 \text{ g} \end{aligned}$$

For 4 g of alumina

$$\begin{aligned} \text{Palladium required} &= (4 \times 0.1) / 99.6 = 0.004016 \text{ g} \\ \text{Silver required} &= (4 \times 0.3) / 99.6 = 0.012048 \text{ g} \end{aligned}$$

Palladium nitrate 0.2 g dissolved in de-ionised water.

$$\begin{aligned} \text{Then Pd content in stock solution} &= \frac{\text{Weight of Pd(NO}_3)_2 \times \text{M.W. of Pd}}{\text{M.W. of Pd(NO}_3)_2} \\ &= (0.2 \times 106.4) / 230.4 \\ &= 0.0924 \quad \text{g} \end{aligned}$$

$$\begin{aligned} \text{Pd(NO}_3)_2 \text{ taken from stock solution (10 g including solvent and solute)} &= (0.004016 \times 10) / 0.0924 \\ &= 0.4346 \quad \text{g} \end{aligned}$$

Silver nitrate 0.5 g dissolved in de-ionised water

$$\begin{aligned} \text{Then Ag content in stock solution} &= \frac{\text{Weight of AgNO}_3 \times \text{M.W. of Ag}}{\text{M.W. of AgNO}_3} \\ &= (0.5 \times 107.9) / 169.9 \\ &= 0.3175 \quad \text{g} \end{aligned}$$

$$\begin{aligned} \text{AgNO}_3 \text{ taken from stock solution (10 g including solvent and solute)} &= (0.012048 \times 10) / 0.3175 \\ &= 0.3795 \quad \text{g} \end{aligned}$$

Since the pore volume of the alumina support is 0.25 ml/g and the total volume of impregnation solution which must be used is 0.5 ml by the requirement of dry impregnation method, the de-ionised water is added until the total volume of impregnation solution is 0.5 ml.

ศูนย์วิทยทรัพยากร
จุฬาลงกรณ์มหาวิทยาลัย

APPENDIX B

CALCULATION CURVES

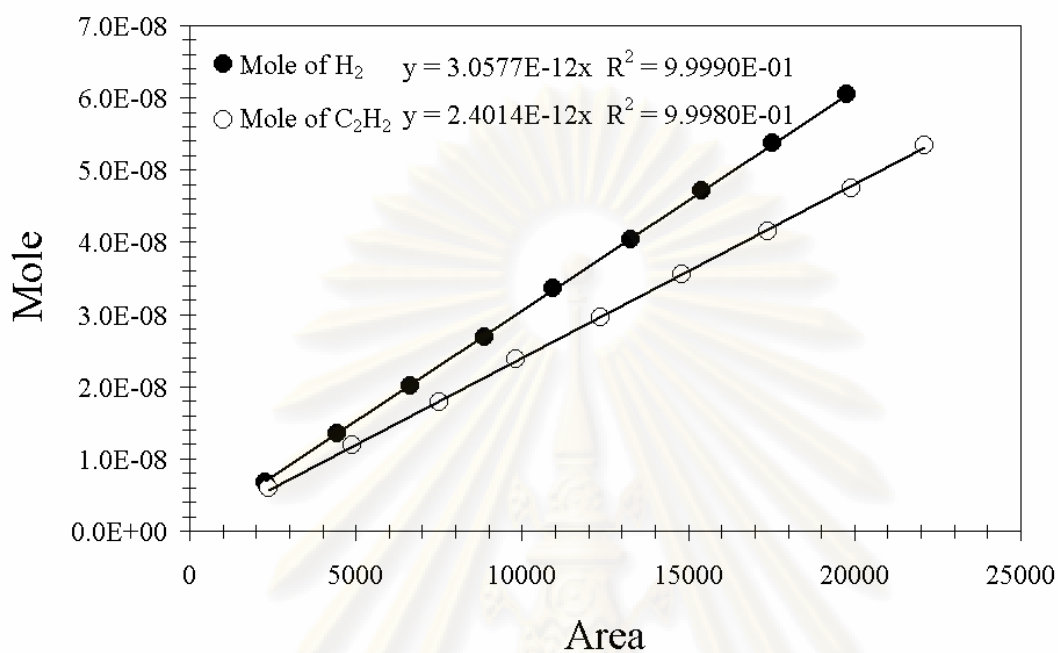


Figure B.1 The calibration curve of acetylene and hydrogen from GC-8APF (FID) and GC-8APT (TCD)

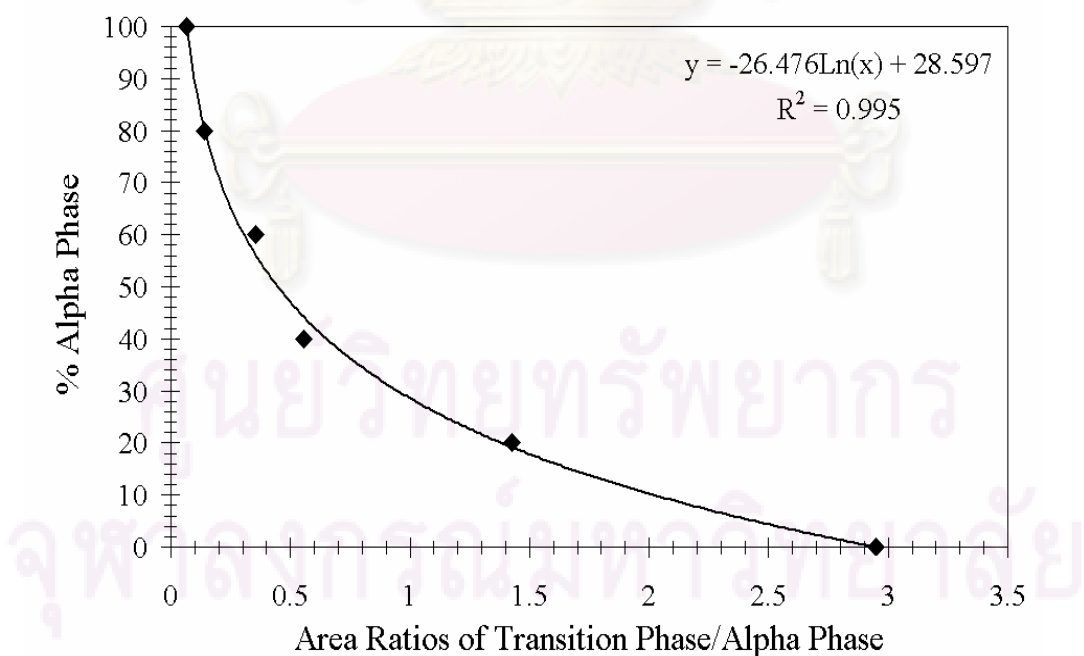


Figure B.2 The calibration curve of transition phase/alpha phase

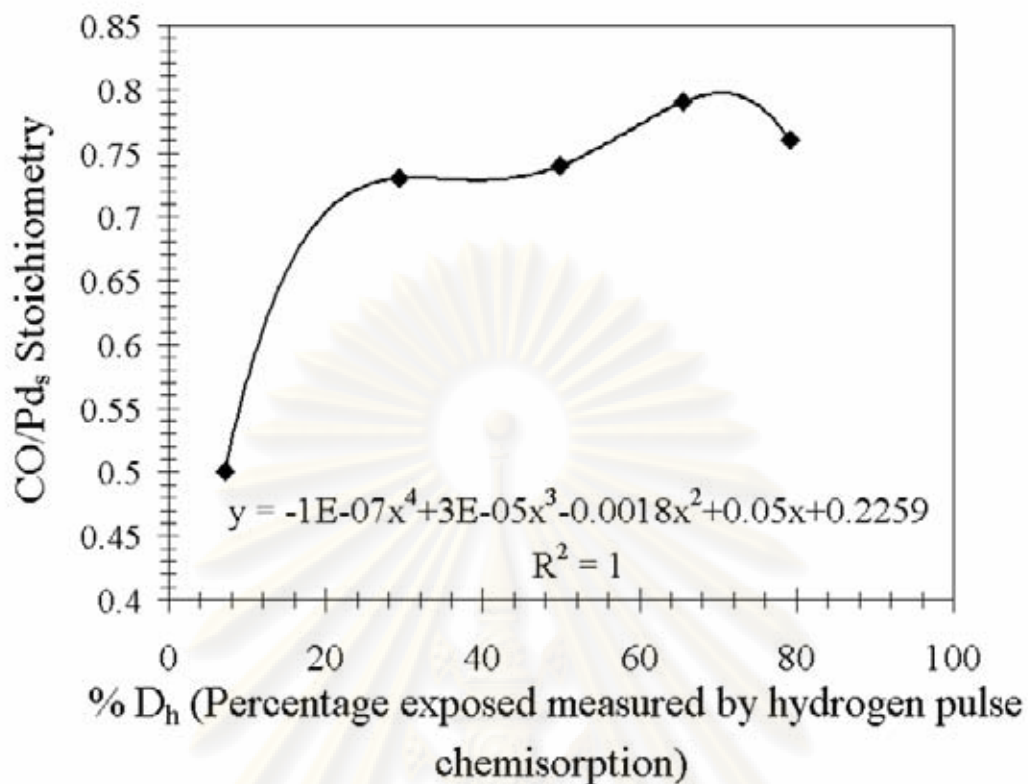


Figure B.3 The calibration curve of CO/Pd_s ratios as a function of D_h for the Pd/SiO₂ series

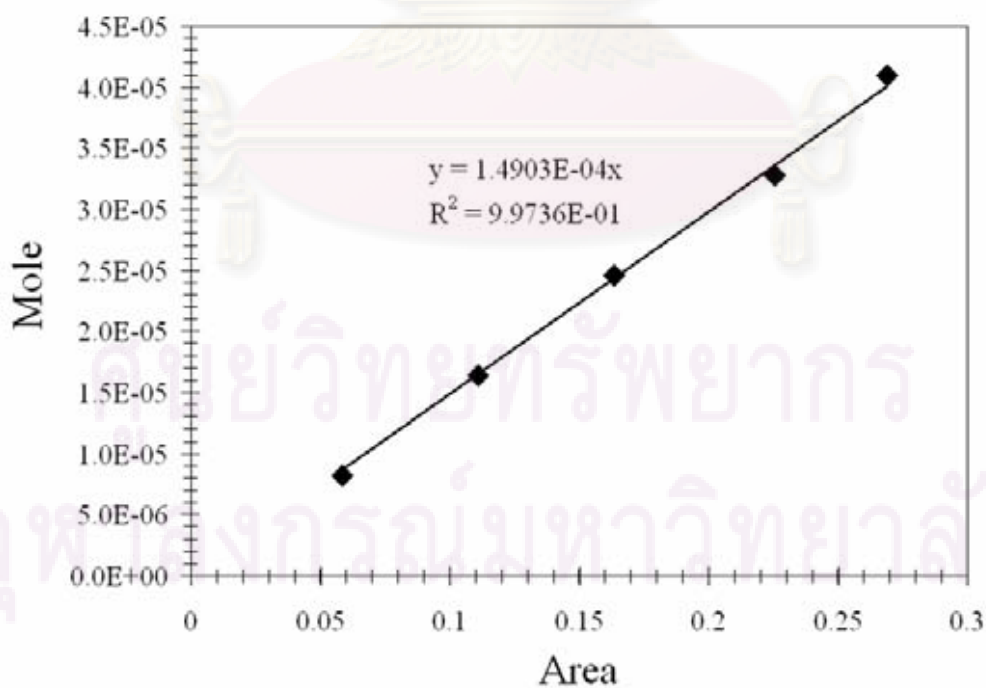


Figure B.4 The calibration curve of ethylene from Micromeritic Chemisorb 2750

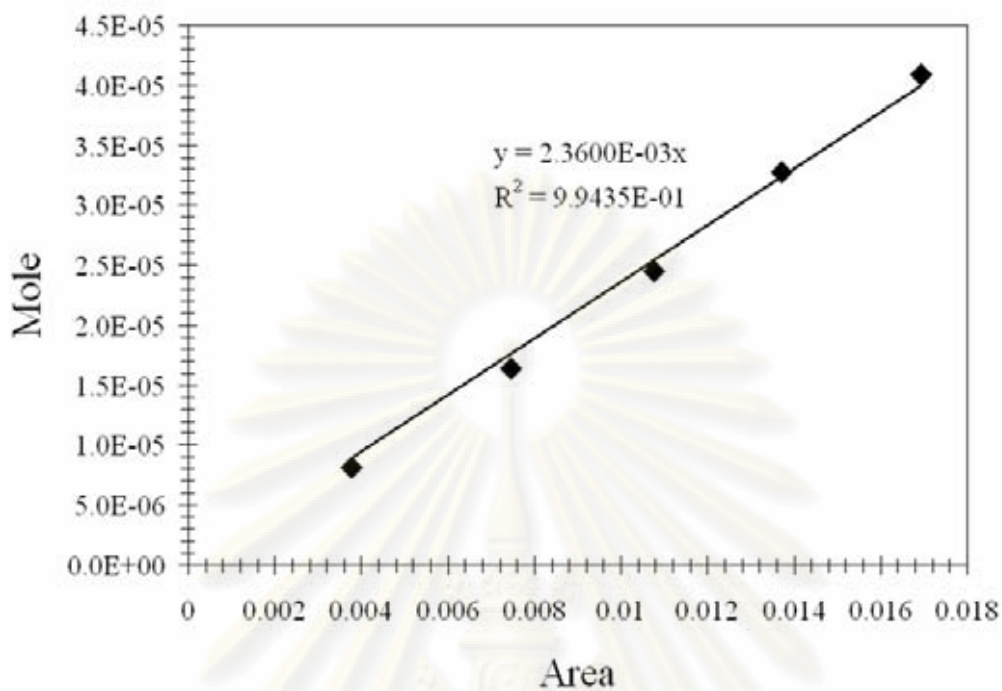


Figure B.5 The calibration curve of hydrogen from Micromeritic Chemisorb 2750

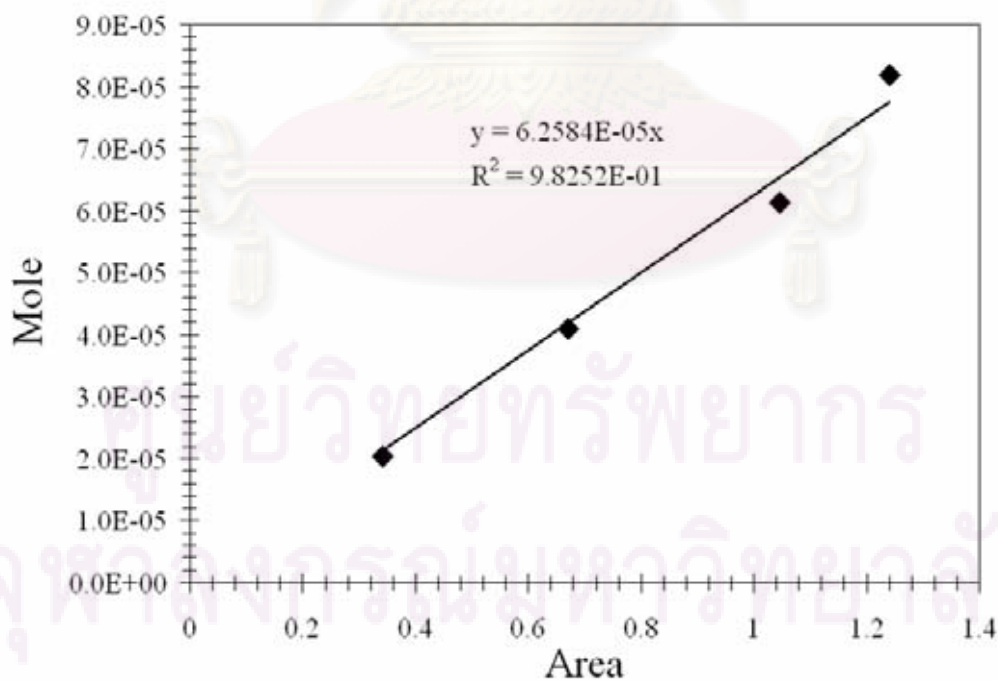


Figure B.6 The calibration curve of carbon monoxide from Micromeritic Chemisorb 2750

APPENDIX C

CALCULATION OF THE CRYSTALLITE SIZE

Calculation of the crystallite size by Debye-Scherrer equation

The crystallite size was calculated from the half-height width of the diffraction peak of XRD pattern using the Debye-Scherrer equation.

From Scherrer equation:

$$D = \frac{K\lambda}{\beta \cos\theta}$$

where

D = Crystallite size, Å

K = Crystallite-shape factor = 0.9

λ = X-ray wavelength, 1.5418 Å for CuK α

θ = Observed peak angle, degree

β = X-ray diffraction broadening, radian

The X-ray diffraction broadening (β) is the corrected width of a powder diffraction free from all broadening due to the instrument. The α -Alumina was used as a standard sample to provide instrumental broadening data (see Figure C.1). The most common correction for the X-ray diffraction broadening (β) can be obtained by using the Warren's formula.

Warren's formula:

$$\beta = \sqrt{B_M^2 - B_S^2}$$

where B_M = The measured peak width in radians at half peak height.

B_S = The corresponding width of the standard material.

Example: Calculation of the crystallite size of α -Al₂O₃

The half-height width of 012 diffraction peak = 0.88° (from the **Figure C.1**)
 = $(2\pi \times 0.88)/360$
 = 0.0154 radian (B_M)

The corresponding half-height width of $\alpha\text{-Al}_2\text{O}_3$ peak (from the B_S value at the 2θ of 25.92° in **Figure C.2**) = 0.0041 radian

$$\begin{aligned} \text{The pure width, } \beta &= \sqrt{0.0154^2 - 0.0041^2} \\ &= 0.0148 \text{ radian} \end{aligned}$$

$$\beta = 0.0148 \text{ radian}$$

$$2\theta = 25.92^\circ$$

$$\theta = 12.96^\circ$$

$$\lambda = 1.5418 \text{ \AA}$$

$$\begin{aligned} \text{The crystallite size} &= \frac{0.9 \times 1.5418 \text{ \AA}}{0.0148 \text{ radian} \times \cos 12.96^\circ} \\ &= 96.21 \text{ \AA} = 9.62 \text{ nm} \end{aligned}$$

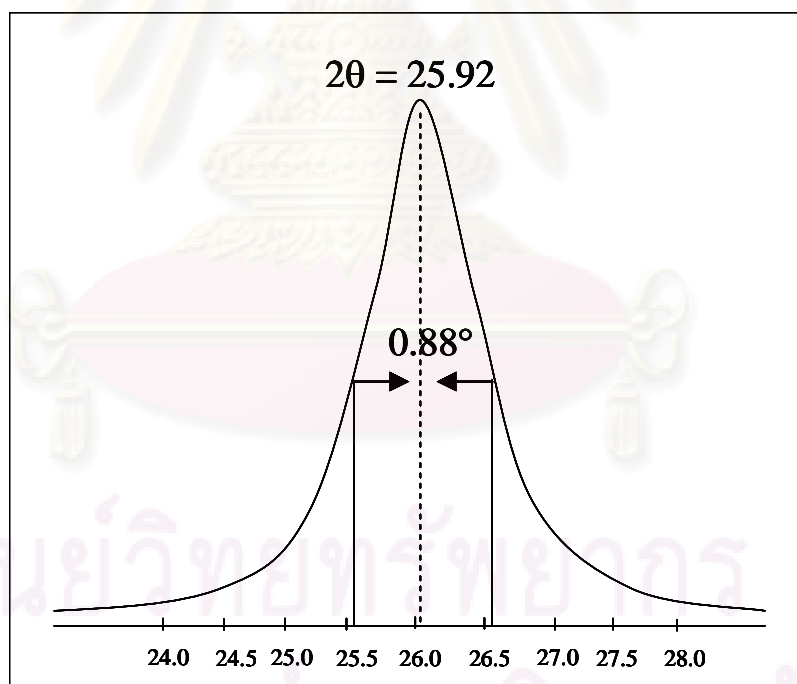


Figure C.1 The observation peak of $\alpha\text{-Al}_2\text{O}_3$ for calculating the crystallite size.

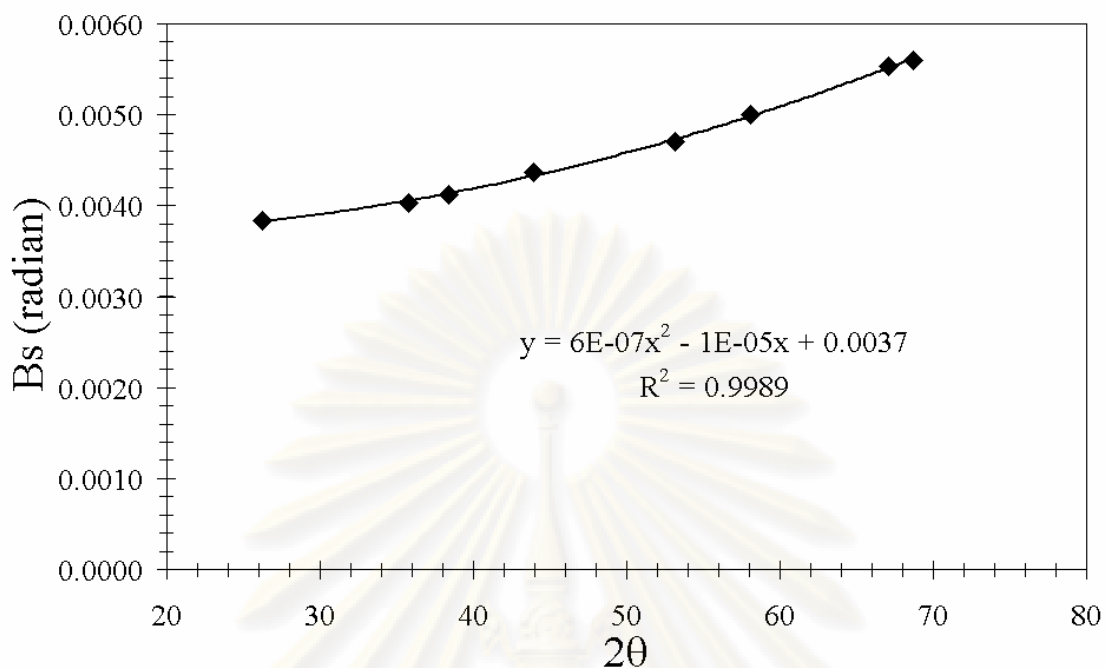


Figure C.2 The graph indicating that value of the line broadening attribute to the experimental equipment from the α - Al_2O_3 standard.

ศูนย์วิทยทรัพยากร
จุฬาลงกรณ์มหาวิทยาลัย

APPENDIX D

CALCULATION OF C₂H₂ CONVERSION AND C₂H₄ GAIN

The catalyst performance for the selective hydrogenation of acetylene was evaluated in terms of activity for acetylene conversion and ethylene gain based on the following equation:



Activity of the catalyst for acetylene conversion is defined as mole of acetylene converted with respect to acetylene in the feed:

$$\text{C}_2\text{H}_2 \text{ conversion (\%)} = \frac{100 \times [\text{mole of C}_2\text{H}_2 \text{ in feed} - \text{mole of C}_2\text{H}_2 \text{ in product}]}{\text{mole of C}_2\text{H}_2 \text{ in feed}}$$

where mole of C₂H₂ can be measured employing the calibration curve of C₂H₂ in **Figure B.1, APPENDIX B.**, i.e.,

$$\text{mole of C}_2\text{H}_2 = (\text{area of C}_2\text{H}_2 \text{ peak from integrator plot on GC-8APF}) \times 2.4014 \times 10^{-12}$$

Ethylene gain was calculated from moles of hydrogen and acetylene:

$$\text{C}_2\text{H}_4 \text{ gain (\%)} = \frac{100 \times [d\text{C}_2\text{H}_2 - (d\text{H}_2 - d\text{C}_2\text{H}_2)]}{d\text{C}_2\text{H}_2}$$

Where $d\text{C}_2\text{H}_2$ = mole of acetylene in feed – mole of acetylene in product

$d\text{H}_2$ = mole of hydrogen in feed – mole of hydrogen in product

mole of H₂ can be measured employing the calibration curve of H₂ in **Figure B.1, APPENDIX B.**, i.e.,

$$\text{mole of H}_2 = (\text{area of H}_2 \text{ peak from integrator plot on GC-8APT}) \times 3.0577 \times 10^{-12}$$

APPENDIX E

CALCULATION FOR CO-CHEMISORPTION

Calculation of the metal active sites, metal dispersion, active metal surface area, and average crystallite size of the catalyst measured by CO-chemisorption is as follows:

Volume of active gas dosed from a loop (V_{inj})

$$V_{inj} = V_{loop} \times \frac{T_{std}}{T_{amb}} \times \frac{P_{amb}}{P_{std}} \times \frac{\%A}{100\%}$$

Example: Volume Dosed Using 100% Active Gas

V_{loop}	=	loop volume injected	50	μL
T_{amb}	=	ambient temperature	295	K
T_{std}	=	standard temperature	273	K
P_{amb}	=	ambient pressure	743	mmHg
P_{std}	=	standard pressure	760	mmHg
$\%A$	=	% active gas	100	%

$$V_{inj} = 50\mu\text{L} \times \frac{273\text{K}}{295\text{K}} \times \frac{743\text{mmHg}}{760\text{mmHg}} \times \frac{100\%}{100\%} = 45.2362\mu\text{L}$$

Volume chemisorbed (V_{ads})

$$V_{ads} = \frac{V_{inj}}{m} \times \sum_{i=1}^n \left[1 - \frac{A_i}{A_f} \right]$$

Example: CO Chemisorption on 0.5wt% Pd/Al₂O₃

V_{inj}	=	volume injected	45.2362	μL
m	=	mass of sample	0.2	g
A_f	=	area of peak last peak	0.02331	

Peak	A_i	$1-A_i/A_f$	V_{ads}^i	ΣV_{ads}^i
1	0.01659	0.2883	13.0411	13.0411
2	0.02231	0.0429	1.9406	14.9817
3	0.02331	0	0	14.9817

$$V_{ads} = 74.9085 \mu\text{L/g} = 0.0749 \text{ cm}^3/\text{g}$$

% Metal dispersion

$$\%D = S_f \times \frac{V_{ads}}{V_g} \times \frac{\text{m.w.}}{\%M} \times 100\% \times 100\%$$

Example: %Dispersion of 0.5wt% Pd/Al₂O₃

S_f	=	stoichiometer factor, CO on Pd	1	
V_{ads}	=	volume adsorbed	0.0749	cm ³ /g
V_g	=	molar volume of gas at STP	22414	cm ³ /mol
m.w.	=	molecular weight of the metal	106.4	g/mol
%M	=	weight percent of the active metal	0.5	%

$$\%D = 1 \times \frac{0.0749 \text{ cm}^3/\text{g}}{22414 \text{ cm}^3/\text{mol}} \times \frac{106.4 \text{ g/mol}}{0.5\%} \times 100\% \times 100\% = 7.1\%$$

Pd active sites

$$\text{Pd active sites} = S_f \times \frac{V_{ads}}{V_g} \times N_A$$

S_f	=	stoichiometry factor, CO on Pd	1	
V_{ads}	=	volume adsorbed	0.0749	cm ³ /g
V_g	=	molar volume of gas at STP	22414	cm ³ /mol
N_A	=	Avogadro's number	6.023×10^{23}	molecules/mol

$$\text{Pd active sites} = 1 \times \frac{0.0749 \text{ cm}^3/\text{g}}{22414 \text{ cm}^3/\text{mol}} \times 6.023 \times 10^{23} \frac{\text{molecules}}{\text{mol}} = 2.01 \times 10^{18} \text{ CO molecules/g}$$

Active metal surface area (per gram of sample)

$$MSA_s = S_f \times \frac{V_{ads}}{V_g} \times \frac{100\%}{\%M} \times N_A \times \sigma_m \times \frac{m^2}{10^{18} \text{ nm}^2}$$

S_f	=	stoichiometry factor, CO on Pd	1
V_{ads}	=	volume adsorbed	0.0749 cm^3/g
V_g	=	molar volume of gas at STP	22414 cm^3/mol
$\%M$	=	weight percent of the active metal	0.5 %
N_A	=	Avogadro's number	6.023×10^{23} molecules/mol
σ_m	=	cross-sectional area of active metal atom	0.0787 nm^2

$$MSA_s = 1 \times \frac{0.0749 \text{ cm}^3/\text{g}}{22414 \text{ cm}^3/\text{mol}} \times \frac{100\%}{0.5\%} \times 6.023 \times 10^{23} \frac{\text{molecules}}{\text{mol}} \times 0.0787 \text{ nm}^2 \times \frac{m^2}{10^{18} \text{ nm}^2}$$

$$= 31.68 \text{ m}^2/\text{g}_{\text{metal}}$$

Average crystallite size

$$d = \frac{F_g}{\rho \times MSA_m} \times \frac{m^3}{10^6 \text{ cm}^3} \times \frac{10^9 \text{ nm}}{m}$$

F_g	=	crystallite geometry factor (hemisphere = 6)	6
ρ	=	specific gravity of the active metal	12.0 g/cm^3
MSA_m	=	active metal surface area per gram of metal	31.68 $\text{m}^2/\text{g}_{\text{metal}}$

$$d = \frac{6}{12 \text{ g}/\text{cm}^3 \times 31.68 \text{ m}^2/\text{g}} \times \frac{m^3}{10^6 \text{ cm}^3} \times \frac{10^9 \text{ nm}}{m} = 15.78 \text{ nm}$$

APPENDIX F

PHYSISORPTION THEORY

Physisorption theory

One form of the well-known BET equation that describes the adsorption of a gas upon a solid surface is

$$\frac{\frac{P}{P_0}}{V\left[1-\frac{P}{P_0}\right]} = \frac{1}{V_m C} + \left(\frac{C-1}{V_m C}\right)\left(\frac{P}{P_0}\right) \quad (1)$$

where

V = the volume (at standard temperature and pressure, STP) of gas adsorbed at pressure P

P_0 = the saturation pressure which is the vapor pressure of liquified gas at the adsorbing temperature

V_m = the volume of gas (STP) required to form an adsorbed monomolecular layer

C = a constant related to the energy of adsorption

The surface area S of the sample giving the monolayer adsorbed gas volume V_m (STP) is then calculated from

$$S = \frac{V_m A}{mM} \quad (2)$$

where

N = Avogadro's number which expresses the number of gas molecules in a mole of gas at standard conditions

m = mass of sample

M = the molar volume of the gas

A = the area of each adsorbed gas molecule

Single-point surface area

The constant C of equation (1) is typically a relatively large number, i.e., $C > 1$, from which equation (1) reduces very nearly to

$$\frac{\frac{P}{P_0}}{V[1-\frac{P}{P_0}]} = \frac{1}{V_m} \left(\frac{1}{C} + \frac{P}{P_0} \right) \quad (3)$$

Now if $P/P_0 \gg 1/C$, equation (3) can be future represented by

$$\frac{\frac{P}{P_0}}{V[1-\frac{P}{P_0}]} = \left(\frac{1}{V_m} \right) \left(\frac{P}{P_0} \right) \quad (4)$$

which rearranges to

$$V_m = V \left[1 - \frac{P}{P_0} \right] \quad (5)$$

Another way of arriving at the same result is by recognizing that the term $1/(V_m C)$ of equation (1) is generally small. Taking it as insignificant changes the slope, and hence the value of V_m and the sample surface area as calculated by equation (2), only a small amount. Equation (1) can be rearranged with the contribution of the intercept term taken to be vanishingly small to also yield equation (5).

Substituting equation (5) into equation (2) yields

$$S = VAN \left[\frac{1 - \frac{P}{P_0}}{M} \right] \quad (6)$$

from which the sample surface area is readily determined once the volume V of gas adsorbed (or desorbed, which must theoretically be identical) is measured and appropriate values for the other terms are incorporated.

For nitrogen gas adsorbed from a mixture of 30 mole % nitrogen and 70 mole % helium using a liquid nitrogen bath, the values are arrived at as follows:

The volume V of gas with which the instrument is calibrated is injected at ambient temperature and atmospheric pressure. This volume must thus be multiplied by the ratios $273.2/(\text{Rm. Temp., K}) \times (\text{Atm. Press., mmHg})/760$ to convert it to standard conditions (0°C and 760 mmHg).

Avogadro's number N is 6.023×10^{23} molecules/g-mole

The molar volume M of a gas at standard conditions is $22414 \text{ cm}^3/\text{g-mole}$

The presently accepted value for the area N of a solid surface occupied by an adsorbed nitrogen molecule is $16.2 \times 10^{-20} \text{ m}^2$ (=16.2 Angstroms).

P is $0.3 \times$ the atmospheric pressure in millimeters of mercury since the gas mixture is 30 % nitrogen and adsorption takes place at atmospheric pressure. P_0 , the saturation pressure of liquid nitrogen is typically a small amount greater than atmospheric due to thermally induced circulation, dissolved oxygen, and other factors. With fresh, relatively pure liquid nitrogen, the saturation pressure is typically about 15 mmHg greater than atmospheric pressure. It can be 40 to 50 mmHg greater if the liquid nitrogen is relatively impure. The saturation pressure should be determined by other means in the latter event.

The result for a 30% $\text{N}_2/70\%$ He mixture adsorbed at liquid nitrogen temperature when room temperature is 22°C and atmospheric pressure is 760 mmHg is the expression.

$$S = v \left[\frac{273.2}{\text{Rm. Temp.}} \right] \left[\frac{\text{Atm. Press.}}{760} \right] \left[\frac{6.023 \times 10^{23} \times 16.2 \times 10^{-20}}{22.414 \times 10^3} \right] \quad (7)$$

$$\left[\frac{(1 - \%N_2/100) \times \text{Atm. Press.}}{\text{Sat. Press.}} \right] = v \cdot \text{constant}$$

where S is the surface area in square meters.

For calibration purposes, this means that a syringe injection of $V = 1.00 \text{ cm}^3$ of nitrogen at 22°C and 760 mmHg should produce an indicated surface area of 2.84, assuming the saturation pressure is 775 mmHg .

The value of S from equation (7) changes when ambient conditions differ significantly from 22°C and 760 mmHg , pressure changes having relatively more effect than temperature. Another value should then be calculated. For example, suppose the gas were $29.33\% \text{ N}_2$, the laboratory were at 22°C , atmospheric pressure were 710 mmHg , and the saturation pressure were measured to be 735 mmHg , the value, instead of being 2.84, should be 2.67

Multipoint surface area

A straight line usually results between P/P_0 values from about 0.05 to 0.25 when experimental data are plotted as $(P/P_0)/V[1-(P/P_0)]$ on the ordinate against P/P_0 as the abscissa. Relative pressures within this prescribed range are typically obtained with gas compositions between about 5% and 25% N_2 with the remainder He. Equation (1) shows then that slope and intercept of this line are, respectively, $(C-1)/V_m C$ and $1/(V_m C)$ and that both the values of V_m and C can be determined

The instrument is calibrated by injecting into it an accurately measured volume of each gas mixture at ambient conditions, calculating the volume of this gas at standard conditions, and setting the instrument to indicate thereafter adsorbed and desorbed gas volumes at standard conditions. When 1 mL of gas mixture is injected, its volume V at STP is given by

$$V = 1.00 \times \frac{273.2}{\text{Rm. Temp.}} \times \frac{\text{Atm. Press.}}{760} \quad (8)$$

The sample specific surface area S in square meters per gram is calculated from equation (2) using appropriate constants and slope and intercept values once the plot is made. Using the constants given above, this relationship becomes

$$S = 6.023 \times 10^{23} \times 16.2 \times \frac{10^{-20}}{22414 (\text{slope} + \text{intercept})} \quad (9)$$

or simply

$$S = \frac{4.353}{\text{slope} + \text{intercept}}$$

(10)

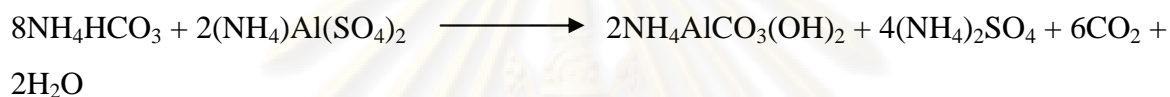


ศูนย์วิทยทรัพยากร
จุฬาลงกรณ์มหาวิทยาลัย

APPENDIX G

CALCULATION OF CONCENTRATION OF BOTH REACTANTS IN PRECIPITATION METHOD

In this study, ammonium aluminum carbonate hydroxide ($\text{NH}_4\text{AlCO}_3(\text{OH})_2$) has been produced by the reaction of ammonium aluminum sulfate solution (AAS solution) and ammonium hydrogencarbonate solution (AHC solution) as following equation:



Ammonium aluminum carbonate hydroxide (AACH) was prepared with the molar ratio of AAS solution to AHC solution equal to 1:4 as the above reaction and calculation procedure is given here.

Calculation of the amount of ammonium hydrogencarbonate (AHC) and ammonium aluminum sulfate (AAS) for AACH preparation

Ammonium aluminum sulfate (AAS) and ammonium hydrogencarbonate (AHC) are used as reactants to prepare AACH.

1. Ammonium aluminum sulfate ($\text{NH}_4\text{Al}(\text{SO}_4)_2 \cdot 12\text{H}_2\text{O}$) has an molecular weight of 237.18 g/mol (not included molecule of water)
2. Ammonium hydrogencarbonate (NH_4HCO_3) has an molecular weight of 79.06 g/mol

Example: Calculation of AACH preparation with concentration of AAS solution to AHC solution equal to 0.2:2.0 mol/l and molar ratio of AAS solution to AHC solution is 0.05:0.2, which is equal to 1:4 as mentioned before, are as following:

AAS solution 0.05 mol consists of: $\text{AAS } 0.05 \times 237.18 = 11.859 \text{ g}$

To get concentration 0.2 mol/l

Distilled water = 250 cm^3

AHC solution 0.2 mol consists of: $\text{AHC } 0.2 \times 79.06 = 15.812 \text{ g}$

To get concentration 2.0 mol/l

Distilled water = 100 cm^3



ศูนย์วิทยทรัพยากร
จุฬาลงกรณ์มหาวิทยาลัย

APPENDIX H

CALCULATION OF Zn MODIFIED ON Al₂O₃ SUPPORT

Preparation of Zn-modified Al₂O₃ with various molar ratio of Zn = 0.3 by solvothermal, sol-gel, precipitation methods.

- Reagent:**
- Aluminum isopropoxide ((CH₃)₂CHO)₃Al
Molecular weight = 203.98 g/mol
 - Aluminium nitrate nonahydrate (Al(NO₃)₃·9H₂O)
Molecular weight = 212.98 g/mol
(not included molecule of water)
 - Ammonium aluminum sulfate (NH₄Al(SO₄)₂·12H₂O)
Molecular weight = 237.18 g/mol
(not included molecule of water)

- Precursors:**
- Zinc (II) nitrate hexahydrate (Zn(NO₃)₂)·6H₂O
Molecular weight = 297.37 g/mol
 - Zinc (II) acetylacetonate ((CH₃COCH=COCH₃)₂Zn)
Molecular weight = 263.59 g/mol

Calculation:

Solvothermal method

For molar ratio Zn/Al = 0.3 is shown as follow:

Aluminum isopropoxide 25 g consisted of aluminium equal to:

$$\begin{aligned} \text{Aluminium} &= (26.98 \times 25) / 203.98 = 3.3067 \text{ g} \\ &= 3.3067 / 26.98 = 0.1226 \text{ mol} \end{aligned}$$

For Zn/Al = 0.3, 0.1226 mol of aluminium

$$\begin{aligned} \text{Zinc required} &= 0.1226 \times 0.3 = 0.0368 \text{ mol} \\ &= 0.0368 \times 65.37 = 2.4036 \text{ g} \end{aligned}$$

Zinc 2.4036 g is used from $((\text{CH}_3\text{COCH}=\text{COCH}_3)_2\text{Zn})$ and molecular weight of Zn is 65.37 g/mol

$$\begin{aligned}\text{Thus, } ((\text{CH}_3\text{COCH}=\text{COCH}_3)_2\text{Zn}) \text{ required} &= (263.59 \times 2.4036) / 65.37 \\ &= 9.6920 \text{ g}\end{aligned}$$

Sol-gel method

For molar ratio Zn/Al = 0.3 is shown as follow:

Aluminium nitrate nonahydrate 24 g consisted of aluminium equal to:

$$\begin{aligned}\text{Aluminium} &= (26.98 \times 24) / 212.98 = 3.0403 \text{ g} \\ &= 3.0403 / 26.98 = 0.1127 \text{ mol}\end{aligned}$$

For Zn/Al = 0.3, 0.1127 mol of aluminium

$$\begin{aligned}\text{Zinc required} &= 0.1127 \times 0.3 = 0.0338 \text{ mol} \\ &= 0.0338 \times 65.37 = 2.2099 \text{ g}\end{aligned}$$

Zinc 2.2099 g is used from $(\text{Zn}(\text{NO}_3)_2) \cdot 6\text{H}_2\text{O}$ and molecular weight of Zn is 65.37 g/mol

$$\begin{aligned}\text{Thus, } (\text{Zn}(\text{NO}_3)_2) \cdot 6\text{H}_2\text{O} \text{ required} &= (297.37 \times 2.2099) / 65.37 \\ &= 10.0529 \text{ g}\end{aligned}$$

Precipitation method

From **APPENDIX G**, concentration of AAS solution to AHC solution equal to 0.2:2.0 mol/l and molar ratio of AAS solution to AHC solution is 0.05:0.2, then AAS 11.859 g is required.

For molar ratio Zn/Al = 0.3 is shown as follow:

Ammonium aluminum sulfate 11.859 g consisted of aluminium equal to:

$$\begin{aligned}\text{Aluminium} &= (26.98 \times 11.859) / 237.18 = 1.3490 \text{ g} \\ &= 1.3490 / 26.98 = 0.0500 \text{ mol}\end{aligned}$$

For Zn/Al = 0.3, 0.0500 mol of aluminium

$$\begin{aligned}\text{Zinc required} &= 0.0500 \times 0.3 = 0.0150 \text{ mol} \\ &= 0.0150 \times 65.37 = 0.9806 \text{ g}\end{aligned}$$

Zinc 0.9806 g is used from $(\text{Zn}(\text{NO}_3)_2) \cdot 6\text{H}_2\text{O}$ and molecular weight of Zn is 65.37 g/mol

$$\begin{aligned}\text{Thus, } (\text{Zn}(\text{NO}_3)_2) \cdot 6\text{H}_2\text{O} \text{ required} &= (297.37 \times 0.9806) / 65.37 \\ &= 4.4608 \text{ g}\end{aligned}$$

APPENDIX I

TABLE OF MESH SIZE

Mesh size conversion table (Alfa Aesar, A Johnson Matthey Company)

A “+” before the mesh size indicates the particles are retained on and are larger than the sieve. A “-” before the mesh size indicates the particles pass through and are smaller than the sieve. For example, -325 mesh indicates the particles pass through and are smaller than the openings of a 325 mesh (44 micron) sieve. Typically 90% or more of the particles will fall within the specified mesh.

MESH SIZE	APPROXIMATE MICRON SIZE	APPROXIMATE MILLIMETERS	INCHES
4	4760	4.76	0.1850
6	3360	3.36	0.1310
8	2380	2.38	0.0930
12	1680	1.68	0.0650
16	1190	1.19	0.0460
20	840	0.84	0.0328
30	590	0.59	0.0232
40	420	0.42	0.0164
50	297	0.29	0.0116
60	250	0.25	0.0097
70	210	0.21	0.0082
80	177	0.17	0.0069
100	149	0.14	0.0058
140	105	0.10	0.0041
200	74	0.07	0.0029
230	62	0.06	0.0024
270	53	0.05	0.0021
325	44	0.04	0.0017
400	37	0.03	0.0015
625	20	0.02	0.0008
1250	10	0.01	0.0004
2500	5	0.005	0.0002

APPENDIX J

CALCULATION OF GAS HOURLY SPACE VELOCITY (GHSV)

For section 5.1

Volume of catalyst

$$\text{Diameter of reactor (d)} = 10.1 \text{ mm}$$

$$\text{High of catalyst (h)} = 1.5 \text{ mm}$$

$$\text{Volume} = \frac{\pi d^2 h}{4}$$

$$= 120.12 \text{ mm}^3$$

Flow rate

$$\text{First } 10 \text{ cm}^3/5.7 \text{ s} = (10*10*10*10*3600)/5.7 = 6315789.5 \text{ mm}^3/\text{h}$$

$$\text{Second } 10 \text{ cm}^3/9.2 \text{ s} = (10*10*10*10*3600)/9.2 = 3913043.5 \text{ mm}^3/\text{h}$$

$$\text{Third } 10 \text{ cm}^3/13.3 \text{ s} = (10*10*10*10*3600)/13.3 = 2706766.9 \text{ mm}^3/\text{h}$$

$$\text{Fourth } 10 \text{ cm}^3/24.2 \text{ s} = (10*10*10*10*3600)/24.2 = 1487603.3 \text{ mm}^3/\text{h}$$

GHSV (h^{-1})

Flow rate/ Volume of catalyst

$$\text{First} \quad 52580$$

$$\text{Second} \quad 32577$$

$$\text{Third} \quad 22534$$

$$\text{Fourth} \quad 12385$$

For section 5.2 and 5.3

$$\text{Volume of catalyst} = 120.12 \text{ mm}^3$$

Flow rate

$$\text{First} \quad 10 \text{ cm}^3/5.7 \text{ s} = (10*10*10*10*3600)/5.7 = 6315789.5 \text{ mm}^3/\text{h}$$

$$\text{Second} \quad 10 \text{ cm}^3/9.2 \text{ s} = (10*10*10*10*3600)/9.2 = 3913043.5 \text{ mm}^3/\text{h}$$

Third	$10 \text{ cm}^3/13.3 \text{ s} = (10*10*10*10*3600)/13.3 = 2706766.9 \text{ mm}^3/\text{h}$
Fourth	$10 \text{ cm}^3/24.2 \text{ s} = (10*10*10*10*3600)/24.2 = 1487603.3 \text{ mm}^3/\text{h}$
Fifth	$10 \text{ cm}^3/32 \text{ s} = (10*10*10*10*3600)/32 = 1125000 \text{ mm}^3/\text{h}$
Sixth	$10 \text{ cm}^3/45 \text{ s} = (10*10*10*10*3600)/45 = 800000 \text{ mm}^3/\text{h}$
Seventh	$10 \text{ cm}^3/70 \text{ s} = (10*10*10*10*3600)/70 = 514285.7 \text{ mm}^3/\text{h}$

GHSV (h^{-1})

Flow rate/ Volume of catalyst

First	52580
Second	32577
Third	22534
Fourth	12385
Fifth	9366
Sixth	6660
Seventh	4282

ศูนย์วิทยทรัพยากร
จุฬาลงกรณ์มหาวิทยาลัย

LIST OF PUBLICATIONS

International publications

1. Sataporn Komhom, Okorn Mekasuwandumrong, Piyasan Prasertthdam, Joongjai Panpranot, Improvement of Pd/Al₂O₃ catalyst performance in selective acetylene hydrogenation using mixed phases Al₂O₃ support, **Catalysis Communications**, **10 (2008), 86-91**
2. Sataporn Komhom, Piyasan Prasertthdam, Okorn Mekasuwandumrong, Joongjai Panpranot, Effects of the support crystallite size and the reduction temperature on the properties of Pd/ α -Al₂O₃ catalysts in selective acetylene hydrogenation, **Reaction Kinetics and Catalysis Letters**, **94 (2008), 233-241**
3. Sataporn Komhom, Okorn Mekasuwandumrong, Joongjai Panpranot, Piyasan Prasertthdam, Influence of preparation method on the nanocrystalline porosity of α -Al₂O₃ and the catalytic properties of Pd/ α -Al₂O₃ in selective acetylene hydrogenation, **(Revised to Industrial & Engineering Chemistry Research)**

Conference contributions

1. Sataporn Komhom, Okorn Mekasuwandumrong, Piyasan Prasertthdam, Joongjai Panpranot, Improvement of Pd/Al₂O₃ catalyst performance in selective acetylene hydrogenation using mixed phases Al₂O₃ support, The 13th Regional Symposium on Chemical Engineering “Advances in Chemical and Biomolecular Engineering”, Singapore from 3-5 December 2006 (Oral)
2. Sataporn Komhom, Piyasan Prasertthdam, Okorn Mekasuwandumrong, Joongjai Panpranot, Effects of the support crystallite size and the reduction temperature on the properties of Pd/ α -Al₂O₃ catalysts in selective acetylene hydrogenation, “RGJ Seminar series LVI conference”, 28 September 2007, Chulalongkorn University, Bangkok (Thailand) (Oral)



Improvement of Pd/Al₂O₃ catalyst performance in selective acetylene hydrogenation using mixed phases Al₂O₃ support

Sataporn Komhom^a, Okorn Mekasuwandumrong^b, Piyasan Praserttham^a, Joongjai Panpranot^{a,*}

^a Center of Excellence on Catalysis and Catalytic Reaction Engineering, Department of Chemical Engineering, Faculty of Engineering, Chulalongkorn University, Bangkok 10330, Thailand

^b Department of Chemical Engineering, Faculty of Engineering and Industrial Technology, Silpakorn University, Nakhonphatom 73000, Thailand

ARTICLE INFO

Article history:

Received 13 February 2008

Received in revised form 24 July 2008

Accepted 29 July 2008

Available online 7 August 2008

Keywords:

Selective acetylene hydrogenation

Mixed phases

Pd/Al₂O₃

α-Al₂O₃

ABSTRACT

The catalytic performances of Pd catalysts supported on γ-Al₂O₃, α-Al₂O₃, and mixed phases Al₂O₃ were investigated in the selective hydrogenation of acetylene in ethylene feed stream. It was found that the use of mixed phases Al₂O₃ with approximately 64% of α-phase resulted in significant improvements in both acetylene conversion and ethylene selectivity. The presence of small amount of transition phase in the alumina supports brought about higher BET surface area and Pd dispersion as well as improvement of reduction ability of the Pd/Al₂O₃ catalysts. On the other hand, significant amount of α-Al₂O₃ is necessary for high ethylene selectivity due to the lower amount of ethylene adsorbed.

© 2008 Elsevier B.V. All rights reserved.

1. Introduction

The effective removal of trace amount of acetylene in ethylene feedstock via selective hydrogenation using supported Pd-based catalysts is of particular challenge in the production of polyethylene since acetylene acts as a poison to the polymerization catalysts. The Pd/α-Al₂O₃ catalyst commonly used for selective acetylene hydrogenation is typically macroporous with a relatively small surface area of approximately 0.1–2 m²/g. In general, α-Al₂O₃ provides low dispersion of active metal than γ-Al₂O₃ due to its lower surface area; however, it is desirable in this reaction because Pd/α-Al₂O₃ catalyst possesses less active sites for direct ethane formation than Pd/γ-Al₂O₃ catalyst [1]. Moreover, α-Al₂O₃ is less acidic than γ-Al₂O₃ thus less oligomer/green oil was formed during acetylene hydrogenation reaction. However, the catalysts are suffered from runaway ethylene hydrogenation especially at high levels of acetylene conversion [2]. Several attempts have been made to improve the selectivity of Pd/Al₂O₃ catalysts and also reduce green oil formation in selective hydrogenation of acetylene such as promotion with a second component such as Ag [3], SiO₂ [4], TiO₂ [5] and pre-treatment of catalysts using oxygen-containing compounds [6–8]. However, development of new efficient catalysts for selective hydrogenation of acetylene has still received

much attention and has been reported continually including Pd on nano-sized TiO₂ [9,10], Pd on Ni modified Al₂O₃ [11], and zeolite-supported Pd–Ag catalysts [12,13].

In general, the more acidic, high surface area alumina hydrates are produced at relatively low temperatures by precipitation from either acidic or basic solutions and are transformed to ‘transition’ β-, γ-, η-, χ-, κ-, δ-, θ-, and α-Al₂O₃ by dehydration and treatment at high temperatures [14]. Differences in crystalline phases may result in changes in physical and chemical properties of Al₂O₃ supports and could play an important role on the catalytic performance of Al₂O₃ supported catalysts. For example, Chary et al. [15] reported that dispersion of vanadium oxide on Al₂O₃ supports as well as their catalytic activities in partial oxidation decreased with increasing calcination temperature due to the transformation of γ-Al₂O₃ into θ-, δ-, and α-Al₂O₃. Moya et al. [16] studied silver nanoparticles supported on α-, η-, and δ-Al₂O₃ prepared by colloidal processing route. It was found that silver particle sizes varied between 1 and 100 nm depending on the Al₂O₃ phases.

In this study, the effect of mixed phases Al₂O₃ (i.e. γ-, θ-, and α-Al₂O₃) on the properties of Pd/Al₂O₃ catalysts was investigated in the gas-phase selective hydrogenation of acetylene in ethylene feed stream. The weights (%) of α-phase were 0, 14, 47, 64, and 100 depending on the calcination conditions of the starting γ-Al₂O₃. The catalysts were characterized by means of X-ray diffraction (XRD), N₂ physisorption, CO pulse chemisorption, H₂-temperature programmed reduction (TPR), X-ray photoelectron spectroscopy (XPS), transmission electron microscope (TEM) and temperature programmed desorption of ethylene (C₂H₄-TPD).

* Corresponding author. Tel.: +66 2 2186869; fax: +66 2 2186877.

E-mail address: joongjai.p@eng.chula.ac.th (J. Panpranot).

2. Experimental

2.1. Catalysts preparation

γ - Al_2O_3 used in this study was the commercial available alumina JRC-ALO-2 (JRC Co., Ltd. Japan). The mixed phases with various phase compositions were prepared by calcination of the γ - Al_2O_3 at 1100 °C for 120, 200, or 240 min. The α - Al_2O_3 was obtained by calcination of the γ - Al_2O_3 at 1175 °C for 120 min. In this paper, the alumina samples consisting of 0, 14, 47, 64, and 100% α -phase are referred to as Al- α 0, Al- α 14, Al- α 47, Al- α 64, and Al- α 100, respectively. The percentage of alpha phase was calculated using a calibration curve from XRD results of the physically mixed γ -, and α - Al_2O_3 (not shown here).

The Pd/ Al_2O_3 catalysts with weight (%) of Pd approximately 1% were prepared by the incipient wetness impregnation technique using an aqueous solution of Pd(NO_3)₂ (Wako, Japan) as the palladium precursor. The catalysts were subsequently dried at 110 °C for 12 h and calcined in air at 550 °C for 2 h.

2.2. Catalyst characterization

The X-ray diffraction (XRD) pattern of the Al_2O_3 supports and Pd/ Al_2O_3 catalysts were carried out using an X-ray diffractometer, SIEMENS XRD D5000, with Cu K α radiation with a Ni filter. The BET surface areas of the Al_2O_3 supports were measured by N_2 physisorption using a Micromeritics ASAP 2000 automated system. The samples were degassed at 200 °C for 1 h prior to N_2 physisorption. The amounts of CO chemisorbed on the Pd/ Al_2O_3 catalysts were measured at room temperature by using a Micromeritics Chemisorb 2750 automated system attached with ChemiSoft TPx software at room temperature. Prior the measurement, 30 ml/min of He gas was introduced into the sample cell in order to remove the remaining air. The system was switched to 50 ml/min of hydrogen and heated to 150 °C with a heating rate of 10 °C/min. The temperature was kept constant for 2 h and then cooled down to the room temperature. Temperature program experiments were carried out in a Micromeritics Chemisorb 2750 automated system. The temperature ramping was controlled by temperature controller, Furnace Power 48 VAC 8A MAX. The XPS analysis was performed using an AMICUS photoelectron spectrom-

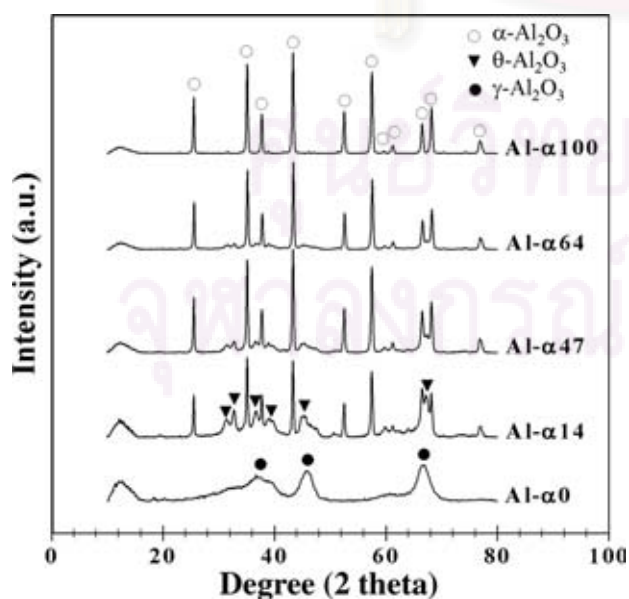


Fig. 1. The XRD patterns of the Al_2O_3 supports containing various % of α -phase.

eter equipped with an Mg K α X-ray as primary excitation and KRATOS VISION2 software. XPS elemental spectra were acquired with 0.1 eV energy step at a pass energy of 75 kV. The C 1s line was taken as an internal standard at 285.0 eV. The distribution of palladium on catalyst supports were observed using JEOL Model JEM-2010 transmission electron microscope operated at 200 keV. A mixture of 10% H_2 in Ar with a flow rate of 15 cm^3/min was used in TPR experiment. Prior the experiment, the sample was treated in N_2 flow at 200 °C for 1 h in order to remove any adsorbed gas. The TPR was performed with a constant heating rate of 10 °C/min from 35 to 200 °C. For ethylene-TPD experiments, the samples were pre-reduced at 150 °C in H_2 for 2 h (flow rate 50 cm^3/min) and cooled down to room temperature. Then adsorption of ethylene was performed at room temperature for 3 h. The temperature programmed desorption was performed with a constant heating rate of 10 °C/min from 35 to 800 °C. The amount of desorbed ethylene was measured by analyzing the effluent gas with a thermal conductivity detector.

2.3. Reaction study

The catalyst performances in selective hydrogenation of acetylene were evaluated using a 10 mm (id) pyrex reactor. Prior to the start of each experimental run, the catalyst was reduced *in situ* with hydrogen by heating from room temperature to 150 °C at a heating rate of 10 °C/min. Then the reactor was purged with argon and cooled down to the reaction temperature 40 °C. The reaction was carried out using a feed composition of 1.5% C_2H_2 , 1.7% H_2 , and balanced C_2H_4 with a vary GHSV of 52,580, 32,577, 22,534 and 12,385 h^{-1} . The products and feeds were analyzed by

Table 1
The physical properties of alumina with various phase compositions

Samples	α -Phase (%)	BET surface area (m^2/g)	Crystallite size (nm) ^a		Pore volume ^b (cm^3/g)	Average pore diameter ^b (Å)
			γ -Phase	α -Phase		
Al- α 100	100	12.3	n.d.	44.5	0.03	90.1
Al- α 64	64	36.1	28.3	45.8	0.14	129.6
Al- α 47	47	45.4	17.8	48.9	0.20	151.9
Al- α 14	14	67.3	11.8	46.0	0.30	143.8
Al- α 0	0	244.1	3.7	n.d.	0.66	78.9

n.d. = Not determined.

^a Calculated from XRD results.

^b Based on BJH method.

Table 2
Physicochemical properties of Pd supported on alumina with various phase compositions

Samples	Pd active sites ^a ($\times 10^{-18}$ CO molecule/g-cat)	% Pd dispersion ^b	dp ^c (Pd ⁰) (nm)	Pd 3d _{5/2} ^d		Atomic concentration ^d Pd/Al
				BE (eV)	FWHM	
Pd/Al- α 100	7.4	12.5	8.9	336.9	1.8	0.034
Pd/Al- α 64	11.0	18.5	6.1	336.9	2.0	0.027
Pd/Al- α 47	25.4	42.9	2.6	336.4	2.4	0.020
Pd/Al- α 14	31.7	53.5	2.1	336.4	2.3	0.011
Pd/Al- α 0	35.1	59.2	1.9	336.4	2.2	0.001

V_{ads} , volume adsorbed; V_g , molar volume of gas at STP; S_f , stoichiometry factor, CO on Pd; MW, molecular weight of the metal; %M, %metal loading.

^a Pd active sites = $(V_{\text{ads}}/V_g) \times (6.02 \times 10^{23})$. Error of measurement = $\pm 5\%$.

^b % Pd dispersion = $[\text{Pd active sites} \times S_f \times (\text{M.W./\% M}) \times 100\% \times 100\%] / (6.02 \times 10^{23})$.

^c Based on $d_p = 1.12/D$ (nm), where D = % Pd dispersion [25].

^d Based on XPS results.

a two gas chromatographs equipped with a FID detector (SHIMADZU FID GC 9A, carbosieve column S-2) and TCD detector (SHIMADZU TCD GC 8A, molecular sieve-5A).

3. Results and discussion

The mixed phases Al_2O_3 supports used for preparation of the $\text{Pd}/\text{Al}_2\text{O}_3$ catalysts in this study were obtained by varying the calcination conditions of the $\gamma\text{-Al}_2\text{O}_3$ (calcination temperature 1100–1175 °C and holding time 2–4 h). The XRD patterns of Al_2O_3 are shown in Fig. 1. The weight (%) of α -phase in these samples were calculated to be 0%, 14%, 47%, 64% and 100% using a calibration from XRD results of the physically mixed γ - and $\alpha\text{-Al}_2\text{O}_3$ (not shown here) and were designated herein as Al- α 0, Al- α 14, Al- α 47, Al- α 64, and Al- α 100, respectively.

Table 1 summarizes physical properties of the various Al_2O_3 supports. The crystallite size of transition phase was increased from 3.7 to 28.3 nm as the weight (%) of α -phase content increased

from 0% to 64%, while the crystal size of α -phase remained constant at around 45 nm. The specific surface area and total pore volume calculated from BJH method decreased from 244 to 12 m^2/g and 0.66 to 0.03 cm^3/g with increasing amount of α -phase alumina. A drastically decrease in BET surface area and total pore volume of alumina during phase transformation can be explained by the rapidly increase of alumina crystal size. It is generally known that calcination of $\gamma\text{-Al}_2\text{O}_3$ at high temperature results in phase transformation from γ - to θ - and then $\alpha\text{-Al}_2\text{O}_3$.

The XRD characteristic peaks of all the $\text{Pd}/\text{Al}_2\text{O}_3$ catalysts were not different from the Al_2O_3 supports after Pd loading. No XRD peaks for PdO or Pd^0 metal were observed due probably to the low loading of palladium (results not shown). The CO chemisorption results such as the number of active Pd atoms, Pd dispersion (%), and average Pd metal particle size are summarized in Table 2. Palladium dispersion was estimated from the amount of CO chemisorbed assuming a stoichiometry of $\text{CO}/\text{Pd} = 1$ [17]. The number of Pd active sites decreased from 35.1 to 7.4×10^{18} sites/

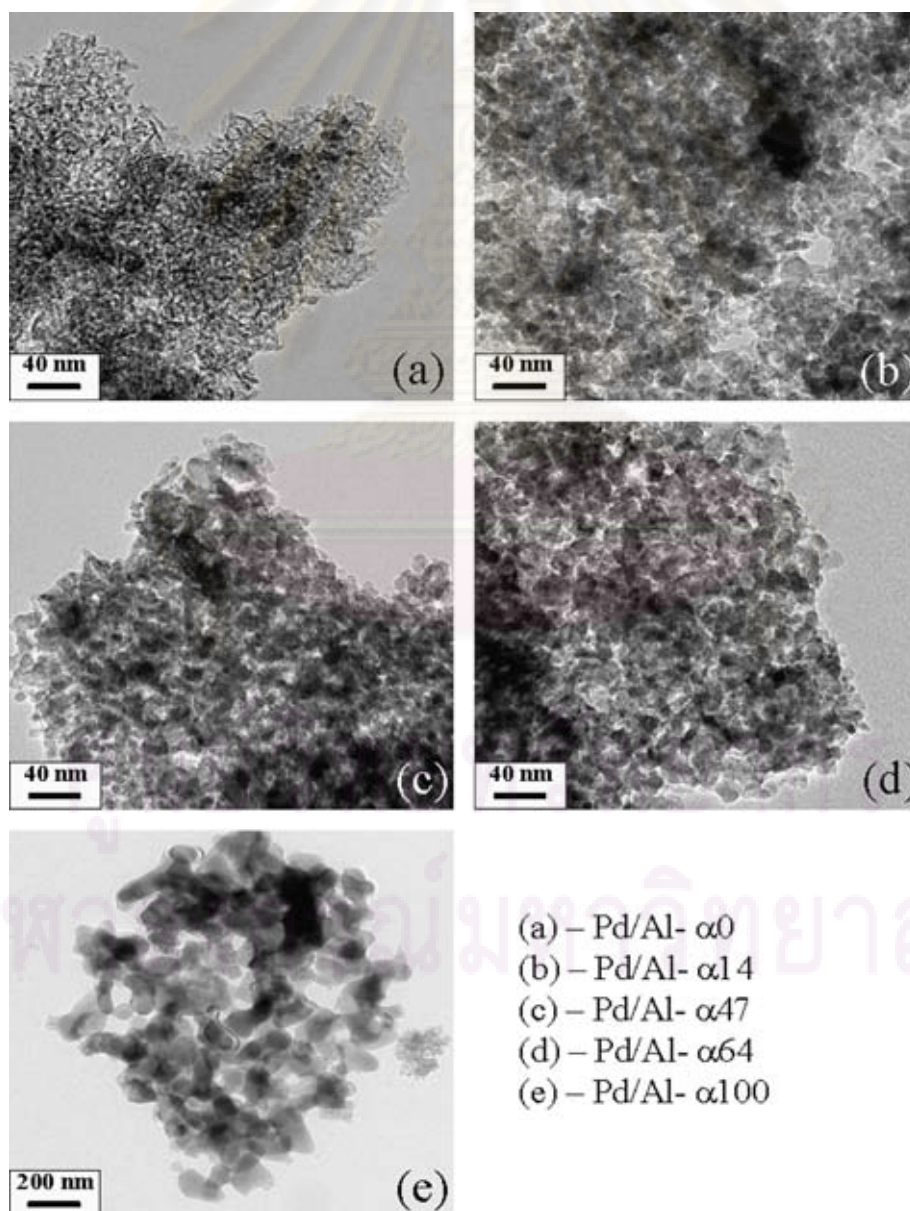


Fig. 2. Transmission electron micrographs of the $\text{Pd}/\text{Al}_2\text{O}_3$ catalysts.

g-catalyst corresponding to a decrease in Pd dispersion (%) from 59.5 to 12.5 and an increase in Pd metal particle size from 1.9 to 8.9 nm as the weight (%) of α -phase contents increased from 0% to 100%.

In order to verify the Pd particle size, TEM micrographs have been acquired and are shown in Fig. 2. The Pd supported on pure γ - Al_2O_3 consisted of particles with primarily spherical shape with some needlelike structure. The particle shape appeared more uniformly spheroidal for those supported on mixed phases Al_2O_3 . Large fingerlike shape particles were observed for the catalysts containing 100% α -phase Al_2O_3 . Increasing α -phase content of the alumina supports from 0 to 100% resulted in an increase of Pd cluster/particle size from about 2 to 10 nm.

XPS is used to determine the surface compositions of the catalysts and the interaction between Pd and the Al_2O_3 supports. The deconvoluted XPS photoelectron spectra for the Pd 3d core level region of all the catalysts are shown in Fig. 3. From the figure, the Pd doublet was clearly evident. A small shoulder at the binding energy around 335.1–335.8 eV was present in every sample and was

attributed to metallic Pd^0 [18]. Such results indicated that partial reduction occurred during analysis. PdO species was observed at the binding energies in the range of 336.9–336.4 eV which was consistent to the values reported in the literature [19,20]. The percentages of atomic concentration, the binding energy, and FWHM of Pd 3d are also given in Table 2. The atomic concentration ratios for Pd/Al decreased with the decrease in α -phase Al_2O_3 contents. The results were consistent with the CO chemisorption results that larger Pd particle sizes were obtained on α - Al_2O_3 . The FWHM values larger than two for Pd $3d_{5/2}$ may be due to some differential charging that contributed to the widening of the palladium peaks [21,22].

Reduction behavior and reducibility of the catalysts were investigated by means of H_2 -temperature programmed reduction and the results are shown in Fig. 4. All the Pd/ Al_2O_3 catalysts exhibited TPR profiles with one main reduction peak which can be assigned to the reduction of PdO to Pd^0 metal. This peak remained constant at around 55 °C for those with the weight (%) of α -phase contents between 0% and 64%. The reduction peak was slightly shifted to

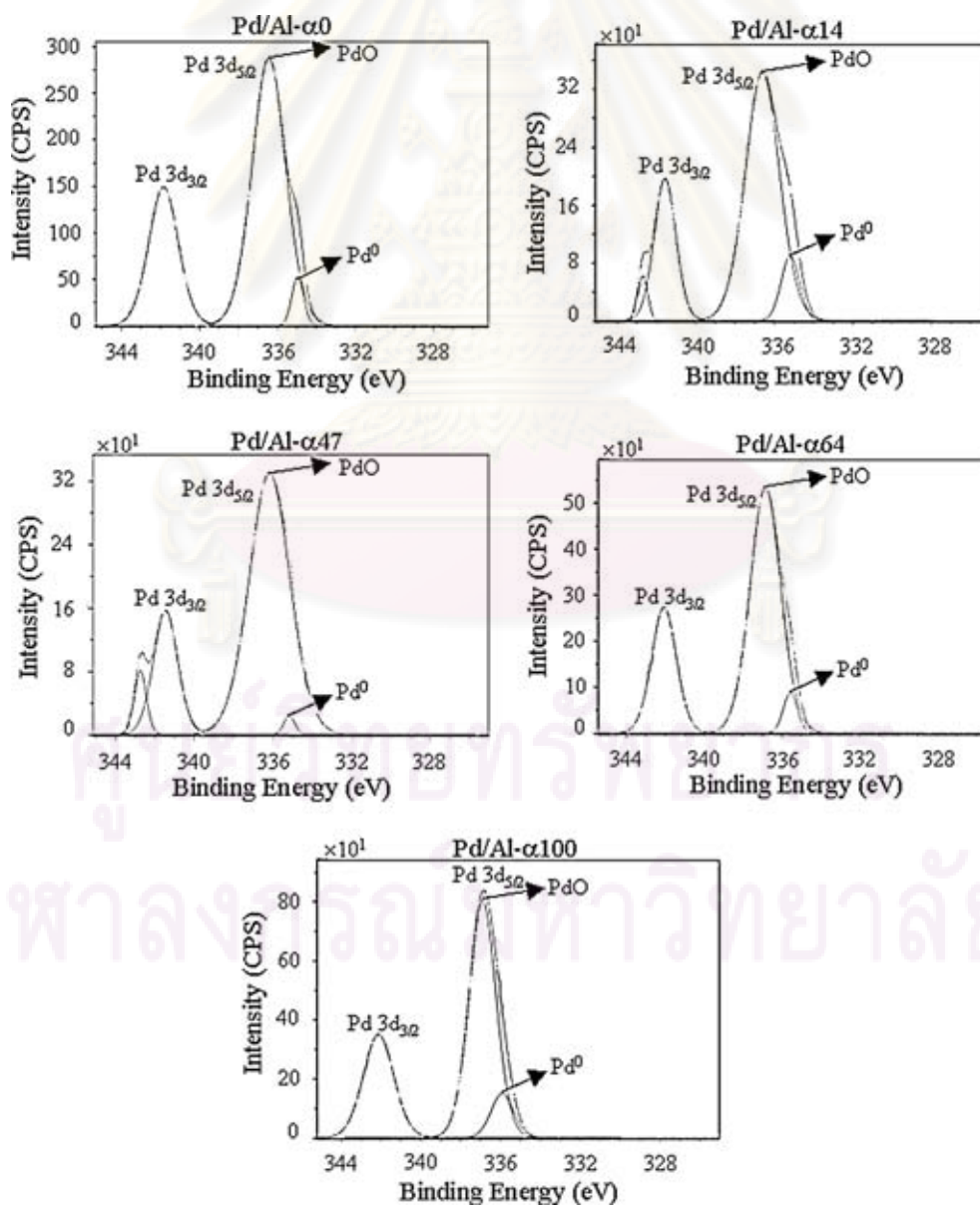


Fig. 3. The XPS deconvoluted spectra of the Pd/ Al_2O_3 catalysts.

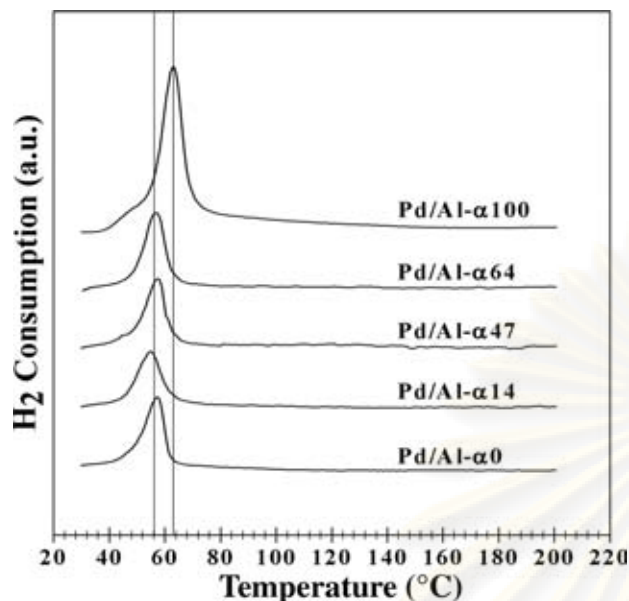


Fig. 4. TPR profiles of the Pd/Al₂O₃ catalysts.

65 °C for the Pd/Al- α 100 catalyst (100% α -phase). It is suggested that the existence of transition phase Al₂O₃ (either γ - or θ -Al₂O₃) in the Al₂O₃ supports facilitated reduction at low temperature. However, the hydrogen consumptions during the transformation of PdO to metallic Pd as determined from the areas of the reduction peak for all the catalysts were essentially the same.

Ethylene-temperature programmed desorption (C₂H₄-TPD) was performed in order to obtain an information about ethylene adsorption behavior on the catalyst surfaces. The C₂H₄-TPD experiments were carried out at 35–800 °C after the samples were reduced in H₂ at 150 °C and purged with He at the same adsorption temperature. The temperature programmed study profiles of the catalysts are shown in Fig. 5. Two main desorption peaks at ca. 80–105 °C and 275–300 °C were observed for all the catalyst samples. As suggested by Moon et al. [23], the lower temperature desorption peak was assigned to π -bonded ethylene spe-

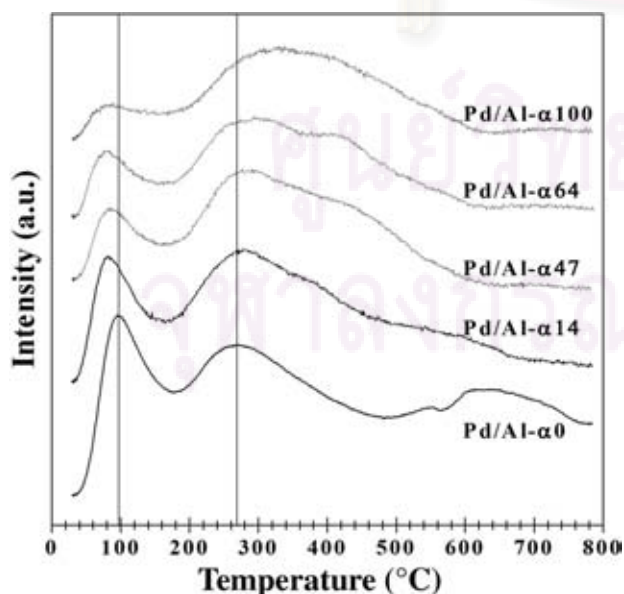


Fig. 5. Ethylene TPD results of the Pd/Al₂O₃ catalysts.

cies while the higher temperature was assigned to di- σ -bonded ethylene. The latter species were suggested to be the species that recombined with surface hydrocarbon and produced ethane. In some cases, the third peak at temperature range around 450–650 °C was observed. It was suggested to be due to decomposition of C₂ hydrocarbons adsorbed on Pd surface [24]. In the present study, the intensities of the TCD signals during ethylene temperature programmed desorption was significantly decreased when the content of α -phase in the Al₂O₃ supports increased from 0 to 100%. In other words, the amount of ethylene adsorbed was much lower when the Al₂O₃ supports contained significant amounts of α -Al₂O₃.

The catalytic performances of Pd/Al₂O₃ catalysts containing α -Al₂O₃, γ -Al₂O₃, or mixed phases alumina were evaluated in the selective hydrogenation of acetylene at 40 °C under various feed flow rates (GHSV 52,580, 32,577, 22,534, and 12,385 h⁻¹). Acetylene conversion is defined as moles of acetylene converted with respect to acetylene in feed. Ethylene gain is defined as the percentage of acetylene hydrogenated to ethylene over totally hydrogenated acetylene. The ethylene being hydrogenated to ethane (ethylene loss) is the difference between all the hydrogen consumed and all the acetylene which has been totally hydrogenated. The plots of acetylene conversion and ethylene selectivity versus GHSV are shown in Figs. 6 and 7, respectively. In general, acetylene conversion decreased with increasing GHSV while ethylene gain increased. Since ethylene is produced as an intermediate in

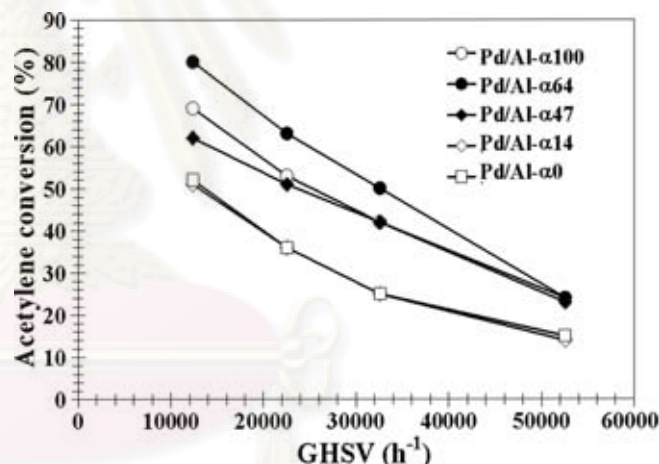


Fig. 6. Catalyst performances in selective hydrogenation of acetylene in terms of GHSV values and acetylene conversion (%).

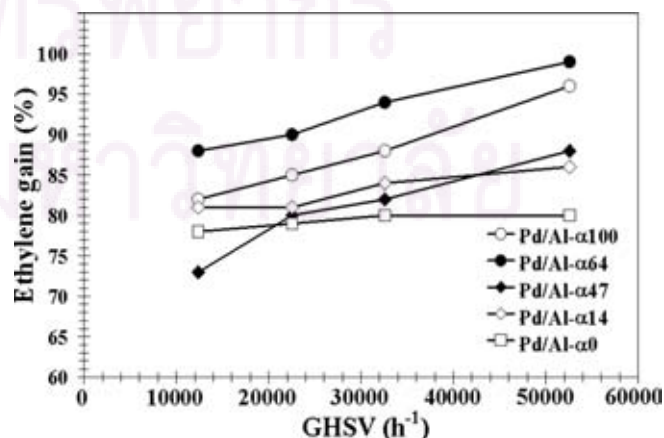


Fig. 7. Catalyst performances in selective hydrogenation of acetylene in terms of GHSV values and ethylene gain (%).

acetylene hydrogenation, which is a typical consecutive reaction, the ethylene selectivity decreases with acetylene conversion [5]. The performance of Pd/Al₂O₃ catalysts was improved in the order of Pd/Al- α 64 > Pd/Al- α 100 > Pd/Al- α 47 > Pd/Al- α 14 > Pd/Al- α 0. It is clearly shown that the Pd catalyst supported on mixed phase Al₂O₃ that contained 64% of α -phase (Pd/Al- α 64) exhibited the best catalytic performance among the five catalysts studied.

Based on the characterization results, the presence of the transition phase in α -Al₂O₃ supports increased the specific surface area, total pore volume, Pd active sites and the dispersion of Pd on Al₂O₃ supports and facilitated the reduction of PdO at lower temperature, which promoted acetylene conversion. However, the TPD profiles suggest that the amount of ethylene adsorbed on the catalyst surface decreased with increasing α -phase content. The feature is important for the improvement of ethylene gain especially at high acetylene conversion. The results in this study revealed that the beneficial properties of both α -Al₂O₃ and transition alumina can be combined to give the best catalytic performance of Pd/Al₂O₃ catalyst in selective acetylene hydrogenation. Among the five catalysts studied, the optimum amount of α -phase content was found to be at 64 wt%.

4. Conclusions

The catalytic performances of Pd/Al₂O₃ catalysts in selective hydrogenation of acetylene were significantly improved when the Al₂O₃ support consisted of mixed transition- Al₂O₃ and α -Al₂O₃ with ca. 64% of α -Al₂O₃. The presence of transition phase Al₂O₃ in α -Al₂O₃ resulted in combined properties of the transition Al₂O₃ such as higher BET surface area, higher Pd dispersion, improved reduction ability and the beneficial properties of α -Al₂O₃ for selective acetylene hydrogenation such as lower amount of ethylene adsorbed. Among the five crystalline phase compositions of alumina used in this study, the one containing 64% α -Al₂O₃ was found to be the best (optimum) composition to prepare Pd/Al₂O₃ catalysts with high acetylene conversion and high ethylene selectivity.

Acknowledgements

The authors would like to thank the Commission for Higher Education, Ministry of Education, Thailand and the Thailand Research Fund (TRF) for the financial supports of this project.

References

- [1] M.J. Vincent, R.D. Gonzalez, Appl. Catal. A: Gen. 217 (2001) 143.
- [2] S. LeViness, V. Nair, A. Weiss, J. Mol. Catal. A: Chem. 25 (1984) 131.
- [3] Y. Jin, A.K. Datye, E. Rightor, R. Gulotty, W. Waterman, M. Smith, J. Catal. 203 (2001) 292.
- [4] E.W. Shin, C.H. Choi, K.S. Chang, Y.H. Na, S.H. Moon, Catal. Today 44 (1998) 137.
- [5] J.H. Kang, E.W. Shin, W.J. Kim, J.D. Park, S.H. Moon, J. Catal. 208 (2002) 310.
- [6] P. Praserthdam, B. Ngamsom, N. Bogdanchikova, S. Phatanasri, M. Pramothana, Appl. Catal. A: Gen. 230 (2002) 41.
- [7] R.N. Lamb, B. Ngamsom, D.L. Trimm, B. Gong, P.L. Silveston, P. Praserthdam, Appl. Catal. A: Gen. 268 (2004) 43.
- [8] B. Ngamsom, N. Bogdanchikova, M.A. Borja, P. Praserthdam, Catal. Commun. 5 (2004) 243.
- [9] J. Panpranot, K. Kontapakdee, P. Praserthdam, Appl. Catal. A: Gen. 314 (2006) 128.
- [10] J. Hong, W. Chu, M. Chen, X. Wang, T. Zhang, Catal. Commun. 8 (2007) 593.
- [11] N. Wongwaranon, O. Mekasuwandumrong, P. Praserthdam, J. Panpranot, Catal. Today 131 (2008) 553.
- [12] W. Huang, J.R. McCormick, R.F. Lobo, J.G. Chen, J. Catal. 246 (2007) 40.
- [13] W. Huang, W. Pyrz, R.F. Lobo, J.G. Chen, Appl. Catal. A: Gen. 333 (2007) 254.
- [14] R.J. Farrauto, C.H. Bartholomew, Fundamentals of Industrial Catalytic Process, third ed., Blackie Academic and Professional, New York, 2002.
- [15] K.V.R. Chary, G. Kishan, C.P. Kumar, G.V. Sagar, Appl. Catal. A: Gen. 246 (2003) 335.
- [16] A. Esteban-Cubillo, C. Díaz, A. Fernández, L.A. Díaz, C. Pecharrómán, R. Torrecillas, J.S. Moya, J. Eur. Ceram. Soc. 26 (2006) 1.
- [17] V.H. Sandoval, C.E. Gigola, Appl. Catal. A: Gen. 148 (1996) 81.
- [18] J.F. Moulder, W.W. Stickle, P.E. Sobol, K.D. Bombier, in: J. Chastain (Ed.), Handbook of X-ray Photoelectron Spectroscopy, Perkin Elmer, Eden Prairie, USA, 1992.
- [19] P. Legare, F. Finck, R. Roche, G. Maire, J. Surf. Sci. 217 (1989) 167.
- [20] M. Brun, A. Berthet, J.C. Bertolini, J. Electron Spectrosc. Relat. Phenom. 104 (1999) 55.
- [21] A.M. Venezia, A. Rossi, L.F. Liotta, A. Martorana, G. Deganello, Appl. Catal. A: Gen. 147 (1996) 81.
- [22] A.B. Gaspar, L.C. Dieguez, Appl. Catal. A: Gen. 201 (2000) 241.
- [23] I.Y. Ahn, W.J. Kim, S.H. Moon, Appl. Catal. A: Gen. 308 (2006) 75.
- [24] E.W. Shin, J.H. Kang, W.J. Kim, J.D. Park, S.H. Moon, Appl. Catal. A: Gen. 223 (2002) 161.
- [25] N. Mahata, V. Vishwanathan, J. Catal. 196 (2000) 262.

RKCL5304

**EFFECTS OF THE SUPPORT CRYSTALLITE SIZE AND THE
REDUCTION TEMPERATURE ON THE PROPERTIES OF Pd/ α -Al₂O₃
CATALYSTS IN SELECTIVE ACETYLENE HYDROGENATION**

**Sataporn Komhom^a, Piyasan Praserttham^a, Okorn Mekasuwandumrong^b
and Joongjai Panpranot^{a,*}**

^aCenter of Excellence on Catalysis and Catalytic Reaction Engineering
Department of Chemical Engineering, Faculty of Engineering
Chulalongkorn University, Bangkok, 10330 Thailand

^bDepartment of Chemical Engineering,
Faculty of Engineering and Industrial Technology, Silpakorn University, Nakhonphatom, 73000
Thailand

Received February 28, 2008, in revised form May 13, 2008, accepted May 16, 2008

Abstract

Pd catalysts supported on the solvothermal-derived nanocrystalline α -Al₂O₃ (45 nm) exhibited superior performances in the selective acetylene hydrogenation than those supported on micron-sized ones (44–149 μ m). Reduction at 500°C led to an improvement of the ethylene yield for the Pd/nanocrystalline α -Al₂O₃, but not for the Pd/micron-sized α -Al₂O₃.

Keywords: Selective hydrogenation, acetylene, crystallite sizes effect, Pd/ α -Al₂O₃

INTRODUCTION

The cracking of petrochemical naphtha usually produces a stream composed mainly of ethylene, paraffins, diolefins, aromatics, and a small amount of acetylene. Ethylene is mainly used in the production of polymers, especially polyethylene [1]. Small amounts of acetylene, in the order of parts per million, are harmful to the catalysts used in polymerization, which should be lowered to

* Corresponding author Tel: 66-2-2186869; Fax: 66-2-2186877
E-mail: joongjai.p@eng.chula.ac.th

below 5 ppm [2]. Therefore, acetylene in the ethylene stream must be hydrogenated aiming at reducing its concentration with a minimum loss of ethylene to ethane. Generally, macroporous alumina-supported palladium catalyst is used for the selective acetylene hydrogenation in ethylene feed stream. The catalyst has a relatively small surface area of 0.1 to 3 m²/g and requires carbon monoxide to enhance its selectivity towards ethylene, which is a limitation in practical use. Several attempts have been made to improve the selectivity of Pd/Al₂O₃ catalysts by addition of a second component [3-5]. Development of new efficient catalysts for the selective hydrogenation has also been reported continually including the glow discharge plasma Pd/ α -Al₂O₃ [6], Pd on nano-sized TiO₂ [7], Pd on nanocrystalline Ni-modified α -Al₂O₃ [8], and zeolite-supported Pd-Ag catalysts [9].

In recent years, nanocrystalline materials have gained considerable interest in the field of catalysis, because they show significant differences in terms of catalytic activity and selectivity as compared with those synthesized in the micron scale. Several techniques have been reported for preparation of nanocrystalline alumina, such as the sol-gel method [10], microwave synthesis [11], emulsion evaporation [12], precipitation [13], and solvothermal synthesis [14]. Among various methods, the products obtained by solvothermal synthesis show uniform morphology, well-controlled chemical composition and narrow size distribution.

It is the aim of this study to investigate the effects of the support crystallite size and the reduction temperature on the catalytic properties of Pd/ α -Al₂O₃ catalysts in selective acetylene hydrogenation. The catalysts were prepared on commercially available micron-sized α -Al₂O₃ and nanocrystalline α -Al₂O₃ prepared via the solvothermal method and characterized by N₂ physisorption, X-ray diffraction (XRD), CO pulse chemisorption, H₂ temperature programmed reduction (H₂-TPR), and ethylene temperature programmed desorption (C₂H₄-TPD).

EXPERIMENTAL

Catalyst preparation

The supports for the catalyst preparation are micron-sized and nanocrystalline α -Al₂O₃. The micron-sized α -Al₂O₃ was the commercially available α -Al₂O₃ from Sigma-Aldrich (-100+325 mesh or 44-149 μ m). The nanocrystalline α -Al₂O₃ was prepared by the solvothermal method according to Ref. [8]. Approximately 25 g of aluminum isopropoxide (AIP) was suspended in 100 mL of toluene in a test tube, which was added to 30 mL of toluene. The autoclave was purged completely by nitrogen before heating up to 300°C at a

rate of 2.5°C/min, and held at this temperature for 2 h. After the system was cooled down, the resulting products were washed repeatedly with acetone, and dried in air overnight. The obtained products were then calcined in depleted-oxygen atmosphere in a box furnace at 1150°C for 1 h with a heating rate of 10°C/min for transformation to α -Al₂O₃.

The 1%Pd/ α -Al₂O₃ catalysts were prepared by an incipient wetness impregnation using Pd(NO₃)₂ (Aldrich) as the palladium precursor. The alumina support (2 g) was placed in an Erlenmeyer flask then the impregnating solution from the palladium solution was gradually dripped into the support. Shaking the flask continuously during impregnation was required to ensure a homogeneous distribution of metal component on the support. After impregnation, the catalysts were let stand at room temperature for 6 h, dried at 110°C in an oven overnight, and then calcined by flowing air at 500°C for 2 h.

Catalyst characterization

The X-ray diffraction (XRD) patterns were collected by using an X-ray diffractometer, SIEMENS XRD D5000, with CuK α radiation with a Ni filter in the 2 θ range of 20-80 degrees, resolution 0.04°. The BET surface areas of the Al₂O₃ supports were measured by N₂ physisorption using a Micromeritic ASAP 2000 automated system. The samples were heated at 200°C for 1 h prior to N₂ physisorption. The amounts of CO chemisorbed on the Pd/Al₂O₃ catalysts were measured using a Micromeritic Chemisorb 2750 automated system attached with a ChemiSoft TPx software at room temperature. Palladium dispersion was estimated from the amount of CO chemisorbed assuming the stoichiometry of CO/Pd = 1 [15]. The XPS analysis was performed using an AMICUS photoelectron spectrometer equipped with a MgK α X-ray as primary excitation and KRATOS VISION2 software. XPS elemental spectra were acquired with 0.1 eV energy steps at a pass energy of 75 kV. The C 1s line was taken as an internal standard at 285.0 eV. Temperature programmed experiments were carried out in a Micromeritic Chemisorb 2750 automated system. A mixture of 10%H₂ in Ar with a flow rate of 15 cm³/min was used in the TPR experiment with a constant heating rate of 10°C/min from 30 to 300°C. For ethylene-TPD experiments, the samples were pre-reduced at 150°C in H₂ for 2 h and cooled down to room temperature. Then, the adsorption of ethylene was performed at room temperature for 3 h. The temperature-programmed desorption was performed with a constant heating rate of 10°C/min from 30 to 780°C.

Reaction study

The catalyst performances in selective hydrogenation of acetylene were evaluated using a 10 mm (i.d.) pyrex reactor. Prior to the start of each experimental run, the catalyst was reduced *in situ* with hydrogen by heating from room temperature to 150 or 500°C at a heating rate of 10°C/min. Then the reactor was purged with argon, and cooled down to the reaction temperature of 60°C. The reaction was carried out using a feed composition of 1.5% C₂H₂, 1.7% H₂, and balanced C₂H₄ with a varying GHSV of 52580, 32577, 22534, 12385, 9366, 6660 and 4282 h⁻¹. The products and feeds were analyzed by two gas chromatographs equipped with an FID detector (SHIMADZU FID GC 9A, carbosieve column S-2) and TCD detector (SHIMADZU TCD GC 8A, molecular sieve-5A).

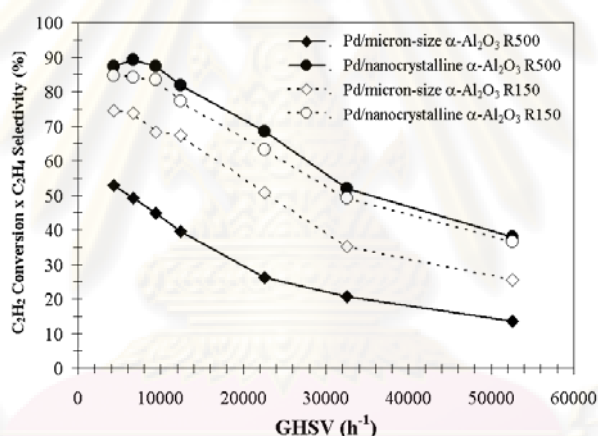


Fig. 1. The catalytic performances of Pd catalysts supported on micron-sized and nanocrystalline α -Al₂O₃ reduced at 150° and 500°C in selective acetylene hydrogenation under various feed flow rates

RESULTS AND DISCUSSION

The plots between acetylene conversion \times ethylene selectivity vs. GHSV are shown in Fig. 1. Acetylene conversion is defined as moles of acetylene converted with respect to acetylene in the feed, and ethylene selectivity is defined as the percentage of acetylene hydrogenated to ethylene over totally hydrogenated acetylene. However, due to the difficulty in the precise measurement of the ethylene change in the feed and product, the indirect calculation using the difference in the amount of hydrogen consumed was used.

The amount of ethylene being hydrogenated to ethane is the difference between all the hydrogen consumed and all the acetylene totally hydrogenated.

It is clearly seen that the ethylene yield (%) was improved in order of Pd/nanocrystalline Al_2O_3 -R500°C > Pd/nanocrystalline Al_2O_3 -R150°C > Pd/micron-sized Al_2O_3 -R150°C > Pd/micron-sized Al_2O_3 -R500°C. The Pd catalysts supported on nanocrystalline α - Al_2O_3 exhibited superior performance to the micron-sized supported ones. It should be noticed that the catalytic performance of Pd/nanocrystalline α - Al_2O_3 was improved by reduction at 500°C while the Pd/micron-sized α - Al_2O_3 showed the opposite trend. The results suggest that the interaction between the Pd metal and the α - Al_2O_3 support was affected by the crystallite size of α - Al_2O_3 . Reduction at 500°C could result in stronger metal-support interaction between the Pd metal and α - Al_2O_3 for the nanocrystalline α - Al_2O_3 supported catalysts and as a consequence, ethylene selectivity was enhanced due to the lower adsorption strength of ethylene as can be found in other catalyst systems such as Pd/TiO₂ [16]. The absence of strong metal-support interaction in the case of Pd/micron-sized α - Al_2O_3 was probably due to a sintering of the Pd⁰ metal during the high temperature reduction.

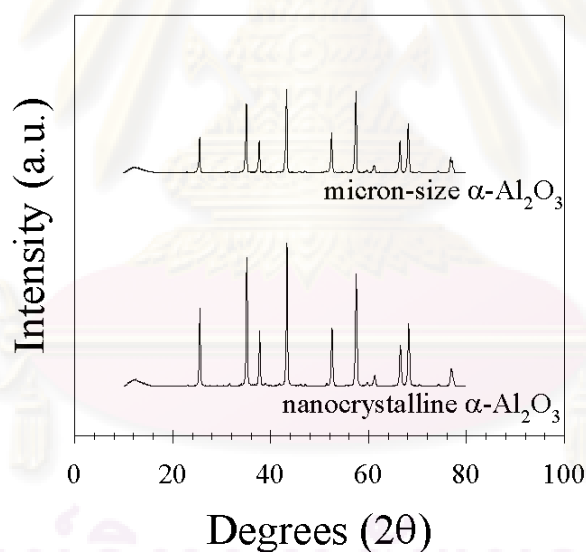


Fig. 2. XRD patterns of the micron-sized and nanocrystalline α - Al_2O_3

Based on XRD results (Fig. 2), both supports showed only the crystal structure for α -phase Al_2O_3 . The average crystallite size of nanocrystalline α - Al_2O_3 calculated from the XRD peak at $2\theta = 43.32^\circ$ using Scherrer's equation

was 45 nm, while those of the commercial one could not be determined by this method due to the calculation limit of the Scherrer equation (the crystallite size may be too large). The physicochemical properties of α -Al₂O₃ supports are summarized in Table 1. The specific surface area of nanocrystalline α -Al₂O₃ was about 6 times higher than that of the micron-sized one. The total pore volume and the average pore diameter of the micron-sized sample cannot be determined, while for the nanocrystalline sample, we could find the total pore volume and average pore diameter. The physical properties of nanocrystalline α -Al₂O₃ promoted the CO chemisorption via the number of active Pd atoms, Pd dispersion (%), and average Pd metal particle size for the Pd/ α -Al₂O₃ catalysts, which was also shown in Table 1. The number of active sites of Pd supported on nanocrystalline α -Al₂O₃ catalyst are higher than those on the micron-sized α -Al₂O₃. The lower Pd dispersion obtained for the Pd/micron-sized α -Al₂O₃ would be due to the lower specific surface area of the α -Al₂O₃ support. The higher acetylene hydrogenation activity obtained over Pd/nanocrystalline α -Al₂O₃ was probably due to the increase in the number of Pd active sites [17].

Table 1
The physicochemical properties of Pd catalysts supported on micron-sized and nanocrystalline α -Al₂O₃

Catalyst	BET surface area (m ² /g)	Pore volume (cm ³ /g)	Average pore diameter (nm)	Pd active sites (x10 ⁻¹⁷ sites/g-catalyst)	%Pd dispersion	Average Pd particle size (nm)	XPS binding energy of Pd 3d _{5/2}
Pd/micron-sized α -Al ₂ O ₃	1.9	n.d. ¹	n.d.	11.6	2.3	48.6	336.0
Pd/nano-crystalline α -Al ₂ O ₃	12.3	0.02259	9.0	41.1	8.2	13.7	337.0

¹n.d. = not determined

Temperature programmed reduction (TPR) was performed in order to determine the reduction behaviors and reducibility of catalysts. The TPR profiles for Pd/nanocrystalline and Pd/micron-sized α -Al₂O₃ catalysts are shown in Fig. 3. Only one main reduction peak was observed which could be assigned to the reduction of PdO to Pd⁰ metal. The reduction peaks were at 65 and 55°C

for the catalysts supported on micron-sized and nanocrystalline α - Al_2O_3 , respectively. The 10°C shift of the TPR profile suggests that PdO/Pd supported on the nanocrystalline α - Al_2O_3 facilitated reduction at lower temperature.

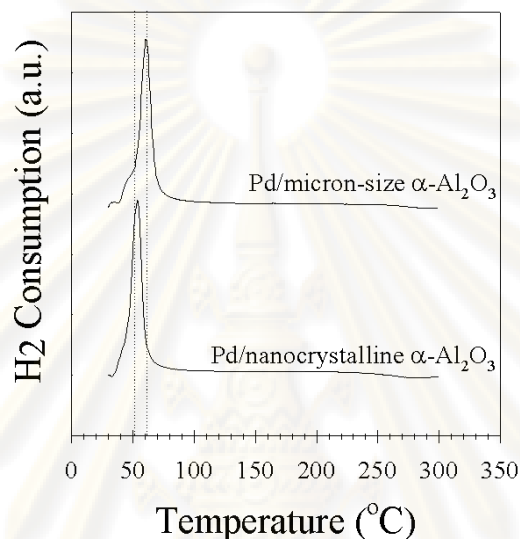


Fig. 3. H_2 temperature programmed reduction results

The behavior for the adsorption and desorption of ethylene on the catalyst surface were investigated by ethylene temperature programmed desorption (ethylene-TPD) and the results are shown in Fig. 4. The amounts of desorbed ethylene increased as the α - Al_2O_3 support changed from micron-sized to nanocrystalline α - Al_2O_3 . This was probably due to the increase in the BET surface area and Pd dispersion of the catalyst. However, the TPD profile of the Pd/nanocrystalline α - Al_2O_3 catalyst exhibited two main peaks ranged around 80°C and 300°C , while the Pd/micron-sized α - Al_2O_3 catalyst exhibited only one broad peak at around 340°C . According to Moon *et al.* [18], the first peak at the low temperature was assigned to π -bonded ethylene species, which were weakly adsorbed on the catalyst surface, and desorbed from Pd without decomposition. The second one was assigned to di- σ -bonded ethylene species, which were desorbed dissociatively followed by the recombination of the surface hydrocarbon species to produce either ethylene or ethane. Disappearance of the first TPD peak and a shift of the second desorption peak to higher temperature for the Pd/micron-sized α - Al_2O_3 indicate that the chemisorption of ethylene on the Pd/micron-sized α - Al_2O_3 was stronger than that on the Pd/nanocrystalline α -

Al_2O_3 . In other words, weaker ethylene chemisorption on the Pd/nanocrystalline $\alpha\text{-Al}_2\text{O}_3$ promoted the selectivity to ethylene [16,19].

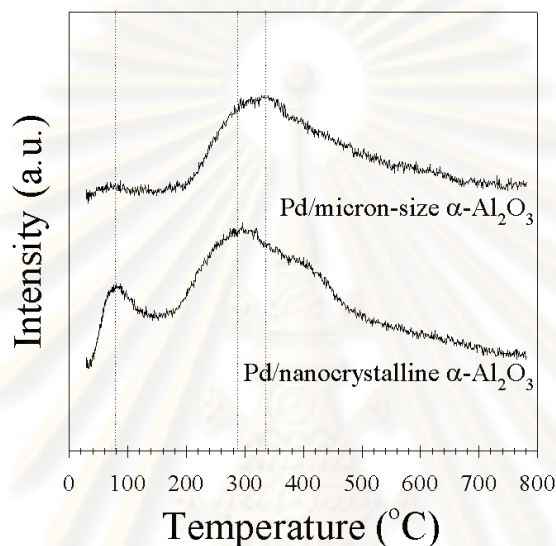


Fig. 4. Ethylene temperature programmed desorption results

Acknowledgements. The authors would like to thank the Commission for Higher Education, Ministry of Education, and Thailand for the financial support of this project.

REFERENCES

1. A.J. Peacock: *Handbook of Polyethylene*, Marcel Dekker, Inc., Basel, New York (2000).
2. N.S. Schbib, M.A. García, C.E. Gígola, A.F. Errazu: *Ind. Eng. Chem. Res.*, **35**, 1496 (1996).
3. W.J. Kim, J.H. Kang, I.Y. Ahn, S.H. Moon: *Appl. Catal. A*, **268**, 77 (2004).
4. A. Sárkány, A. Horváth, A. Beck: *Appl. Catal. A.*, **229**, 117 (2002).
5. E.W. Shin, C.H. Choi, K.S. Chang, Y.H. Na, S.H. Moon: *Catal. Today*, **44**, 137 (1998).
6. M.H. Chen, W. Chu, X.Y. Dai, X.W. Zhang: *Catal. Today*, **89**, 201 (2004).
7. J. Hong, W. Chu, M. Chen, X. Wang, T. Zhang: *Catal. Commun.*, **8**, 593 (2007).
8. N. Wongwaranon, O. Mekasuwandumrong, P. Prasertdam, J. Panpranot: *Catal. Today*, **131**, 553 (2008).
9. W. Huang, J.R. McCormick, R.F. Lobo, J.G. Chen: *J. Catal.*, **246**, 40 (2007).
10. C.J. Brinker, G.W. Scherrer: *Sol-Gel Science: The Physics and Chemistry of Sol-Gel processing*, San Diego, Academic Press (1990).

11. S.G. Deng, Y.S. Lin: *J. Mater. Sci. Lett.*, **16**, 1291 (1997).
12. Y. Sarikaya, I. Sevinc, M. Akinc: *Powder Technol.*, **116**, 109 (2001).
13. W.B. Scott, E. Matijevic: *J. Colloid. Interf. Sci.*, **66**, 447 (1978).
14. M. Inoue, H. Kominami, T. Inui: *J. Am. Ceram. Soc.*, **73**, 1100 (1990).
15. V.H. Sandoval, C.E. Gigola: *Appl. Catal. A*, **148**, 81 (1996).
16. J.H. Kang, E.W. Shin, W.J. Kim, J.D. Park, S.H. Moon: *J. Catal.*, **208**, 310, (2002).
17. J. Panpranot, K. Kontapakdee, P. Prasertdam: *Appl. Catal. A*, **314**, 128 (2006).
18. I.Y. Ahn, W.J. Kim, S.H. Moon: *Appl. Catal. A*, **308**, 75 (2006).
19. G.C. Bond: *Catalysis by Metals*, Academic Press, London (1962).



ศูนย์วิจัยทรัพยากร
จุฬาลงกรณ์มหาวิทยาลัย

VITA

Sataporn Komhom was born in December 3, 1981 in Phetchaburi, Thailand. After graduating from Hua-Hin School in 1999, Prachuapkhirikhan, he spent 4 years at Rangsit University and eventually earned the Second Class Honors in the Bachelor's Degree, from the Department of Chemical Engineering, graduating in May 2003. After that he started to work at Electronics Industry Public Company Limited, Lat Krabang Industrial Estate, Bangkok, he spend one's life at there for one year. Thereafter, he received the Scholarship from the Department of Chemical Engineering at Chulalongkorn University since May 2004 and joined catalysis and catalytic reaction engineering research group.



ศูนย์วิทยทรัพยากร
จุฬาลงกรณ์มหาวิทยาลัย